Exploration de nouvelles approches en radiothérapie interne vectorisée à l'aide d'analogues de neuropeptides

Adrien Chastel

université de BORDEAUX

THÈSE PRÉSENTÉE

POUR OBTENIR LE GRADE DE

DOCTEUR DE

L'UNIVERSITÉ DE BORDEAUX

ÉCOLE DOCTORALE DES SCIENCES DE LA VIE ET DE LA SANTÉ

SPÉCIALITÉ BIOIMAGERIE

Par Adrien CHASTEL

Exploration de nouvelles approches en radiothérapie interne vectorisée à l'aide d'analogues de neuropeptides

Sous la direction du Professeur Elif HINDIÉ

Soutenue le 18 Décembre 2020

JURY

Président :	Madame le Professeur Laurence BORDENAVE
1er rapporteur :	Monsieur le Professeur David TAÏEB
2ème rapporteur :	Monsieur le Docteur David KRYZA
Invité :	Monsieur le Docteur Clément MORGAT

Remerciements

Merci à tous les membres du jury d'avoir accepté d'évaluer ma thèse.

À la Présidente du jury

Professeur Laurence Bordenave

Merci de faire à nouveau partie de mon jury de thèse et de me faire l'honneur de présider ce jury.

Aux membres du jury

Professeur David Taïeb

Merci de faire partie de mon jury de thèse et d'avoir accepté d'être rapporteur.

Docteur David Kryza

Je vous remercie d'avoir accepté d'être rapporteur ainsi que de faire partie de mon jury.

Professeur Elif Hindié

Merci beaucoup d'avoir dirigé cette thèse. Vos conseils et votre soutien ont été précieux.

Docteur Clément Morgat

Merci pour toute ton aide, elle m'a été indispensable durant toutes ces années. Tu m'as toujours encouragé et as toujours été disponible pour encadrer mes travaux de recherche depuis le Master 2.

À l'équipe de l'INCIA : Merci à tous et plus particulièrement Delphine Vimont, Frédéric Masmejean, Catherine Savona-Baron et Laura Cardoit. J'ai également une pensée pour Pr. Philippe Fernandez.

Merci également à Isabel Alves, pour son aide et pour le temps investi dans ce projet.

Au sein de l'équipe de l'IBMM, je souhaite remercier notamment Santo Previti et Florine Cavelier pour leur aide.

Merci à l'équipe de l'université de Leipzig, plus pércisément Dennis Worm et Pr. Beck-Sickinger.

Merci à l'équipe du Cerimed à Marseille, plus particulièrement Samantha Fernandez et à Philippe Garrigue.

Merci à Melina Petrel et Dr Etienne Gontier du pôle d'imagerie électronique pour votre aide dans la mise en place du nouveau protocole.

Merci à Dr Philippe Barberet, Dr Guillaume Devès et Dr Stéphanie Sorieul du CENBG.

À ma famille, merci d'avoir été là depuis le début de mes études, 13 ans c'est long !
À ma femme, Marie-Caroline, merci pour ton soutien tout au long de ma thèse.

Sommaire

Liste des abréviations / Glossaire

BIBP3226 : Antagoniste spécifique Y_1R

eV : electron-volt

^{68}Ga : Gallium 68

IC50 : Half Maximum inhibitory concentration

^{111}In : Indium 111

^{131}I : Iode 131

Levocabastine : Antagoniste spécifique NTS_2

^{177}Lu : Lutetium 177

MIBG : MetaIodoBenzylGuanidine

NT : Neurotensine

NTS_1 : Récepteur de la neurotensine 1

NTS_2 : Récepteur de la neurotensine 2

NPY : Neuropeptide Y

NPYR : Récepteurs du neuropeptide Y

PP : pancreatic polypeptide

PPY : peptide YY

RIV : Radiothérapie Interne Vectorisé

RT-PCR : Reverse Transcription Polymerase Chain Reaction

SR48692 : Antagoniste spécifique NTS_1

TDM : Tomodensitométrie

TEMP : Tomographie à émission monophotonique

TEP : Tomographie à émission de positons

^{90}Y : Yttrium 90

Y_1R : Récepteur 1 du neuropeptide Y

hY_1R : Récepteur 1 du neuropeptide Y humain

Y_2R : Récepteur 2 du neuropeptide Y

Y_5R : Récepteur 5 du neuropeptide Y

Table des Figures

Introduction : Ciblage de récepteurs de neuropeptides pour l'imagerie de tumeurs et radiothérapie interne vectorisée.

La radiothérapie interne vectorisée (RIV) consiste en l'administration de médicaments radiopharmaceutiques pour irradier les tumeurs. Selon l'atome radioactif attaché à la molécule vectrice, un radiopharmaceutique sera employé à visée thérapeutique ou à visée diagnostique. Lorsque l'imagerie diagnostique est utilisée en prélude au traitement on parle d'approche théranostique (contraction de thérapie et de diagnostic).

Depuis les années 50, l'iode-131 est employé en thérapie grâce à ses émissions bêta moins (β^-) et les émissions gamma (γ) associées permettent l'imagerie post-traitement. Ses indications sont notamment dans le cancer de la thyroïde après chirurgie pour prévenir les récidives et détecter et traiter la maladie métastatique[1,2,3,4]. Associé à des molécules vectrices spécifiques, l'iode-131 est également utilisé pour ciblage d'autres tumeurs, par exemple sous forme de ^{131}I-MIBG pour traiter les neuroblastomes et les phéochromocytomes métastatiques[5]. Signalons que si l'imagerie par γ caméra de l'iode-131 n'offre pas une résolution optimale et ne permet pas une quantification précise, il est possible dès l'étape diagnostique de substituer l'iode-131 par l'iode-124, émetteurs de positons, permettant une imagerie quantitative en TEP[6].

Dans les années 90, différentes molécules vectrices marquées par le radiométal yttrium-90 ont fait leur entrée en thérapie : utilisation d'anticorps anti-CD20 marqués à l'^{90}Y dans le traitement des lymphomes ; utilisation d'analogues de la somatostatine marqués à l'^{90}Y dans le traitement de tumeurs neuroendocrines, en association avec des analogues marqués à l'indium-111 (^{111}In-pentetreotide) émetteur γ servant l'étape diagnostique[7,8,9,10]. Le ^{90}Y est un émetteur quasi-exclusivement β^-, d'une énergie relativement élevée avec un maximum de 2280 keV expliquant que dans des essais menés avec les analogues peptidiques de la somatostatine radiomarqués à l'^{90}Y, dont le mode d'élimination est principalement urinaire, un des inconvénients majeurs relevés était une toxicité rénale élevée. Cette toxicité a persisté malgré l'administration d'acides aminés à visée néphroprotectrice pour réduire la capitation par les cellules tubulaires proximales[11].

Début des années 2000 le lutétium-177 a fait son entrée dans le champ de la RIV et s'est retrouvé privilégié du fait de ses caractéristiques de sécurité et d'efficacité plus adaptés à un emploi en pratique clinique. En effet le ^{177}Lu a une émission β^- de moyenne énergie (maximum

500 keV). Ces particules ß$^-$ ont une pénétration tissulaire maximale de 2mm permettant une bonne efficacité d'irradiation au sein des lésions tumorales, tout en épargnant au maximum les tissus sains périphériques[12] offrant ainsi un bon rapport efficacité/toxicité dans les essais cliniques. De plus, le ^{177}Lu émet deux rayonnements γ (208 keV : 10,4% ; et 113 keV : 6,2%) permettant l'imagerie post-traitement qui est actuellement réalisée en mode planaire corps entier, complétée par des acquisitions en mode tomoscintigraphique TEMP (tomographie par émission monophotonique) couplé au scanner (TEMP-TDM) sur les γ-caméra hybrides actuelles.

En routine clinique, le lutétium-177 est actuellement utilisé couplé aux analogues de la somatostatine, notamment le [^{177}Lu]Lu-DOTATATE, bénéficiant d'une AMM dans la prise en charge de tumeurs neuro-endocrines (Lutathera®, d'où l'utilisation en France du terme lutathérapie). Ces mêmes analogues sont également radiomarqués au ^{68}Ga pour un emploi à visée diagnostique en imagerie TEP préalable à la thérapie ([^{68}Ga]Ga-DOTATOC en France ou [^{68}Ga]Ga-DOTATATE aux Etats-Unis). Les résultats obtenus avec le [^{177}Lu]Lu-DOTATATE en essai clinique de phase 3 incluant 229 patients avec une tumeur neuroendocrine (essai NETTER-1) sont particulièrement prometteurs avec une survie sans progression à 20 mois de 65,2% (contre 10,8% dans le groupe contrôle). Plus récemment, des ligands du Prostate Specific Membrane Antigen (PSMA) ont montré une bonne efficacité dans le cancer de la prostate métastatique résistant à la castration dans plusieurs études cliniques[13,14]. Un large essai randomisé de phase 3 (Essai Vision) est en cours d'analyse comparant l'efficacité du lutétium [^{177}Lu]Lu-PSMA-617 en association au traitement de référence par rapport au traitement de référence seul, chez des patients ayant un cancer de la prostate métastatique, résistant à la castration, évolutif et positif en TEP au PSMA[15].

Un avantage majeur de la RIV est sa capacité à atteindre des métastases disséminées, localisées à différents endroits, ceci représentant un avantage fondamental par rapport à la radiothérapie externe. En effet, la plupart des radiopharmaceutiques employés en oncologie ont pour caractéristique de cibler le tissu tumoral, indépendamment du fait qu'il s'agisse de la tumeur primitive ou des métastases. Une approche alternative étant le ciblage d'antigènes de surface par des anticorps spécifiques, ou radio-immuno-thérapie. L'exigence fondamentale est que la molécule vectrice ait toujours une forte sélectivité/affinité pour le tissu tumoral afin d'obtenir la meilleure efficacité avec une toxicité minime pour les organes et tissu sains.

Parmi les caractéristiques intéressantes du ciblage par petites molécules, la cinétique rapide de clairance plasmatique et de captation tumorale et la capacité de radiomarquer ces

ligands et petites molécules par des radioéléments émetteurs de positons, comme le gallium-68 (^{68}Ga), pour une imagerie par tomographie d'émission de positons (TEP) permettant une détection précise de la maladie métastatique et l'évaluation quantitative de la captation tumorale avant RIV[16,17,18]. L'avantage du ^{68}Ga c'est la possibilité de production par un générateur germanium-68/gallium-68 (^{68}Ge/^{68}Ga) ou par cyclotron, lui conférant une disponibilité croissante[19]. Par ailleurs, la demi-vie du ^{68}Ga est compatible avec les propriétés pharmacocinétiques de nombreux vecteurs auxquels il peut être associé, à savoir des molécules de faible poids moléculaire (peptides ou fragments d'anticorps) qui se distribuent rapidement.

La plupart des ligands ayant pour but d'être radiomarqués contiennent un chélateur tel que le DOTA par exemple, permettant de lier solidement le radiométal choisi à visée thérapeutique ou d'imagerie. Un des avantages du DOTA est sa polyvalence car on peut lui attacher du ^{68}Ga mais aussi du ^{177}Lu par exemple, permettant ainsi un double emploi pour une même molécule.

Ainsi, deux molécules à même base vectrice pourront être utilisées, soit pour la thérapie ou pour le diagnostic, en faisant simplement varier l'atome radioactif employé lors du radiomarquage (selon le type d'émission souhaitée : β^+ pour imagerie TEP ou γ pour imagerie TEMP, et pour la thérapie β^-, voir alpha ou Auger). C'est le concept de « théranostique » ou « imager et traiter » qui est un excellent exemple de prise en charge personnalisée associant diagnostic et thérapie dans la prise en charge individualisée de la maladie[20]. Ce concept est en pleine expansion.

Parmi les approches en RIV, celle basée sur des analogues de peptides radiomarqués ciblant des récepteurs à la surface de cellules tumorales (PRRT) est en pleine expansion. Si le ciblage des récepteurs de la somatostatine est un exemple phare, divers autres récepteurs de peptides et neuropeptides sont surexprimés à la surface de cellules tumorales dans diverses tumeurs ou sous-types tumoraux associés à une faible présence dans les tissus sains périphériques[21]. De plus, les avancées récentes dans le domaine de la biologie et de la chimie ont rendu certains récepteurs accessibles avec des ligands hautement sélectifs. Lorsque le ciblage s'effectue à l'aide d'analogues radiomarqués de type « agonistes », similaires aux peptides naturels, et suite à la liaison spécifique de ces analogues aux récepteurs peptidiques surfaciques, le complexe peptide/récepteur est ensuite internalisé pour partie, ce qui conduit à une accumulation de radioactivité dans les cellules néoplasiques. Mais le ciblage peut également s'effectuer à l'aide d'analogues de type « antagonistes » et même si dans ce cas la liaison aux récepteurs n'est en général pas suivie d'une internalisation cellulaire, il a été

démontré dans certains cas que les liaisons peuvent être très stables au cours du temps amenant à un ciblage remarquable[22,23].

L'objectif de ce travail de Thèse est d'étendre le développement du ciblage de tumeurs par des analogues de neuropeptides ciblant des récepteurs surexprimés à leur surface. Nous nous intéresserons plus spécifiquement aux analogues peptidiques de la neurotensine et du neuropeptide Y dont les récepteurs sont connus pour être surexprimés dans divers cancers, notamment des cancers qui ne répondent pas ou ne sont pas éligibles aux autres traitements par RIV actuellement disponibles comme le [^{177}Lu]Lu-DOTATATE ou le [^{177}Lu]Lu-PSMA. Notre travail consistera en la caractérisation de plusieurs nouveaux analogues radiomarqués.

PARTIE I : Ciblage du récepteur de la neurotensine NTS_1

Chapitre 1 : Contexte scientifique

a) La neurotensine

Découverte par Carraway et Leeman en 1973[24], la neurotensine (NT – **Figure 1**) est un peptide composé de treize acides aminés[25] agissant comme neuromodulateur dans le système nerveux central en intervenant notamment sur la transmission dopaminergique[26]. La NT présente également une action analgésique centrale[27] via la substance grise périaqueducale ainsi que la moelle rostrale ventromédiale. En périphérie, la NT est sécrétée par les cellules N-entéro-endocrines du tube digestif en réponse à l'ingestion de lipides intraluminaux[28]. Le peptide exerce principalement une action de régulation hormonale et neurocrine dans le processus digestif, notamment l'inhibition de la motilité de l'intestin grêle et des sécrétions stomacales, la stimulation des sécrétions pancréatiques (insuline et glucagon) et biliaires[29], ainsi que la facilitation de l'absorption des acides gras[30]. La neurotensine a également un rôle dans le système cardiovasculaire en agissant sur la perméabilité vasculaire[31].

pGlu[1]-Leu[2]-Tyr[3]-Glu[4]-Asn[5]-Lys[6]-Pro[7]-Arg[8]-Arg[9]-Pro[10]-Tyr[11]-Ile[12]-Leu[13]

Figure 1 : Structure peptidique de la neurotensine

b) Les récepteurs de la neurotensine

L'action de la neurotensine est médiée par deux récepteurs couplés aux protéines G (RCPG) avec sept domaines transmembranaires, les récepteurs NTS_1 et NTS_2, respectivement de haute affinité et de faible affinité[32], mais également par un récepteur transmembranaire unique non-spécifique NTS_3 également appelé Sortilin, codé par le gène SORT1[33]. Chez la souris, NTS_1 a été retrouvé par RT-PCR principalement au niveau du système nerveux central (noyaux hypothalamiques principalement ainsi que cortex préfrontal et striatum et dans une moindre mesure le cervelet). En périphérie, l'ARN messager NTS_1 a été détecté dans le côlon, ainsi que le foie, le duodénum et le pancréas[34]. L'expression de NTS_1 a été détectée dans la muqueuse colique saine par immunohistochimie[35], ainsi que par autoradiographie dans les cellules musculaires lisses du côlon sain chez l'homme[36].

L'affinité de la NT pour NTS_1 est très forte, de l'ordre de 2-3nM (IC_{50})[37], et son plus petit fragment pharmacologiquement actif est le fragment C-terminal [8-13] (cf. **Figure 1**)[38]. L'équipe de Barroso[39] a également montré l'importance de plusieurs résidus de la NT[8-13] pour sa liaison à NTS_1, comme la Tyr^{11}, l'Ile^{12} ou la Leu^{13}, ce qui a été confirmé plus récemment par les travaux de P. Kitabgi[40].

Le site de liaison à la neurotensine de NTS_1 se situe principalement au niveau de la troisième boucle extracellulaire[39]. Plus récemment, l'équipe de White et al a déterminé par cristallographie que la majorité des sites d'interaction entre la NT et NTS_1 (

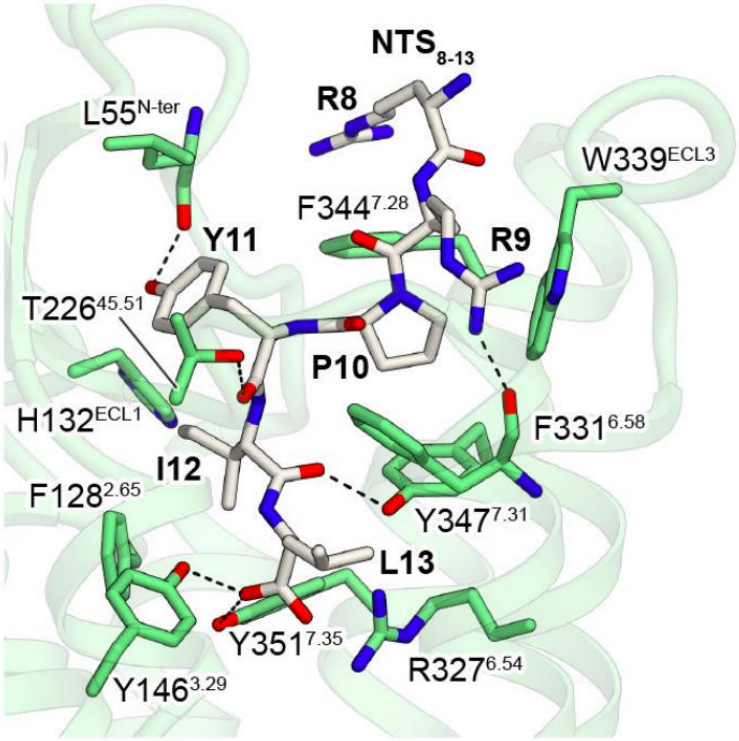

Figure 2) se situaient sur les 2e et 3e boucles extracellulaires, ainsi que sur les 6e et 7e domaines transmembranaires du récepteur. De façon générale les interactions ligand/récepteur nécessitent des liaisons hydrogène, des liaisons van der Waals et des interactions ioniques. Plus précisément la liaison de la neurotensine à NTS_1 nécessite une charge positive apportée par l'arginine au niveau de la NT, afin de se lier au bord électronégatif du site de liaison au récepteur[41]. Les interactions ioniques ont été déterminées notamment à l'aide d'analogues de la NT(8-13) avec des substitutions d'acides aminés à chaque position. Ces travaux ont mis en évidence que l'Arg^9 de la neurotensine interagit avec la Phe^{331} de NTS_1, la Tyr^{11} avec Met^{208}, Phe^{344} et plus particulièrement avec Tyr^{347}, que l'Ile^{12} interagit avec Met^{208} et la Leu^{13} avec Met^{208} et Phe^{331}. La fonction carboxyle de l'extrémité C-terminale du peptide interagit elle avec Arg^{327} [39].

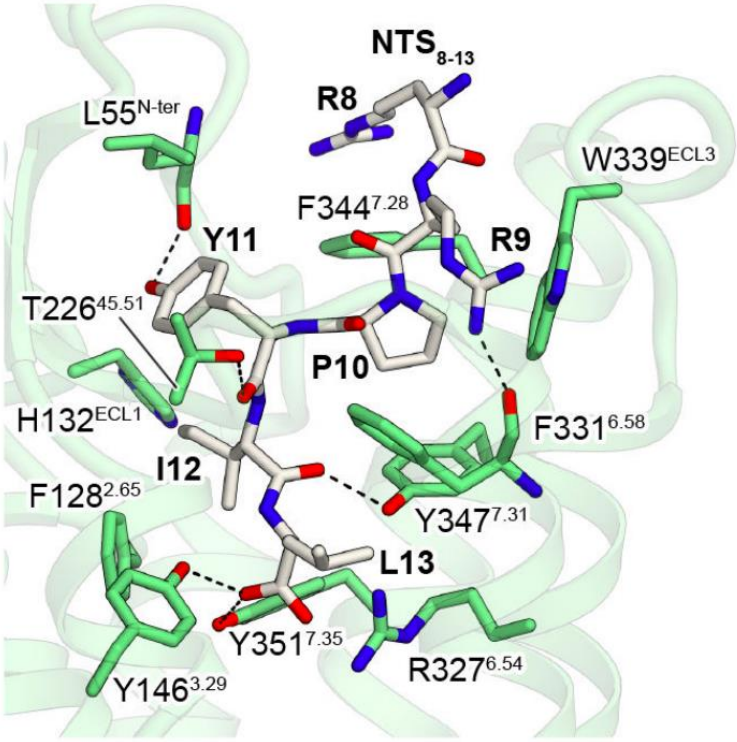

Figure 2 : Liaison NT/NTS_1 d'après Kato et al[42]

La NT stimule, via NTS_1, préférentiellement la cascade de signalisation intracellulaire de la protéine $G_{q/11}$[43]. Les voies impliquant les sous unités Gs et Gi/G0 existent également mais sont secondaires[44]. Dans plusieurs types de tumeurs, la liaison de NT à NTS_1 est un facteur stimulant la cancérogénèse en favorisant la motilité, l'invasion, la prolifération et la survie[45]. La voie de signalisation pro-oncogénique est la suivante (**Figure 3**) : à la liaison de la NT à NTS_1 la sous unité $G_{q/11}$ du récepteur active la phospholipase C (PLC), suivie de l'hydrolyse du phosphatidylinositol 4,5-bisphosphate membranaire en diacylglycérol (DAG) et inositol triphosphate (IP3). Le DAG va ensuite stimuler la protéine kinase C (PKC) alors que l'IP3 va induire la mobilisation de calcium intracellulaire via le réticulum endoplasmique. Les effets pro-oncogénique sont principalement dépendants de la PKC qui joue un rôle dans la prolifération et la survie cellulaire[45]. Comme la plupart des RCPG, lorsque NTS_1 est exposé à un agoniste à haute concentration, le récepteur est activé puis sujet à une désensibilisation. Le mécanisme de désensibilisation relève de l'internalisation du récepteur médiée par la clathrine et dépendant de la liaison de la bêta-arrestine au récepteur phosphorylé[46]. Dans des modèles cellulaires animaux (CHO)[47] ou humains (HEK)[48], la majorité des récepteurs internalisés n'est pas recyclée vers la membrane mais dégradée par voie lysosomale[49]. D'autres protéines sont impliquées dans le mécanisme d'internalisation, mais ce mécanisme diffère selon la lignée cellulaire étudiée. En effet, dans la lignée COS-7 (singe) et HEK 293 (humain), ce processus implique la beta arrestine et la dynamine mais pas l'amphiphysine. L'intersectine joue un rôle

dans la lignée COS-7 mais n'est pas nécessaire à l'endocytose des récepteurs dans la lignée HEK 293[50].

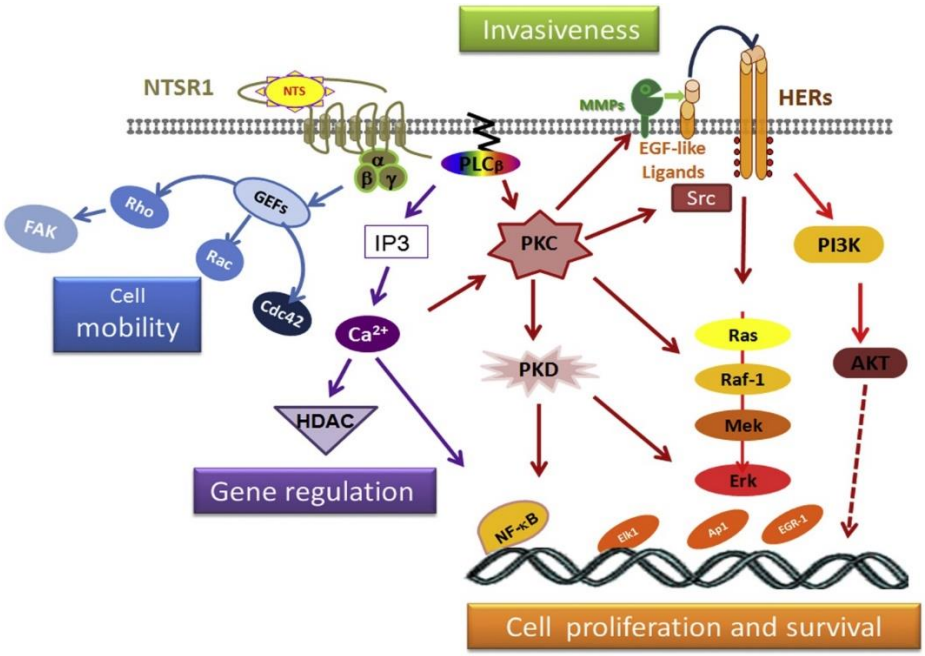

Figure 3 : Cascade de signalisation intracellulaire après activation de NTS_1 par NT[45]

c) NTS_1 en oncologie

Le complexe NT/NTS_1 contribue à l'agressivité des tumeurs et l'activation chronique du complexe NT/NTS_1 stimule l'EGFR. Une augmentation de la croissance des tumeurs et de l'apparition de métastases pour des tumeurs exprimant le complexe NT/NTS_1 a été observée chez des souris nude[51].

Il a été également démontré que la protéine NTS_1 n'est pas ou peu détectée dans les tissus sains, mais elle est connue pour être surexprimée dans divers cancers, qui sont détaillés ci-dessous :

Dans le carcinome canalaire pancréatique, l'expression de la protéine NTS_1 a été mise en évidence par autoradiographie dans 73% (8/11) des tumeurs primitives, et 63% (14/23) des métastases hépatiques. La densité des récepteurs était importante dans les tumeurs NTS_1 positives alors que les tissus sains (pancréas et foie) adjacents étaient NTS_1 négatifs[52]. Ceci suggère que le NTS_1 pourrait être une nouvelle cible des tumeurs pancréatiques de haut grade.

Dans le cancer du sein, une étude sur 51 échantillons de carcinomes canalaires invasifs (CCI) a retrouvé une expression du peptide neurotensine dans 34% des cas, une expression de NTS_1 dans 91% des cas et une co-expression de NT et NTS_1 dans 30% des cas. Le complexe NT/NTS_1 stimule la croissance tumorale ainsi que la progression métastatique via l'activation d'EGFR, HER2 et HER3[53]. Par ailleurs, il a été également observé que 106 patientes ayant un CCI et une forte expression de NTS_1 avaient une moins bonne survie à 10 ans que les patientes

avec une faible expression de NTS_1 (66,2 % versus 96,5 %, $p = 0,01$). De plus, il a été constaté que les tumeurs NTS_1 positives étaient de plus grande taille ($p = 0,007$) et de plus haut grade ($p = 0,036$) que les tumeurs n'exprimant pas NTS_1, et les patientes avec des tumeurs NTS_1 positives avaient un taux de mortalité supérieur ($p = 0,0025$). Enfin, il a été également constaté une forte association entre l'expression de récepteurs à la neurotensine et la positivité des récepteurs aux œstrogènes[54]. L'association entre l'expression du complexe NT/NTS_1 et l'expression de HER2 et/ou HER3 a été évaluée 1883 échantillons de cancer du sein. NTS_1 a été retrouvé dans 28% (375/1347) des échantillons, NT et NTS_1 ont été retrouvés dans 23% (301/1347) des échantillons, tandis que HER2 et HER3 étaient trouvés dans 28% (361/1268) et 53% (753/1410) de ces échantillons respectivement. Parmi la population positive à NTS_1, 19% (244/1410) exprimaient HER3 alors que seul 8% (102/1268) exprimaient HER2. L'expression de HER3 était positivement corrélée à celle de NTS_1 (p <0,0001) et celle de NT/NTS_1 (p<0,0001). En contrepartie, il n'a pas été retrouvé de relation significative entre HER2 et NTS_1 ou entre HER2 et NT/NTS_1. Seuls 5% (62/1410) des échantillons ont surexprimé les 4 marqueurs de façon concomitante. Cette surexpression n'est pas associée à une transcription de gènes ou une activité post-transcriptionelle, suggérant que la NT induit un nouvel équilibre dans le trafic cellulaire de HER[53].

Dans le cancer du poumon non à petites cellules, NTS_1 est présent dans 59% (160/271) des cas, et cette surexpression est associée à un plus faible taux de survie global à 5 ans des patients : 36,5% *vs* 55,4% chez les patients exprimant peu NTS_1 ; ($p = 0,039$)[55]. Une seconde étude incluant 74 patients a retrouvé par analyse univariée que l'expression de NTS_1 était associée à un moins bon taux de survie à cinq ans ($p = 0,0081$) ainsi qu'à une moins bonne survie sans rechute ($p = 0,0024$). L'analyse multivariée retrouva qu'un âge supérieur à 65 ans et l'expression de NTS_1 étaient des facteurs indépendants de mauvais pronostic ($p = 0,0018$ et $p = 0,0034$ respectivement)[56].

Dans le cancer de la prostate, la surexpression de NTS_1 a été retrouvée dans des cellules tumorales peu différenciées notamment n'exprimant pas les récepteurs aux androgènes (AR) (lignées PC3 et DU145)[57,58]. Ceci est particulièrement intéressant car les cancers AR négatifs sont souvent agressifs et ne répondent pas ou peu aux thérapies basées sur la suppression androgénique[59,60]. Une étude menée sur la lignée LNCaP a démontré que l'acquisition des propriétés invasives médiées par la gelsoline faisait suite à l'activation de NTS_1 par la neurotensine[61]. Notre équipe a également mené une étude sur l'expression de NTS_1 dans le cancer de la prostate, mettant en évidence une surexpression de NTS_1 plus importante dans les ganglions métastatiques que dans les tumeurs primitives ($p=0,038$)[62].

Cette forte expression du récepteur dans les lésions primitives et métastatiques de plusieurs cancers invasifs, encourage le développement d'analogues radiomarqués de la neurotensine à visée diagnostique et thérapeutique.

d) Stratégies de stabilisation des analogues de la neurotensine

La NT[8-13] possède trois sites de clivage par les endopeptidases, à savoir les sites Arg^{8}-Arg^{9}, Pro^{10}-Tyr^{11} et Tyr^{11}-Ile^{12} (**Figure 4**). L'enzyme de conversion de l'angiotensine (ACE) clive rapidement la liaison Tyr^{11}-Ile^{12} alors que la neural endopeptidase (NEP) clive la liaison Pro^{10}-Tyr^{11} ainsi que la liaison Tyr^{11}-Ile^{12}. Les metalloendopeptidases 24.15 (thimet oligopeptidase) et 24.16 (neurolysin) sont respectivement responsables du clivage des liaisons Arg^{8}-Arg^{9} et Pro^{10}-Tyr^{11} [63].

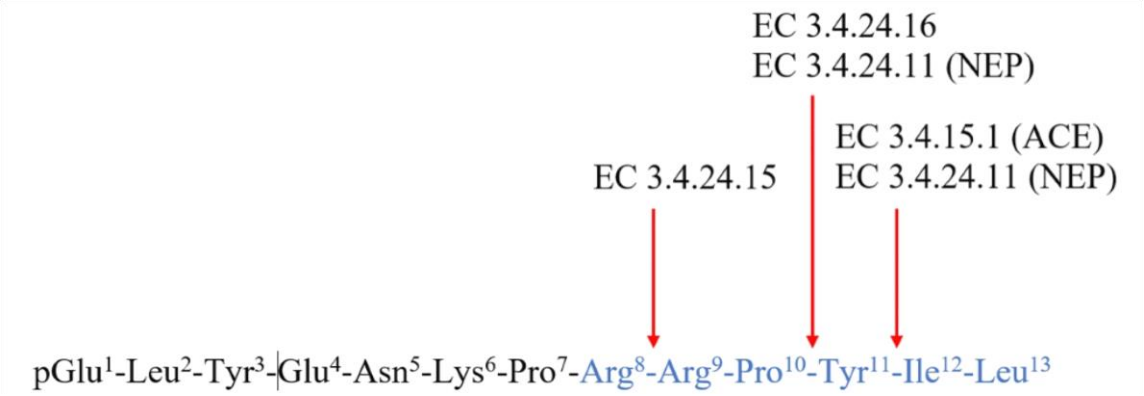

Figure 4 : Endopeptidases impliquées dans le clivage de la neurotensine[8-13] et sites de clivage

Une étude ex vivo menée sur des analogues radiomarqués du fragment [8-13] comportant des modifications successives de l'extrémité N-terminale a permis de déterminer que le clivage de la liaison Arg^{8}-Arg^{9} survenait en premier, suivi de la liaison Tyr^{11}-Ile^{12}. La liaison Pro^{10}-Tyr^{11} est donc la dernière à être clivée[64].

Ces sites de clivage entraînent une dégradation rapide in vivo, rendant le fragment NT[8-13] inutilisable en l'état en pratique clinique.

Afin d'améliorer la demi vie plasmatique de la NT pour atteindre sa cible NTS_1, deux possibilités existent : agir sur la stabilité plasmatique du peptide en protégeant les sites de clivage ou injecter la NT (ou analogue de la neurotensine) avec un (ou plusieurs) inhibiteurs des endopeptidases[65]. Cependant, tous les inhibiteurs d'endopeptidases n'ont pas été étudiés in

vivo, ce qui à ce jour limite leur emploi chez l'homme. Une stratégie intéressante est donc de modifier les acides aminés présents au niveau des sites de clivage en vue d'améliorer la stabilité plasmatique des analogues radiomarqués basés sur le fragment NT[8-13]. Il est également possible de modifier les liaisons peptidiques via une réduction, une méthylation,…

Par exemple, dans une étude menée sur la lignée HT-29, il a été rapporté que la substitution de l'Arg^8 par une lysine a permis une amélioration de la stabilité plasmatique (atteignant 20 min) avec un maintien d'une excellente affinité pour NTS_1 avec un Kd de 0,6 nM. Par la suite, la réduction de la liaison Lys^8-Arg^9 (NT-VI) a permis l'obtention d'une stabilité encore plus importante (3h) tout en maintenant l'affinité (Kd = 0,3 nM)[66]. Dans ce même analogue, une substitution de la liaison réduite Lysψ(CH_2NH)Arg par Arg-NMeArg a mené à une plus faible captation rénale et un meilleur rapport tumeur/rein, tout en gardant une bonne affinité pour NTS_1 et bonne stabilité plasmatique in vitro[67].

Une autre approche a été la réduction de l'arginine N-terminale (du fragment actif de NT) et a permis l'obtention d'un analogue plus stable et plus affin pour NTS_1[68].

La substitution de la Leu^{13} par une $ß^3$hLeu puis la substitution de l'Arg^8 par une $ß^2$hArg dans des analogues basés sur la DOTA-neurotensine(8-13) avait notamment permis l'obtention de résultats très prometteurs in vitro avec une meilleure stabilité ainsi qu'une bonne affinité pour NTS_1, mais après injection in vivo chez des souris des analogues radiomarqués au ^{68}Ga, il s'est avéré que la stabilité plasmatique était très faible[69].

Une autre possibilité de modification est l'emploi d'acides aminés silylés tels que la silaproline ou la TMS-Ala. La substitution de la Pro^{10} par la silaproline augmente la lipophilie et améliore la stabilité de la NT et la substitution de la leucine par la TMS-Ala majore l'affinité pour NTS_1[70]. Un des avantages de l'emploi de ces acides aminés sylilés est qu'ils n'impactent pas la conformation du peptide[71]. Cependant leur positionnement dans le peptide peut avoir un impact notable, par exemple, la TMS-Ala en position 13 dans la NT[8-13] a induit une nette diminution de l'affinité pour NTS_1 qui n'a pas été retrouvée lorsque la TMS-Ala était en position 12[72].

Ainsi, on remarque que la substitution des arginines en 8 et 9 par des lysines et la substitution de l'isoleucine par la tert-leucine sont des approches fréquentes pour stabiliser les analogues de la neurotensine[73]. Cependant, l'amélioration de la stabilité par ces modifications a induit une baisse de l'internalisation des analogues par les cellules HT-29 (cancer colorectal) et une diminution de l'affinité pour NTS_1. Par ailleurs, la substitution des résidus Arg en 8 et 9 par des Lys semble majorer l'hydrophilie[66]. Une réduction de la Lys substituant l'Arg^8 dans

l'analogue cité précédemment (NT-VI) et une substitution de l'Ile^{12} par une Tle ont résulté en une amélioration notable de la stabilité de l'analogue radiomarqué au ^{99m}Tc[74].

L'un des analogues radiomarqués de la NT les plus étudiés dans la littérature à ce jour est le DOTA-NT-20.3 dont la séquence est Ac-Lys(DOTA)-Pro-Me-Arg-Arg-Pro-Tyr-Tle-Leu-OH. Dans cet analogue, la NT[8-13] a subi trois modifications avec l'ajout d'une proline N-terminale et la méthylation d'Arg^8 pour protéger le site de clivage Arg^8-Arg^9. Au niveau C-terminal, l'Ile^{12} a été substituée par la tert-leucine qui augmente l'hydrophobie ainsi que l'affinité pour NTS_1. Son affinité pour NTS_1 (in vitro, cellules HT-29), lorsque radiomarqué au ^{68}Ga est de 14 ± 2 nM (IC_{50})[75].

Il existe un antagoniste non peptidique spécifique de NTS_1 (IC_{50} = 30,3 ± 1,5nM), le SR48692 (**Figure 5**)[76]. Cet antagoniste a été modifié pour donner le SR142948A (IC_{50} = 0,32 ± 0,08nM) (**Figure 6**) qui est à la base d'une famille d'analogues non peptidiques antagonistes de NTS_1, cependant le SR142948A est peu sélectif pour NTS_1. Elle diffère de la molécule de référence par le remplacement de la chloroquinoline en position 1 du pyrazole par un cycle phényle bisubstitué[77]. Le dérivé du SR142948A ayant les meilleurs résultats à ce jour est le 3-BP227 (**Figure 7**). Un avantage majeur est l'inaction des endopeptidases sur les analogues non peptidiques ainsi que leur excellente affinité pour NTS_1, avec une captation tumorale importante (8,4 ± 3,1 %ID/g à 6h chez des souris nude)[78]. Cet analogue, radiomarqué au ^{177}Lu, a également été injecté chez 6 patients avec adénocarcinome pancréatique, avec une bonne tolérance[79].

Cependant, le caractère antagoniste des analogues non peptidiques empêche leur internalisation ce qui limite la possibilité de potentialisation de l'action thérapeutiques des radioéléments et plus particulièrement en cas d'emploi d'émetteurs Auger ou alpha.

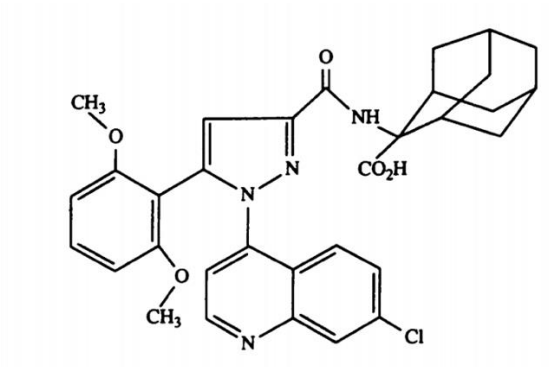

Figure 5 : Antagoniste non peptidique de NTS_1 : SR48692

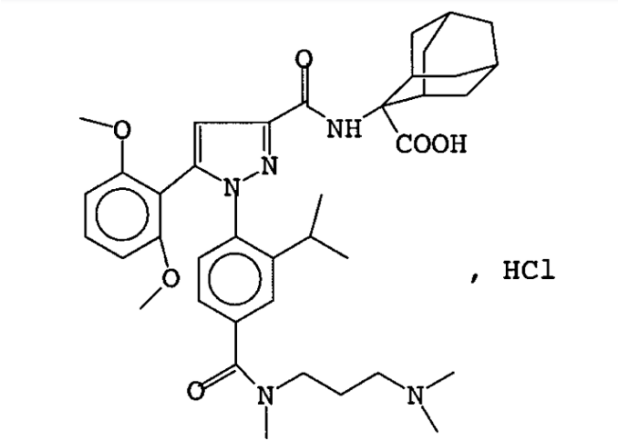

Figure 6 : Antagoniste non peptidique de NTS_1 : SR142948A

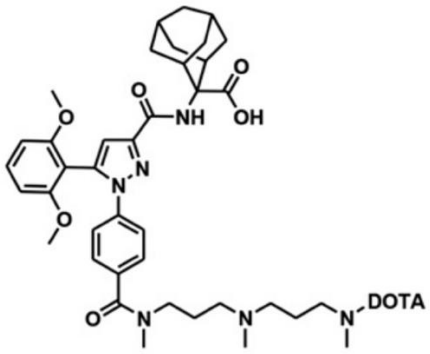

Figure 7 : Antagoniste non peptidique de NTS_1 : 3-BP227

Les différences principales entre les analogues peptidiques et non peptidiques de la neurotensine sont résumées dans le **Tableau 1** ci-dessous.

	Avantages	**Inconvénients**
Analogues peptidiques	Internalisation Bonne biodistribution	Pro-oncogénique Demi-vie courte
Analogues non peptidiques	Antagoniste Demi-vie longue Meilleure captation tumorale	Absence d'internalisation (limite l'emploi d'émetteurs alpha et Auger)

Tableau 1 : Récapitulatif des principaux avantages et inconvénients des analogues peptidiques et non peptidiques ciblant NTS_1

L’objectif de notre première partie du travail de thèse décrit dans le chapitre suivant a donc été de développer de nouveaux analogues peptidiques de la neurotensine à l’aide d’introduction d’acides aminés non-naturels afin d’obtenir une meilleure stabilité plasmatique tout en conservant une bonne affinité pour NTS_1 en vue d’une application théranostique. Ce projet a bénéficié de financements de France Life Imaging (projet PINK) et de l’Institut National du Cancer (projet THERACAN). Ce projet a été réalisé en collaboration avec l’Institut des Biomolécules Max Mousseron, Laboratoire des Acides Aminés, Peptides et Protéines du Dr Florine Cavelier (Université de Montpellier) et avec le CERIMED (Université Aix-Marseille, Pr B. Guillet) pour la partie imagerie in vivo.

Chapitre 2 : Évaluation de radiopharmaceutiques issus de modifications structurales (C-term et N-term) du squelette de la neurotensine [8-13]

Introduction : Plusieurs études indépendantes ont signalé la surexpression de NTS_1 dans diverses tumeurs malignes telles que le carcinome mammaire canalaire invasif, le cancer de la prostate ou encore l'adénocarcinome pancréatique[53,62,52]. Ceci rend ce récepteur intéressant dans des perspectives d'imagerie et de thérapie. Toutefois, comme indiqué dans le chapitre précédent, à ce jour, les analogues de neurotensine peptidique radiomarqués souffrent d'une faible stabilité plasmatique due aux endopeptidases présentes physiologiquement chez l'homme et donc d'une disponibilité insuffisante pour une captation élevée par les tumeurs[80]. D'autre part, les analogues non peptidiques de la neurotensine[78], très stables, ont cependant le désavantage d'avoir une pharmacocinétique trop lente pour un emploi en imagerie TEP au ^{68}Ga. Aussi, notre objectif a été de participer au développement de nouveaux analogues peptidiques de la neurotensine, basés sur l'introduction d'acides aminés non-naturels afin d'obtenir une meilleure stabilité plasmatique tout en conservant une bonne affinité pour NTS_1 pouvant permettre des applications futurs théranostiques, et de tester ces analogues suite à leur marquage. Les premiers résultats qui ont fait l'objet d'une publication récente dans Bioconjugate Chemistry (cf. article complet Partie 2, Chapitre 4) sont résumés et discutés ci-après :

Résultats : Parmi la série de nouveaux analogues de la neurotensine développés grâce au partenariat entre notre laboratoire de l'INCIA et l'Institut des Biomolécules Max Mousseron, nous avons identifié comme bon candidat (lead compound) le [^{68}Ga]Ga-JMV6659. Cet analogue radiomarqué présente une hydrophilie élevée ($LogD_{7,4}$ = -3,41 ± 0,14), une affinité élevée dans la gamme nanomolaire basse vis-à-vis de NTS_1 (Kd = 6,29 ± 1,37 nM), une bonne sélectivité (Kd NTS_1 / Kd NTS_2 = 35,9), une internalisation médiée par NTS_1 élevée, un efflux plus faible et demi-vie plasmatique prolongée dans le plasma humain par rapport au composé de référence, le [^{68}Ga]Ga-JMV6661. Chez les souris nude portant une xénogreffe HT-29, la captation tumorale du [^{68}Ga]Ga-JMV6659 atteint 7,8 ± 0,54 %ID/g 2h après l'injection. L'injection d'un excès de neurotensine froide diminue la captation à 1,38 ± 0,71 %ID/g. La dose efficace extrapolée à l'homme a été estimée à 2,35 ± 0,6 mSv, pour une activité injectée de 100 MBq.

Conclusion : Les résultats présentés dans ce travail ont montré que l'incorporation d'acides aminés contenant du silicium dans les analogues de la neurotensine améliore leur

affinité de liaison, la stabilité plasmatique et les propriétés radiopharmaceutiques. Le [^{68}Ga]Ga-JMV6659 est donc un candidat prometteur pour étudier l'expression de NTS_1 à visée diagnostique à l'aide de l'imagerie TEP dans de futurs essais cliniques.

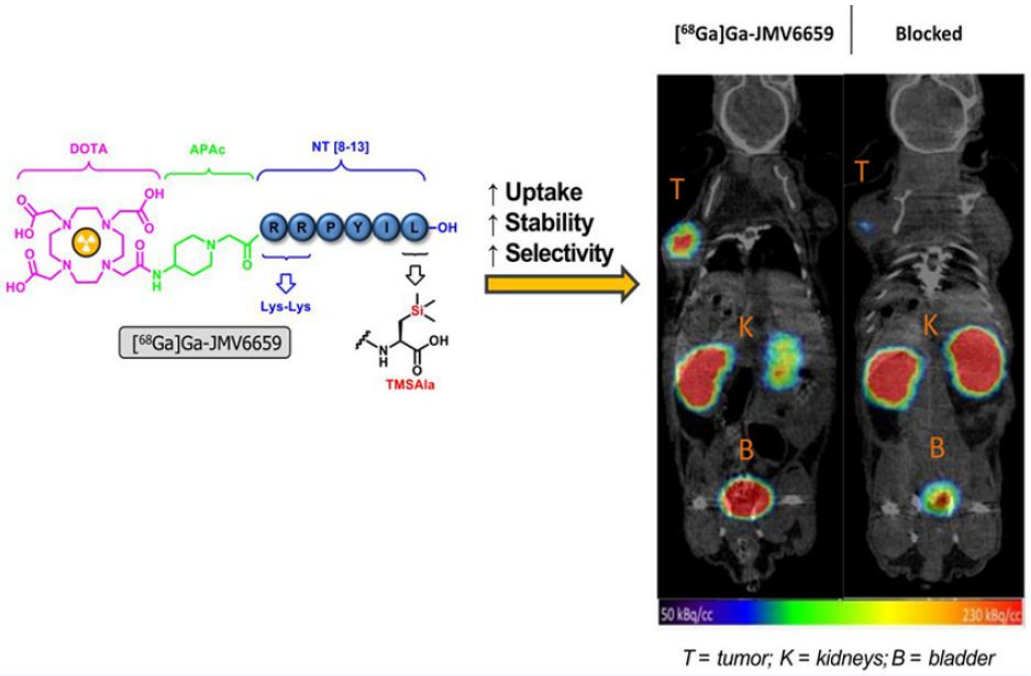

Figure 8 : Lead Compound : [^{68}Ga]Ga-JMV6659

Chapitre 3 : Discussion sur NTS_1 et poursuite de ce travail

L'introduction de l'acide aminé sylilé TMSAla majore l'hydrophobie et l'affinité pour le récepteur. En effet, le site principal de liaison à la neurotensine comporte une poche hydrophobe qui interagit principalement avec l'extrémité C-terminale de NT[8-13]. Ceci explique également pourquoi sa position en 12 vs 13 a un impact significatif sur cette modification d'affinité (qui est nettement améliorée lorsque la TMSAla est en position 13 vs 12). Un avantage majeur est la conservation du caractère agoniste suite à l'ajout de la TMSAla et de l'internalisation cellulaire et donc de la possibilité d'employer par la suite des émetteurs Auger ou alpha avec les analogues comportant cet AA non naturel. Le [^{68}Ga]Ga-JMV6659 a une très bonne captation tumorale à 2h (7,8 ± 0,54 %ID/g), meilleure que celle de l'analogue peptidique radiomarqué au ^{68}Ga le plus prometteur décrit à ce jour, le [^{68}Ga]Ga-[8][81] et du même ordre que celle du [^{68}Ga]Ga-NT20.3[82] (dont l'absence d'effets indésirables chez l'homme a par ailleurs pu être constatée[83]). Sa captation tumorale est également du même ordre que celle du [^{177}Lu]Lu-3BP-227[84], récemment employé chez l'homme[79]. Un autre avantage majeur du [^{68}Ga]Ga-JMV6659 et sa biodistribution rapide (captation tumorale dès 5 min, avec un maximum atteint à 40 min et retrouvé dans le tissu tumoral jusqu'à 2h post-injection), minimisant l'irradiation des tissus autre que le tissu tumoral cible, contrairement à l'[^{111}In]In-3BP227 qui présente une cinétique de captation tumorale plus lente, avec une captation tumorale décrite à partir de 3h et un maximum atteint 6h après injection[78].

Le composé le plus prometteur parmi ceux étudiés ici est donc le [^{68}Ga]Ga-JMV6659, c'est pourquoi la suite de nos travaux se sont concentrés sur cet analogue. Ainsi, nous l'avons dans un second temps radiomarqué à l'^{111}In (substitut au ^{177}Lu, car peu disponible pour notre équipe aujourd'hui), qui a une demi vie plus longue que le ^{68}Ga, afin d'apprécier la pharmacocinétique tardive dans un but d'utilisation future en thérapie. Au cours de ces travaux nous démontrons in vitro que l'[^{111}In]In-JMV6659, conserve les mêmes propriétés radiopharmaceutiques in vitro que le [^{68}Ga]Ga-JMV6659 mais à des temps plus tardifs. Ceci suggère que, dans ce cas précis, le radioélément utilisé ne semble pas modifier profondément les caractéristiques pharmacocinétiques/pharmacodynamiques du radiopharmaceutique. La captation sanguine du JMV6659 radiomarqué justifiera une attention particulière sur les paramètres de laboratoire lorsqu'un usage thérapeutique chez l'Homme sera envisagé. L'imagerie µSPECT/CT a été réalisée, les données sont en cours d'analyse. Ces travaux feront l'objet d'un article prochainement.

Bien que la demi-vie plasmatique courte corresponde bien à la cinétique de distribution du JMV6659 radiomarqué, d'autres stratégies de modulation des sites potentiels de clivage doivent être envisagées pour augmenter la captation tumorale. Parmi ces pistes de travail, un axe de recherche est la modulation du site de clivage supplémentaire introduit par l'utilisation d'un linker et d'un chélate pour le radiomarquage. En effet, il a été montré avec un analogue de la bombésine, qu'un site important de clivage est localisé entre le macrocycle DOTA et le linker APAc[85] introduit dans la séquence du JMV6659. Ainsi, une nouvelle série d'analogue de la neurotensine a été synthétisée, toujours avec le squelette du JMV6659, mais d'autres linker ont été introduits. Des variations de longueurs et de charges ont notamment été testées. Enfin, une autre piste de modulation chimique, est d'explorer l'impact de la réduction de la liaison peptidique entre les deux lysines. Cette modification est connue pour stabiliser encore plus la séquence NT[8-13][67] mais son impact sur un radiopharmaceutique comprenant en plus un linker, un chélate et un radioélément n'a jamais été démontré. Au total, 4 composés ont donc été synthétisés et évalués parmi cette nouvelle génération. Les premiers enseignements déduits de ces modifications chimiques sont que le linker APAc introduit effectivement un site important de clivage. En effet son remplacement par un autre linker de type $(\beta ala)_2$, stabilise grandement la molécule sans impacter l'affinité et la sélectivité. Par contre l'introduction de la liaison Lys-Lys réduite stabilise également la molécule mais cette insertion est mal tolérée en présence du linker APAc, en termes d'affinité. Cependant, lorsqu'un linker de type $(\beta ala)_2$ est introduit, la molécule résultante est fortement stabilisée. Un des écueils connus de cette liaison Lys-Lys réduite est un impact sur la sélectivité NTS_1/NTS_2, élément qui est mieux toléré dans cette série. Une des explications pourrait être que l'ensemble linker-DOTA-^{68}Ga pourrait jouer un rôle dans l'affinité/sélectivité, et ainsi contre-balancer l'impact de la liaison Lys-Lys réduite. Une autre caractéristique commune à cette deuxième génération est un efflux cellulaire bien plus important que le composé initial [^{68}Ga]Ga-JMV6659. Les mécanismes moléculaires sous-jacents sont aujourd'hui mal connus, mais la structure et la charge du radiopharmaceutique semble jouer un rôle dans le processus d'efflux sur notre lignée cellulaire. Ainsi, dans cette nouvelle génération, des composés stables, affins et sélectifs ont été synthétisés. L'efflux cellulaire se trouve par contre grandement augmenté. Une étude micro-TEP du meilleur analogue dans cette série est prévue, la comparaison avec le composé [^{68}Ga]Ga-JMV6659 sera intéressante pour obtenir des données générales guidant le design de radiopharmaceutiques ciblant NTS_1.

Ces résultats et perspectives contribuent à l'approfondissement du développement de nouveaux radiopharmaceutiques ciblant les récepteurs de neuropeptides surexprimés par

certains cancers. Ceci encourage la poursuite d'une approche théranostique, dont les patients pourraient bénéficier dans un futur proche. En effet, il s'est avéré très intéressant de modifier les analogues peptidiques de la NT à l'aide d'acides aminés non naturels. Toutefois, d'autres approches pour maximiser la délivrance d'énergie à l'ADN cellulaire en RIV sont possibles, telle que l'internalisation nucléaire de l'atome radioactif. Nous avons donc exploré la faisabilité de cette approche dans la partie IV de ce travail de Thèse.

Chapitre 4 : Article 1

Silicon-Containing Neurotensin Analogues as Radiopharmaceuticals for NTS1-Positive Tumors Imaging

Bioconjugate Chemistry

pubs.acs.org/bc

Article

Silicon-Containing Neurotensin Analogues as Radiopharmaceuticals for NTS_1-Positive Tumors Imaging

Roberto Fanelli, Adrien Chastel, Santo Previti, Elif Hindié, Delphine Vimont, Paolo Zanotti-Fregonara, Philippe Fernandez, Philippe Garrigue, Frédéric Lamare, Romain Schollhammer, Laure Balasse, Benjamin Guillet, Emmanuelle Rémond, Clément Morgat,*,∇ and Florine Cavelier*,∇

Cite This: https://dx.doi.org/10.1021/acs.bioconjchem.0c00419

Read Online

ACCESS | Metrics & More | Article Recommendations | Supporting Information

ABSTRACT: Several independent studies have demonstrated the overexpression of NTS_1 in various malignancies, which make this receptor of interest for imaging and therapy. To date, radiolabeled neurotensin analogues suffer from low plasmatic stability and thus insufficient availability for high uptake in tumors. We report the development of ^{68}Ga-radiolabeled neurotensin analogues with improved radiopharmaceutical properties through the introduction of the silicon-containing amino acid trimethylsilylalanine (TMSAla). Among the series of novel radiolabeled neurotensin analogues, [^{68}Ga]**Ga**-JMV6659 exhibits high hydrophilicity (log $D_{7.4}$ = −3.41 ± 0.14), affinity in the low nanomolar range toward NTS_1 (K_d = 6.29 ± 1.37 nM), good selectivity (K_d NTS_1/K_d NTS_2 = 35.9), and high NTS_1-mediated internalization. It has lower efflux and prolonged plasmatic half-life in human plasma as compared to the reference compound ([^{68}Ga]Ga-JMV6661 bearing the minimum active fragment of neurotensin and the same linker and chelate as other analogues). In nude mice bearing HT-29 xenograft, [^{68}Ga]Ga-JMV6659 uptake reached 7.8 ± 0.54 %ID/g 2 h post injection. Uptake was decreased to 1.38 ± 0.71 %ID/g with injection of excess of non-radioactive neurotensin. Radiation dose as extrapolated to human was estimated as 2.35 ± 0.6 mSv for a standard injected activity of 100MBq. [^{68}Ga]Ga-JMV6659 was identified as a promising lead compound suitable for PET imaging of NTS_1-expressing tumors.

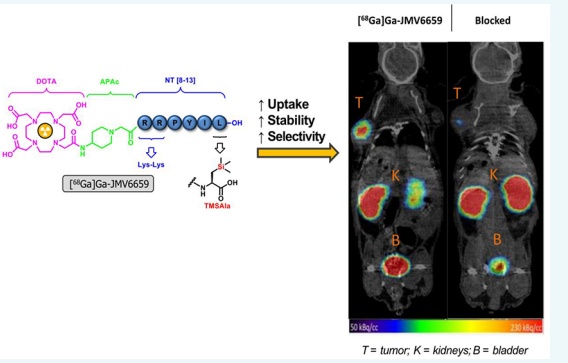

INTRODUCTION

Neurotensin (NT) is an endogenous 13-amino acid peptide distributed in the central nervous system (CNS) and in peripheral tissues.[1] NT shows a wide range of biological activities: in the brain, it is involved in the dopaminergic system modulation, hypothermia, and analgesia, while in periphery it modulates digestive and cardiovascular functions and proinflammatory responses.[2,3] NT effects occur via the activation of the neurotensin receptors NTS_1 and NTS_2, which belong to the GPCR family, and NTS_3, a receptor with a single transmembrane domain.[4] The natural ligand NT has high affinity and specificity to these receptors, and it has been demonstrated that the shortest active sequence is the fragment NT[8−13] (Figure 1).[5] Several independent studies demonstrated the overexpression of NTS_1 in a panel of tumors, such as pancreatic adenocarcinoma, non-small cell lung cancer, invasive ductal breast carcinoma, and prostate cancer, among others.[6−9] Interestingly, the NT/NTS_1 system is today highlighted as a pro-oncogenic factor in many tumors.[10−12] Consequently, NT represents a peptide of choice to develop tumors targeting vectors for the elaboration of diagnostic and therapeutic agents. However, the high sensitivity of NT to peptidases, which should be countered while preserving the fast pharmacokinetics and high tumor uptake necessary for imaging procedures, makes the design of peptide analogues challenging. Neurotensin stabilization techniques account for reduction or *N*-methylation of amide bonds in [^{68}Ga]Ga-DOTA-NT20.3,[13] amino acids substitutions in [^{68}Ga]Ga-(8),[14] or replacement of amide bonds with enzymatically stable 1,2,3 triazoles in [^{177}Lu]Lu-NT-VI or IX.[15] Despite excellent in vitro behaviors of the stabilized peptide compounds, novel artifices are required to also improve tumor uptake.[16] Some authors used a radically different strategy based on the compound SR142948A (Figure 1), which bears an adamantane moiety and is known as a potent NTS_1 antagonist, to lead to 3BP-227, that was elongated with a DOTA chelator for radiolabeling with ^{177}Lu.[17] As a nonpeptide compound, it is intrinsically resistant to proteases but exhibits much slower pharmacokinetics not suitable for PET imaging with short-lived positron-emitters like ^{68}Ga.

Received: July 24, 2020
Revised: August 29, 2020
Published: September 4, 2020

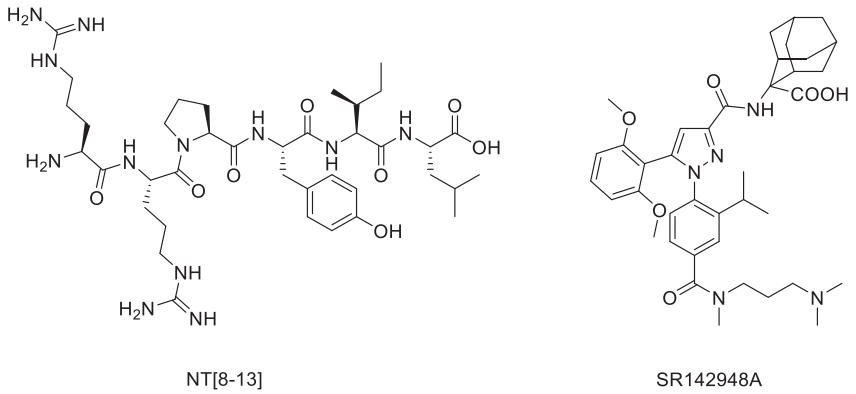

Figure 1. NT[8−13] and SR142948A chemical structures.

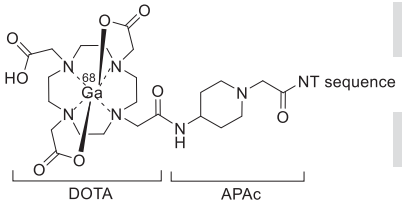

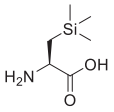

[^{68}Ga]Ga-JMV6658

NT sequence = -Lys^{8}-Lys^{9}-Pro^{10}-Tyr^{11}-TMSAla^{12}-Leu^{13}-OH (JMV2006)

[^{68}Ga]Ga-JMV6659

NT sequence = -Lys^{8}-Lys^{9}-Pro^{10}-Tyr^{11}-Ile^{12}-TMSAla^{13}-OH (JMV2007)

[^{68}Ga]Ga-JMV6660

NT sequence = -Lys^{8}-Lys^{9}-Pro^{10}-Tyr^{11}-Ile^{12}-Leu^{13}-OH (JMV438)

[^{68}Ga]Ga-JMV6661

NT sequence = -Arg^{8}-Arg^{9}-Pro^{10}-Tyr^{11}-Ile^{12}-Leu^{13}-OH (NT[8-13])

Figure 2. Chemical structure of NT conjugates and the unnatural amino acid L-TMSAla used in this study.

In this work, our strategy has been to base our efforts on peptide neurotensin analogues, which retain high affinity and selectivity to NTS_1, high tumor uptake, and exhibit fast kinetics suitable for clinical procedures.

Engineered peptides often feature improved biological properties.[18] For example, introduction of unnatural amino acids brings resistance to proteolysis, while allowing the modulation of physicochemical properties thanks to the wide variety of side chains.[19,20] Silicon/carbon switch is reported in drug design to provide lipophilicity when carbon atom is replaced with silicon: only with this difference are log *D* values slightly higher in silicon-containing derivatives.[21−24] Incorporation of silicon-containing amino acids in bioactive peptides,[25−30] as we already reported for NT[8−13], increases both binding affinity and resistance toward enzyme degradation.[31,32]

Herein, we describe the synthesis of bioconjugates based on stabilized NT[8−13] analogues radiolabeled with ^{68}Ga using a DOTA macrocycle complex chelator. The full characterization of this series allowed us to select a lead compound as a promising radiopharmaceutical for NTS_1-positive tumors imaging.

RESULTS

Chemical Synthesis of NT-Conjugates. All NT analogues prepared in this study were linked to DOTA as radionuclide chelator through the amino piperidin-1-yl-acetic acid ((4)-APAc) attached to the N-terminal amine of the peptide fragment (Figure 2).

The linker APAC and the protected chelator DOTA(tBu)$_3$−OH were consecutively coupled to the peptide. The reference compound JMV6661 was built with NT[8−13]. JMV6660 is correlated to hexapeptide JMV438 (H-Lys-Lys-Pro-Tyr-Ile-Leu-OH)[32] (Figure 2), in which the two Arg residues in positions 8 and 9 have been replaced by Lys. As known, this double substitution is well tolerated in terms of binding[33,34] and facilitates the synthesis. JMV6658 and JMV6659 contain both of these two Lys residues and also include the unnatural amino acid (L)-trimethylsilylalanine (TMSAla, Figure 2) in positions 12 and 13, respectively. Fmoc-TMSAla-OH was prepared on a large scale in very good overall yield (58%, five steps) with 98% enantiomeric excess, with use of hydroxypinan-3-one as the chiral inductor as previously reported.[35]

To prepare the conjugates, two different strategies were considered depending on the sequence: (i) automatic solid-phase peptide synthesis (SPPS) was adopted for basic sequences, while (ii) manual SPPS was preferred when using the noncommercially available amino acid TMSAla. When TMSAla was located at the C-terminal position, solution-phase synthesis was initially performed, because the anchorage of Fmoc-TMSAla-OH on Wang resin failed. However, despite the steric hindrance, Fmoc-TMSAla-OH was successfully attached to 2-chlorotrityl resin, with a good loading (0.8 mmol/g) using only 1 equiv of Fmoc-TMSAla-OH to perform JMV6659 synthesis efficiently. When using this solid support, this strategy led to higher yields and purity as expected (>80% and >95%, respectively). For JMV6658, the manual strategy starting from commecially available Leu-preloaded Wang resin allowed us to monitor and stir the coupling reaction up to the completion of it. All four peptides were obtained in satisfactory yields and further purified on preparative HPLC (Table S1).

https://dx.doi.org/10.1021/acs.bioconjchem.0c00419
Bioconjugate Chem. XXXX, XXX, XXX−XXX

^{68}Ga-Radiolabeling and In Vitro Studies. All compounds were radiolabeled with ^{68}Ga with 60% yield, high radiochemical purity (>95% after purification), high volumic activity of 100 MBq/mL, and high apparent molar activity of 12.5 ± 1.3 GBq/μmol. Representative radio-HPLC and radio-TLC chromatograms are available in Figures S1 and S2. Radiochemical purity was stable (≥95%) in PBS (Figure S3), and no ^{68}Ga-transchelation was seen in human plasma up to 45 min (Figure S4). On RP-HPLC, relative retention times (normalized from the front solvent) were 3.17 ± 0.14 for [^{68}Ga]Ga-JMV6658, 3.07 ± 0.21 for [^{68}Ga]Ga-JMV6659, 2.99 ± 0.01 for [^{68}Ga]Ga-JMV6660, and 3.01 ± 0.09 for [^{68}Ga]Ga-JMV6661. We also looked at hydrophilicity of the ^{68}Ga-compounds using the PBS-octanol partition method. All radiolabeled analogues were highly hydrophilic with subtle differences. As expected, [^{68}Ga]Ga-JMV6658 and [^{68}Ga]Ga-JMV6659, which bear silicon-containing amino acids, exhibit statistically significantly higher lipophilicity $p < 0.05$ (Table 2) that leads to slightly higher retention times on RP-HPLC.

NTS_1 and NTS_2 Expression on HT-29 Cells. Western blot performed on HT-29 lysates showed a single band of 55 kDa at the expected molecular weight of NTS_1 and a band at 45 kDa corresponding to the molecular weight of NTS_2 (Figure 3A). NTS_1 and NTS_2 expressions were further confirmed by immunofluorescence. NTS_1 labeling was granular mainly located in the cytoplasm with localized reinforcements at the plasma membrane. NTS_2 labeling showed preferential staining at the plasma membrane (Figure 3B and C).

Binding Affinity of Non-labeled and ^{68}Ga-Labeled Conjugates. The ability of our series of four non-metalated conjugates to inhibit the binding of [^{125}I]I-Tyr^3-NT (K_d = 0.22 nM) on human recombinant CHO cells transfected with human NTS_1 showed that the conjugate JMV6659 is the most potent compound to NTS_1 receptor in this series with IC_{50} = 34.5 ± 1.4 nM. Other conjugates do not retain significant NTS_1 affinity (Table 1). K_d values were next determined for the ^{68}Ga-labeled conjugates. Similarly, [^{68}Ga]Ga-JMV6659 displayed the highest NTS_1 affinity among the four analogues investigated, with a K_d value of 6.29 ± 1.37 nM toward the NTS_1 (Table 1).

Cellular Studies. Specific internalization and efflux of this series of ^{68}Ga-neurotensin analogues was investigated in HT-29 cells. All analogues were highly internalized (>60%, which corresponds to 0.5−1% of applied dose) with the exception made of [^{68}Ga]Ga-JMV6658 (Figure 4A). As additional experiments, we also investigated potential NTS_2-mediated internalization or membrane binding of [^{68}Ga]Ga-JMV6659 due to the NTS_2 affinity around 0.2 μM. We observed a transient and weak NTS_2-mediated internalization of 9.0 ± 3.8% and 10.5 ± 0.7% at 10 and 30 min, respectively. At 60 min, NTS_2-mediated internalization decreased below 5%. NTS_2-membrane binding of [^{68}Ga]Ga-JMV6659 was <5% at any time points (Table 4). After being internalized, efflux of the radiopeptides was also studied. [^{68}Ga]Ga-JMV6660 and [^{68}Ga]Ga-JMV6661 demonstrated high efflux (>60%) at 45 min, while [^{68}Ga]Ga-JMV6659 exhibited significantly lower efflux than the reference compound at all time points ($p < 0.05$) (Figure 4B).

Blood Plasma Stability. The ^{68}Ga-neurotensin analogues were investigated in human plasma to determine their blood plasma stability. Interestingly, [^{68}Ga]Ga-JMV6658 and [^{68}Ga]Ga-JMV6659, which bear the TMSAla amino acid, retain significantly higher stability than the reference compound [^{68}Ga]Ga-JMV6661 at 15 min. At 30 min, only [^{68}Ga]Ga-JMV6659 showed increased stability as compared to the reference compound. At 45 min, all radiolabeled neurotensin analogues were metabolized (Figure 4C). No significant differences were seen between the [^{68}Ga]Ga-JMV6660 and the reference compound ($p > 0.05$) at any time. After curve fitting, the 95% confidence interval (95%CI) of the [^{68}Ga]Ga-JMV6659 half-life was [7.17−24.63] min as compared to the [3.71−4.02] min 95%CI of the reference compound [^{68}Ga]Ga-JMV6661 (Table 2).

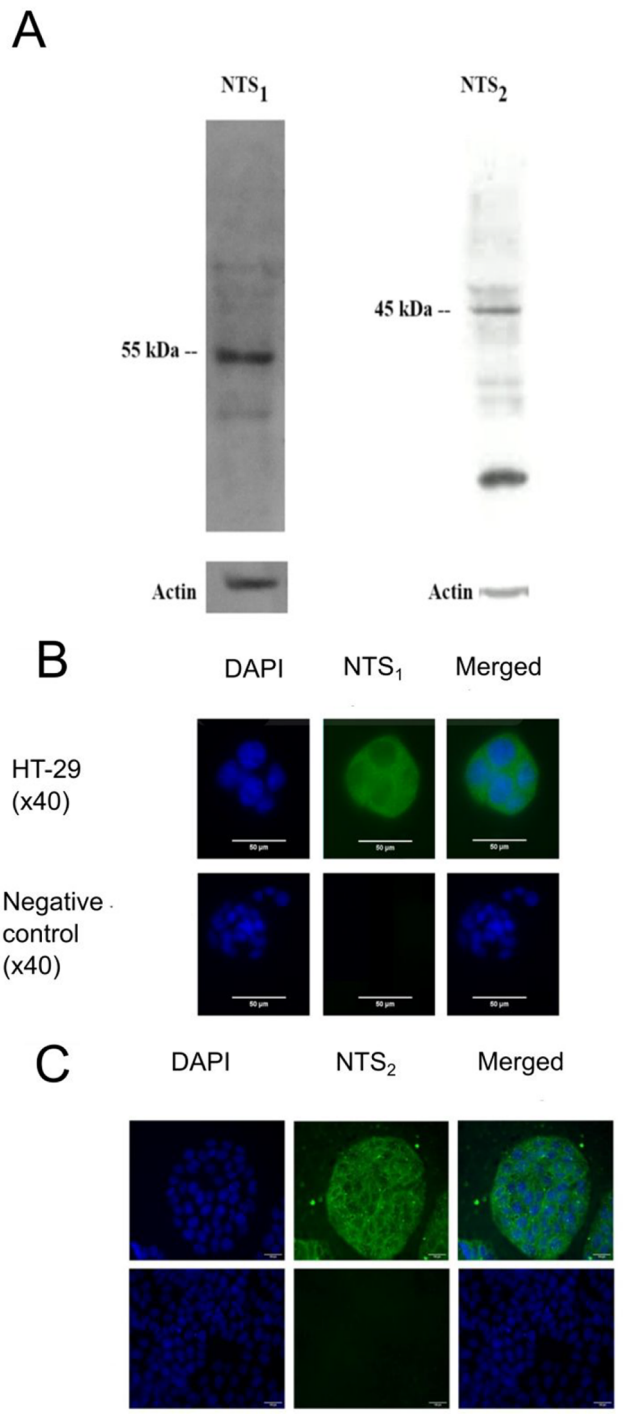

Figure 3. (A) Representative Western blots of NTS_1 and NTS_2 in HT-29 cells. Immunofluorescence of NTS_1 (B) and NTS_2 (C) in HT-29 cells. Negative controls correspond to HT-29 cells without the primary antibody. Images were obtained at 40× magnification.

https://dx.doi.org/10.1021/acs.bioconjchem.0c00419
Bioconjugate Chem. XXXX, XXX, XXX−XXX

Table 1. Binding Affinity of Non-metalated and ^{68}Ga-Labeled Analogues

Analogues	Affinity toward NTS_1 (nM)	selectivity NTS_1/NTS_2[a]
JMV6658	4877 ± 1173 (IC_{50})	nd
[^{68}Ga]Ga-JMV6658	>1000 (K_D)	na
JMV6659	34.5 ± 1.4 (IC_{50})	nd
[^{68}Ga]Ga-JMV6659	6.29 ± 1.37 (K_D)	35.9
JMV6660	1919 ± 1253 (IC_{50})	nd
[^{68}Ga]Ga-JMV6660	246.5 ± 75.39 (K_D)	0.2
JMV6661	540.5 ± 129 (IC_{50})	nd
[^{68}Ga]Ga-JMV6661	83.26 ± 22.49 (K_D)	>12

[a]nd, not determined; na, not applicable.

Preclinical PET/CT Imaging, Biodistribution, and Dosimetry Analysis. For animal studies, [^{68}Ga]Ga-JMV6659 was used at a volumic activity greater than 700 MBq/mL, RCP > 97% and formulated in 30% EtOH (50 μL, ~0.71 μg injected). After injection of [^{68}Ga]Ga-JMV6659 in nude mice bearing HT-29 tumor, whole-body dynamic μPET/CT imaging clearly showed an early uptake in HT-29 tumor of 2.82 ± 1.58 %ID/g at 3 min (Figure 5D and Table S2). Maximum uptake of 4.35 ± 2.15 %ID/g was reached 40 min after injection and remained roughly constant over time (at 2 h, uptake was 3.67 ± 1.90 %ID/g). Elimination of the radiotracer was urinary-exclusive (Figure 5A−C). On biodistribution experiments, a high uptake of 7.8 ± 0.54 %ID/g at 2 h in tumor was also seen, Figure 5C and Table S2. Analysis of PET images and ex vivo biodistribution showed strong significant positive correlation (Spearman coefficient r = 0.883, p = 0.008).

Specificity of [^{68}Ga]Ga-JMV6659 was demonstrated by preinjection of an excess of 180 μg of neurotensin, which resulted in significantly lower uptake in tumor both in PET images (p < 0.01) and in ex vivo biodistribution as compared to the unblocked experiment (Table S2). Interestingly, blood, kidneys, and spleen showed also NTS_1-mediated uptake in biodistribution experiments (8.18 ± 1.00, 19.63 ± 1.57, 7.83 ± 4.39 %ID/g for the unblocked group vs 0.09 ± 0.02, 4.39 ± 7.60, 0.33 ± 0.12 %ID/g after blocking with 180 μg of neurotensin, respectively; Table S2). In PET images, a similar pattern of NTS_1-uptake was seen on kidneys at 2 h after injection (Table S2 and Figure 5D). Spleen exhibited also a high uptake in PET images, to reach 7.89 ± 3.39 %ID/g at 40 min postinjection. However, the NTS_1-mediated process was less evident in PET images possibly due to the manual delineation of the CT images. To investigate more precisely the receptor-mediated uptake on spleen and blood, another group of mice was preinjected with a small dose of 50 μg of neurotensin to produce a dose−response effect. Again, in this group, lower uptake on spleen and blood was shown (Table S2). Clearance of [^{68}Ga]Ga-JMV6659 from other organs was fast (Figure 5D). Only colon and intestines showed a different kinetics with an increasing signal starting at 1 h post-injection. It was not possible to derive TACs for blood because the aorta volume is too small to provide reliable data.

Organ-absorbed doses were estimated by using OLINDA software to extrapolate to the adult phantom the mouse distribution data of [^{68}Ga]Ga-JMV6659. Table 3 summarizes the organ-absorbed doses. Among normal organs, kidneys had the highest absorbed dose (0.121 ± 0.135 mSv/MBq). The effective dose was estimated at 0.0235 ± 0.006 mSv/MBq.

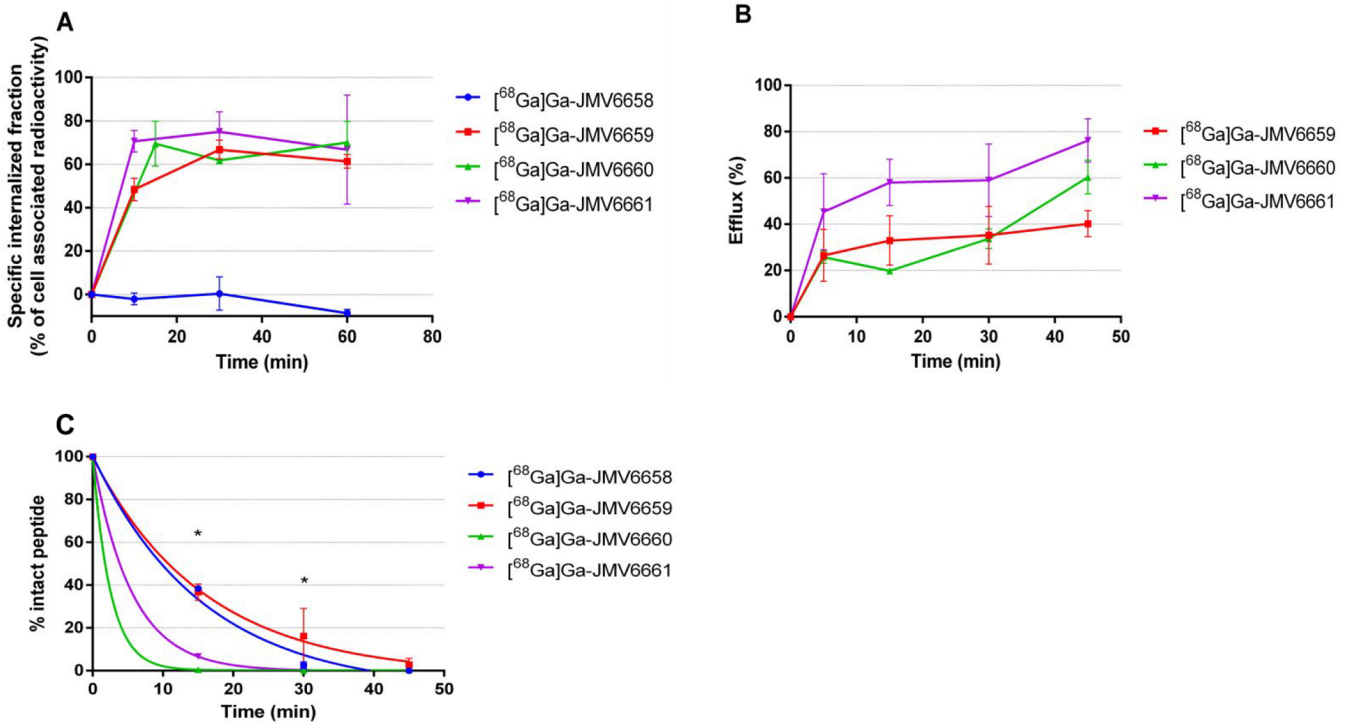

Figure 4. Internalization (A), efflux (B), and blood plasma stability (C) of the series of radiolabeled neurotensin analogues investigated in this work. The "*" indicates a significant difference (p < 0.05). At 15 min, [^{68}Ga]Ga-JMV6658 and [^{68}Ga]Ga-JMV6659 exhibit significantly higher blood plasma stability than [^{68}Ga]Ga-JMV6661. At 30 min, only [^{68}Ga]Ga-JMV6659 showed increased stability as compared to the reference compound [^{68}Ga]Ga-JMV6661. For better clarity, statistical analysis of internalization and efflux is not figured out.

https://dx.doi.org/10.1021/acs.bioconjchem.0c00419
Bioconjugate Chem. XXXX, XXX, XXX−XXX

Table 2. Summary of In Vitro Radiopharmaceutical Properties of a Series of Novel Neurotensin Conjugates

Analogues	Log D	95%CI of blood plasma half-life (min)	NTS_1-internalized fraction (%, 1 h)	NTS_1-membrane-bound fraction (%, 1 h)	efflux (% of internalized, 45 min)[a]
[^{68}Ga]Ga-JMV6658	−3.21 ± 0.43	[7.36−21.61]	<5	<5	nr
[^{68}Ga]Ga-JMV6659	−3.41 ± 0.14	[7.17−24.63]	61.3 ± 2.4	12.5 ± 7.3	39.4 ± 5.7
[^{68}Ga]Ga-JMV6660	−3.66 ± 0.06	[1.21−3.28]	70.1 ± 9.7	24.7 ± 9.4	60.4 ± 7.3
[^{68}Ga]Ga-JMV6661	−3.77 ± 0.38	[3.71−4.02]	66.8 ± 25.1	16.7 ± 4.8	76.2 ± 9.3

[a]nr = not reported.

DISCUSSION

Targeting the NTS_1 receptor holds promise in nuclear oncology as this receptor is expressed in many tumors[36] and therefore offers the possibility of targeting these tumors with radiolabeled NT analogs for imaging or therapy.[37] Several groups have been very active at producing radiolabeled neurotensin analogues with better stability, but current analogues still leave room for improvement in term of pharmacokinetics[17] or tumor uptake.[13,14] In this work, we present a novel series of peptidic neurotensin analogues. All conjugates bear the APAc linker given its ability to protonate being described as an advantage for improving affinity due to its positive charge.[38,39] The JMV6660 conjugate was constructed with two lysine residues instead of arginine, given that this substitution was demonstrated to be well-tolerated in terms of binding and biological activities of the NT analogues,[40] although in our conditions the plasmatic stability was not significantly improved by the use of lysine substitution alone. Additionally, *Nε*-Boc-*Nα*-Fmoc-Lys-OH is easier to handle as compared to the corresponding Arg analogue, which carries Pdf or Pmc as the *Nε*-protecting group. Finally, conjugates JMV6658 and JMV6659 were synthesized by replacing hydrophobic natural amino acids with the highly hydrophobic TMSAla at C-terminal position, which has already been proven by our research group to lead to improved NTS_1 affinity.[32,41] Lipophilicity at the C-terminal end of the NT[8−13] is required for high affinity binding to the NTS_1 pocket. Considering the high lipophilicity of TMSA-Ala, we replaced the two positions, 12 and 13, respectively, of the lipophilic tail of the NT sequence. The replacement of Leu in position 13 resulted in improved affinity.[32]

After validation steps confirming NTS_1 and NTS_2 expression in HT-29 cells (Figure 3), cellular experiments were carried out. Thus, we determined the affinity and selectivity of unlabeled bioconjugates and radiolabeled counterparts regarding NTS_1 (Table 1). Results from competition experiments indicate that the unlabeled bioconjugates suffer from a dramatic loss in affinity as compared to their respective binding sequences[32] due to the introduction of the APAc linker and the DOTA macrocycle. Nevertheless, ^{68}Ga-bioconjugates showed an apparent improvement in affinity by a factor ∼5 as compared to their unlabeled counterparts. However, differences in the testing systems used make direct comparisons hazardous. Overall, [^{68}Ga]Ga-JMV6659 exhibits affinity in the nanomolar range, similar to some radiolabeled neurotensin analogues, but importantly shows the best affinity and selectivity among ^{68}Ga-labeled monomeric neurotensin analogues.[42] The impact of other metallic isotopes (^{111}In, ^{177}Lu, or ^{161}Tb, for example) is currently being investigated.

We pursued our efforts to characterize our series by determining affinity to NTS_2 and thus selectivity to NTS_1. [^{68}Ga]Ga-JMV6659 exhibits also good selectivity to NTS_1 receptor. We here show that [^{68}Ga]Ga-JMV6659 has the highest reported selectivity to NTS_1 (Table 1). Selectivity is unfortunately rarely investigated during radiopharmaceutical characterization of neurotensin analogues. This point is crucial because little is known regarding physiological expression of NTS_2 in periphery[43,44] and unselective targeting may increase the background. NTS_1-mediated internalization of [^{68}Ga]Ga-JMV6659, [^{68}Ga]Ga-JMV6660, and reference [^{68}Ga]Ga-JMV6661 was up to 60−70% at 1 h (similar to other peptide analogues[13,14]), unlike [^{68}Ga]Ga-JMV6658, which did not internalize in HT-29 cells in line with its low NTS_1 affinity (Table 2 and Figure 4).

Good internalization is of major importance for future targeted radionuclide therapy applications with short-range particle emitters such as metallic emitters rich in Auger electrons (^{161}Tb, ^{58m}Co...) or *α*-emitters (^{225}Ac, ^{213}Bi, ^{227}Th...).[45−48] We also investigated the membrane-bound fraction of our ^{68}Ga-neurotensin analogues. None of the analogues remained bound to the membrane NTS_1 (and NTS_2 for [^{68}Ga]Ga-JMV6659) in high amount, which revealed that all analogues might behave like agonists (antagonists do not promote Ca^{2+} release and internalization and remain located at the cell membrane).[36] Efflux experiments were also carried out and indicated that [^{68}Ga]Ga-JMV6660 and [^{68}Ga]Ga-JMV6661 were more released from the cells (∼60−70%) as compared to [^{68}Ga]Ga-JMV6659 (∼40% efflux) (Table 2 and Figure 4).

Modification at position 13 seems to be critical to also modulate cellular efflux. We are working to decipher the molecular mechanisms involved in this cellular efflux. [^{68}Ga]Ga-JMV6659 was then injected in mice for in vivo imaging. As expected, uptake in HT-29 xenograft was high and increased over time to reach a maximum of 7.8 %ID/g at 2 h on biodistribution experiments. This value is substantially higher than the uptake found with peptide neurotensin analogues reported so far and in the same range as the nonpeptide antagonist [^{177}Lu]Lu-3BP-227 that has been recently used in patients.[14,17,49] For instance, [^{68}Ga]Ga-(8) uptake in nude mice bearing HT-29 tumor was reported to reach a maximum 10 min after injection (2.77 ± 0.47 %ID/g) and then decrease to 1.55 ± 0.35 %ID/g at 1 h.[14] Similarly, uptake of [^{68}Ga]Ga-DOTA-NT-20.3 was only detectable at 45 min postinjection,[13] while we herein noted very early uptake of [^{68}Ga]Ga-JMV6659, which begins at 3 min post injection on the *μ*PET/CT images, reaches its maximum at 40 min, and then remains constant.

The increase of [^{68}Ga]Ga-JMV6659 uptake over time in the tumor reflects the higher stability of this compound as compared to the reference compound. Although more stable peptide analogues have been reported in the literature,[42] the stability should fit with the kinetics of the distribution process. Therefore, a high stability would be required for probes with long retention in blood and thus slow distribution. Indeed, our lead compound does not show the highest stability reported, but this value is high enough given the early and high uptake of [^{68}Ga]Ga-JMV6659 in HT-29 tumor (Figure 5).

https://dx.doi.org/10.1021/acs.bioconjchem.0c00419
Bioconjugate Chem. XXXX, XXX, XXX−XXX

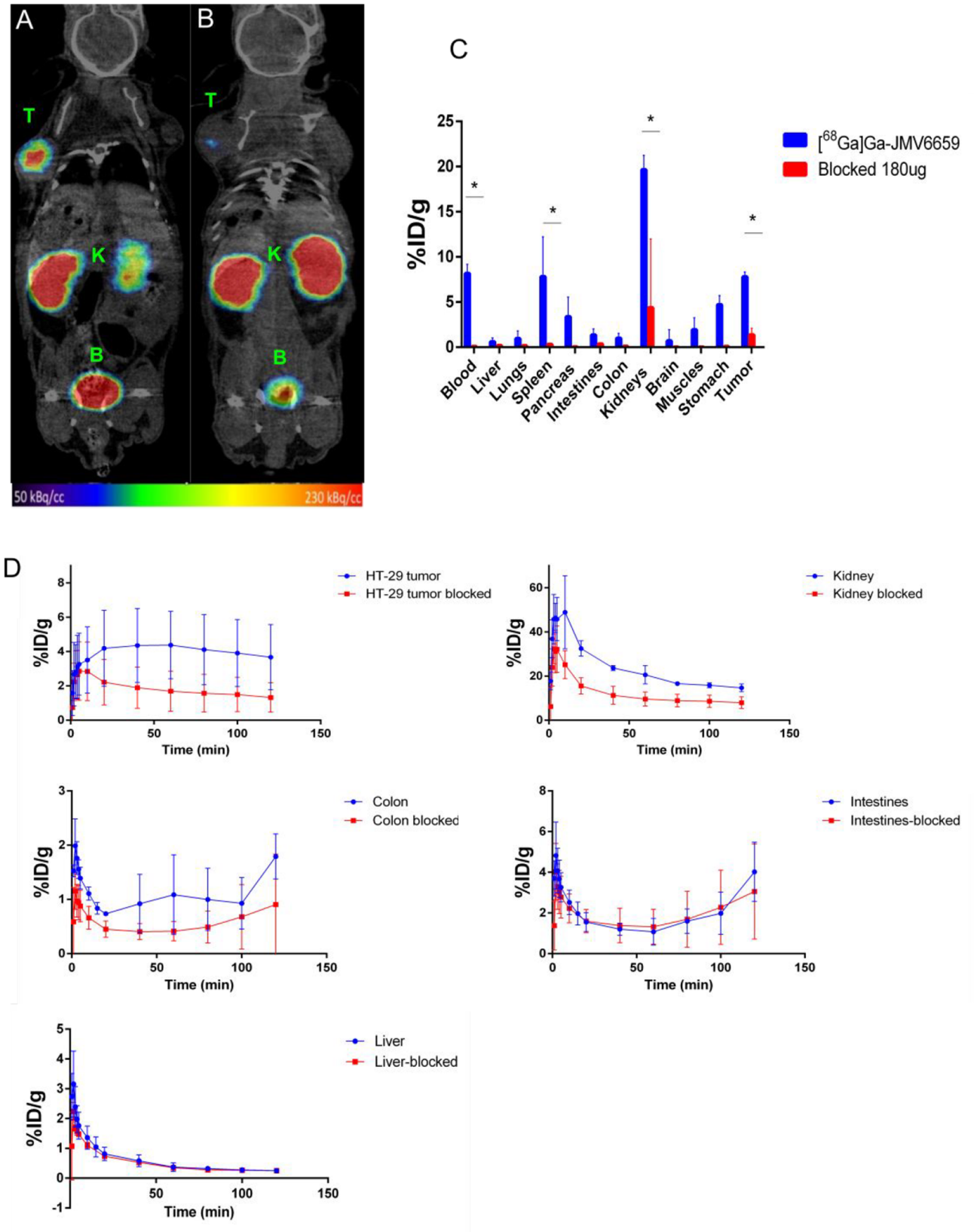

Figure 5. μPET/CT imaging, biodistribution, and image-derived time−activity curves of [^{68}Ga]Ga-JMV6659 in HT-29 tumor-bearing nude mice. (A) Fused coronal PET/CT image at 2 h postinjection of nude mice injected with [^{68}Ga]Ga-JMV6659 alone. (B) Fused coronal PET/CT image at 2 h post injection of nude mice injected with [^{68}Ga]Ga-JMV6659 and excess of neurotensin (180 μg) that demonstrates specificity of NTS_1 targeting. T indicates the HT-29 tumor, K stands for kidneys, and B means bladder. (C) Biodistribution after animal sacrifice 2 h after injection. A group of three mice received only [^{68}Ga]Ga-JMV6659 ([^{68}Ga]Ga-JMV6659 group), while the blocked group of three additional mice was preinjected with 180 μg of neurotensin. (D) PET image-derived time−activity curves (TACs) in HT-29 tumor, kidney, colon, intestines, and liver.

https://dx.doi.org/10.1021/acs.bioconjchem.0c00419
Bioconjugate Chem. XXXX, XXX, XXX−XXX

Table 3. Radiation Dose Estimates (mGy/MBq) of [^{68}Ga]Ga-JMV6659

Organs	mean	SD
adrenals	1.47×10^{-02}	9.07×10^{-04}
brain	3.54×10^{-03}	5.10×10^{-04}
breasts	1.15×10^{-02}	5.51×10^{-04}
gallbladder wall	1.43×10^{-02}	2.65×10^{-04}
lower large intestine wall	4.64×10^{-02}	1.05×10^{-02}
small intestine	1.47×10^{-02}	3.21×10^{-04}
stomach wall	5.60×10^{-02}	6.84×10^{-02}
upper large intestine wall	1.44×10^{-02}	3.00×10^{-04}
heart wall	1.35×10^{-02}	6.08×10^{-04}
kidneys	1.21×10^{-01}	1.35×10^{-01}
liver	6.08×10^{-03}	2.63×10^{-03}
lungs	9.44×10^{-03}	3.31×10^{-03}
muscle	1.27×10^{-02}	4.58×10^{-04}
ovaries	1.48×10^{-02}	4.36×10^{-04}
pancreas	7.79×10^{-03}	1.40×10^{-03}
red marrow	1.08×10^{-02}	3.06×10^{-04}
osteogenic cells	1.80×10^{-02}	7.64×10^{-04}
skin	1.12×10^{-02}	5.03×10^{-04}
spleen	2.29×10^{-02}	8.11×10^{-03}
testes	1.25×10^{-02}	6.11×10^{-04}
thymus	1.28×10^{-02}	6.00×10^{-04}
thyroid	1.27×10^{-02}	6.56×10^{-04}
urinary bladder wall	1.40×10^{-02}	5.69×10^{-04}
uterus	1.45×10^{-02}	5.29×10^{-04}
total body	1.35×10^{-02}	3.21×10^{-04}
effective dose (mSv/MBq)	2.35×10^{-02}	6.40×10^{-03}

Therefore, [^{68}Ga]Ga-JMV6659 displays fast pharmacokinetics common with other radiopeptides[42] as demonstrated by the distribution kinetics of the free fraction of [^{68}Ga]Ga-JMV6659 in NTS_1-positive organs (Figure 5). This contrasts with the slow uptake of [^{111}In]In-3BP227 in tumor cells, which is 6 h after injection.[17] A ^{18}F-labeled glycoconjugate of 3BP227 has been developed with much faster pharmacokinetics, but the uptake in HT-29 tumors was dramatically decreased to 0.74 % ID/g at 1 h.[50,51] In biodistribution experiments, we also noted significant dose−response NTS_1-mediated uptake in blood, kidneys, and spleen like in other previous studies.[17,42] In the study of Schulz et al., the high blood uptake of [^{111}In]In-3BP227 was 5-fold higher in mice bearing NTS_1-positive xenograft than in NTS_1-negative xenografted mice, which suggests a receptor-mediated process. To get more insight on this binding that can be limiting for future therapeutic trials, the plasma protein binding of [^{68}Ga]Ga-JMV6659 was studied ex vivo. Results showed that the radiopeptide effectively binds to plasma proteins in a nonspecific manner (21.0 ± 3.2%) (Table 4 and Table S3). This value illustrates well the ∼18% fraction of [^{68}Ga]Ga-JMV6659 not displaced in the in vivo 180 μg blocked-experiment (Figure 5) and is similar to previous works[52] but much lower than the In-, Lu-, and Y-labeled derivatives of the nonpeptide antagonist SR142948A, which showed ∼90% binding on human plasma protein.[53] Additionally, the literature reported that human blood cells (macrophages and neutrophils) express NTS_1 as well as circulating B cells[54−56] to support the specific uptake of [^{68}Ga]Ga-JMV6659 in blood and by extension the spleen. Using [^{111}In]In-JMV6659, we found that NTS_1 and NTS_2 are present on human neutrophils (but not on lymphocytes; data will be presented in a separate article), which explains the tumor-to-blood ratio of [^{68}Ga]Ga-JMV6659 ∼1 at 2 h, lower than other peptide probes developed to target NTS_1,[42] but very similar to that observed in some patients.[16] Investigation of later time points is scheduled with the ^{111}In-version of JMV6659. Overall, the blood uptake is a combination of two mechanisms that includes a specific binding to blood cells and a nonspecific binding to plasma proteins. One can argue that this value may hinder clinical translation of this radiopeptide for imaging, but uptake in blood may be easily separated from that of tumor lesions thanks to the associated anatomical imaging routinely performed with PET using computerized tomography or magnetic resonance imaging. However, the hematological toxicity of the ^{177}Lu-labeled version should be carefully studied for future therapeutic trials using high activities. In the first in-human study performed with [^{177}Lu]Lu-3BP227, which presents uptake in blood similar to that of [^{68}Ga]Ga-JMV6659, the hematoxicity profile looks reassuring after intravenous infusion of 5.5 GBq of the radiopharmaceutical.[49]

Table 4. Summary of Radiopharmaceutical Properties of Lead Compound [^{68}Ga]Ga-JMV6659

K_d (nM)	
NTS_1	NTS_2
6.29 ± 1.37	225.5 ± 34.0
Selectivity NTS_1/NTS_2	
35.9	
Plasmatic half-life (95%CI)	
[7.17 – 24.63] min	
LogD	
-3.41 ± 0.14	
Internalized fraction (%)	
NTS_1	NTS_2
61.3 ± 2.4	∼5
Membrane-bound fraction (%)	
NTS_1	NTS_2
12.5 ± 7.3	< 5
Efflux (%)	
39.4 ± 5.7	
Binding to plasma protein (%)	
21.04 ± 3.15	
Uptake in HT-29 tumor (%ID/g at 2h)	
7.8 ± 0.54	

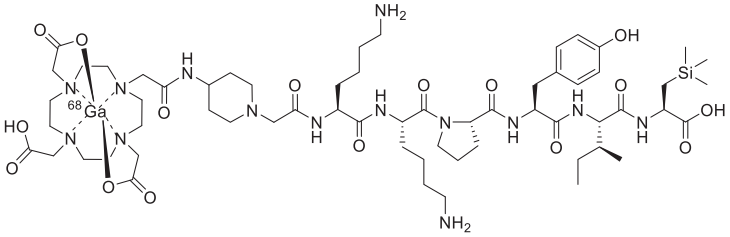

[^{68}Ga]Ga-JMV6659

https://dx.doi.org/10.1021/acs.bioconjchem.0c00419
Bioconjugate Chem. XXXX, XXX, XXX−XXX

Also, organs could be at risk when considering the high NTS_1-mediated uptake in mice kidneys of 19.66 ± 1.57 %ID/g, but, for comparison, therapeutic infusion [^{177}Lu]Lu-PSMA-617 does not require kidney protection, while this radiopharmaceutical exhibits a very high and PSMA-specific uptake of 137.2 ± 77.8 % ID/g in mice.[57] Given the high tumor uptake, [^{68}Ga]Ga-JMV6659 provides therefore a tumor-to-kidney ratio of 0.4 at 2 h, similar to or even better than other radiolabeled neurotensin peptides[13−15] but indeed lower than nonpeptide antagonists due to their hepatic clearance.[17,58] Consequently, the tumor-to-liver ratio, which was as high as 15.45 ± 6.80 at 2 h, follows the opposite pattern. The tumor-to-muscle ratio reaches 5.22 ± 2.84 at 2 h and reflects the low unspecific binding of the radiopharmaceutical. Finally, [^{68}Ga]Ga-JMV6659 was rapidly eliminated from other organs excepted from colon and intestines, which demonstrated a kind of redistribution process after 1 h (Figure 5). Currently, we could not explain this phenomenom, but this was already seen with other probes targeting NTS_1 ([^{68}Ga]Ga-6 showed a ∼50% increase of uptake in intestines between 30 and 60 min).[14] Finally, we performed a radiation dosimetry estimate. This is the first estimation of human absorbed dose from radiolabeled neurotensin analogue. For a proposed median activity of 100 MBq, the extrapolated radiation dose is 2.35 mSv, which is comparable to those of other ^{68}Ga-based agents used in clinics.[59,60]

CONCLUSION

We have reported a series of novel ^{68}Ga-radiolabeled neurotensin analogues, in which the Arg^8-Arg^9 sequence was replaced with Lys^8-Lys^9 and silicon-containing amino acid (L)-trimethylsilylalanine (TMSAla) was inserted in position 12 or 13. Interestingly, the conjugate [^{68}Ga]Ga-JMV6659 exhibited the highest binding affinity toward NTS_1 (K_d = 6.29 ± 1.37 nM), good selectivity over NTS_2 (K_d NTS_1/K_d NTS_2 = 35.9), and increased stability in human plasma with respect to the reference analogue [^{68}Ga]Ga-JMV6661 (>5-fold). High NTS_1-mediated internalization, moderate efflux in cells, and a very promising specific tumor uptake of 7.8 ± 0.54 %ID/g at 2 h in mice were also demonstrated with [^{68}Ga]Ga-JMV6659. The blood uptake of 8.18 ± 1.00 %ID/g deserves further investigations. At the light of these data, summarized in Table 4, [^{68}Ga]Ga-JMV6659 was identified, among this series, as the most promising radiopharmaceutical for NTS_1-targeted tumor imaging.

EXPERIMENTAL PROCEDURES

Radiochemistry. *^{68}Ga-Radiolabeling.* Radiolabeling was achieved using the FastLab automate cassette system (GE Healthcare). 1.1 mL of $^{68}GaCl_3$ (∼600 MBq) in HCl 0.1 M (Galli Eo, IRE-EliT, Belgium) was incubated, without further purification, with 50 μg (37−39 nmol) of each analogue in acetate buffer (0.1M, pH 4.6, final volume 2 mL) and heated using a microwave (GE MicroWave System 100; 100−240 vac; 50−60 Hz; 500 W; fuses 2xT6AH 250 V) at 90 °C for 5 min. The crude peptide was then purified by a Sep-Pak Light C_{18} cartridge (WAT023501) using 0.5 mL of ethanol and then formulated in PBS to obtain a final volume of 1.1 mL. Radiochemical purity was monitored with UV-radio HPLC and TLC analysis. A full description of the material used for quality control is available in the Supporting Information. Nondecay corrected apparent molar activities were determined by dividing the activity obtained at the end of synthesis by the amount of precursor used for radiolabeling.

Radiolabeling Stability in PBS and Human Plasma. At each time point, an aliquot (4 μL) was taken, and radiochemical purity was determined by TLC analysis. The study of the radiolabeled analogues was performed at different time points (0, 15, 30, and 45 min). Experiments were performed twice in triplicate for each radiolabeled neurotensin analogue.

Biological Evaluation. Cells were obtained from the University of Bordeaux, and no additional authentication was performed by the authors of this study. As validation steps, the HT-29 cells were checked regarding NTS_1 and NTS_2 expression (see Supporting Information). For all in vitro experiments, the volume of radiolabeled neurotensin analogues used was <1% of the total volume of each well.

Binding Affinity of Non-metalated Peptide Conjugates. Binding assays were performed using competition experiments as previously described.[17]

Stability of ^{68}Ga-Radiolabeled Neurotensin Analogues in Human Plasma. 37 MBq of each radiolabeled analogue (∼0.3 nmol in ∼20 μL) were incubated in 2 mL of human plasma. At various time points (0, 15, 30, and 45 min), an aliquot of 50 μL was taken, and proteins were precipitated using 100 μL of ethanol. After centrifugation at 13 000 rpm for 5 min, 50 uL of the supernatant was diluted in 150 μL of water and analyzed with radio-UV HPLC. Experiments were performed twice. 95%CI of plasmatic half-lives were calculated by monoexponential fitting using the GraphPad prism software (v6.01).

Hydrophilicity Studies. The hydrophilicity of each radiolabeled analogue was assessed by the PBS−octanol distribution coefficient method as previously described in triplicate for three independent experiments.[14]

Saturation Binding Assay of ^{68}Ga-NT-Conjugates. The affinity of the ^{68}Ga-labeled peptides was studied on HT-29 cells seeded at a density of 1 million cells per well in six-well plates (Corning, area of each well was 9.5 cm^2) and incubated overnight with complete medium. Well plates were first set on ice 30 min before the beginning of the experiment. ^{68}Ga-labeled radiopeptides were then added to the medium at concentrations of 0.1, 1, 10, 100, and 1000 nM, and cells were incubated (in triplicate) for 2 h at 4 °C. Incubation was stopped by removing medium and washing cells twice with ice-cold PBS. Finally, cells were treated with NaOH (1 M), and the radioactivity was measured in a gamma counter. To assess for nonspecific affinity, excess nonradioactive neurotensin (final concentration 1 μM) or levocabastine (a selective antagonist for NTS_2, final concentration 1 μM) was added to selected wells.

In Vitro Internalization and Efflux Studies. HT-29 cells were cultured as described in saturation binding experiments above. Internalization and efflux experiments were performed according to published procedures[14] with only minor modification (1 MBq, 8−15 pmol, of the respective ^{68}Ga-labeled radiopeptides was used, and NTS_2-mediated internalization and NTS_2-membrane-bound fraction of [^{68}Ga]Ga-JMV6659 were determined using 1 μM of levocabastine). To also verify the NTS_1 specificity, blocking experiments were performed for all radiopeptides by using 1 μM of neurotensin.

Small Animal PET Imaging and Biodistribution Study. Animal experiments were authorized by APAFiS #14191 on 2018/12/05 for 5 years after evaluation by the Ethics committee CE71. Animals were handled following national guidelines R.214-87 and R.214-126. HT-29 tumor-bearing mice (n = 3) were injected intravenously with 4.6 ± 0.6 MBq of [^{68}Ga]Ga-JMV6659 under 2% isoflurane anesthesia. PET dynamic images were acquired for 2 h (5 × 1 min, 3 × 5 min, 5 × 20 min) and

https://dx.doi.org/10.1021/acs.bioconjchem.0c00419
Bioconjugate Chem. XXXX, XXX, XXX−XXX

began 10 s before injection on a Nanoscan PET/CT camera (Mediso). For blocking experiments, three other mice were intravenously injected with an excess (180 μg) of neurotensin 25 min before [^{68}Ga]Ga-JMV6659 injection, and PET images were acquired for 2 h with the same dynamic acquisition protocol. A second group of three mice was blocked with a smaller dose of neurotensin (50 μg). For biodistribution studies, mice were sacrificed after PET imaging. The tumors and other tissues (lung, liver, kidneys, brain, spleen, muscle, stomach, intestines, pancreas, and colon), as well as blood, were removed and weighed. Radioactivity of the samples was measured using a γ-counter and expressed as %ID/g. Processing of reconstructed images was performed using PMOD software (version 3.5). For each mouse, the following organs, lungs, whole brain, spleen, stomach, liver, colon, tumor, kidney, and intestines, were manually delineated on CT images and subsequently applied to the dynamic PET image series. Data were expressed in %ID/g after normalization of standard PET value expressed in kBq/mL by the volume of the ROI, the injected activity, and the weight of the organ measured after sacrifice. The decay-corrected mean time−activity curves (TACs) were determined for each target organ.

Radiation Dose Estimates. Human radiation dosimetry estimates of [^{68}Ga]Ga-JMV6659 were calculated from mouse biodistribution data by using the MIRD methodology to calculate the internal organ radiation dose and extrapolate to humans. Briefly, the radiation dose to a given organ is

$$D_T = \sum_S A_S DF(T \leftarrow S)$$

A_S stands for the cumulative activity within an internal source organ expressed in unit of Bq s per Bq administrated, and $DF(T \leftarrow S)$ are the dose factors for source organ S irradiating the target organ T. The summation is performed on all source-to-target organ combinations and for every target organ in the body. The cumulative activity is obtained by integration of time−activity data for each organ (tumor, brain, lung, kidneys, stomach, spleen, liver, intestines, and pancreas), and the residence time was therefore derived for each mouse organ and then extrapolated to humans using the ratio in organ weights of mouse and human. The residence time of the rest of the body was calculated by subtracting the sum of organ residence times from the total residence time $\langle t_{1/2}|60|\ln(2)\rangle$. Extrapolated human residence times were used as input to the dosimetry software OLINDA/EXM. Absorbed doses to the organs were derived for the reference male phantom.

Statistical Analyses. All statistical analyses were performed with the GraphPad Prism software package. The unpaired student t test was used to determine statistical significance between two groups. For comparison between three or more groups, a two-way ANOVA with multiple comparison test correction was used. Differences at the 95% confidence level ($p < 0.05$) were considered significant.

■ ASSOCIATED CONTENT

Supporting Information

The Supporting Information is available free of charge at https://pubs.acs.org/doi/10.1021/acs.bioconjchem.0c00419.

Synthesis and control of peptides, characterization of NTS_1 and NTS_2 expressions in HT-29 cells, quality controls of ^{68}Ga-neurotensin analogues, stability of ^{68}Ga-radiolabeling in PBS and in human plasma, biodistribution assessed on PET images and after animal sacrifice, and plasma protein binding of [^{68}Ga]Ga-JMV6659 (PDF)

■ AUTHOR INFORMATION

Corresponding Authors

Clément Morgat − *University of Bordeaux, CNRS, EPHE, INCIA, UMR 5287, Bordeaux F-33000, France; Nuclear Medicine Department, University Hospital of Bordeaux, Bordeaux F-33000, France;* orcid.org/0000-0002-9432-9223; Email: clement.morgat@chu-bordeaux.fr

Florine Cavelier − *Institut des Biomolécules Max Mousseron, IBMM, UMR-5247, CNRS, Université de Montpellier, ENSCM, Montpellier 34095 Cedex 5, France;* orcid.org/0000-0001-5308-6416; Email: florine.cavelier@umontpellier.fr

Authors

Roberto Fanelli − *Institut des Biomolécules Max Mousseron, IBMM, UMR-5247, CNRS, Université de Montpellier, ENSCM, Montpellier 34095 Cedex 5, France*

Adrien Chastel − *University of Bordeaux, CNRS, EPHE, INCIA, UMR 5287, Bordeaux F-33000, France; Nuclear Medicine Department, University Hospital of Bordeaux, Bordeaux F-33000, France*

Santo Previti − *Institut des Biomolécules Max Mousseron, IBMM, UMR-5247, CNRS, Université de Montpellier, ENSCM, Montpellier 34095 Cedex 5, France*

Elif Hindié − *University of Bordeaux, CNRS, EPHE, INCIA, UMR 5287, Bordeaux F-33000, France; Nuclear Medicine Department, University Hospital of Bordeaux, Bordeaux F-33000, France*

Delphine Vimont − *University of Bordeaux, CNRS, EPHE, INCIA, UMR 5287, Bordeaux F-33000, France*

Paolo Zanotti-Fregonara − *Houston Methodist Research Institute, Houston, Texas 77030, United States*

Philippe Fernandez − *University of Bordeaux, CNRS, EPHE, INCIA, UMR 5287, Bordeaux F-33000, France; Nuclear Medicine Department, University Hospital of Bordeaux, Bordeaux F-33000, France*

Philippe Garrigue − *Aix-Marseille University, INSERM, Institut National de la Recherche Agronomique, Centre de Recherche en Cardiovasculaire et Nutrition, Marseille 13385, France; Aix-Marseille University, Centre Européen de Recherche en Imagerie Médicale, Marseille 13005, France*

Frédéric Lamare − *University of Bordeaux, CNRS, EPHE, INCIA, UMR 5287, Bordeaux F-33000, France; Nuclear Medicine Department, University Hospital of Bordeaux, Bordeaux F-33000, France*

Romain Schollhammer − *University of Bordeaux, CNRS, EPHE, INCIA, UMR 5287, Bordeaux F-33000, France; Nuclear Medicine Department, University Hospital of Bordeaux, Bordeaux F-33000, France*

Laure Balasse − *Aix-Marseille University, INSERM, Institut National de la Recherche Agronomique, Centre de Recherche en Cardiovasculaire et Nutrition, Marseille 13385, France*

Benjamin Guillet − *Aix-Marseille University, INSERM, Institut National de la Recherche Agronomique, Centre de Recherche en Cardiovasculaire et Nutrition, Marseille 13385, France; Aix-Marseille University, Centre Européen de Recherche en Imagerie Médicale, Marseille 13005, France*

Emmanuelle Rémond − *Institut des Biomolécules Max Mousseron, IBMM, UMR-5247, CNRS, Université de*

https://dx.doi.org/10.1021/acs.bioconjchem.0c00419
Bioconjugate Chem. XXXX, XXX, XXX−XXX

Montpellier, ENSCM, Montpellier 34095 Cedex 5, France;
orcid.org/0000-0002-3201-4365

Complete contact information is available at:
https://pubs.acs.org/10.1021/acs.bioconjchem.0c00419

Author Contributions

[▽]C.M. and F.C. contributed equally.

Notes

The authors declare no competing financial interest.

■ ACKNOWLEDGMENTS

This work was partly funded by France Life Imaging (grant ANR-11-INBS-0006) from the French program "Investissements d'Avenir" and by the Institut National du Cancer (INCa PLBIO 2017, THERACAN project). This work was achieved within the context of the Laboratory of Excellence TRAIL ANR-10-LABX-57.

■ REFERENCES

(1) Carraway, R., and Leeman, S. E. (1973) The Isolation of a New Hypotensive Peptide, Neurotensin, from Bovine Hypothalami. *J. Biol. Chem. 248*, 6854−6861.

(2) St−Gelais, F., Jomphe, C., and Trudeau, L. E. (2006) The Role of Neurotensin in Central Nervous System Pathophysiology: What Is the Evidence? *J. Psychiatry Neurosci. 31*, 229−245.

(3) Boules, M., Li, Z., Smith, K., Fredrickson, P., and Richelson, E. (2013) Diverse Roles of Neurotensin Agonists in the Central Nervous System. *Front. Endocrinol. 4* (1−16), 1 DOI: 10.3389/fendo.2013.00036.

(4) Sarret, P., and Cavelier, F. (2017) Neurotensin and Its Receptors. *Neurosci. Biobehav. Psychol.*, 1−17.

(5) Carraway, R., and Leeman, S. E. (1975) The Amino Acid Sequence of a Hypothalamic Peptide, Neurotensin. *J. Biol. Chem. 250*, 1907−1911.

(6) Korner, M., Waser, B., Strobel, O., Buchler, M., and Reubi, J. C. (2015) Neurotensin Receptors in Pancreatic Ductal Carcinomas. *EJNMMI Res. 5*, 17−23.

(7) Alifano, M., Souaze, F., Dupouy, S., Camilleri−Broet, S., Younes, M., Ahmed−Zaid, S. M., Takahashi, T., Cancellieri, A., Damiani, S., Boaron, M., et al. (2010) Neurotensin Receptor 1 Determines the Outcome of Non−Small Cell Lung Cancer. *Clin. Cancer Res. 16*, 4401−4410.

(8) Morgat, C., Chastel, A., Molinie, V., Schollhammer, R., Macgrogan, G., Velasco, V., Malavaud, B., Fernandez, P., and Hindie, E. (2019) Neurotensin Receptor−1 Expression in Human Prostate Cancer: A Pilot Study on Primary Tumors and Lymph Node Metastases. *Int. J. Mol. Sci. 20*, 1721−1730.

(9) Dupouy, S., Doan, V. K., Wu, Z., Mourra, N., Liu, J., De Wever, O., Llorca, F. P., Cayre, A., Kouchkar, A., Gompel, A., et al. (2014) Activation of EGFR, HER2 and HER3 by Neurotensin/Neurotensin Receptor 1 Renders Breast Tumors Aggressive yet Highly Responsive to Lapatinib and Metformin in Mice. *Oncotarget 5*, 8235−8251.

(10) Kim, J. T., Weiss, H. L., and Evers, B. M. (2017) Diverse Expression Patterns and Tumorigenic Role of Neurotensin Signaling Components in Colorectal Cancer Cells. *Int. J. Oncol. 50*, 2200−2206.

(11) Dupouy, S., Mourra, N., Doan, V. K., Gompel, A., Alifano, M., and Forgez, P. (2011) The Potential Use of the Neurotensin High Affinity Receptor 1 as a Biomarker for Cancer Progression and as a Component of Personalized Medicine in Selective Cancers. *Biochimie 93*, 1369−1378.

(12) Norris, E. J., Zhang, Q., Jones, W. D., DeStephanis, D., Sutker, A. P., Livasy, C. A., Ganapathi, R. N., Tait, D. L., and Ganapathi, M. K. (2019) Increased Expression of Neurotensin in High Grade Serous Ovarian Carcinoma with Evidence of Serous Tubal Intraepithelial Carcinoma. *J. Pathol. 248*, 352−362.

(13) Alshoukr, F., Prignon, A., Brans, L., Jallane, A., Mendes, S., Talbot, J. N., Tourwe, D., Barbet, J., and Gruaz−Guyon, A. (2011) Novel Dota−Neurotensin Analogues for ^{111}In Scintigraphy and ^{68}Ga PET Imaging of Neurotensin Receptor−Positive Tumors. *Bioconjugate Chem. 22*, 1374−1385.

(14) Maschauer, S., Einsiedel, J., Hubner, H., Gmeiner, P., and Prante, O. (2016) ^{18}F− and ^{68}Ga−Labeled Neurotensin Peptides for PET Imaging of Neurotensin Receptor 1. *J. Med. Chem. 59*, 6480−6492.

(15) Mascarin, A., Valverde, I. E., Vomstein, S., and Mindt, T. L. (2015) 1,2,3−Triazole Stabilized Neurotensin−Based Radiopeptidomimetics for Improved Tumor Targeting. *Bioconjugate Chem. 26*, 2143−2152.

(16) Buchegger, F., Bonvin, F., Kosinski, M., Schaffland, A. O., Prior, J., Reubi, J. C., Blauenstein, P., Tourwe, D., Garcia Garayoa, E., and Bischof Delaloye, A. (2003) Radiolabeled Neurotensin Analog, ^{99m}Tc−NT−XI, Evaluated in Ductal Pancreatic Adenocarcinoma Patients. *J. Nucl. Med. 44*, 1649−1654.

(17) Schulz, J., Rohracker, M., Stiebler, M., Goldschmidt, J., Grosser, O. S., Osterkamp, F., Pethe, A., Reineke, U., Smerling, C., and Amthauer, H. (2016) Comparative Evaluation of the Biodistribution Profiles of a Series of Nonpeptidic Neurotensin Receptor−1 Antagonists Reveals a Promising Candidate for Theranostic Applications. *J. Nucl. Med. 57*, 1120−1123.

(18) Jackson, J. A., Hungnes, I. N., Ma, M. T., and Rivas, C. (2020) Bioconjugates of Chelators with Peptides and Proteins in Nuclear Medicine: Historical Importance, Current Innovations, and Future Challenges. *Bioconjugate Chem. 31*, 483−491.

(19) Blaskovich, M. A. (2016) Unusual Amino Acids in Medicinal Chemistry. *J. Med. Chem. 59*, 10807−10836.

(20) Hapau, D., Rémond, E., Fanelli, R., Vivancos, M., René, A., Côté, J., Besserer−Offroy, É., Longpré, J.−M., Martinez, J., Zaharia, V., et al. (2016) Stereoselective Synthesis of β−(5−Arylthiazolyl) α−Amino Acids and Use in Neurotensin Analogues. *Eur. J. Org. Chem. 2016*, 1017−1024.

(21) Fujii, S., Miyajima, Y., Masuno, H., and Kagechika, H. (2013) Increased Hydrophobicity and Estrogenic Activity of Simple Phenols with Silicon and Germanium−Containing Substituents. *J. Med. Chem. 56*, 160−166.

(22) Ramesh, R., and Reddy, D. S. (2018) Quest for Novel Chemical Entities through Incorporation of Silicon in Drug Scaffolds. *J. Med. Chem. 61*, 3779−3798.

(23) Dalkas, G. A., Marchand, D., Galleyrand, J. C., Martinez, J., Spyroulias, G. A., Cordopatis, P., and Cavelier, F. (2010) Study of a Lipophilic Captopril Analogue Binding to Angiotensin I Converting Enzyme. *J. Pept. Sci. 16*, 91−97.

(24) Cavelier, F., Marchand, D., and Martinez, J. (2008) α, α'−Disubstituted Amino Acids with Silylated Side Chains as Lipophilic Building Blocks for the Synthesis of Peptaibol Analogues. *Chem. Biodiversity 5*, 1279−1287.

(25) Cavelier, F., Marchand, D., Martinez, J., and Sagan, S. (2004) Biological Activity of Silylated Amino Acid Containing Substance P Analogues. *J. Pept. Res. 63*, 290−296.

(26) Meanwell, N. A. (2011) Synopsis of Some Recent Tactical Application of Bioisosteres in Drug Design. *J. Med. Chem. 54*, 2529−2591.

(27) Pujals, S., Fernandez−Carneado, J., Kogan, M. J., Martinez, J., Cavelier, F., and Giralt, E. (2006) Replacement of a Proline with Silaproline Causes a 20−Fold Increase in the Cellular Uptake of a Pro−Rich Peptide. *J. Am. Chem. Soc. 128*, 8479−8483.

(28) Rémond, E., Martin, C., Martinez, J., and Cavelier, F. (2016) Silicon−Containing Amino Acids: Synthetic Aspects, Conformational Studies, and Applications to Bioactive Peptides. *Chem. Rev. 116*, 11654−11684.

(29) Rémond, E., Martin, C., Martinez, J., and Cavelier, F. (2015) Silaproline, a Silicon−Containing Proline Surrogate. *Top. Heterocycl. Chem. 48*, 27−50.

(30) Fanelli, R., Berthomieu, D., Didierjean, C., Doudouh, A., Lebrun, A., Martinez, J., and Cavelier, F. (2017) Hydrophobic α, α−

Disubstituted Disilylated Tesdpg Induces Incipient 310−Helix in Short Tripeptide Sequence. *Org. Lett. 19*, 2937−2940.
(31) Cavelier, F., Vivet, B., Martinez, J., Aubry, A., Didierjean, C., Vicherat, A., and Marraud, M. (2002) Influence of Silaproline on Peptide Conformation and Bioactivity. *J. Am. Chem. Soc. 124*, 2917−2923.
(32) Fanelli, R., Besserer−Offroy, E., Rene, A., Cote, J., Tetreault, P., Collerette−Tremblay, J., Longpre, J. M., Leduc, R., Martinez, J., Sarret, P., et al. (2015) Synthesis and Characterization in Vitro and in Vivo of (L)−(Trimethylsilyl)Alanine Containing Neurotensin Analogues. *J. Med. Chem. 58*, 7785−7795.
(33) Granier, C., Van Rietschoten, J., Kitabgi, P., Poustis, C., and Freychet, P. (1982) Synthesis and Characterization of Neurotensin Analogues for Structure/Activity Relationship Studies. *Eur. J. Biochem. 124*, 117−125.
(34) St−Pierre, S., Lalonde, J. M., Gendreau, M., Quirion, R., Regoli, D., and Rioux, F. (1981) Synthesis of Peptides by the Solid−Phase Method. 6. Neurotensin, Fragments, and Analogues. *J. Med. Chem. 24*, 370−376.
(35) René, A., Vanthuyne, N., Martinez, J., and Cavelier, F. (2013) (L)−(Trimethylsilyl)Alanine Synthesis Exploiting Hydroxypinanone−Induced Diastereoselective Alkylation. *Amino Acids 45*, 301−307.
(36) Morgat, C., Mishra, A. K., Varshney, R., Allard, M., Fernandez, P., and Hindie, E. (2014) Targeting Neuropeptide Receptors for Cancer Imaging and Therapy: Perspectives with Bombesin, Neurotensin, and Neuropeptide−Y Receptors. *J. Nucl. Med. 55*, 1650−1657.
(37) Herrmann, K., Schwaiger, M., Lewis, J. S., Solomon, S. B., McNeil, B. J., Baumann, M., Gambhir, S. S., Hricak, H., and Weissleder, R. (2020) Radiotheranostics: A Roadmap for Future Development. *Lancet Oncol. 21*, e146−e156.
(38) Mansi, R., Wang, X., Forrer, F., Waser, B., Cescato, R., Graham, K., Borkowski, S., Reubi, J. C., and Maecke, H. R. (2011) Development of a Potent Dota−Conjugated Bombesin Antagonist for Targeting Grpr−Positive Tumours. *Eur. J. Nucl. Med. Mol. Imaging 38*, 97−107.
(39) Jia, Y., Zhang, W., Fan, W., Brusnahan, S., and Garrison, J. (2016) Investigation of the Biological Impact of Charge Distribution on a NTR_1−Targeted Peptide. *Bioconjugate Chem. 27*, 2658−2668.
(40) Doulut, S., Rodriguez, M., Lugrin, D., Vecchini, F., Kitabgi, P., Aumelas, A., and Martinez, J. (1992) Reduced Peptide Bond Pseudopeptide Analogues of Neurotensin. *Pept. Res. 5*, 30−38.
(41) Fanelli, R., Floquet, N., Besserer−Offroy, E., Delort, B., Vivancos, M., Longpré, J. M., Renault, P., Martinez, J., Sarret, P., and Cavelier, F. (2017) Use of Molecular Modeling to Design Selective NTS_2 Neurotensin Analogues. *J. Med. Chem. 60*, 3303−3313.
(42) Maschauer, S., and Prante, O. (2018) Radiopharmaceuticals for Imaging and Endoradiotherapy of Neurotensin Receptor−Positive Tumors. *J. Labelled Compd. Radiopharm. 61*, 309−325.
(43) Maschauer, S., Greff, C., Einsiedel, J., Ott, J., Tripal, P., Hubner, H., Gmeiner, P., and Prante, O. (2015) Improved Radiosynthesis and Preliminary in Vivo Evaluation of a ^{18}F−Labeled Glycopeptide−Peptoid Hybrid for PET Imaging of Neurotensin Receptor 2. *Bioorg. Med. Chem. 23*, 4026−4033.
(44) Swift, S. L., Burns, J. E., and Maitland, N. J. (2010) Altered Expression of Neurotensin Receptors Is Associated with the Differentiation State of Prostate Cancer. *Cancer Res. 70*, 347−356.
(45) Hindie, E., Zanotti−Fregonara, P., Quinto, M. A., Morgat, C., and Champion, C. (2016) Dose Deposits from ^{90}Y, ^{177}Lu, ^{111}In, and ^{161}Tb in Micrometastases of Various Sizes: Implications for Radiopharmaceutical Therapy. *J. Nucl. Med. 57*, 759−764.
(46) Champion, C., Quinto, M. A., Morgat, C., Zanotti−Fregonara, P., and Hindie, E. (2016) Comparison between Three Promising Beta−Emitting Radionuclides, ^{67}Cu, ^{47}Sc and ^{161}Tb, with Emphasis on Doses Delivered to Minimal Residual Disease. *Theranostics 6*, 1611−1618.
(47) Kratochwil, C., Bruchertseifer, F., Giesel, F. L., Weis, M., Verburg, F. A., Mottaghy, F., Kopka, K., Apostolidis, C., Haberkorn, U., and Morgenstern, A. (2016) ^{225}Ac−PSMA−617 for PSMA−Targeted Alpha−Radiation Therapy of Metastatic Castration−Resistant Prostate Cancer. *J. Nucl. Med. 57*, 1941−1944.
(48) Muller, C., Umbricht, C. A., Gracheva, N., Tschan, V. J., Pellegrini, G., Bernhardt, P., Zeevaart, J. R., Koster, U., Schibli, R., and van der Meulen, N. P. (2019) Terbium−161 for PSMA−Targeted Radionuclide Therapy of Prostate Cancer. *Eur. J. Nucl. Med. Mol. Imaging 46*, 1919−1930.
(49) Baum, R. P., Singh, A., Schuchardt, C., Kulkarni, H. R., Klette, I., Wiessalla, S., Osterkamp, F., Reineke, U., and Smerling, C. (2018) ^{177}Lu−3BP−227 for Neurotensin Receptor 1−Targeted Therapy of Metastatic Pancreatic Adenocarcinoma: First Clinical Results. *J. Nucl. Med. 59*, 809−814.
(50) Misu, R., Noguchi, T., Ohno, H., Oishi, S., and Fujii, N. (2013) Structure−Activity Relationship Study of Tachykinin Peptides for the Development of Novel Neurokinin−3 Receptor Selective Agonists. *Bioorg. Med. Chem. 21*, 2413−2417.
(51) Lang, C., Maschauer, S., Hubner, H., Gmeiner, P., and Prante, O. (2013) Synthesis and Evaluation of a ^{18}F−Labeled Diarylpyrazole Glycoconjugate for the Imaging of NTS_1−Positive Tumors. *J. Med. Chem. 56*, 9361−9365.
(52) Teodoro, R., Faintuch, B. L., Nunez, E. G., and Queiroz, R. G. (2011) Neurotensin(8−13) Analogue: Radiolabeling and Biological Evaluation Using Different Chelators. *Nucl. Med. Biol. 38*, 113−120.
(53) Osterkamp, F., Smerling, C., Reineke, U., Hasse, C., and Ungewib, J. (2014) Neurotensin Receptor Ligands. WO 2014/086499.
(54) Bar−Shavit, Z., and Goldman, R. (1982) Tuftsin and Substance P as Modulators of Phagocyte Functions. *Adv. Exp. Med. Biol. 141*, 549−558.
(55) Goldman, R., Bar−Shavit, Z., and Romeo, D. (1983) Neurotensin Modulates Human Neutrophil Locomotion and Phagocytic Capability. *FEBS Lett. 159*, 63−67.
(56) Saada, S., Marget, P., Fauchais, A. L., Lise, M. C., Chemin, G., Sindou, P., Martel, C., Delpy, L., Vidal, E., Jaccard, A., et al. (2012) Differential Expression of Neurotensin and Specific Receptors, $NTSR_1$ and $NTSR_2$, in Normal and Malignant Human B Lymphocytes. *J. Immunol. 189*, 5293−5303.
(57) Benesova, M., Schafer, M., Bauder−Wust, U., Afshar−Oromieh, A., Kratochwil, C., Mier, W., Haberkorn, U., Kopka, K., and Eder, M. (2015) Preclinical Evaluation of a Tailor−Made Dota−Conjugated PSMA Inhibitor with Optimized Linker Moiety for Imaging and Endoradiotherapy of Prostate Cancer. *J. Nucl. Med. 56*, 914−920.
(58) Schulz, J., Rohracker, M., Stiebler, M., Goldschmidt, J., Stober, F., Noriega, M., Pethe, A., Lukas, M., Osterkamp, F., Reineke, U., et al. (2017) Proof of Therapeutic Efficacy of a ^{177}Lu−Labeled Neurotensin Receptor 1 Antagonist in a Colon Carcinoma Xenograft Model. *J. Nucl. Med. 58*, 936−941.
(59) Afshar−Oromieh, A., Hetzheim, H., Kubler, W., Kratochwil, C., Giesel, F. L., Hope, T. A., Eder, M., Eisenhut, M., Kopka, K., and Haberkorn, U. (2016) Radiation Dosimetry of ^{68}Ga−Psma−11 (Hbed−Cc) and Preliminary Evaluation of Optimal Imaging Timing. *Eur. J. Nucl. Med. Mol. Imaging 43*, 1611−1620.
(60) Sandstrom, M., Velikyan, I., Garske−Roman, U., Sorensen, J., Eriksson, B., Granberg, D., Lundqvist, H., Sundin, A., and Lubberink, M. (2013) Comparative Biodistribution and Radiation Dosimetry of ^{68}Ga−Dotatoc and ^{68}Ga−Dotatate in Patients with Neuroendocrine Tumors. *J. Nucl. Med. 54*, 1755−1759.

https://dx.doi.org/10.1021/acs.bioconjchem.0c00419
Bioconjugate Chem. XXXX, XXX, XXX−XXX

Supporting Information

Silicon-Containing Neurotensin Analogues as Radiopharmaceuticals for NTS_1-Positive Tumors Imaging

Roberto Fanelli,[1] Adrien Chastel,[2,3] Santo Previti,[1] Elif Hindié,[2,3] Delphine Vimont,[2] Paolo Zanotti Fregonara[4], Philippe Fernandez,[2,3] Philippe Garrigue,[5,6] Frédéric Lamare, [2,3] Romain Schollhammer, [2,3] Laure Balasse,[5] Benjamin Guillet,[5,6] Emmanuelle Rémond,[1] Clément Morgat,[2,3,‡] Florine Cavelier,[1,‡,*]

[1]*Institut des Biomolécules Max Mousseron, IBMM, UMR-5247, CNRS, Université de Montpellier, ENSCM, Place Eugène Bataillon, 34095 Montpellier cedex 5, France.*

[2]*Univ. Bordeaux, CNRS, EPHE, INCIA, UMR 5287, F-33000 Bordeaux, France*.

[3]*Nuclear Medicine Department, University Hospital of Bordeaux, F-33000 Bordeaux, France.*

[4]*Houston Methodist Research Institute, Houston, TX, 77030, USA.*

[5]*Aix-Marseille University, INSERM, Institut National de la Recherche Agronomique, Centre de Recherche en Cardiovasculaire et Nutrition, 13385 Marseille, France.*

[6]*Aix-Marseille University, Centre Européen de Recherche en Imagerie Médicale, 13005 Marseille, France.*

Table of content

Table of figures

I. Chemistry.

All solvents and reagents for the synthesis were purchased from Sigma Aldrich, Fluka and Alfa Aesar in gradient grade or reagent quality. 2-[4-(tert-Butoxycarbonylamino)piperidin-1-yl]acetic acid (Boc-(4)APAc-OH) was purchased from Fluorochem. 4-(9-Fluorenylmethyloxycarbonylamino)-phenylacetic acid (Fmoc-(4)APAc-OH) was purchased from Iris Biotech GMBH. Tri-tert-butyl 1,4,7,10-Tetraazacyclododecane-1,4,7,10-tetraacetate (DOTA(tBu)$_3$-OH) was purchased from TCI. All reactions involving air-sensitive reagents were performed under nitrogen or argon. JMV6658 and JMV6659 were synthesized using a VWR Microplate Shaker starting from Wang resin preloaded with Fmoc-Leucine (loading 0.7 mmol/g, 0.1 mmol scale) and 2-Cl trityl chloride resin (loading 0.8 mmol/g). JMV6660 and JMV6661 were synthesized using a Liberty Blue CEM microwave-assisted peptide synthesizer at 0.25 mmol scale, on a Wang resin preloaded with Fmoc-Leucine (loading 0.7 mmol/g). Purifications were performed with column chromatography using silica gel (Merck 60, 230–400 mesh). LC/MS system consisted of a Waters Alliance 2690 HPLC, coupled to a ZQ spectrometer (Manchester, UK) fitted with an electrospray source operated in the positive ionization mode (ESI^+). All the HPLC analyses were carried out using a C18 Chromolith Flash 25 x 4.6 mm column operated at a flow rate of 3 ml/min. A gradient of 0% of 0.1% aqueous TFA (solvent A) to 100% of acetonitrile containing 0.1% TFA (solvent B) was developed over 3 min. Positive-ion electrospray mass spectra were acquired at a solvent flow rate of 100-200 µL/min. Nitrogen was used for both the nebulizing and drying gas. The data were obtained in a scan mode ranging from 200 to 1700 m/z in 0.1 s intervals. A total of 10 scans were summed up to get the final spectrum. All final compounds were purified using a gradient composed of water/acetonitrile with 0.1% TFA at 50 mL/min flow rate performed on a Gilson PLC 2250 preparative apparatus equipped with a C18 Deltapak column (100 mm x 40 mm, 15µm, 100 Å). Purity was determined by RP-Analytic HPLC performed on an Agilent 1220 using a 50 x 4.6 mm Chromolith® High Resolution column. Compounds were separated using a linear gradient system (0 to 100% solvent B in 10 min) using a constant flow rate of $3mL.min^{-1}$. All the key target compounds showed a purity degree > 95%. High-resolution mass spectra (HRMS) were performed by the "Laboratoire de Mesures Physiques" of Montpellier University on a Micromass Q-Tof spectrometer

equipped with electrospray source ionization (ESI), using phosphoric acid as internal standard. Unnatural amino acids FmocTMSAla-OH and BocTMSAla-OH were prepared following already published procedure.[1]

Synthesis of JMV6658: DOTA-(4)-APAc-Lys-Lys-Pro-Tyr-TMSAla-Leu-OH.

JMV6658 was prepared (Scheme S1, SI) by at a 0.2 mmol scale on a Wang resin preloaded with Fmoc-Leucine (loading 0.8 mmol/g). The resin was swollen in DCM in a 5 ml plastic syringe equipped with a Teflon filter for 30 min. Fmoc deprotection was carried out with 20% piperidine in DMF (2 × 10 min.). Resin beads were washed with DMF (× 3). All Fmoc-amino acids (4 eq.) were coupled by using a solution of HATU in DMF (4 eq.) and DIPEA (10 eq.) in DMF. The syringe was shaken for 2h. After this time, the solution was sucked off and the resin was washed three times with DMF and once with DCM. For the coupling Fmoc-4-APAc-OH and DOTA-$(tBu)_3$-OH, the reaction time for the coupling was increased up to 5 hours. After each deprotection cycle, the solvent was removed by filtration and the resin washed with DMF. For the cleavage from the resin and final deprotection, the resin was suspended in a mixture of TFA/TIS (97/3 by volume) and stirred for 12 h at room temperature. The solution was filtered and the peptide precipitated with ice-cold diethyl ether. After centrifugation and elimination of the supernatant, the crude was purified by preparative HPLC. Yield: 74%: purity: 98%; ESI-MS: 659.5 $[M+2H]^{2+}/2$; 440.1 $[M+3H]^{3+}/3$; 326.4 $[M+4H]^{4+}/4$; HPLC: t_R 3.639 min (over 10 min); RP-LC: t_R = 1.01 min; HRMS: cald. For $C_{61}H_{105}N_{14}O_{16}Si$ $[M+H]^+$: 1317.7602; found: 1317.7611.

Synthesis of JMV6659 in solution: DOTA-(4)-APAc-Lys-Lys-Pro-Tyr-Ile-TMSAla-OH (Scheme S2).

General procedure (GP) for coupling reaction in solution (GP1).

To a solution of the appropriate Boc-protected amino acid (1.5 eq.) in dry DMF (10 mL/mmol), HATU (1.5 eq.) and N,N-diisopropylethylamine (3 eq.) were added. After 10 min, the amino acid

methyl ester hydrochloride or peptide methyl ester trifluoroacetate was added, and the mixture was maintained in stirring for 24 h at room temperature. After this time, solvent was evaporated in vacuo and the resulting residue was diluted with EtOAc and washed with 1M $KHSO_4$ (x 2), saturated $NaHCO_3$ solution (x 2) and brine (x 2), dried over anhydrous $MgSO_4$ and concentrated under reduced pressure to afford the crude coupling product, which was purified by chromatography on a silica gel column and subsequently characterized by LC-MS.

General procedure for the Boc deprotection in solution (GP2).

The *N*-Boc-protected peptide was dissolved in TFA/CH_2Cl_2 (1:1, 4 mL/mmol). The mixture was stirred until HPLC showed complete disappearance of starting material (ranging from 1h to 2h). After, CH_2Cl_2 was removed *in vacuo*, diethyl ether was added and evaporated (repeatedly, from 2 to 5 times), in order to obtain the corresponding trifluoroacetic salt, which was used for next step without further purification.

General procedure for methyl ester saponification (GP3)

The peptide methyl ester was dissolved in methanol (10 ml/mmol) and a solution of 4N KOH (5 eq.) was added. The reaction was stirred until disappearance of the starting material. The solvent was removed under reduced pressure, and the resulting residue was dissolved in water (10 mL/mmol) and acidified with citric acid 15% to pH 4-5. The organic product was extracted with ethyl acetate (x 4), dried over $MgSO_4$ and concentrated *in vacuo*, to afford the corresponding carboxylic acid, which was used for the next step without further purification.

General procedure for the deprotection of N-benzyloxycarbonyl in solution (GP4).

The *N*-Cbz-protected peptide in dry MeOH (5 ml/0.2 mmol) was degassed and subsequently, 10 weight % Pd/C was added. The mixture was degassed again, charged with H_2 and maintained in stirring overnight. The mixture was diluted with MeOH, filtered on a bed of Celite and washed with methanol (x 5). The filtrate was dried over anhydrous $MgSO_4$, filtered and concentrated *in vacuo* to provide the corresponding free amine.

Procedure for Boc and t-butyl deprotection in solution (GP5).

For the final deprotection, peptide was suspended in a mixture of TFA/TIS (95:5 by volume) and stirred for overnight at room temperature. Subsequently, diethyl ether was added and evaporated (repeatedly, from 2 to 5 folds) to afford the corresponding TFA salt, which was purified by preparative HPLC.

Boc-Tyr(Bn)-Ile-TMSAla-OMe.

Boc-Ile-TMSAla-OMe was deprotected following general procedure GP2. The TFA salt was directly coupled with Boc-Tyr(Bn)-OH following the general procedure GP1. The tripeptide Boc-Tyr(Bzl)-Ile-TMSAla-OMe was obtained as a white foam (690 mg, 79%). R_f: 0.25 (cyclohexane/ethylacetate 7:3), ESI-MS: 642.4 $[M+H]^+$, RP-LC: t_R = 2.15 min.

Boc-Lys(Z)-Lys(Z)-Pro-Tyr(Bn)-Ile-TMSAla-OMe.

Boc-Tyr(Bn)-Ile-TMSAla-OMe was deprotected following procedure GP2. Without further purification, it was directly coupled with Boc-Lys(Z)-Lys(Z)-Pro-OH, following the procedure GP1. The hexapeptide was obtained as a white foam (335 mg, 43%).

R_f: 0.32 (dichloromethane/methanol 95:5), ESI-MS: 639.4 $[M+2H]^{2+}/2$, RP-LC: t_R = 2.43 min.

Boc-(4)-APAC-Lys(Z)-Lys(Z)-Pro-Tyr(Bn)-Ile-TMSAla-OMe.

Boc-Lys(Z)-Lys(Z)-Pro-Tyr(Bn)-Ile-TMSAla-OMe was deprotected following procedure GP2. Without further purification it was directly coupled with Boc-(4)-APAC-OH, following the procedure GP1. The expected product was obtained as a white solid (299 mg, 81%). R_f: 0.21 (dichloromethane/methanol 95:5), ESI-MS: 702.9 $[M+2H]^{2+}/2$, RP-LC: t_R = 1.85 min.

DOTA(tBu)$_3$-(4)-APAC-Lys(Z)-Lys(Z)-Pro-Tyr(Bn)-Ile-TMSAla-OMe.

Boc-(4)-APAC-Lys(Z)-Lys(Z)-Pro-Tyr(Bn)-Ile-TMSAla-OMe was deprotected following procedure GP2. Without further purification, it was directly coupled with DOTA(tBu)$_3$-OH, following the procedure GP1. The expected product was obtained as a white solid (236 mg, 60%). R_f: 0.14 (dichloromethane/methanol 95:5), ESI-MS: 930.1 $[M+2H]^{2+}/2$, RP-LC: t_R = 1.73 min.

DOTA(tBu)$_3$-(4)-APAC-Lys(Z)-Lys(Z)-Pro-Tyr(Bn)-Ile-TMSAla-OH.

The entitled compound was obtained starting from DOTA(tBu)$_3$-(4)-APAC-Lys(Z)-Lys(Z)-Pro-Tyr(Bn)-Ile-TMSAla-OMe, following the procedure GP3 (150 mg, 65%) as a white foam. ESI-MS: 923.2 $[M+2H]^{2+}/2$, RP-LC: t_R = 1.71 min.

DOTA-(4)-APAC-Lys-Lys-Pro-Tyr-Ile-TMSAla-OH (JMV6659).

The entitled compound was obtained starting from DOTA(*t*Bu)$_3$-(4)-APAc-Lys(Z)-Lys(Z)-Pro-Tyr(Bn)-Ile-TMSAla-OH, which was first deprotected following general procedure GP4 to remove Z and Bn protecting groups. Without further purification, the residue was treated with TFA following the general procedure GP5, to obtain the desired product (135 mg, 100%) as a white solid and purified by preparative HPLC. ESI-MS: 659.5 $[M+2H]^{2+}/2$;440.1 $[M+3H]^{3+}/3$; 326.4 $[M+4H]^{4+}/4$. HPLC: t_R 1.967 min (over 3 min); RP-LC: t_R = 0.99 min. HR-MS: cald. For $C_{61}H_{105}N_{14}O_{16}Si$ $[M+H]^+$: 1317.7602; found: 1317.7593.

Synthesis of JMV6659 by Solid-Phase Peptide Approach (Scheme S3).

JMV6659 was synthesized in SPPS approach using 2-Chlorotritylchloride resin (Scheme S3, SI). Anchoring of the first amino acid was carried out starting from 2Cl-Trt resin (1.6 mmol/g), which was dried overnight and subsequently treated with $SOCl_2$ (1.5 eq/resin loading) in CH_2Cl_2 (2 mL/100 mg resin) for 2h at rt. After this time, the resin was washed with CH_2Cl_2 (10 ml x 5) and dried *in vacuo* for 2h. Fmoc-TMSAla-OH (1 eq.) was dissolved in CH_2Cl_2 (1 ml/100 mg of resin) and added to the resin. DIPEA (1 eq.) was added and the mixture was stirred for 5 minutes, followed by the adding of a DIPEA excess (1.5 eq.). The mixture was maintained in stirring overnight. To end cap any remaining reactive trityl groups, methanol was added (80 µL/100 mg of resin) and stirred for 30 min. After, resin was filtered and washed with CH_2Cl_2 (3 x 5 mL), DMF (2 x 5 mL) and methanol (2 x 5 mL). The resin was dried *in vacuo* and the loading was measured spectrophotometrically. After the TMSAla loading, synthesis of **2** by SPPS was carried out following the same procedure used for JMV6658. Yield: 81%; purity: 99%.

Synthesis of JMV6660: DOTA-(4)-APAc-Lys-Lys-Pro-Tyr-Ile-Leu-OH.

JMV6660 was synthesized (Scheme S4) using a Liberty Blue CEM microwave-assisted peptide synthesizer at a 0.25 mmol scale on a Wang resin preloaded with Fmoc-Leucine (loading 0.7 mmol/g). All Fmoc-amino acids (4 eq.) were double coupled by using a solution of Oxima Pure in DMF (4 eq.) and DIC in DMF (4 eq.) as coupling reagent under microwave irradiation at 170 watts for 15 sec at 75°C and at 30 watts for 110 sec at 90°C. The reactant and solvent were then filtered and the resin washed with DMF (3 x 5 ml). After each deprotection cycle, the solvent was removed by filtration and the resin washed with DMF (3 x 5 ml). For the cleavage from the resin and final deprotection, the resin was suspended in a mixture of TFA/TIS (97/3 by volume) and stirred for 12h at room temperature. The solution was filtered and the peptide was precipitated with ice-cold diethyl ether. After centrifugation and elimination of the supernatant, the crude was purified by preparative HPLC. Yield: 67%; purity: 96%; ESI-MS: 1289.3 $[M+H]^+$; 644.6 $[M+2H]^{2+}/2$, 430.2 $[M+3H]^{3+}/3$; HPLC: t_R 1.901 min (over 3 min); RP-LC: t_R = 0.84 min.; HRMS: cald. $[M+2H]^{2+}/2$: 644.3878; found: 644.3869.

Synthesis of JMV6661: DOTA-(4)-APAc-Arg-Arg-Pro-Tyr-Ile-Leu-OH.

JMV6661 was synthesized (Scheme S5) following the same procedure used for conjugate JMV6660. Yield: 58%; purity: 96%; ESI-MS: 1344.1 $[M+H]^+$: 672.6 $[M+2H]^{2+}/2$; 448.5 $[M+3H]^{3+}/3$; RP-LC: t_R = 0.85 min; HPLC: t_R 1.942 min (over 3 min); HRMS: cald. $[M+2H]^{2+}/2$: 672.3939; found: 672.3942.

Table S1. Characterization of final conjugates.

	Sequence	Yield	Purity	Formula	Molecular Weight	HRMS	
						Calculated	Found
JMV6658	DOTA-APAc-Lys-Lys-Pro-Tyr-TMSAla-Leu-OH	74%	98%	$C_{61}H_{105}N_{14}O_{16}Si$	1317.64	1317.7602	1317.7611
JMV6659	DOTA-APAc-Lys-Lys-Pro-Tyr-Ile-TMSAla-OH	81%[a]	99%[a]	$C_{61}H_{105}N_{14}O_{16}Si$	1317.64	1317.7602	1317.7593
JMV6660	DOTA-APAc-Lys-Lys-Pro-Tyr-Ile-Leu-OH	67%	96%	$C_{61}H_{102}N_{14}O_{16}$	1287.54	644.3878[b]	644.3869[b]
JMV6661	DOTA-APAc-Arg-Arg-Pro-Tyr-Ile-Leu-OH	58%	96%	$C_{61}H_{102}N_{18}O_{16}$	1343.57	672.3939[b]	672.3942[b]

[a]Yield and purity refer to the SPPS approach.
[b]Calculated and found mass for JMV6660 and JMV6661 were reported as $[M+2H]^{2+}/2$.

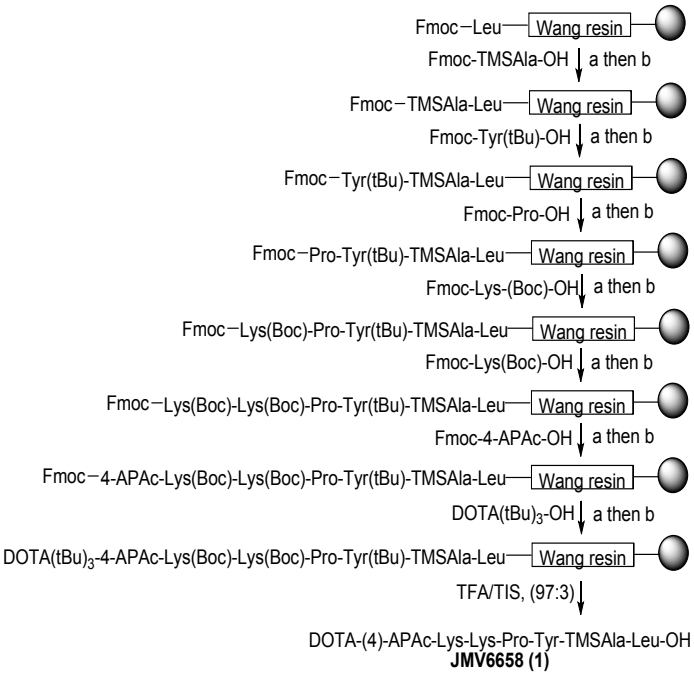

a: 20% piperidine in DMF
b: AA (4 eq.), HATU (4 eq.), DIPEA (10 eq.) in DMF.

Scheme S1. Synthesis of JMV6658.

IBMM-UMR5247 - Laboratoire des acides aminés, peptides et protéines

Sample name:	FR-DOTA-JMV2006
Data file:	C:\CHEM32\LC1220_000\AGILENT1220_000\DATA\ROBERTOFANELLI\FR-DOTA-JMV2006 2017-02-14 14-07-08.D
Description:	
Injection volume:	5.000
Instrument:	LC 1220
Injection date:	2/14/2017 2:08:31 PM
Acq. method:	0 à 100% 10min 214nm.M

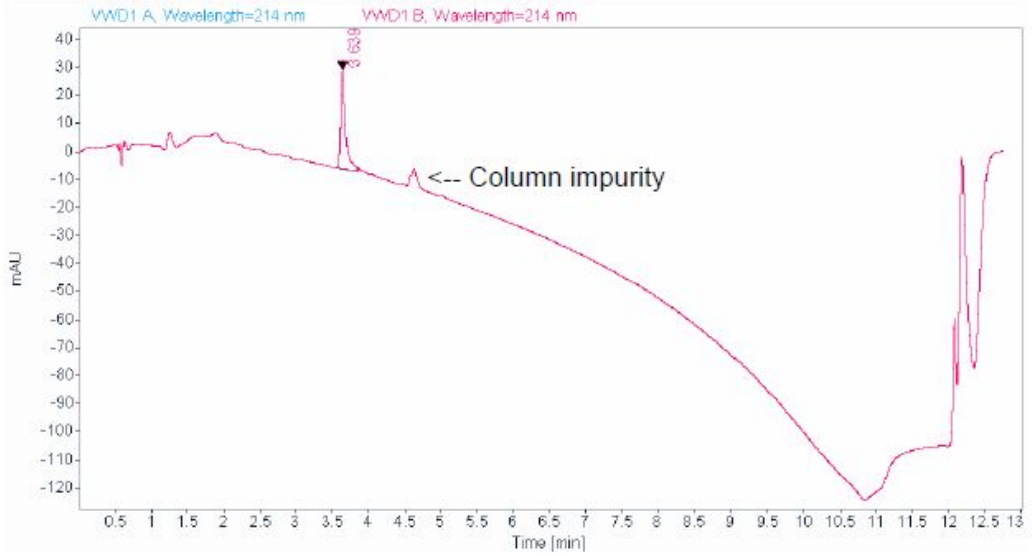

Signal: VWD1 A, Wavelength=214 nm

RT [min]	Area	Height	Peak Area Percent
3.639	163.15813	35.26292	100.00

Signal: VWD1 B, Wavelength=214 nm

RT [min]	Area	Height	Peak Area Percent
3.639	163.54102	35.22461	100.00

Chart S1. HPLC profile of **JMV6658**.

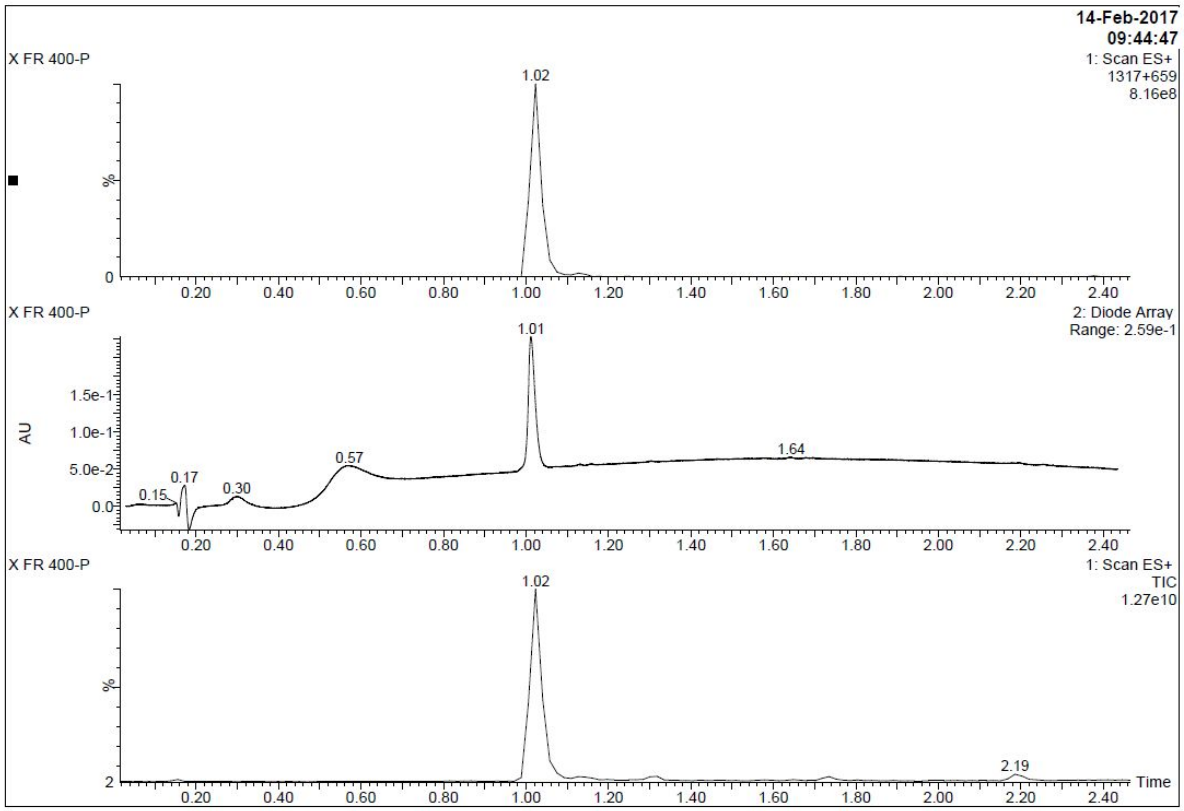

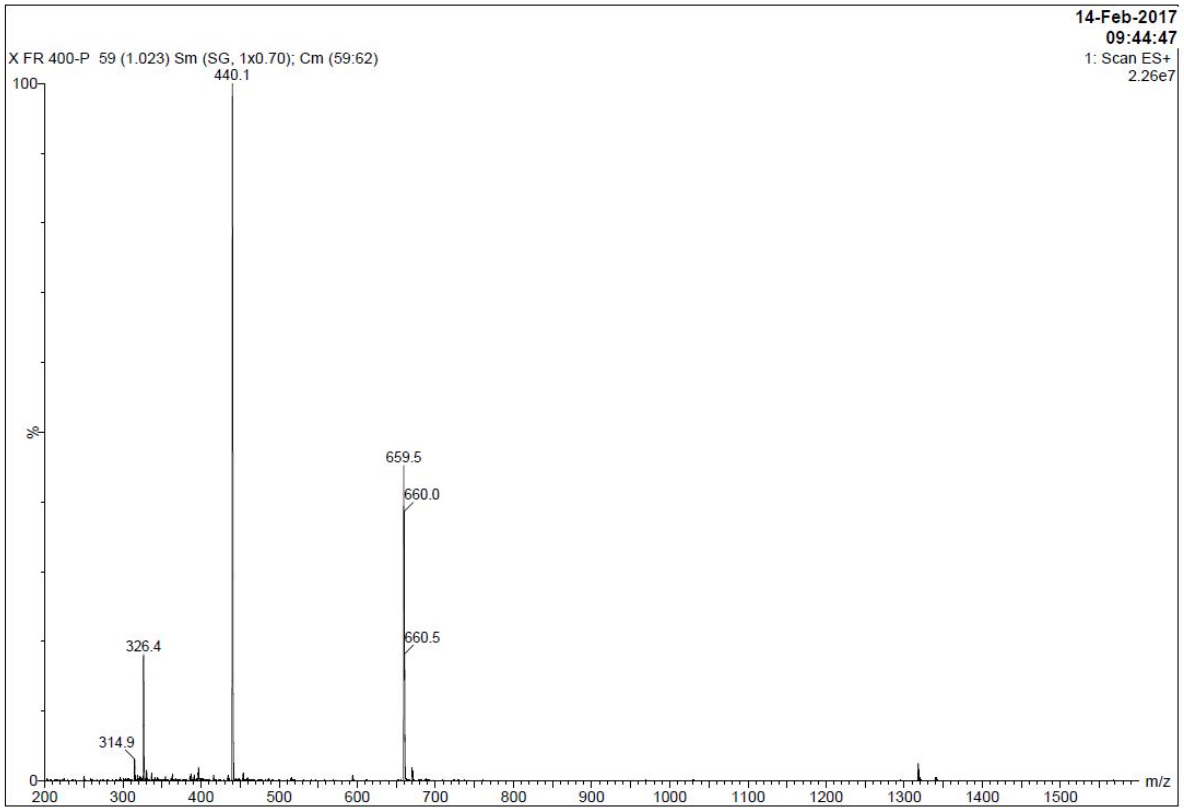

Chart S2. LC-MS of **JMV6658**.

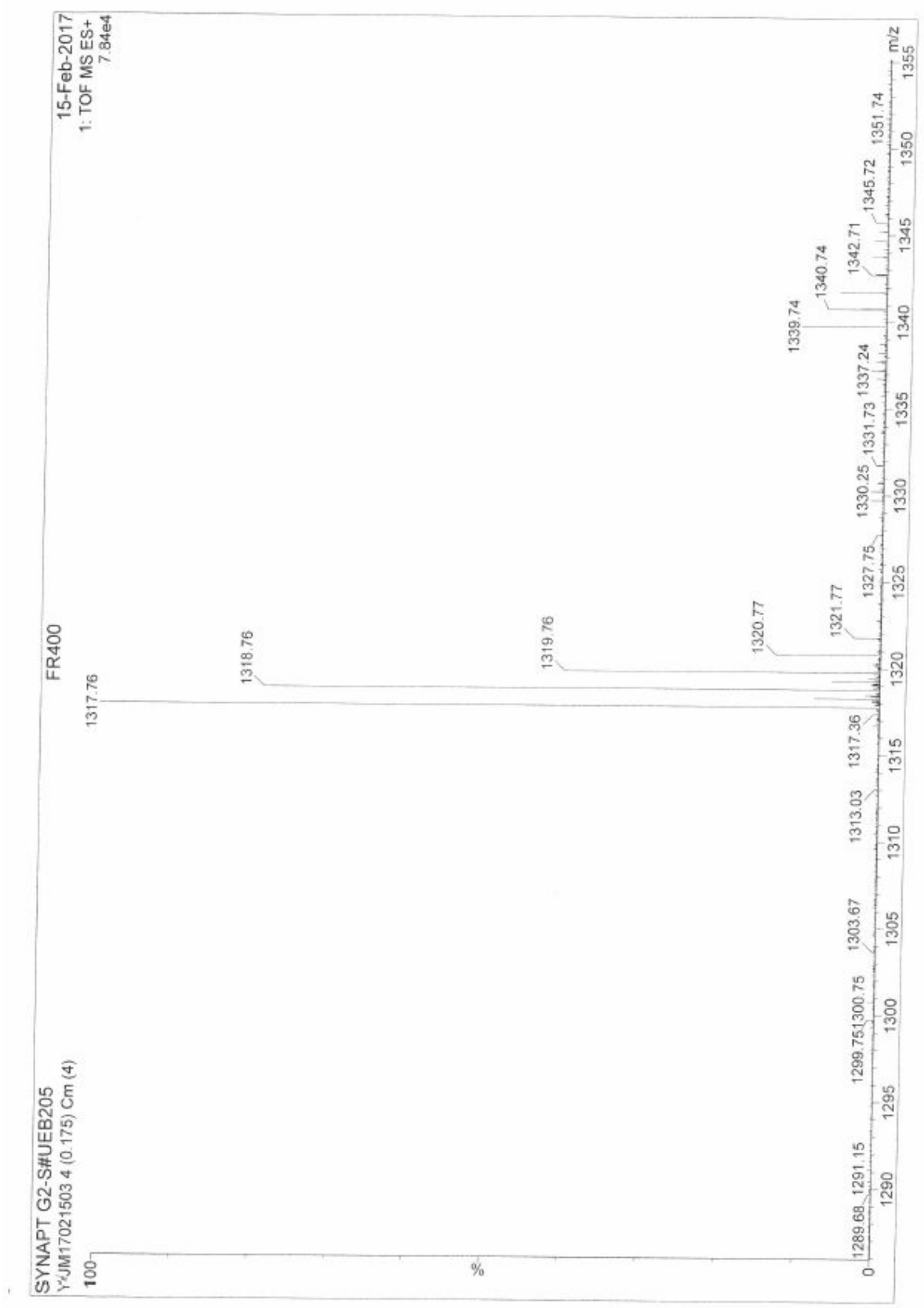

Chart S3. HRMS of **JMV6658**.

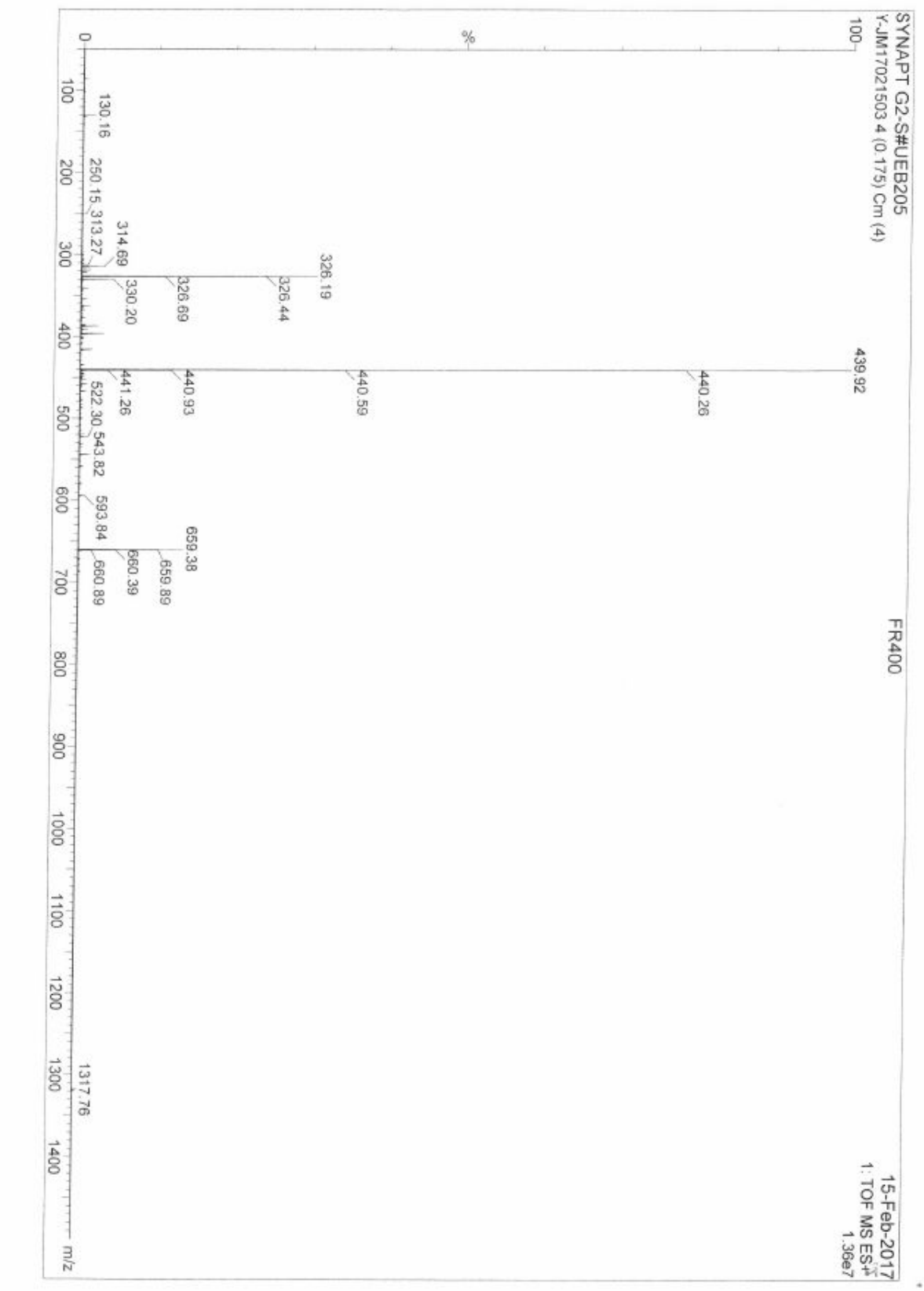

Chart S4. Detailed HRMS of **JMV6658** around the exact mass.

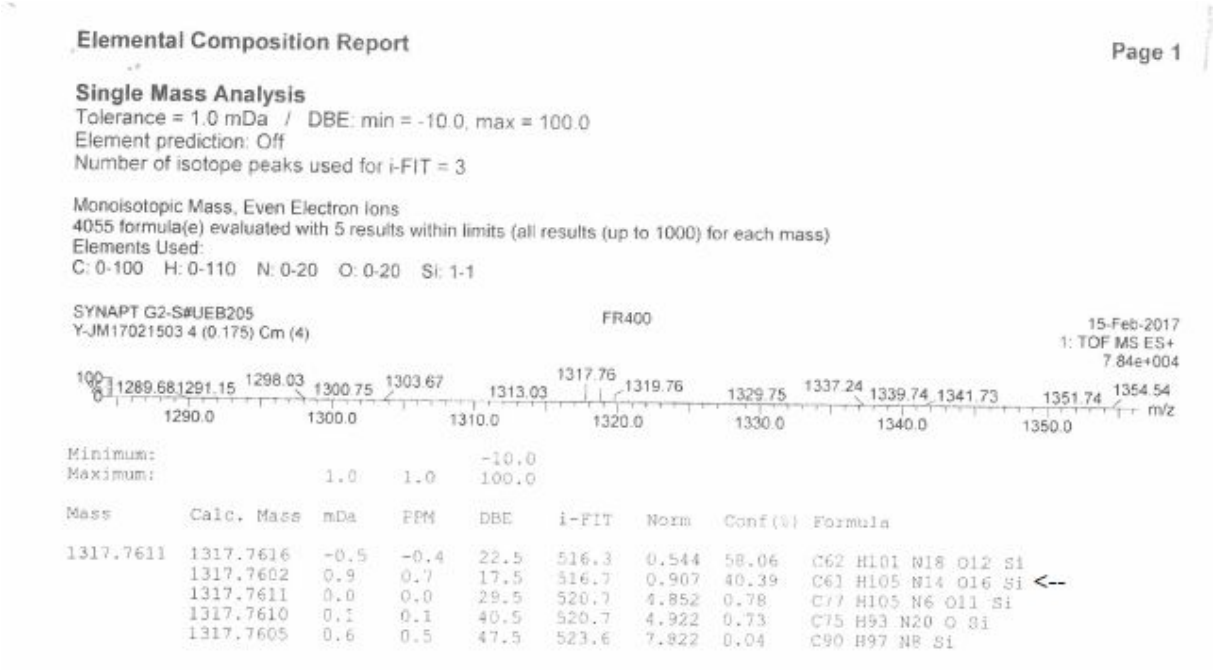

Elemental Composition Report Page 1

Single Mass Analysis
Tolerance = 1.0 mDa / DBE: min = -10.0, max = 100.0
Element prediction: Off
Number of isotope peaks used for i-FIT = 3

Monoisotopic Mass, Even Electron Ions
4055 formula(e) evaluated with 5 results within limits (all results (up to 1000) for each mass)
Elements Used:
C: 0-100 H: 0-110 N: 0-20 O: 0-20 Si: 1-1

SYNAPT G2-S#UEB205
Y-JM17021503 4 (0.175) Cm (4)
FR400
15-Feb-2017
1: TOF MS ES+
7.84e+004

Mass	Calc. Mass	mDa	PPM	DBE	i-FIT	Norm	Conf(%)	Formula	
Minimum:				-10.0					
Maximum:		1.0	1.0	100.0					
1317.7611	1317.7616	-0.5	-0.4	22.5	516.3	0.544	58.06	C62 H101 N18 O12 Si	
	1317.7602	0.9	0.7	17.5	516.7	0.907	40.39	C61 H105 N14 O16 Si	<--
	1317.7611	0.0	0.0	29.5	520.7	4.852	0.78	C77 H105 N6 O11 Si	
	1317.7610	0.1	0.1	40.5	520.7	4.922	0.73	C75 H93 N20 O Si	
	1317.7605	0.6	0.5	47.5	523.6	7.822	0.04	C90 H97 N8 Si	

Chart S5. HRMS for **JMV6658**, with calculated and found mass.

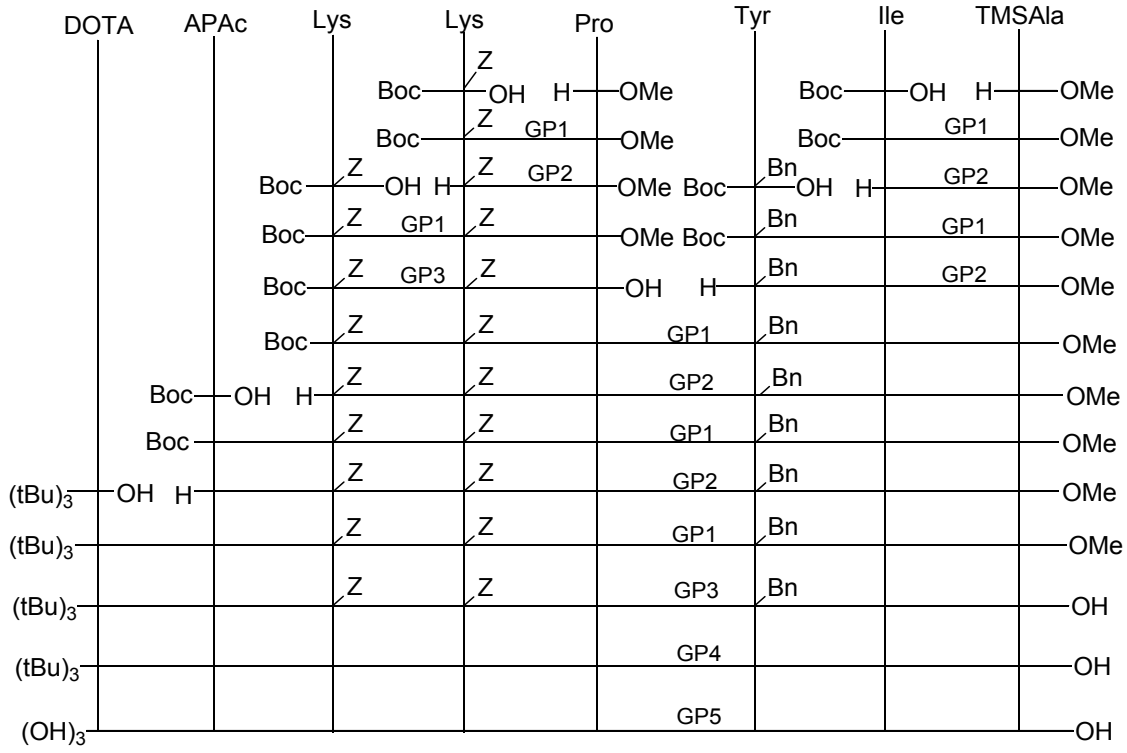

Scheme S2. Synthesis of **JMV6659** in solution. Reagents and conditions = GP1: HATU, DIPEA, DMF, overnight, rt; GP2: TFA/DCM (1:1), until starting material disappearance (1-2h), rt; GP3: 4N KOH, methanol, until starting material disappearance (9-12h), rt; GP4: 10% Pd/C, dry methanol, H_2, overnight, rt; GP5: TFA/TIS (95:5), overnight, rt.

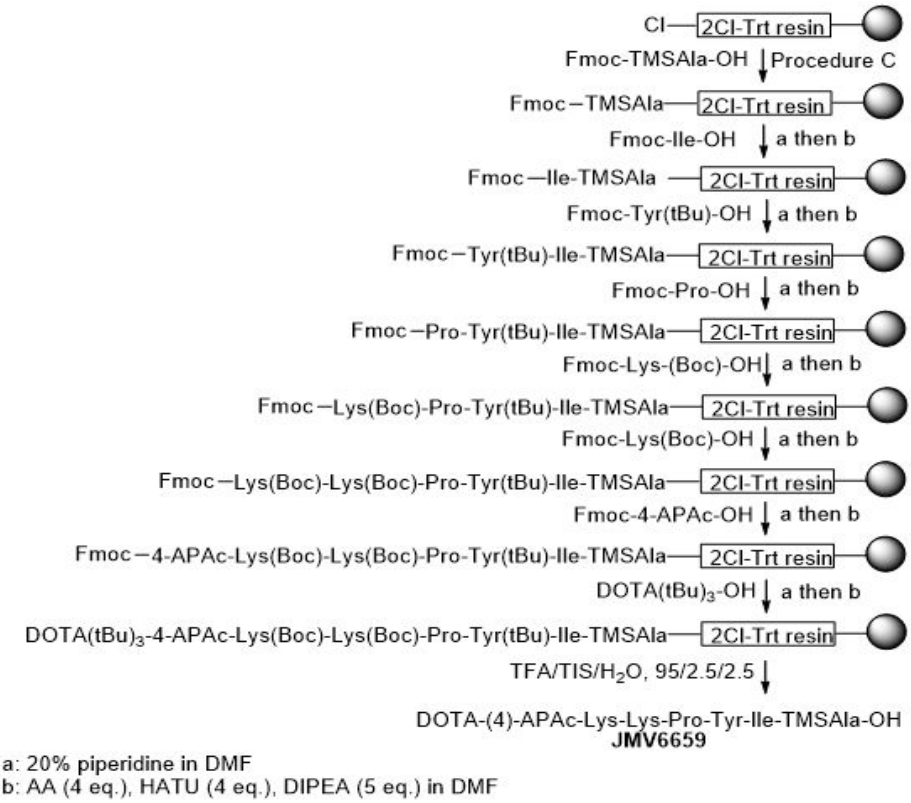

Scheme S3. Synthesis of **JMV6659** in SPPS. Reagents and conditions = a: 20% piperidine in DMF (5 mi x 3); b: HATU, DIPEA, DMF, ranging from 30 and 60 min. Final cleavage was performed overnight.

IBMM-UMR5247 - Laboratoire des acides aminés, peptides et protéines

Sample name:	FR422-F2
Data file:	C:\CHEM32\LC1220_000\AGILENT1220_000\DATA\ROBERTOFANELLI\FR422-F2 2017-02-15 17-44-57.D
Description:	
Injection volume:	5.000
Instrument:	LC 1220
Injection date:	2/15/2017 5:54:48 PM
Acq. method:	0a100_3min_214nm.M

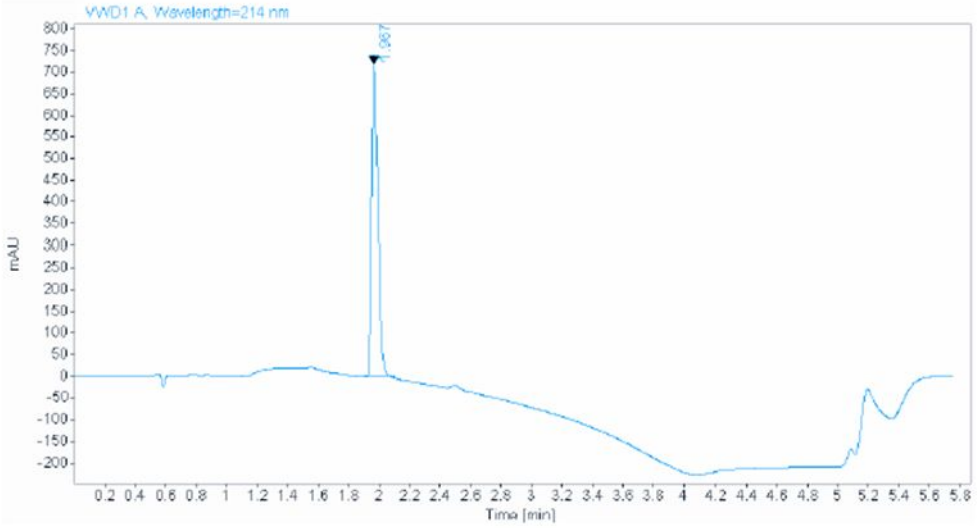

Signal: VWD1 A, Wavelength=214 nm

RT [min]	Area	Height	Peak Area Percent
1.967	2018.31860	717.05151	100.00

Chart S6. HPLC profile of **JMV6659**.

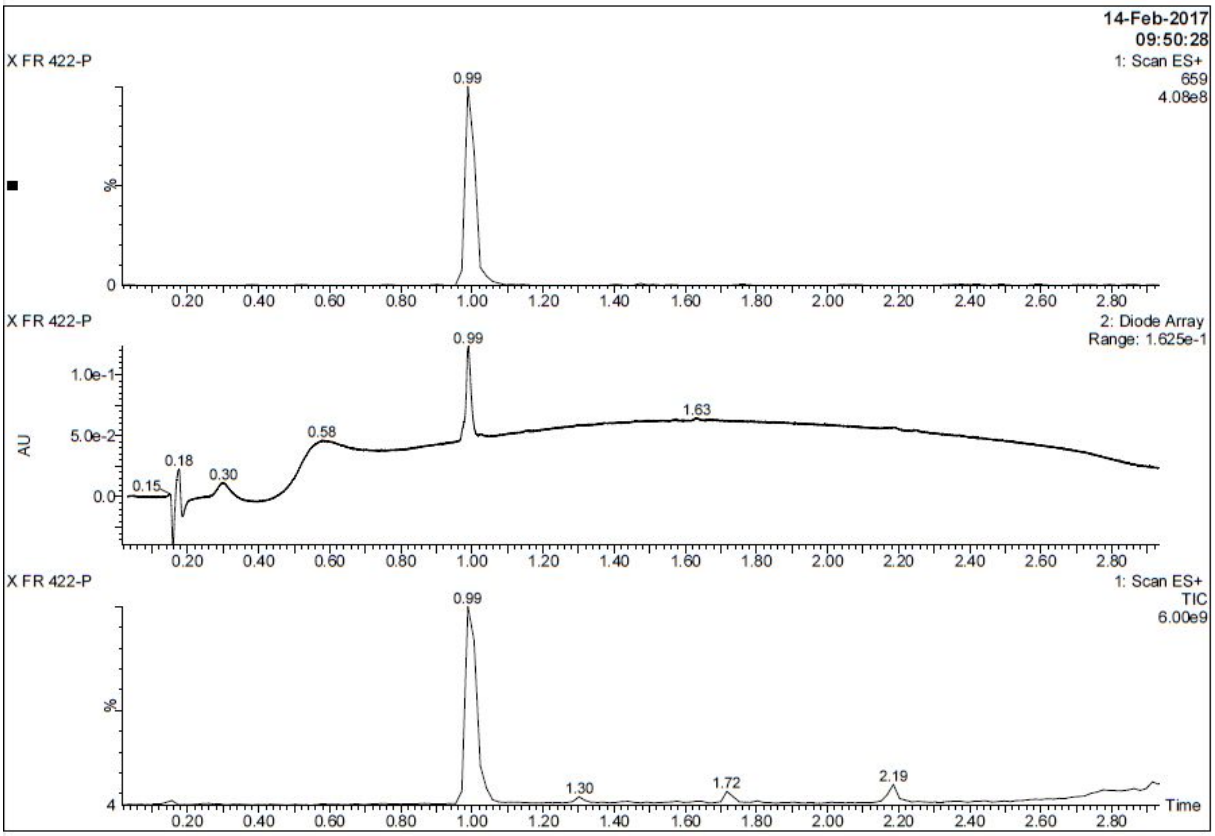

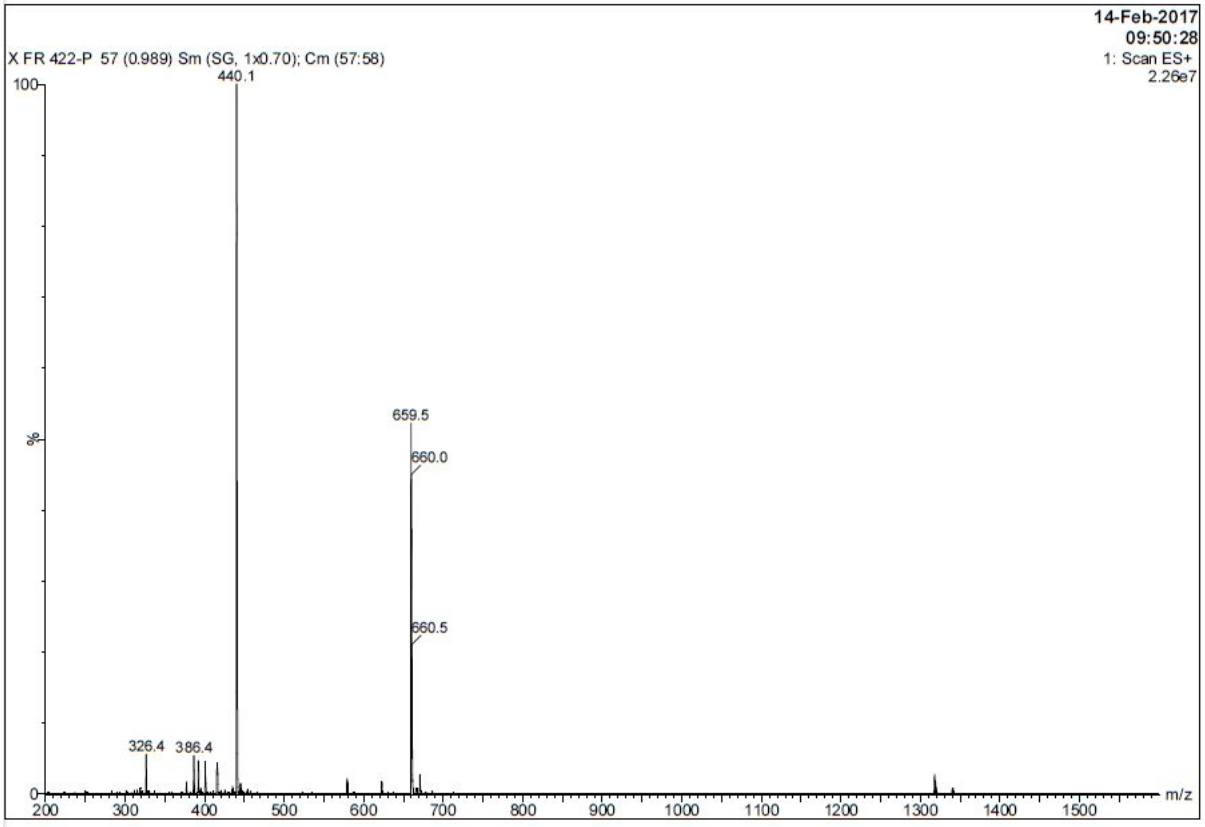

Chart S7. LC-MS of **JMV6659**.

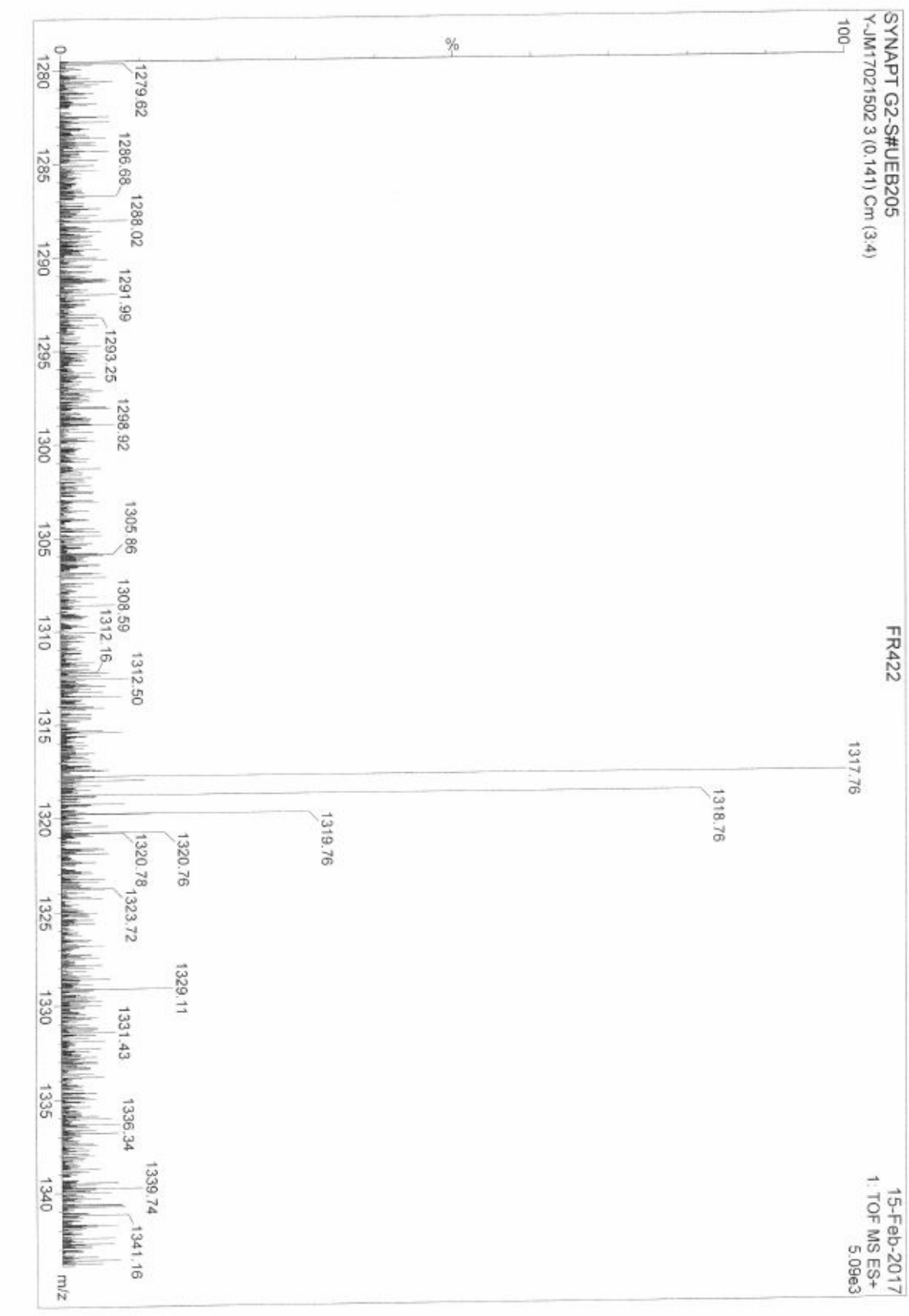

Chart S8. HRMS of **JMV6659** around the exact mass.

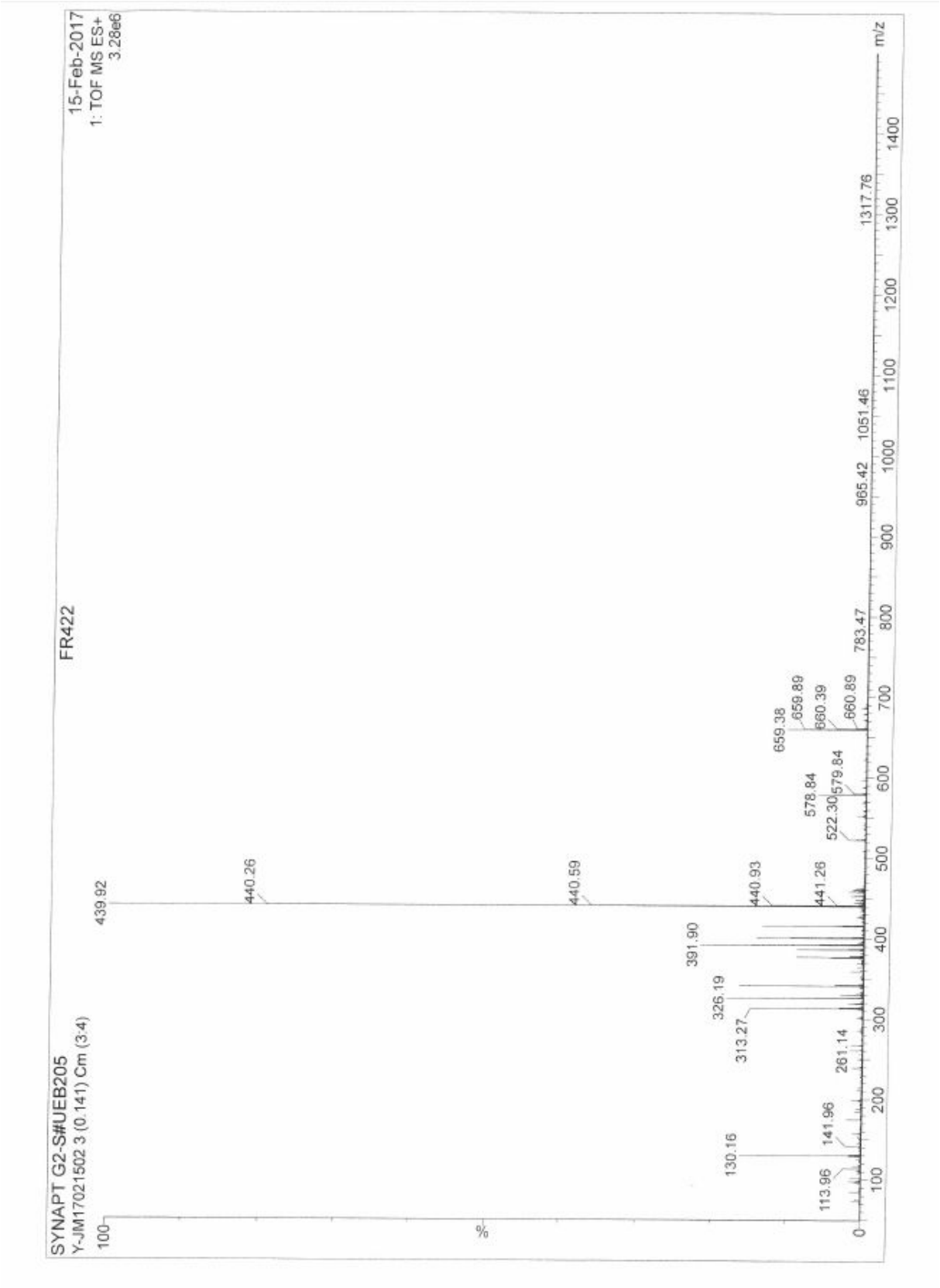

Chart S9. HRMS of **JMV6659**.

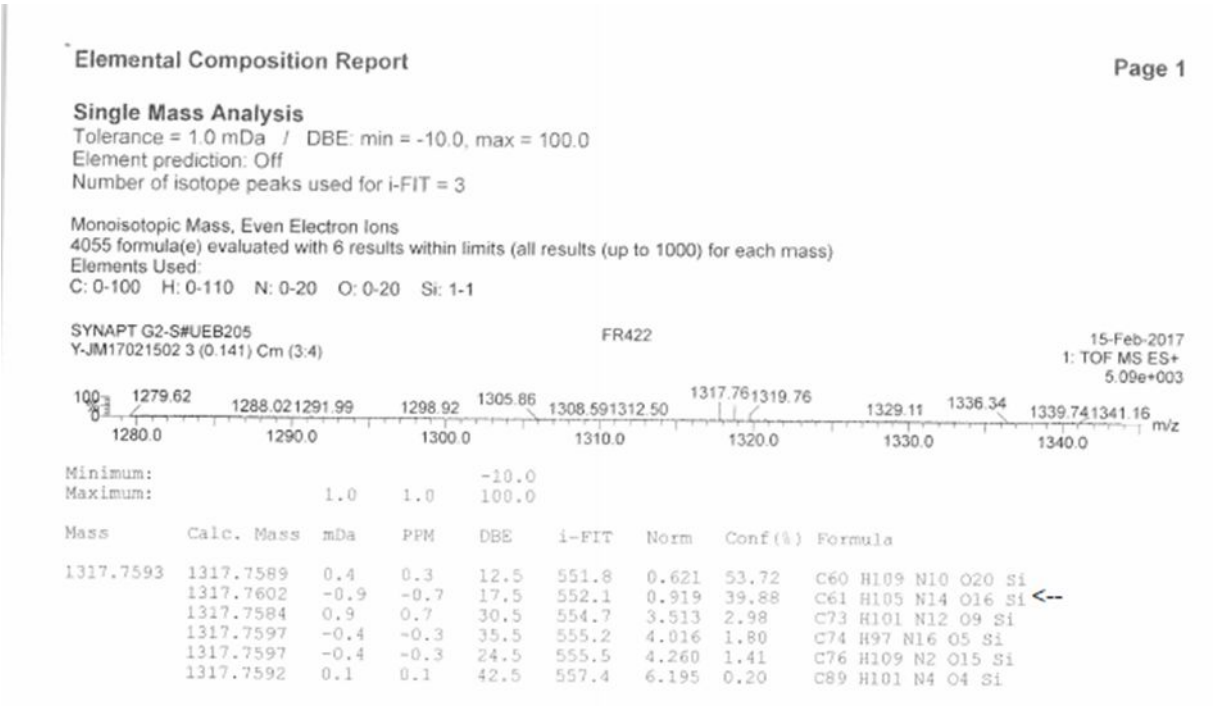

Elemental Composition Report

Page 1

Single Mass Analysis
Tolerance = 1.0 mDa / DBE: min = -10.0, max = 100.0
Element prediction: Off
Number of isotope peaks used for i-FIT = 3

Monoisotopic Mass, Even Electron Ions
4055 formula(e) evaluated with 6 results within limits (all results (up to 1000) for each mass)
Elements Used:
C: 0-100 H: 0-110 N: 0-20 O: 0-20 Si: 1-1

SYNAPT G2-S#UEB205
Y-JM17021502 3 (0.141) Cm (3:4)

FR422

15-Feb-2017
1: TOF MS ES+
5.09e+003

Minimum:				-10.0				
Maximum:		1.0	1.0	100.0				
Mass	Calc. Mass	mDa	PPM	DBE	i-FIT	Norm	Conf(%)	Formula
1317.7593	1317.7589	0.4	0.3	12.5	551.8	0.621	53.72	C60 H109 N10 O20 Si
	1317.7602	-0.9	-0.7	17.5	552.1	0.919	39.88	C61 H105 N14 O16 Si <--
	1317.7584	0.9	0.7	30.5	554.7	3.513	2.98	C73 H101 N12 O9 Si
	1317.7597	-0.4	-0.3	35.5	555.2	4.016	1.80	C74 H97 N16 O5 Si
	1317.7597	-0.4	-0.3	24.5	555.5	4.260	1.41	C76 H109 N2 O15 Si
	1317.7592	0.1	0.1	42.5	557.4	6.195	0.20	C89 H101 N4 O4 Si

Chart S10. HRMS for **JMV6659**, with calculated and found mass.

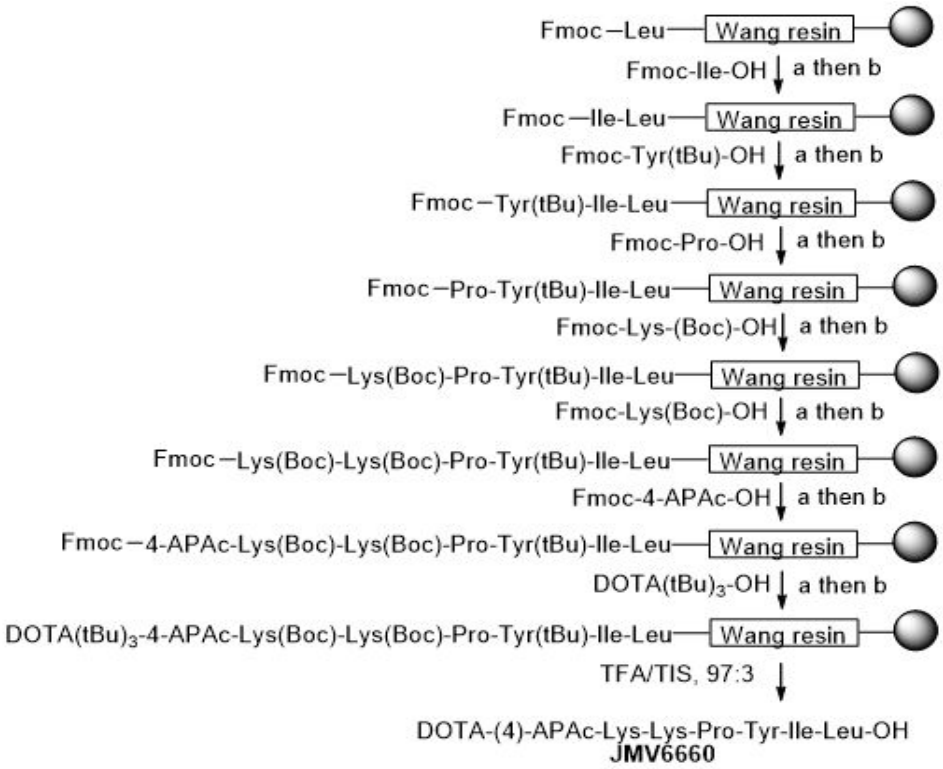

Scheme S4. Synthesis of **JMV6660**.

IBMM-UMR5247 - Laboratoire des acides aminés, peptides et protéines

Sample name:	JMV6660
Data file:	C:\CHEM32\LC1220_000\AGILENT1220_000 \DATA\ROBERTOFANELLI\JMV6660 2017-03-06 11-48-38.D
Description:	
Injection volume:	5.000
Instrument:	LC 1220
Injection date:	3/6/2017 11:49:58 AM
Acq. method:	0a100_3min_214nm.M

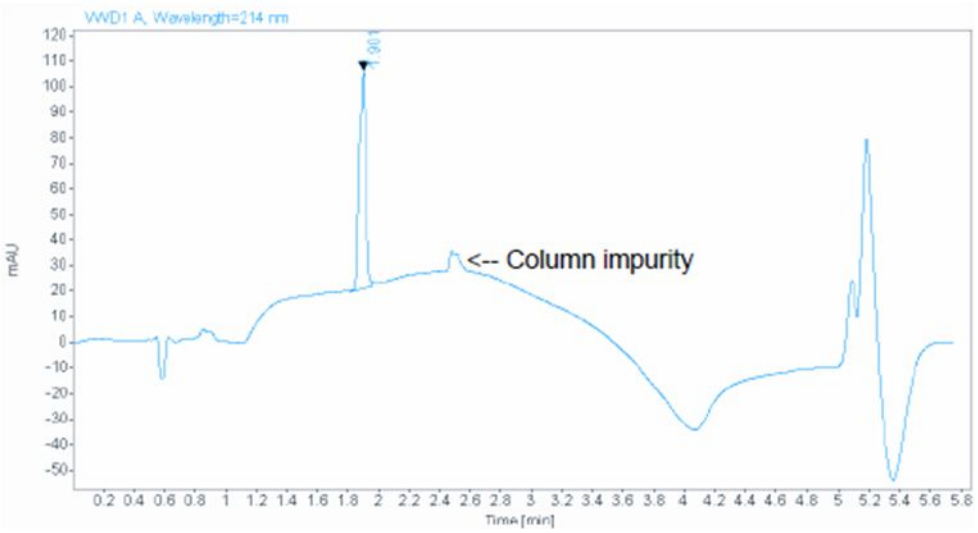

Signal: VWD1 A, Wavelength=214 nm

RT [min]	Area	Height	Peak Area Percent
1.901	260.38647	85.37262	100.00

Chart S11. HPLC profile of **JMV6660**.

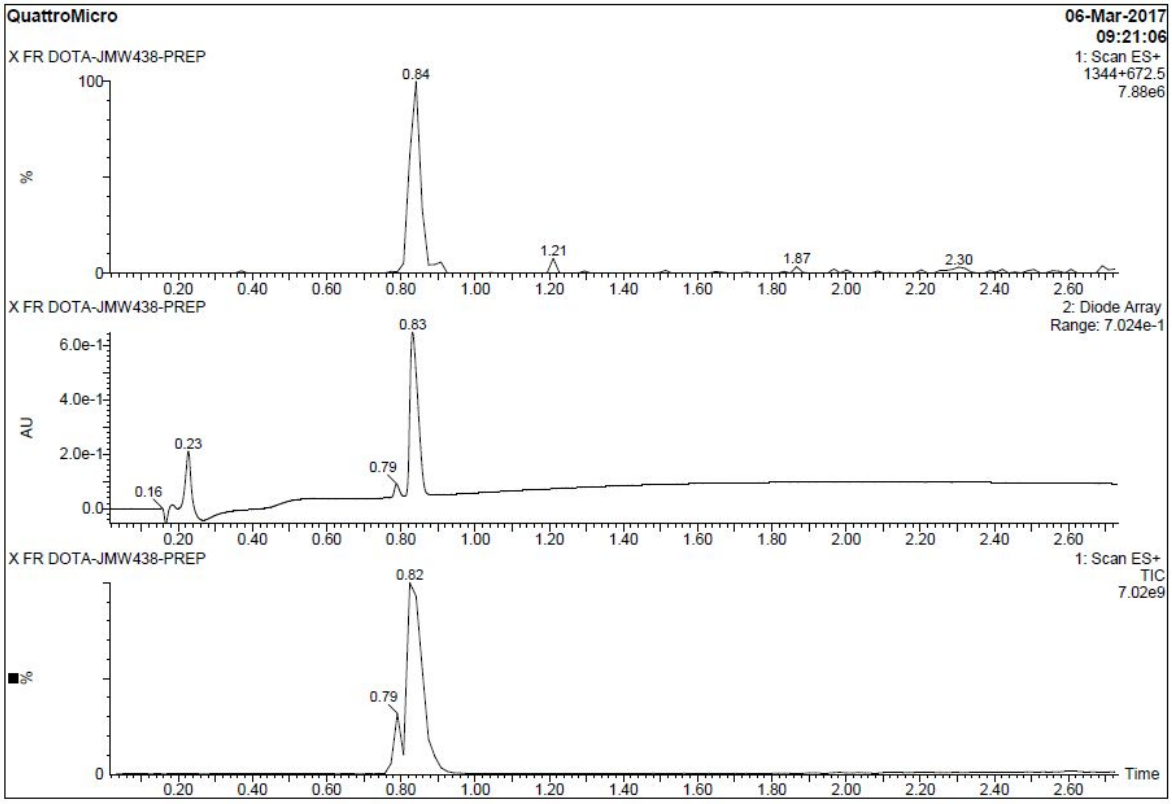

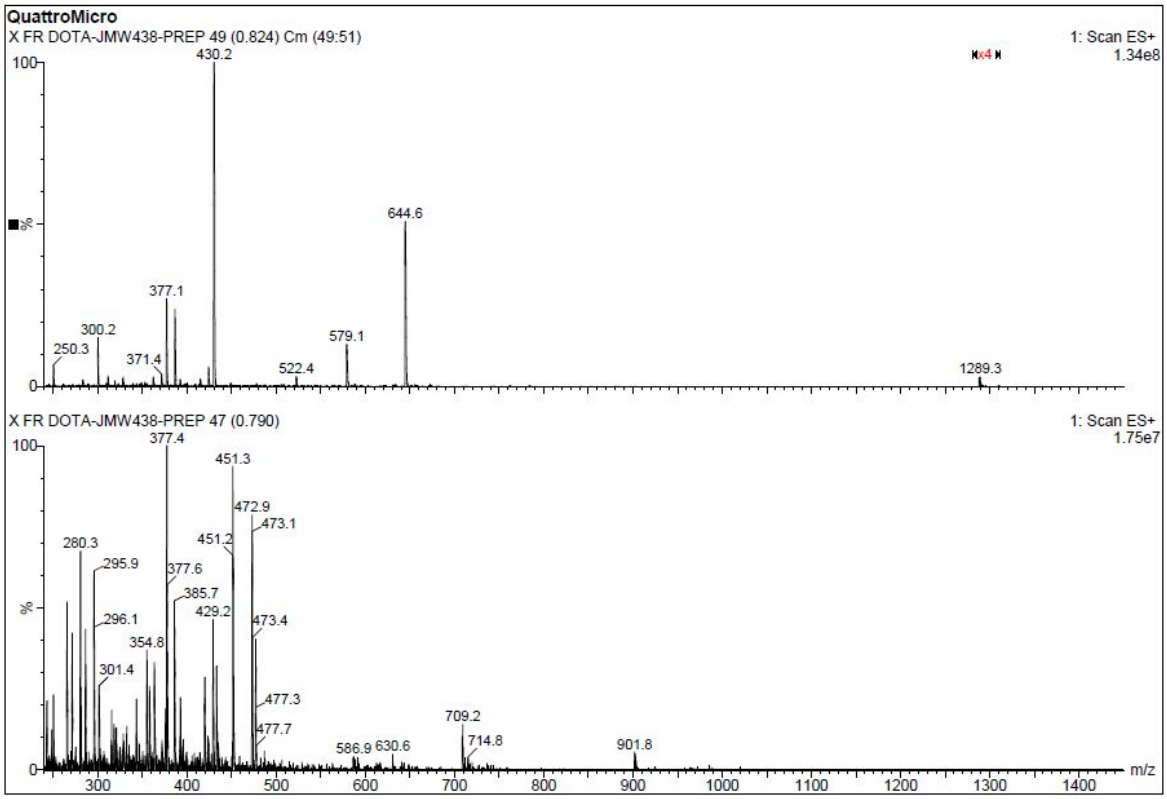

Chart S12. LC-MS of **JMV6660**.

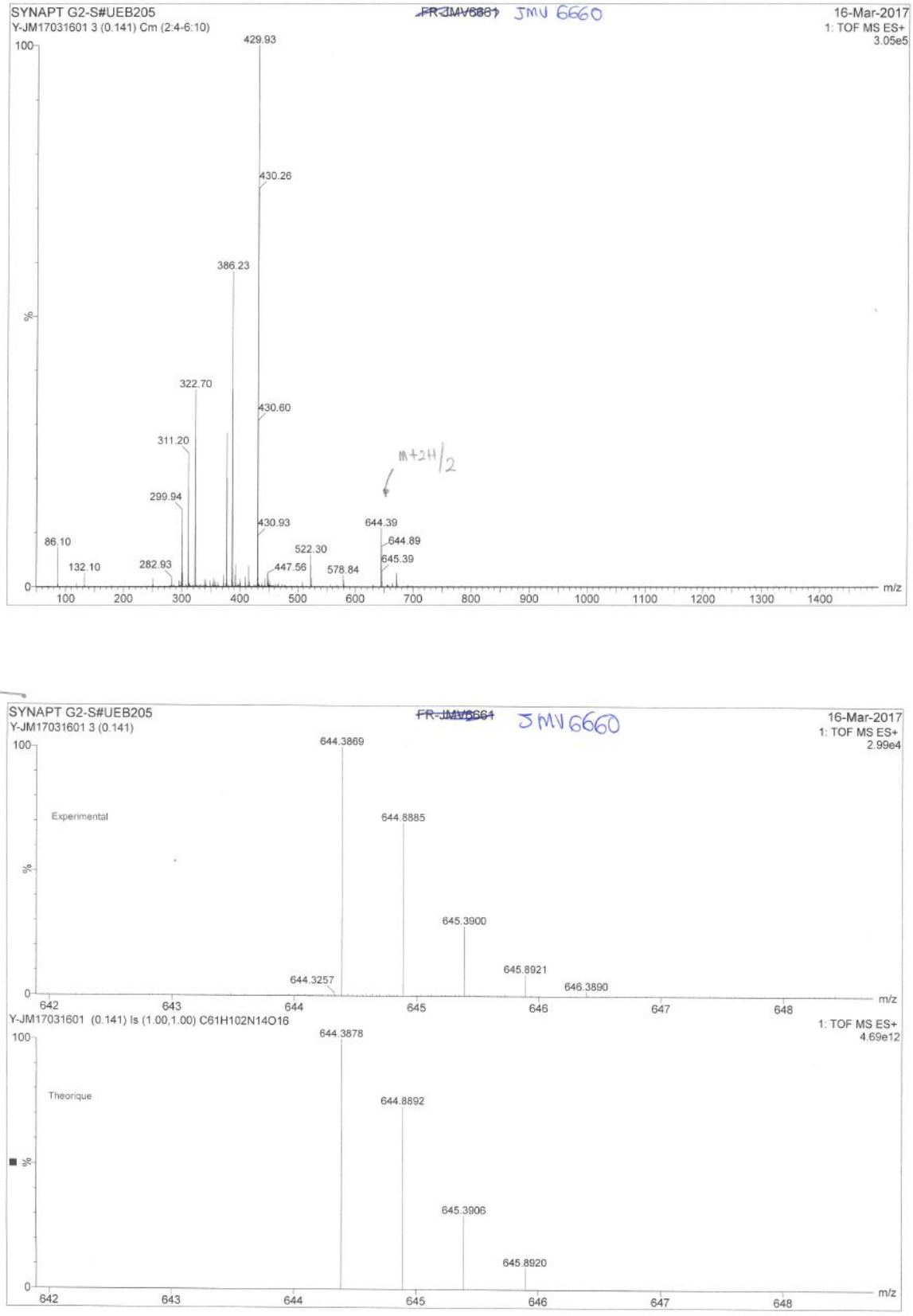

Chart S13. HRMS of **JMV6660.**

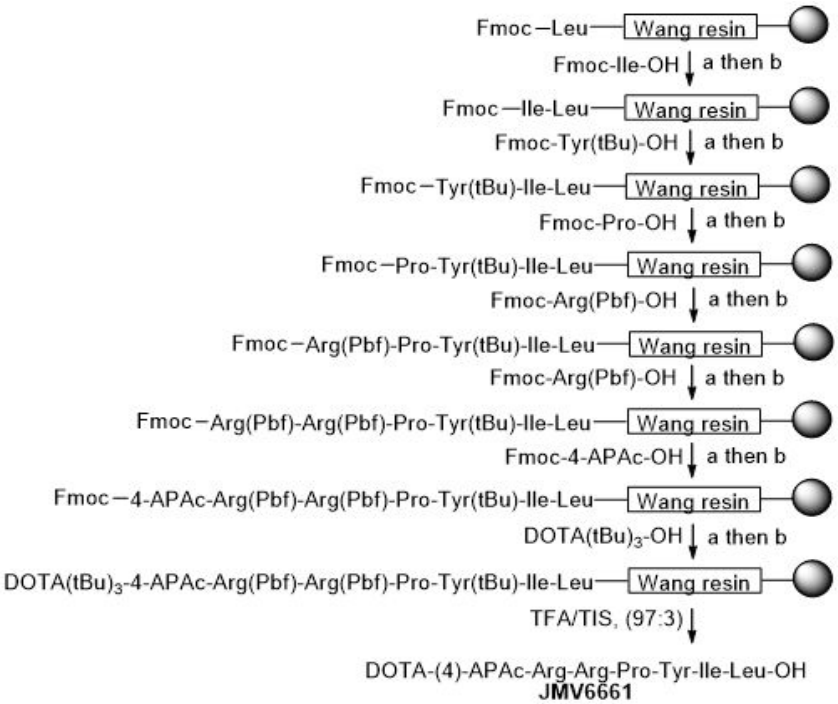

Scheme S5. Synthesis of **JMV6661**.

IBMM-UMR5247 - Laboratoire des acides aminés, peptides et protéines

Sample name:	JMV6661
Data file:	C:\CHEM32\LC1220_000\AGILENT1220_000 \DATA\ROBERTOFANELLI\JMV6661 2017-03-06 11-48-47.D
Description:	
Injection volume:	5.000
Instrument:	LC 1220
Injection date:	3/6/2017 11:57:08 AM
Acq. method:	0a100_3min_214nm.M

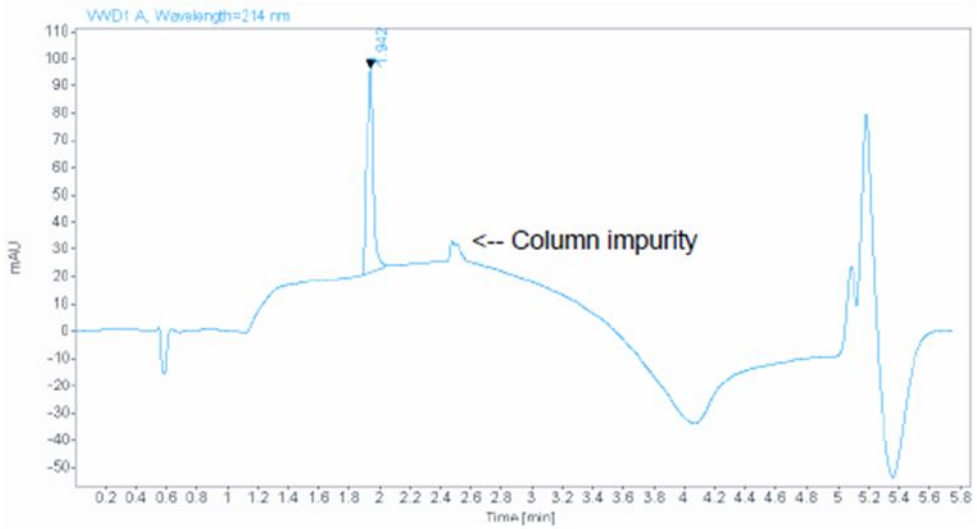

Signal: VWD1 A, Wavelength=214 nm

RT [min]	Area	Height	Peak Area Percent
1.942	227.60481	74.73854	100.00

Chart S14. HPLC profile of **JMV6661**.

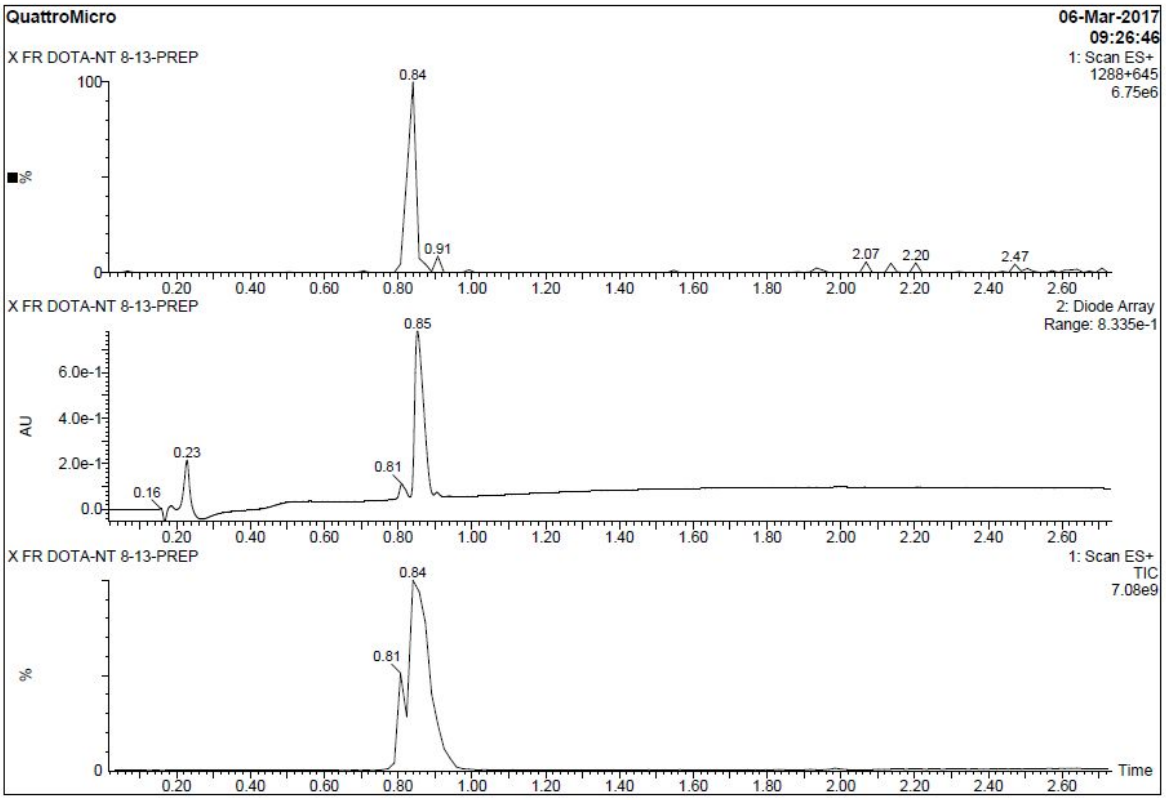

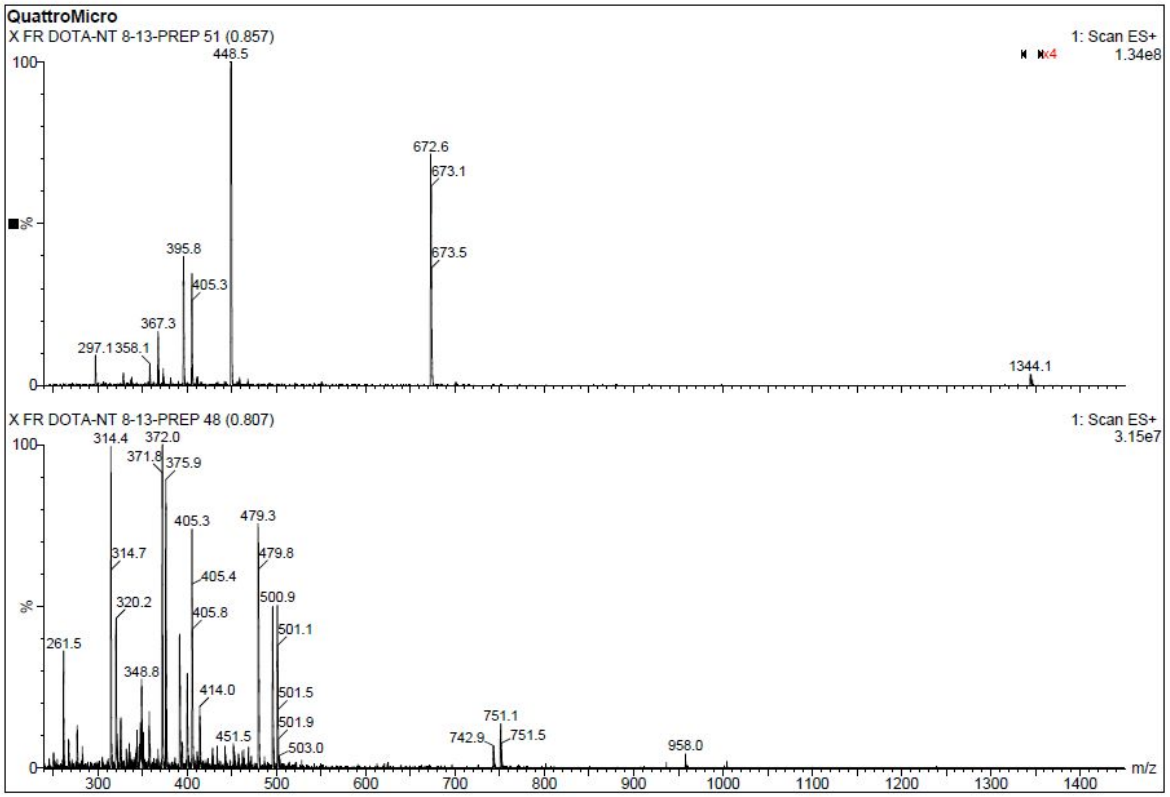

Chart S15. LC-MS of **JMV6661**.

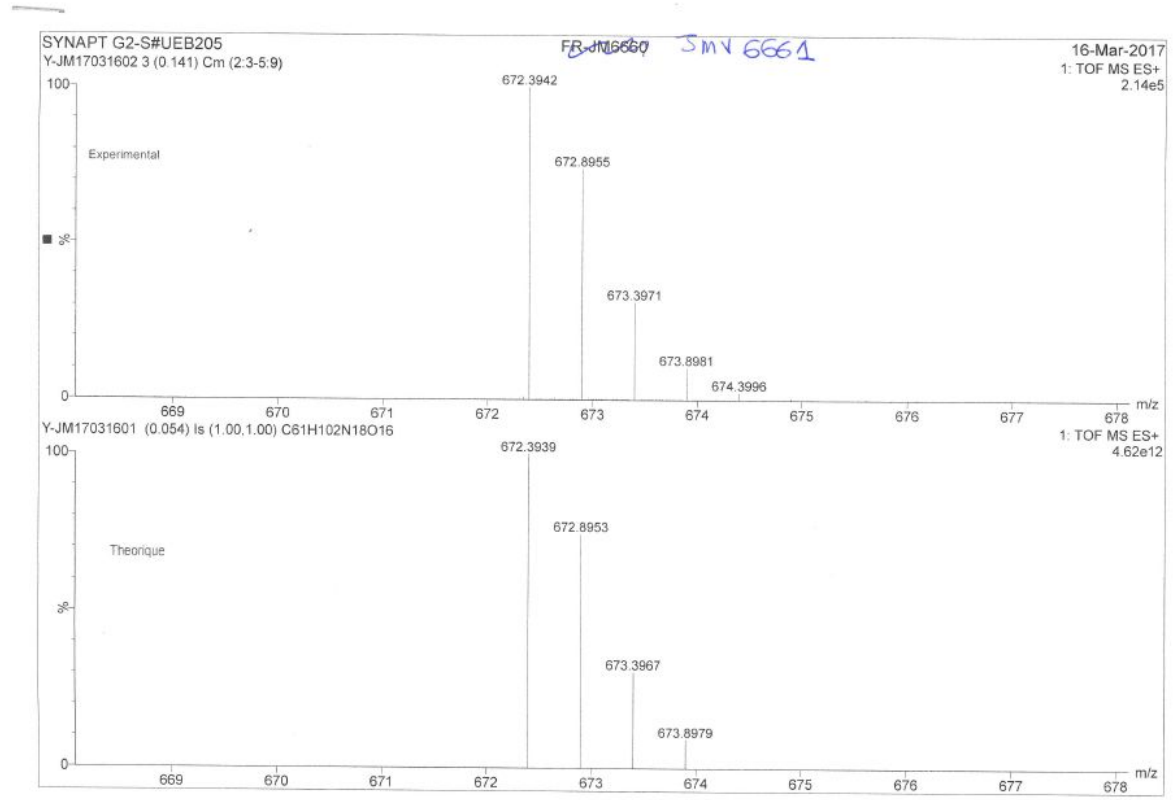

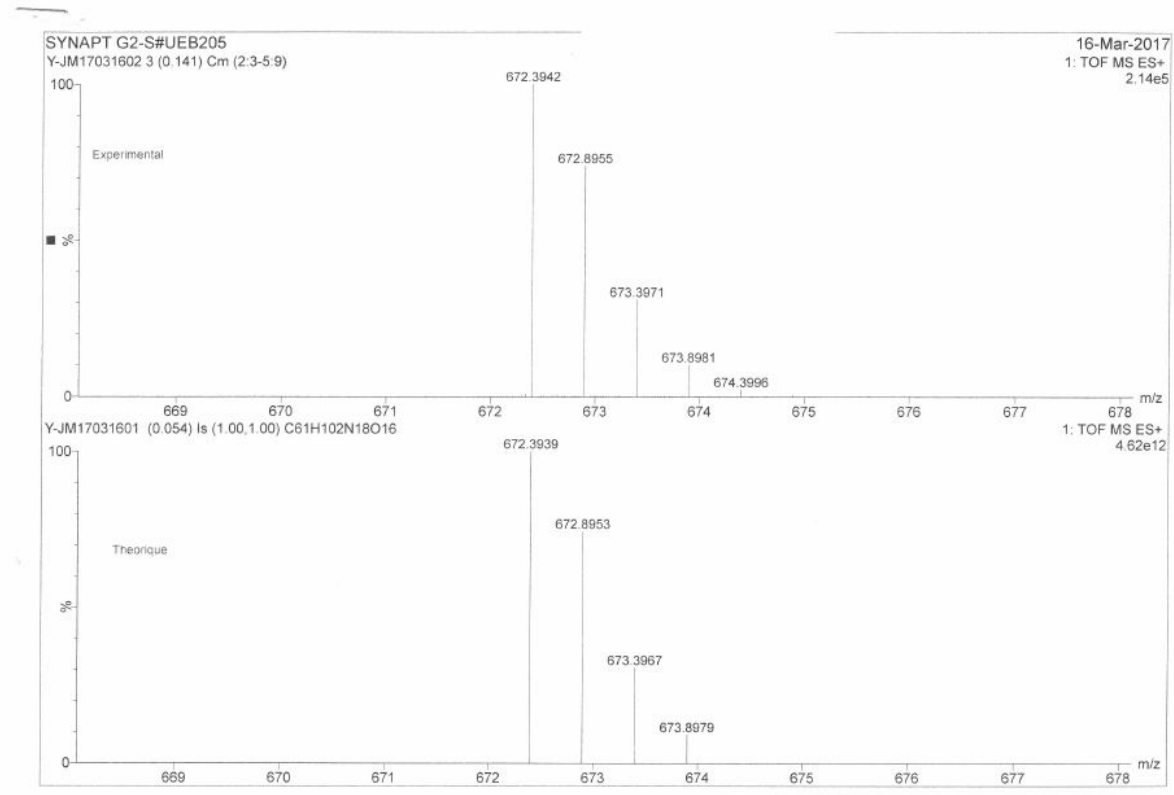

Chart S16. HRMS of **JMV6661**.

II. Characterization of NTS_1 and NTS_2 expressions in HT-29 cells.

Cell line.

The HT-29 human colorectal cancer cell line was cultivated in RPMI 1640 (21875-034 ;Gibco®), supplemented with 10%(v/v) fetal bovine serum (FBS ;10270-106 ;Gibco®), 100µL/mL Penicillin-Streptomycin (15070-063 ; Gibco®) and grown at 37°C in a humidified atmosphere containing 5% CO_2 and protected from light.

Western Blot.

Protein samples (80µg for NTS_1 and 88µg for NTS_2) were denatured for 5 minutes at 90°C and then loaded onto 10% SDS polyacrylamide gels (70V for 30min then 150V for 1h). Following electrophoresis, proteins were transferred onto nitrocellulose membranes (Immobilon®-P) (300mA for 1h30). Membrane was blocked with 5% non-fat milk at room temperature for 1h, and incubated for 1h at room temperature with the following primary antibodies : Anti-NTS_1 (sc-376958; SantaCruz®; 1:25), anti-NTS_2 (PAB0151; Abnova®; 1:400) and anti-actin (A2066; Sigma-Aldrich®) (1:5000). Membranes were subsequently incubated with anti-mouse IgG peroxidase-conjugated secondary antibodies (1:10.000) or anti-Rabbit IgG (111-035-144; Jackson Immunoresearch®) peroxidase-conjugated secondary antibodies (1:10.000), at room temperature for 45min. Finally, the immunoreactive bands of NTS_1 were visualized using ECL Western Blotting detection reagents (RPN2209; GE Healthcare®). Semi-quantitative analysis was conducted using ImageJ (V1.52c) to measure densitometric values for each band.

Immunofluorescence.

Cells were seeded onto glass cover slips and incubated for 24 hours with culture medium. The cells were then rinsed with 2mL of DPBS (14190-094; Gibco®), and fixed with 3% paraformaldehyde for 90 minutes. Before the experiment, cells were rinsed three times during 10 minutes with DPBS. The slides were saturated for 90 minutes with 50µL of PBS/Triton 0,3% (127K0048 ; Sigma-Aldrich®) / BSA 1% (A2153; Sigma-Aldrich®) and then set in the damp chamber overnight with the primary antibody (Anti-NTS_1; 1/500 – anti-NTS_2; 1/100) and PBS/Triton 0.3% / BSA 1%. Cells were then

rinsed three times for 10 minutes with DPBS and then placed in the damp chamber, protected from light, with the secondary antibody (1/500) and 50µL of PBS/Triton 0.3% / BSA 1%. The glass cover slips were rinsed once more with DPBS for three times 10 minutes and then mounted on microscope sliders with Prolonlog (P36931; Invitrogen®) and DAPI (1/5000). A negative control was also included but without the primary antibody. All images obtained were analyzed using ImageJ (V1.52c) software.

III. Radiochemistry

Quality controls of ^{68}Ga-neurotensin analogues developed in this work.

All analogues were subjected to TLC and HPLC analysis before running experiments. Radio-UV-HPLC analysis were performed using a Phenomenex Luna C18 column (4mL/min, λ = 220nm C18; 150mm x 4,6mm x 5µm). HPLC conditions were: 0-2min: 90% ACN (A), 10% water in 0.1%TFA (B), 2-10min: 90%→10% A ; 10%→90% B, 10-12min: 10% A ; 90% B, 12-14min: 10%→90% A; 90%→10% B. The analytical HPLC system used was a JASCO system with ChromNAV software, a PU-2089 Plus quaternary gradient pump, a MD-2018 Plus photodiode array detector and Raytest Gabi Star detector. TLC analysis were also carried out (miniGITA plate reader, acquisition time of 1min, Rf impurities ≤ 0.1, Rf ^{68}Ga-bioconjugates ≥ 0.8 as described in the monograph of the European Pharmacopeia for ^{68}Ga-edoctreotide n°01/2013:2482 corrected 8.6 using methanol/ammonium acetate (1:1) as mobile phase and ITLC-SG as stationary phase. Representative radio-HPLC chromatograms are displayed in Fig S6 below. Representative radio-TLC chromatograms are also displayed in Fig S7.

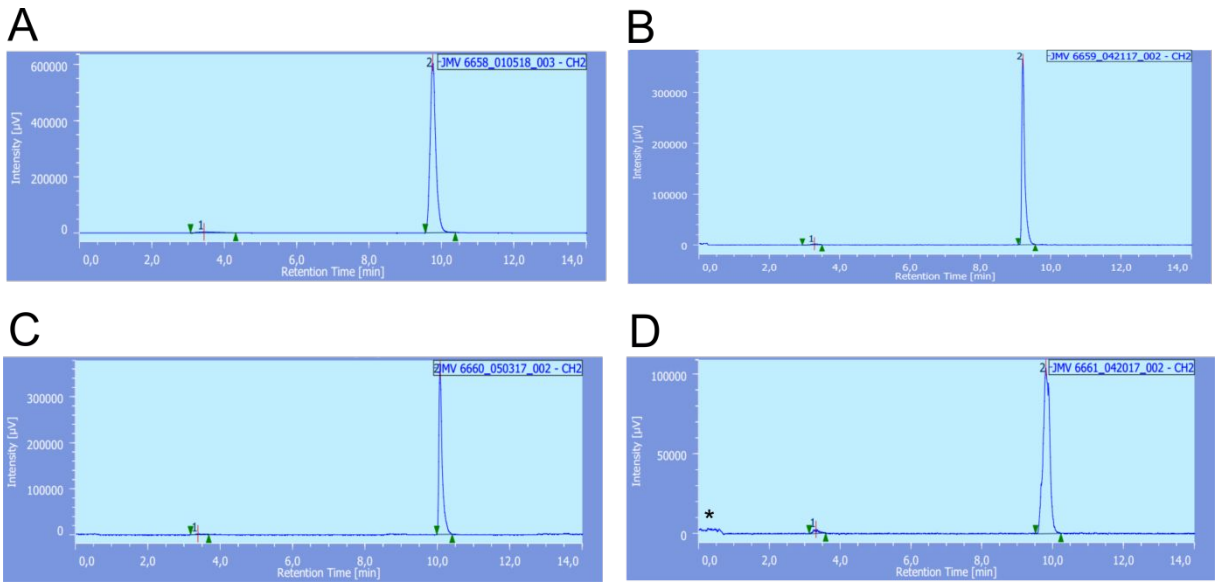

Fig S1: Representative radio-HPLC chromatograms of [^{68}Ga]Ga-JMV6658 (A), [^{68}Ga]Ga-JMV6659 (B), [^{68}Ga]Ga-JMV6660 (C) and [^{68}Ga]Ga-JMV6661 (D). ^{68}Ga-bioconjugates are depicted by peak 2 and impurities by peak 1. In the radio-HPLC chromatogram D, the weak radioactive signal marked "*" between 0 and 0.6 minute is due to the presence of the shielded vial containing the radiolabeled compound closed to the gamma-detector.

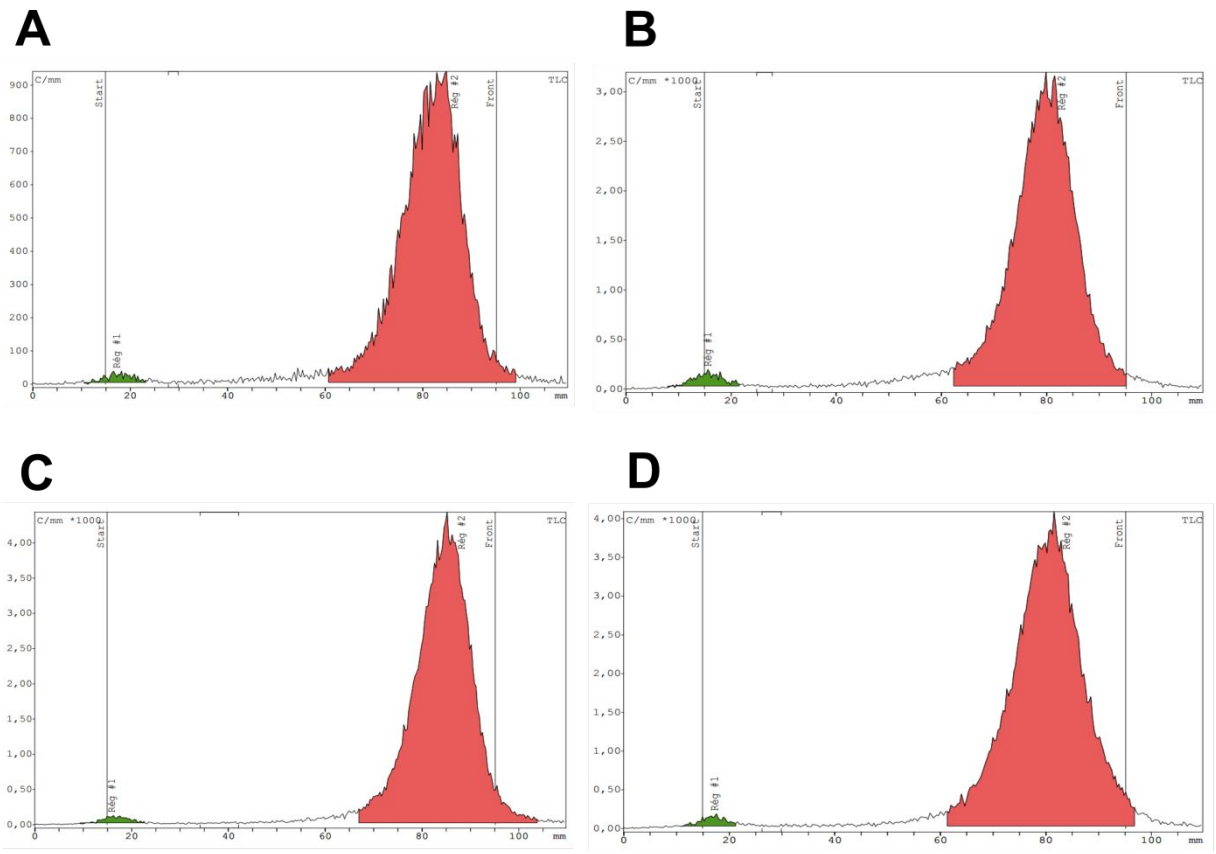

Figure S2: Representative radio-TLC chromatograms of [^{68}Ga]Ga-JMV6658 (A), [^{68}Ga]Ga-JMV6659 (B), [^{68}Ga]Ga-JMV6660 (C) and [^{68}Ga]Ga-JMV6661 (D). Radiolabeled compounds with a retention factor ≤ 0.1 were impurities (marked in green) and ^{68}Ga-bioconjugates developed in this work exhibit a retention factor ≥ 0.8 (marked in red).

Stability of ^{68}Ga-radiolabeling in PBS and in human plasma

Radiochemical purity of the ^{68}Ga-bioconjugates was stable in human PBS at least for 45 min (Fig S8). Moreover, no ^{68}Ga-transchelation was seen in human plasma during the same period of incubation (Fig S9).

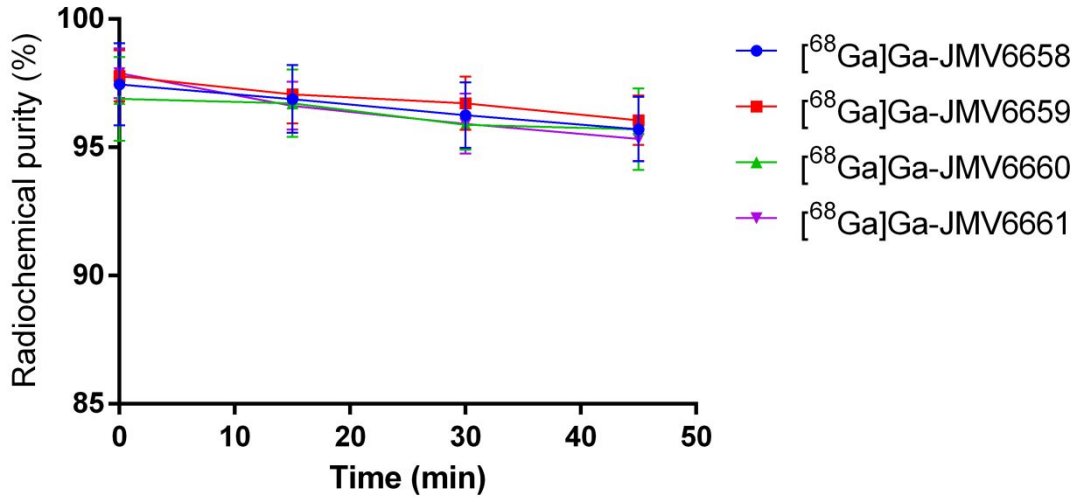

Fig S3: Radiochemical purity of the ^{68}Ga-bioconjugate over time in PBS. All ^{68}Ga-neurotensin analogues remains stable up to 45 min.

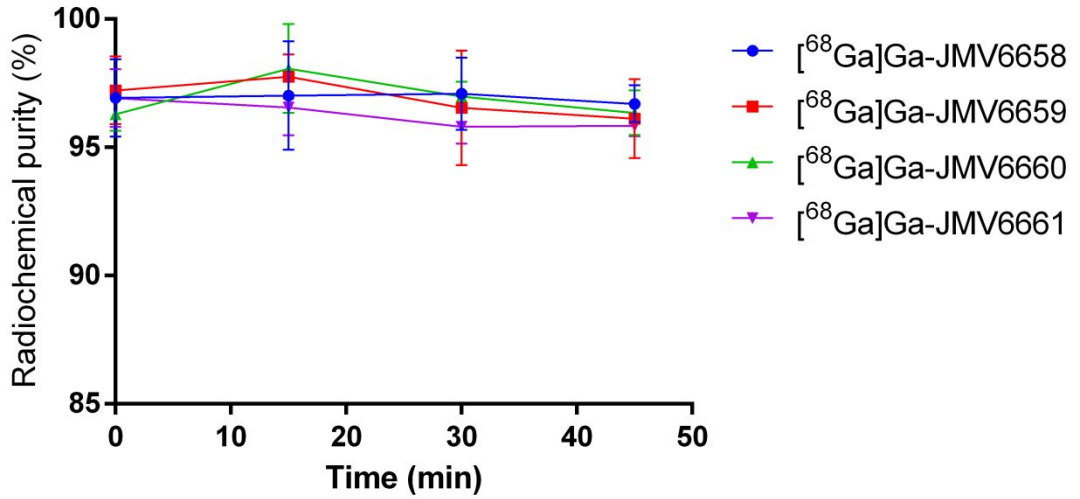

Fig S4: Radiochemical purity of the ^{68}Ga-bioconjugate over time in human plasma. No ^{68}Ga-transchelation was seen over the 45 min of the study.

Table S2: Biodistribution of [^{68}Ga]Ga-JMV6659

	On µPET/CT imaging (%ID/g)								*On sacrificed animals (%ID/g)*		
Organ	5min p.i.	5min p.i. blocked	20min p.i.	20min p.i. blocked	1h p.i.	1h p.i. blocked	2h p.i.	2h p.i. blocked	2h p.i.	2h p.i. blocked 50µg	2h p.i. blocked 180µg
Tumor	3.26 ± 1.81	2.86 ± 1.70	4.19 ± 2.22	2.21 ± 1.32*	4.38 ± 1.96	1.69 ± 1.17*	3.67 ± 1.90	1.32 ± 0.86*	7.80 ± 0.54	3.44 ± 0.56*	1.38 ± 0.71*
Lungs	7.53 ± 1.36	7.54 ± 2.09	3.42 ± 0.65	3.59 ± 0.91	1.07 ± 0.17	1.26 ± 0.55	0.51 ± 0.09	0.40 ± 0.13	0.97 ± 0.82	0.26 ± 0.05	0.17 ± 0.06
Kidney	45.77 ± 9.78	32.17 ± 10.49	32.48 ± 3.47	15.52 ± 3.68*	20.56 ± 4.15	9.62 ± 3.19*	14.67 ± 1.76	7.96 ± 2.62*	19.63 ± 1.57	32.33 ± 7.90	4.39 ± 7.60*
Liver	1.76 ± 0.45	1.48 ± 0.08	0.82 ± 0.22	0.74 ± 0.05	0.37 ± 0.14	0.35 ± 0.05	0.25 ± 0.06	0.25 ± 0.06	0.62 ± 0.41	0.33 ± 0.05	0.20 ± 0.03
Spleen	22.88 ± 9.00	20.21 ± 11.56	10.75 ± 4.26	10.49 ± 6.20	5.35 ± 2.68	4.97 ± 3.32	3.10 ± 1.51	2.55 ± 1.58	7.83 ± 4.39	0.36 ± 0.15*	0.33 ± 0.12*
Intestine	3.26 ± 0.72	2.78 ± 1.03	1.55 ± 0.46	1.60 ± 0.57	1.08 ± 0.65	1.32 ± 0.86	4.02 ± 1.45	3.06 ± 2.34	1.36 ± 0.67	0.85 ± 0.08	0.37 ± 0.06
Pancreas									3.38 ± 2.18	0.13 ± 0.06	0.06 ± 0.02
Colon	3.19 ± 0.20	0.88 ± 0.29	0.74 ± 0.04	0.45 ± 0.15	1.09 ± 0.73	0.41 ± 0.18	1.79 ± 0.42	0.91 ± 0.93	1.01 ± 0.52	0.40 ± 0.24	0.11 ± 0.03
Stomach	3.74 ± 1.87	2.28 ± 0.35	2.03 ± 0.93	1.53 ± 0.42	1.07 ± 0.37	0.83 ± 0.29	0.75 ± 0.18	0.62 ± 0.12	4.71 ± 0.10	0.25 ± 0.20	0.09 ± 0.02
Blood									8.18 ± 1.00	0.14 ± 0.06*	0.09 ± 0.02*
Muscle									1.95 ± 1.32	0.20 ± 0.24	0.03 ± 0.01
Brain	1.42 ± 0.12	1.04 ± 0.24	0.73 ± 0.01	0.55 ± 0.12	0.23 ± 0.02	0.18 ± 0.07	0.11 ± 0.01	0.07 ± 0.02	0.72 ± 1.24	0.09 ± 0.03	0.03 ± 0.02
Tumor/blood									0.98 ± 0.05	25.12 ± 10.01	14.88 ± 5.70
Tumor/liver	1.80 ± 0.70	1.98 ± 1.26	3.68 ± 1.24	3.09 ± 2.00	7.49 ± 2.26	4.99 ± 3.69	13.49 ± 2.98	6.11 ± 5.58	15.45 ± 6.80	10.71 ± 0.73	6.70 ± 2.60
Tumor/muscle									5.22 ± 2.84	9.38 ± 1.51	50.17 ± 18.33
Tumor/kidney	0.08 ± 0.06	0.10 ± 0.08	0.10 ± 0.05	0.14 ± 0.07	0.18 ± 0.08	0.16 ± 0.06	0.25 ± 0.14	0.16 ± 0.07	0.40 ± 0.01	0.14 ± 0.06	0.11 ± 0.05

* indicate a significant difference. Blood and muscle were not analyzable on µPET/CT images due to their very small volumes. Pancreas was not clearly visible on images as CT was not injected.

Binding to plasma protein.

The binding of [^{68}Ga]Ga-JMV6659 to human plasma protein was investigated using Amicon-4-ultra filter according to manufacturer's instructions. Briefly, 3.7MBq were added to 0.5mL of human plasma with or without 1µM of neurotensin or levocabastine to determine receptor specificity and incubated 60 min at 37°C. After centrifugation, fractions were separated and γ-counted. Results are expressed in mean ± SD of radioactivity added of two independent experiments.

Table S3. Ex vivo plasma protein binding of [^{68}Ga]Ga-JMV6659

Analogue	Total binding	NTS_1-blocked	NTS_2-blocked
[^{68}Ga]Ga-JMV6659	21.04±3.15	22.83±1.08	20.29±2.45

IV. References

1. René, A., Vanthuyne, N., Martinez, J. and Cavelier, F. (2013) (L)-(Trimethylsilyl)Alanine Synthesis Exploiting Hydroxypinanone-Induced Diastereoselective Alkylation. *Amino Acids 45,* 301-307.

PARTIE II : ciblage du récepteur Y_1 du neuropeptide Y

Chapitre 1 : Contexte.

a) Le neuropeptide Y

Le neuropeptide Y (NPY) est un peptide de 36 acides aminés (AA) dont la séquence est présentée **Figure 9**. Il tient son nom de sa richesse en Tyrosine (Y)[86].

Tyr-Pro-Ser-Lys-Pro-Asp-Asn-Pro-Gly-Glu-Asp-Ala-Pro-Ala-Glu-Asp-Leu-Ala-Arg-Tyr-Tyr-Ser-Ala-Leu-Arg-His-Tyr-Ile-Asn-Leu-Ile-Thr-Arg-Gln-Arg-Tyr-NH_2

Figure 9 : Séquence peptidique du neuropeptide Y

Par ailleurs, NPY comporte de nombreux sites de clivage ce qui en fait une molécule à demi-vie courte in vivo (**Figure 10**).

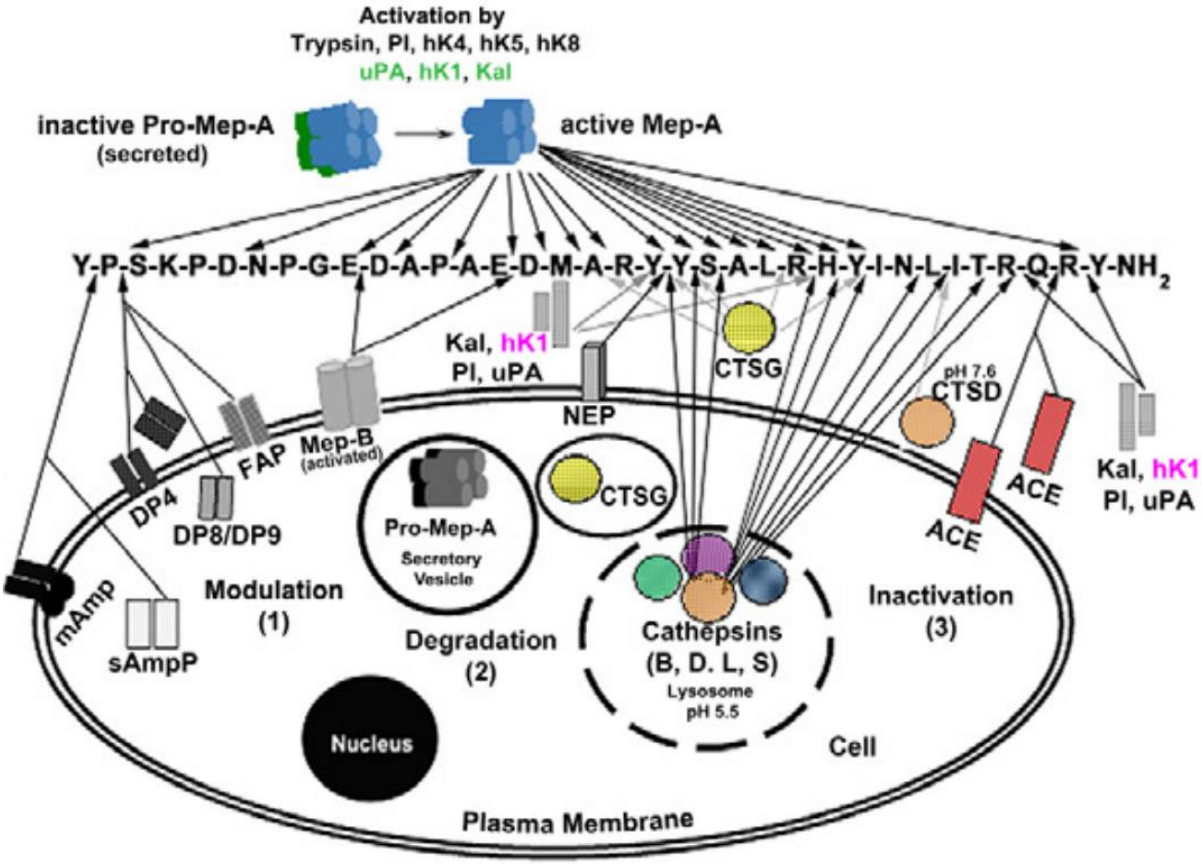

Figure 10 : Endopeptidases impliquées dans le clivage du NPY et sites de clivage (d'après Wagner et al. Journal of neurochemistry, 2015[87]).

PYY (peptide YY) et PP (pancreatic polypeptide), comme NPY, ont 36 AA. Bien que ces peptides aient une séquence d'AA différente, ils présentent des similitudes structurelles. NPY et PYY présentent près de 70% d'homologie entre eux et ces deux peptides ont environ 50% de similitudes avec PP. Ainsi, NPY, PYY et PP ont été classés dans une famille d'hormones homologues[86].

Depuis, il s'est avéré que NPY est l'un des peptides les plus largement distribués dans le système nerveux central et périphérique des mammifères. Il a également été retrouvé dans plusieurs organes, notamment le système gastro-intestinal, les glandes salivaires, la glande thyroïde, le pancréas, le système urogénital, les voies respiratoires et le cœur.

Au niveau central, NPY est impliqué dans la régulation du comportement alimentaire et de l'homéostasie anergique, ainsi que dans l'inhibition de l'anxiété[88].

En périphérie, le NPY joue un rôle dans la vasomotricité en réponse aux stimulations adrénergiques. Il a également un effet stimulant sur la croissance des cellules musculaires lisses humaines, de rat et de porc[89].

b) Les récepteurs du neuropeptide Y

Les actions de NPY sont médiées par des récepteurs, dont 5 sous-types ont été trouvés chez l'homme : Y_1R, Y_2R[90], Y_4R[91], et Y_5R. Les récepteurs Y_1R, Y_2R, Y_4R, et Y_5R sont bien caractérisés et leur expression physiologique a été démontrée[92]. Ils ont notamment été retrouvés au niveau du cerveau, de la rate, des membranes intestinales et des cellules musculaires lisses aortiques[93].

De nombreux travaux ont étudié l'interaction NPY/Y_1R (**Figure 11**) et ont démontré l'importance des extrémités N et C-terminales du peptide[94,95], ainsi que l'importance de plusieurs acides aminés (dont Pro2, Pro5, Arg19 et Tyr20). Les acides aminés des positions 27 à 36 notamment, se sont révélés indispensables, en particulier la position 27. Les arginines en positions 33 et 35 se sont également avérées extrêmement importantes, ainsi que la fonction Tyr36-amide N-terminale[96,97,98].

Au niveau de Y_1R, Asp2.68 et Asp6.59 sont également importants pour la liaison de NPY au récepteur car le peptide perd de son affinité lorsqu'ils sont mutés en Ala[99,100,101,102]. En outre, Asp6.59 se lie à l'Arg35 de pNPY, et il s'agit de la première interaction démontrée pour ce récepteur[103].

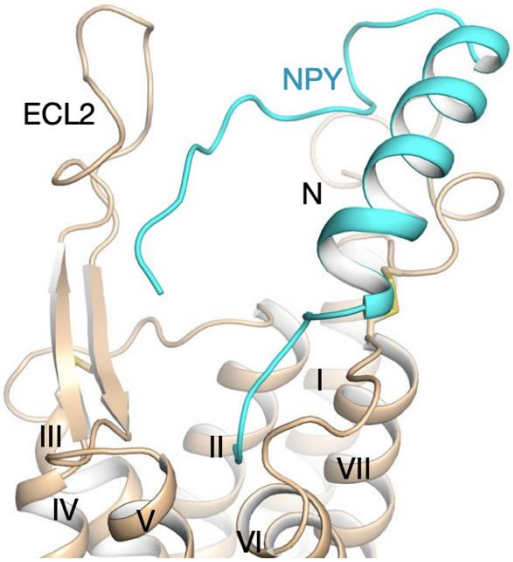

Figure 11 : Modélisation de la liaison NPY-Y_1R (d'après Yang et al, Nature 2018[104])

Sur le plan fonctionnel, les récepteurs du NPY (NPYR) appartiennent à la super famille des récepteurs couplés aux protéines G (RCPG). Ces récepteurs agissent en transmettant le signal provoqué par la liaison de NPY, à un complexe intracellulaire lié à la GTP. Ce complexe de protéines G active alors plusieurs systèmes de second messagers différents qui à leur tour induiront une diminution de l'AMP cyclique et une augmentation du calcium intracellulaire[93].

La stimulation des récepteurs de NPY activera différentes voies de signalisation intracellulaire selon leur localisation. Par exemple, lorsque Y_1R est activé au niveau de l'épithélium intestinal, la sous unité beta-gamma de la protéine Gq activera la voie des MAP kinases[105], alors que son activation au niveau des précurseurs neuronaux va stimuler leur prolifération via une cascade intracellulaire impliquant la protéine kinase C (PKC) et ERK1/2 (extracellular regulated kinase 1/2). Une voie similaire impliquant ERK1/2 mais dépendant de la phosphoinositide 3-kinase (PI_3K) induit l'hypertrophie des cardiomyocytes[106].

Concernant les différents sous-types de récepteurs, NPY a une affinité de l'ordre du nanomolaire pour Y_1R et Y_2R et leur activation est suivie d'une internalisation du récepteur, alors que l'activation de Y_5R n'induit pas d'internalisation[107].

Les différents sous-types de récepteurs se trouvent dans différents types de tissus et leurs rôles diffèrent. Le sous-type de NPYR d'intérêt dans notre travail est Y_1R.

Chez l'homme, Y_1R est retrouvé dans les cellules musculaires lisses vasculaires, le cortex cérébral, le côlon et les adipocytes[108]. Parmi les effets rapportés, on note une vasoconstriction,

l'anxiolyse/sédation, la régulation de la croissance de l'épithélium colique humain ainsi qu'un rôle dans l'induction de la prise alimentaire (faisant également intervenir Y_5R)[109].

L'un des mécanismes impliqués dans la régulation du système NPY/récepteur Y est l'internalisation du récepteur. Il a été démontré qu'Y_1R a une cinétique d'internalisation rapide. Les taux d'internalisation sont spécifiques à chaque sous-type et non affectés par la dimérisation du sous-type de récepteur ou par la lignée cellulaire qui l'exprime. La différence de structure des récepteurs explique la différence entre les taux d'internalisation, en effet Y_5R a une troisième boucle intracellulaire très longue et une extrémité C-terminale très courte comparée aux Y_1R, Y_2R et Y_4R qui ont des taux d'internalisation beaucoup plus rapides. Par ailleurs, l'internalisation de Y_1R et Y_2R n'est induite que lorsqu'ils sont stimulés par des agonistes et non pas en présence d'antagonistes[107].

c) Les récepteurs du NPY en oncologie

Les récepteurs du NPY sont particulièrement intéressants pour les perspectives de ciblage tumoral car l'expression de Y_1R et Y_2R a été observée dans les carcinomes du sein, des glandes surrénales et les tumeurs apparentées (carcinomes corticosurrénaux, phéochromocytome et paragangliomes), ainsi que les cancers du rein et le cancer de l'ovaire[110]. Les récepteurs de NPY ont également été retrouvés dans les tumeurs de haut grade du système nerveux central[111].

Les NPYR ont été signalés pour la première fois dans les cancers du sein en 2001 par Reubi et al. : 89 échantillons de tissus cancéreux (dont 69 carcinomes canalaires et 12 carcinomes lobulaires) ont été analysés et comparés à 45 échantillons de tissus non néoplasiques. Les NPYR ont été exprimés dans 76/89 (85%) des carcinomes du sein testés, plus précisément dans 61/69 carcinomes canalaires (58/64 invasifs et 3/5 in situ) et 10/12 carcinomes lobulaires. Y_1R a été retrouvé dans 100% des échantillons néoplasiques positifs aux récepteurs, tandis que Y_2R n'a été trouvé que dans 24% des tumeurs positives aux récepteurs. Dans 58 des 76 (76%) tumeurs positives au récepteur, Y_1R s'est avéré être le seul ou le sous-type de récepteur prédominant exprimé. Notamment, lorsqu'Y_2R était exprimé dans les tumeurs, il était invariablement associé à Y_1R. Un groupe supplémentaire de 6 patients a été analysé (pour lesquels des tumeurs primaires du sein et toutes les métastases ganglionnaires lymphatiques ont été obtenues), et Y_1R a été retrouvé dans toutes les tumeurs primaires ainsi que toutes les métastases. Concernant les 45 échantillons de tissus non néoplasiques, des NPYR ont été trouvés dans 45/45 (100%) des échantillons. Dans 42% des cas, Y_2R a été exprimé seul, tandis que dans les 58% restants des échantillons Y_1R et Y_2R ont été exprimés de manière concomitante. Cela suggère qu'Y_1R a un rôle fonctionnel potentiel dans la prolifération des

cellules tumorales, et au vu de sa densité élevée et son incidence élevée dans le cancer du sein, il pourrait représenter une cible importante pour les analogues de NPY.

Dans le carcinome rénal (CR), des récepteurs de NPY ont été trouvés dans 14/24 (56%) des échantillons analysés, parmi lesquels 67% des CR sont de type à cellules claires, dont un avec différenciation sarcomateuse focale. Cependant, les trois CR chromophobes et papillaires n'exprimaient pas le NPYR. Le seul sous-type de NPYR exprimé par les CR s'est avéré être Y_1. Des NPYR ont été trouvés dans 80% des néphroblastomes analysés (8/10 échantillons) et observés dans les trois composants tissulaires (différenciation blastémale, mésenchymateuse et épithéliale), dans certains cas, même simultanément[112].

Sur 43 tumeurs ovariennes analysées, 7/22 adénocarcinomes exprimaient NPYR, et 10/14 tumeurs cordo-stromales sexuelles exprimaient NPYR (dont 0/4 fibromes/fibrothécomes exprimaient NPYR), aucun des adénomes (3), tumeurs borderline (3) ou des tumeurs de cellules germinales (1) se sont révélées exprimer le NPYR. Les sous-types de récepteurs Y_1R et Y_2R ont été trouvés, souvent exprimés de manière concomitante dans des tumeurs individuelles[113].

Des études, menées sur les trois différentes lignées cellulaires de cancer de la prostate humaines LNCaP (androgéno-dépendantes), DU145 et PC3 (androgéno-indépendantes), indiquent que le gène et la protéine Y_1R sont exprimés dans tous ces clones[114,115], alors que seules les cellules PC3 expriment Y_2R. Les actions du NPY sur les cellules de cancer de la prostate sont spécifiques de la prolifération cellulaire, car il a été rapporté qu'elle n'a aucun effet sur l'invasion et la migration in vitro des cellules PC3, LNCaP et DU145[116]

Les récepteurs du NPY s'avèrent donc être des cibles attractives en oncologie et de multiples analogues radiomarqués du NPY ont été développés pour des perspectives de ciblage tumoral.

d) Analogues radiomarqués de NPY ciblant Y_1R

Trois stratégies principales ont été développées pour développer des analogues innovants du NPY : la création d'analogues non peptidiques, d'antagonistes peptidiques tronqués ou d'agonistes peptidiques entiers.

Parmi les analogues non peptidiques le BIBP3226 (**Figure 12**) est particulièrement intéressant : il s'agit d'un antagoniste spécifique et ayant une très bonne affinité pour Y_1R[117].

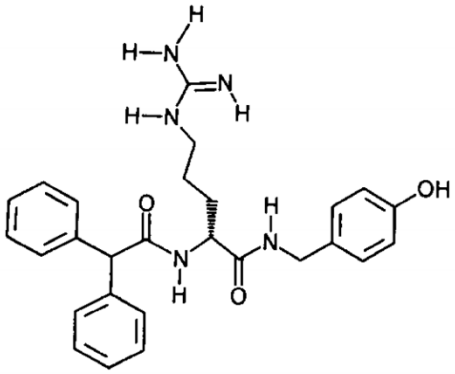

Figure 12 : BIBP3226

Cet analogue non peptidique a ensuite été modifié et radiomarqué au Fluor-18 pour donner l'analogue (R)-N^{α}-(2,2-diphenylacetyl)-N^{ω}-[4-(2-[^{18}F]-fluoropropanoylamino)butyl] aminocarbonyl-N-(4-hydroxybenzyl)-argininamide ou [^{18}F]F-**23** (**Figure 13**)[118] qui, malgré une accumulation au niveau de la vésicule biliaire, a pu être employé pour une imagerie TEP de tumeurs MCF-7 (carcinome mammaire exprimant Y_1R) chez des souris nude.

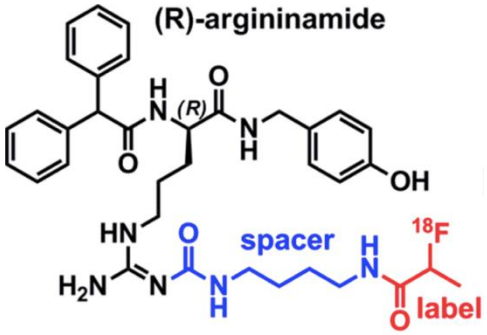

Figure 13 : [^{18}F]F-**23**

Le développement d'analogues peptidiques tronqués a été motivé par une synthèse chimique plus simple que celle des analogues entiers et une plus grande facilité pour introduire des modifications afin d'améliorer la stabilité métabolique du peptide. Ainsi on peut citer le [Pro^{30}, Tyr^{32}, Leu^{34}]NPY(28-36)NH_2 ou BVD15 (**Figure 14**)[119] qui a une forte affinité pour Y_1R et à partir duquel le [Lys (Pip-Ga-DOTA) 4, Bip5]BVD15 (ou CCZ01055 **Figure 15**) a été synthétisé. Le CCZ01055 a une bonne affinité pour Y_1R (K_i de 23,4 ± 9 nM) cependant sa faible stabilité plasmatique (14% à 1h), clairance rapide avec accumulation intravésicale à 1h

post-injection (captation rénale >10 %ID/g à 5 min), et faible captation tumorale (0,98 ± 0,21 %ID/g) le rendent peu adapté à la pratique clinique[120].

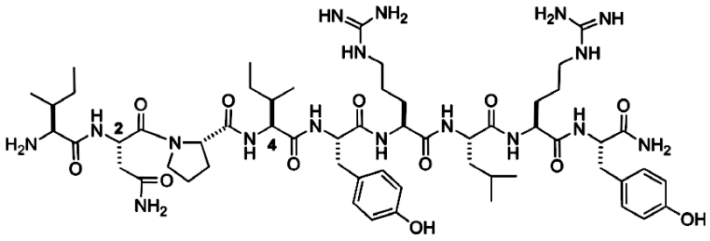

Figure 14 : BVD15

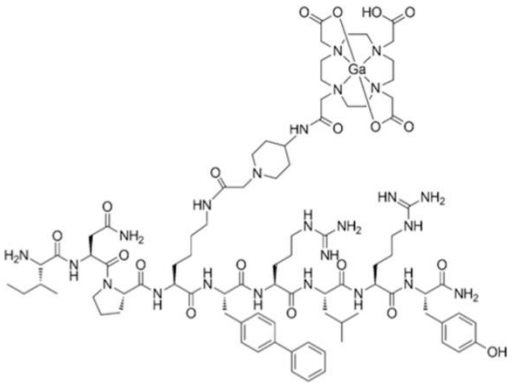

Figure 15 : CZ01055

Le [F^7,P^{34}]-NPY est un agoniste peptidique entier avec une affinité subnanomolaire pour Y_1R[121]. Cet analogue a été glycosylé pour donner le [^{18}F][Pra(F-Glc), F^7,P^{34}]-NPY ([^{18}F]F-3b) qui a une EC_{50} de 8,51 ± 0,10 nM et une IC_{50} de 8,63 ± 0,09 nM pour Y_1R. Son injection chez des souris nude porteuses de xénogreffes MCF-7 a permis de déterminer que cet analogue avait une élimination rénale rapide avec une captation rénale de 29,55 ± 9,65 %ID/g à 2h post injection versus 62,45 ± 4,93 %ID/g à 20min post injection, et une captation tumorale de 1,8 %ID/g à 20 min post-injection et 0,7 %ID/g à 2h post injection[122].

Y_1R est particulièrement intéressant du fait de son internalisation cellulaire et du ciblage effectué principalement par des agonistes. Il nous a donc paru utile dans le développement d'analogue du NPY ciblant Y_1R de doter ces radiopharmaceutiques de radioéléments à faible parcours et fort dépôt d'énergie locale, comme c'est le cas pour certains émetteurs Auger.

Parmi les radionucléides pouvant être potentiellement employés en RIV, le Terbium 161 (^{161}Tb) suscite plus particulièrement l'intérêt de la communauté scientifique du fait de son spectre d'émission β^- et de l'émission concomitante d'électrons d'Auger. Müller et al. ont été

les premiers à employer des molécules radiomarqués par ^{161}Tb dans le cadre d'études précliniques sur souris porteuses de xénogreffes tumorales[123]. Un meilleur effet thérapeutique avec le ^{161}Tb par rapport à celui obtenu avec le ^{177}Lu a été décrit dans 3 études précliniques indépendantes utilisant pour la première un ciblage tumoral par folate et pour la 2ème un ciblage par un anticorps anti L1CAM et pour la troisième un ciblage par le PSMA[124,125,126]. De plus, bien que la dose déposée au niveau tumoral et l'effet thérapeutique soient supérieur au ^{177}Lu, cela ne s'accompagne pas d'un excès de toxicité[127]. Les électrons Auger semblent être favorables à des fins thérapeutiques, mais la supériorité clinique du ^{161}Tb sur ^{177}Lu reste à évaluer. Deux études in silico concluent en faveur du ^{161}Tb dans le cas d'un ciblage de micro-métastases. En effet, la dose déposée par le ^{161}Tb (en considérant 1 MeV libéré par µm^3) est 1,8 fois plus élevée que celle délivrée par le ^{177}Lu dans une micrométastase de 100 µm et 3,6 fois plus élevée que le ^{177}Lu dans une cellule de 10 µm. Le ^{161}Tb dépose une plus grande quantité d'énergie par MeV que ^{177}Lu sur une distance de 30 µm. Ainsi, le ^{161}Tb délivrerait probablement une dose plus élevée que le ^{177}Lu, non seulement à la cellule ciblée, mais également à ses voisins immédiats[128]. À l'échelle de la cellule tumorale isolée, le terbium délivre une dose d'énergie supérieure à celle délivrée par le ^{177}Lu au noyau de la cellule, quelle que soit sa localisation (membranaire ou nucléaire), avec toutefois une plus forte potentialisation lorsque la localisation est nucléaire[129]. Il est donc particulièrement intéressant d'employer le ^{161}Tb avec des analogues pouvant atteindre le noyau des cellules tumorales ciblées afin de déposer un maximum d'énergie au plus proche de l'ADN cellulaire.

Les objectifs de ce travail sont l'évaluation d'un analogue peptidique du neuropeptide Y pour adresser les radiolanthanides à visée thérapeutique (et plus particulièrement le ^{161}Tb riche en émissions Auger) au noyau de cellules surexprimant naturellement le récepteur Y_1 humain (Y_1R) à l'aide d'une séquence d'adressage nucléaire et d'un site de clivage par la cathepsine B pour permettre l'échappement de l'endosome après internalisation. Ce projet a bénéficié d'un financement local TRAIL et a été réalisé en collaboration avec le Pr Annette Beck-Sickinger (Université de Leipzig, Allemagne, en charge de la synthèse chimique), du Centre des Biologie des Membranes et Nano-Objets (Dr Isabel Alves, Université de Bordeaux, en charge des expérimentations PWR), de l'accélérateur AIFIRA de l'Université de Bordeaux (Dr Philippe Barberet, pour la réalisation des expériences PIXE) et du CERIMED (Université Aix-Marseille, Pr B. Guillet), en charge des expérimentations in vivo.

Chapitre 2 : Résumé Article 2

Introduction : Le ciblage des récepteurs couplés aux protéines G à la surface des cellules cancéreuses avec des ligands peptidiques est un concept prometteur pour l'administration sélective aux tumeurs de cargaisons thérapeutiquement actives, y compris des radiométaux pour la radiothérapie interne vectorisée (RIV). Récemment, le radiolanthanide terbium-161 (^{161}Tb) a suscité un intérêt significatif pour les applications en RIV, car il se désintègre avec un rayonnement β de moyenne énergie mais émet également une quantité importante d'électrons de conversion et Auger avec une courte plage de pénétration tissulaire. L'efficacité thérapeutique des radiométaux émettant des électrons Auger, comme le ^{161}Tb, peut donc être fortement augmentée par une délivrance subcellulaire supplémentaire dans le noyau, afin de faciliter le dépôt de dose maximale au niveau de l'ADN. Il est possible d'adresser un peptide dans le noyau d'une cellule à l'aide d'une séquence d'adressage nucléaire (Nuclear Localisation Sequence ou NLS).

Dans cette étude, nous décrivons la conception d'un conjugué multifonctionnel radiomarqué, du neuropeptide-Y (NPY), pour adresser les radiolanthanides au noyau de cellules surexprimant naturellement le récepteur Y_1 humain (hY_1R). En utilisant la synthèse peptidique en phase solide, l'analogue [F^7,P^{34}]-NPY (ciblant hY_1R) a été modifié avec un acide gras, un espaceur clivable par la cathepsine B, suivi d'une séquence d'adressage nucléaire (NLS, PKKKRKV), et un chélateur (DOTA) pour obtenir le composé pb12. Dans cette étude de validation de principe, le marquage a été effectué soit avec du terbium-159 natif (^{nat}Tb), comme substitut de ^{161}Tb, soit avec de l'indium-111 (^{111}In). Les résultats qui ont fait l'objet d'une publication récente dans EJNMMI Research (article complet Partie II, Chapitre 4) sont résumés et discutés ci-après.

Résultats : Le composé [^{nat}Tb]Tb-pb12 a montré une forte affinité (K_D 3 ± 3,7 nM) pour hY_1R endogène sur les cellules MCF-7 et était capable d'induire l'activation du récepteur hY_1R et une internalisation similaire à l'agoniste de référence [F^7,P^{34}]-NPY. Une internalisation spécifique du conjugué marqué au ^{111}In dans des cellules MCF-7 a été observée (atteignant un maximum de 32 ± 9,7 % d'internalisation à 4h), et surtout, l'internalisation nucléaire en fonction du temps de ^{111}In-Pb12 a été démontrée (avec une fraction nucléaire de 24,1 %). L'incubation avec un inhibiteur de la cathepsine B a causé une diminution significative de l'internalisation nucléaire (p<0,01). L'étude in vitro de la stabilité métabolique a montré que le peptide n'est pas suffisamment stable dans le plasma humain. En effet il ne restait que 20 % de peptide intact après 1h d'incubation à 37°C. Ceci a été confirmé par l'injection de [^{111}In]In-

pb12 chez des souris nude portant une xénogreffe MCF-7 qui a montré une captation tumorale spécifique à 12 minutes après injection avec un ratio tumeur/muscle significatif (p=0,001), mais sans renforcement du signal au-delà en raison de la dégradation du peptide circulant.

Conclusion : Le conjugué NPY multifonctionnel avec une unité DOTA-NLS libérable représente un concept prometteur pour une RIV améliorée avec des radiolanthanides émetteurs d'électrons Auger. Notre recherche se concentre maintenant sur l'amélioration de la stabilité plasmatique de ce conjugué prometteur ciblant Y_1 et dotés de fonctionnalité d'adressage nucléaire.

Chapitre 3 : Discussion sur ciblage de Y_1R

Dans ce travail, nous avons cherché à explorer la faisabilité de la RIV plus finement ciblée, capable de délivrer un émetteur d'électrons Auger comme le ^{161}Tb, dans le noyau de tumeurs surexprimant Y_1R. L'objectif est l'étude des caractéristiques radiopharmacologiques du composé pb12 qui possède une séquence NLS liée à un chélateur DOTA pour véhiculer le terbium dans le noyau à l'aide d'importines intra-cytoplasmiques[130]. Le marquage de cet analogue au ^{nat}Tb entraîne une diminution de son affinité pour Y_1R d'un log. Il a également été radiomarqué avec du ^{111}In comme «substitut » des lanthanides, et son affinité pour Y_1R était nettement supérieure (Kd = 5,1 ± 3,5 nM). La différence d'affinité entre la version marquée au ^{111}In de pb12 et son homologue au ^{nat}Tb illustre la nécessité de déterminer soigneusement l'affinité des composés métallisés pour l'imagerie et la thérapie[131]. L'affinité du [^{111}In]In-pb12 est du même ordre de grandeur que les peptides entiers[122] ou les composés non peptiques[118], voir même meilleurs que les peptides tronqués[120]. L'[^{111}In]In-pb12 a montré une internalisation spécifique dépendant du temps atteignant 30% de la liaison totale correspondant au maximum de la capacité d'internalisation de hY_1R, reflétant le comportement agoniste entier de [^{111}In]In-pb12[132]. Cet analogue a montré également sa capacité à atteindre le noyau grâce à la séquence NLS qui est libérée après le clivage par la cathepsine B intra-endosomale. Une autre exigence pour les radiopeptides employés en RIV est leur faible d'efflux assurant ainsi une rétention tumorale maximale. En effet, un efflux élevé entraînerait une irradiation sous-optimale des cellules tumorales, en particulier avec des particules à courte portée, et une administration de dose hors cible plus élevée. [^{111}In]In-pb12 a démontré un efflux élevé qui n'a pas été inhibé par l'inhibiteur d'efflux probénécide. Cet efflux est probablement surestimé, dû à l'association du peptide avec la membrane cellulaire puisque le pb12 interagit avec les lipides membranaires d'une manière non spécifique. Cependant le [^{111}In]In-pb12 est rapidement métabolisé ex-vivo dans du plasma humain ce qui a été confirmé après l'injection de cet analogue chez des souris nude porteuse d'une xénogreffe MCF-7. Il est donc nécessaire d'améliorer la stabilité plasmatique de ce composé pour le ciblage tumoral. Ce concept d'amener un émetteur Auger au plus près du noyau est retrouvé chez des analogues ciblant d'autres récepteurs, par exemple SST_2[133]. Il s'agit donc d'un concept très intéressant qui pourra être appliqué à de nombreux analogues peptidiques en oncologie. Une dernière limite à ce travail est pour l'instant la faible disponibilité du terbium 161 dans le monde. Toutefois, l'intérêt grandissant pour ce radioélément a amené plusieurs équipes européennes à s'intéresser à des moyens de production à grande échelle.

Chapitre 4 : Article 2

Design, synthesis, and biological evaluation of a multifunctional neuropeptide-Y conjugate for selective nuclear delivery of radiolanthanides

Chastel et al. EJNMMI Research (2020) 10:16
https://doi.org/10.1186/s13550-020-0612-8

EJNMMI Research

ORIGINAL RESEARCH Open Access

Design, synthesis, and biological evaluation of a multifunctional neuropeptide-Y conjugate for selective nuclear delivery of radiolanthanides

Adrien Chastel[1,2,3], Dennis J. Worm[4], Isabel D. Alves[5], Delphine Vimont[2,3], Melina Petrel[6], Samantha Fernandez[7,8], Philippe Garrigue[7,8], Philippe Fernandez[1,2,3], Elif Hindié[1,2,3], Annette G. Beck-Sickinger[4] and Clément Morgat[1,2,3*]

Abstract

Background: Targeting G protein-coupled receptors on the surface of cancer cells with peptide ligands is a promising concept for the selective tumor delivery of therapeutically active cargos, including radiometals for targeted radionuclide therapy (TRT). Recently, the radiolanthanide terbium-161 (^{161}Tb) gained significant interest for TRT application, since it decays with medium-energy β-radiation but also emits a significant amount of conversion and Auger electrons with short tissue penetration range. The therapeutic efficiency of radiometals emitting Auger electrons, like ^{161}Tb, can therefore be highly boosted by an additional subcellular delivery into the nucleus, in order to facilitate maximum dose deposition to the DNA. In this study, we describe the design of a multifunctional, radiolabeled neuropeptide-Y (NPY) conjugate, to address radiolanthanides to the nucleus of cells naturally overexpressing the human Y_1 receptor (hY_1R).
By using solid-phase peptide synthesis, the hY_1R-preferring [F^7,P^{34}]-NPY was modified with a fatty acid, a cathepsin B-cleavable linker, followed by a nuclear localization sequence (NLS), and a DOTA chelator (compound pb12). In this proof-of-concept study, labeling was performed with either native terbium-159 (^{nat}Tb), as surrogate for ^{161}Tb, or with indium-111 (^{111}In).

Results: [^{nat}Tb]Tb-pb12 showed a preserved high binding affinity to endogenous hY_1R on MCF-7 cells and was able to induce receptor activation and internalization similar to the hY_1R-preferring [F^7,P^{34}]-NPY. Specific internalization of the ^{111}In-labeled conjugate into MCF-7 cells was observed, and importantly, time-dependent nuclear uptake of ^{111}In was demonstrated. Study of metabolic stability showed that the peptide is insufficiently stable in human plasma. This was confirmed by injection of [^{111}In]In-pb12 in nude mice bearing MCF-7 xenograft which showed specific uptake only at very early time point.

Conclusion: The multifunctional NPY conjugate with a releasable DOTA-NLS unit represents a promising concept for enhanced TRT with Auger electron-emitting radiolanthanides. Our research is now focusing on improving the reported concept with respect to the poor plasmatic stability of this promising radiopeptide.

Keywords: ^{161}Tb, Neuropeptide-Y, Sub-cellular delivery, Auger-emitter, Breast cancer

* Correspondence: clement.morgat@u-bordeaux.fr; clement.morgat@chu-bordeaux.fr
[1]Department of Nuclear Medicine, University Hospital of Bordeaux, F-33076 Bordeaux, France
[2]University of Bordeaux, INCIA UMR 5287, F-33400 Talence, France
Full list of author information is available at the end of the article

Background

Targeted radionuclide therapy (TRT) uses radioisotopes linked to a vector (peptides, small molecules, antibodies, and other targeting agents) in order to target tumor cells or their natural environment and deliver cytotoxic radiations. Encouraging results have been obtained in metastatic neuro-endocrine tumors with [^{177}Lu]Lu-DOTATATE, a somatostatin analog radiolabeled with lutetium-177 (^{177}Lu), that targets SST_2R, the somatostatin receptor subtype 2 [1]. Similar success is envisioned with ^{177}Lu-labeled prostate specific membrane antigen (PSMA) inhibitors in patients with castration-resistant metastatic prostate cancer [2]. However, about 20% of these patients will not respond to therapy or rapidly relapse with re-growth of micrometastases [2]. It is therefore necessary to increase toxicity of TRT to tumor cells. Modeling studies have identified terbium-161 (^{161}Tb) as a potential alternative to ^{177}Lu to deliver higher cytotoxic radiation doses without kidney damage [3]. ^{161}Tb is a radiolanthanide that is chemically similar to ^{177}Lu but is expected to outperform ^{177}Lu due to its emission spectra rich in Auger electrons [4, 5]. Recent preclinical findings confirm the higher tumor control of [^{161}Tb]Tb-PSMA compared with [^{177}Lu]Lu-PSMA [6, 7]. Due to the short range of Auger electrons (few micrometers), the efficacy of such Auger-electron emitters can be maximized if located inside or close to the nucleus. A nuclear delivery of ^{161}Tb after cellular internalization could therefore significantly increase the dose deposited to the genomic DNA and enhance the cancer cell-killing effect of this radiolanthanide [8].

Our team works on improving the efficacy of TRT and extending applications to other targetable receptors that are overexpressed in tumors [9, 10]. One promising target is the human Y_1 receptor (hY_1R) which was found to be overexpressed in some tumors, such as estrogen receptor (ER)-positive breast cancer [11].

Here, we describe the combination of a full-length hY_1R-targeting peptide with a releasable NLS-DOTA unit in order to deliver radiolanthanides for better efficacy.

Materials and methods

Synthesis of the novel pb12 NPY conjugate; its labeling with natural terbium (^{159}Tb), or its radio-labeling with indium-111 (^{111}In)

The synthesis of the new NPY-conjugates is summarized below. Additional details are available in supporting information.

For the DOTA-NLS-NPY conjugate pb12, newly developed in our laboratories, the backbone sequence of [F^7,P^{34}]-NPY was synthesized by robot-assisted SPPS using the Fmoc/*t*Bu strategy [12]. As modification point, the natural Lys^4 in [F^7,P^{34}]-NPY was chosen. In previous studies, modification of Lys^4 with toxic agents or carboranes did not change the activity and selectivity profile of the peptide [13, 14]. To facilitate side-specific modification in pb12, the N_ε-amino group of Lys^4 was orthogonally protected by Dde. After the removal of the Dde group with hydrazine, the amino acid Dde-Lys(Fmoc)-OH was coupled as branching unit to the N_ε-amino group of Lys^4 (Fig. 1). Subsequently, manual Fmoc deprotection was performed and the free N_ε-amino group of the Lys branching unit could be extended with the amino acid sequence βAla-PAAKRVKLDGLFG by automated SPPS. GLFG thereby acts as cleavage site for the lysosomal protease cathepsin B [15], while PAAKRVKLD represents the NLS from the c-Myc protein [16]. β-Ala was introduced as short spacer. Next, the bifunctional chelating agent DOTA was manually coupled to the *N*-terminus of the β-alanine spacer with DIC/HOBt by using the protected building block DOTA-tris(*t*Bu)ester. Finally, the Dde protecting group at the N_α-amino group of the Lys branching unit was removed, and palmitic acid was manually coupled with DIC/HOBt to yield conjugate pb12. For the control peptide pb13, the peptide backbone [F^7,A^{33},P^{34},A^{35}]-NPY was used and modification at Lys^4 was performed as described for pb12. Replacement of the Arg^{33} and Arg^{35} residues in [F^7,P^{34}]-NPY with alanine was previously shown to delete the binding affinity of the peptide and is therefore suitable for the generation of a negative control peptide [17].

For first biological in vitro experiments, the DOTA-containing NPY conjugates pb12 and pb13 were labeled with ^{nat}Tb or ^{111}In as surrogate for radiolanthanides as described below:

The pb12 and pb13 conjugates (0.34 μmol) were dissolved in 500 μL of 0.4 M aqueous ammonium acetate solution (pH 5), and 100 μL of 0.01 M aqueous $^{nat}TbCl_3$ solution were added. The mixture was incubated for 30 min at 37 °C and 500 rpm in a dry block heater and subsequently cooled to room temperature. Removal of salts was accomplished by using Amicon® Ultra-4 MWCO 3000 centrifugal filter units (Merck) or PD MidiTrap G-25 desalting columns (GE Healthcare, Chicago, IL, USA) to obtain conjugates [^{nat}Tb]Tb-pb12 and [^{nat}Tb]Tb-pb13.

For radiolabeling with ^{111}In, $^{111}InCl_3$ (Curium Netherlands B.V, ~ 250 MBq) was incubated at room temperature with 50 μg of DOTA-peptide (pb12 or pb13) in 500 μL of 0.1 M acetate buffer (pH 5) for 1.5 h under gentle agitation. The raw product was diluted to 3 mL with acetate buffer and purified on a PD-10 size exclusion column (GE Healthcare) according to the manufacturer's instructions. Elution was performed with 3.5 mL of acetate buffer, and fractions of 0.5 mL were collected. The two fractions with the highest activities were pooled. Radiochemical purity was monitored by UV-radio RP-HPLC using a Phenomenex Luna C18 column (150 mm × 4.6 mm, 5 μm, 4 mL/min) with a linear gradient of 20–70% eluent B (ACN) in eluent A (0.1% (v/v) TFA in water) over 10 min and detection at λ = 220 nm.

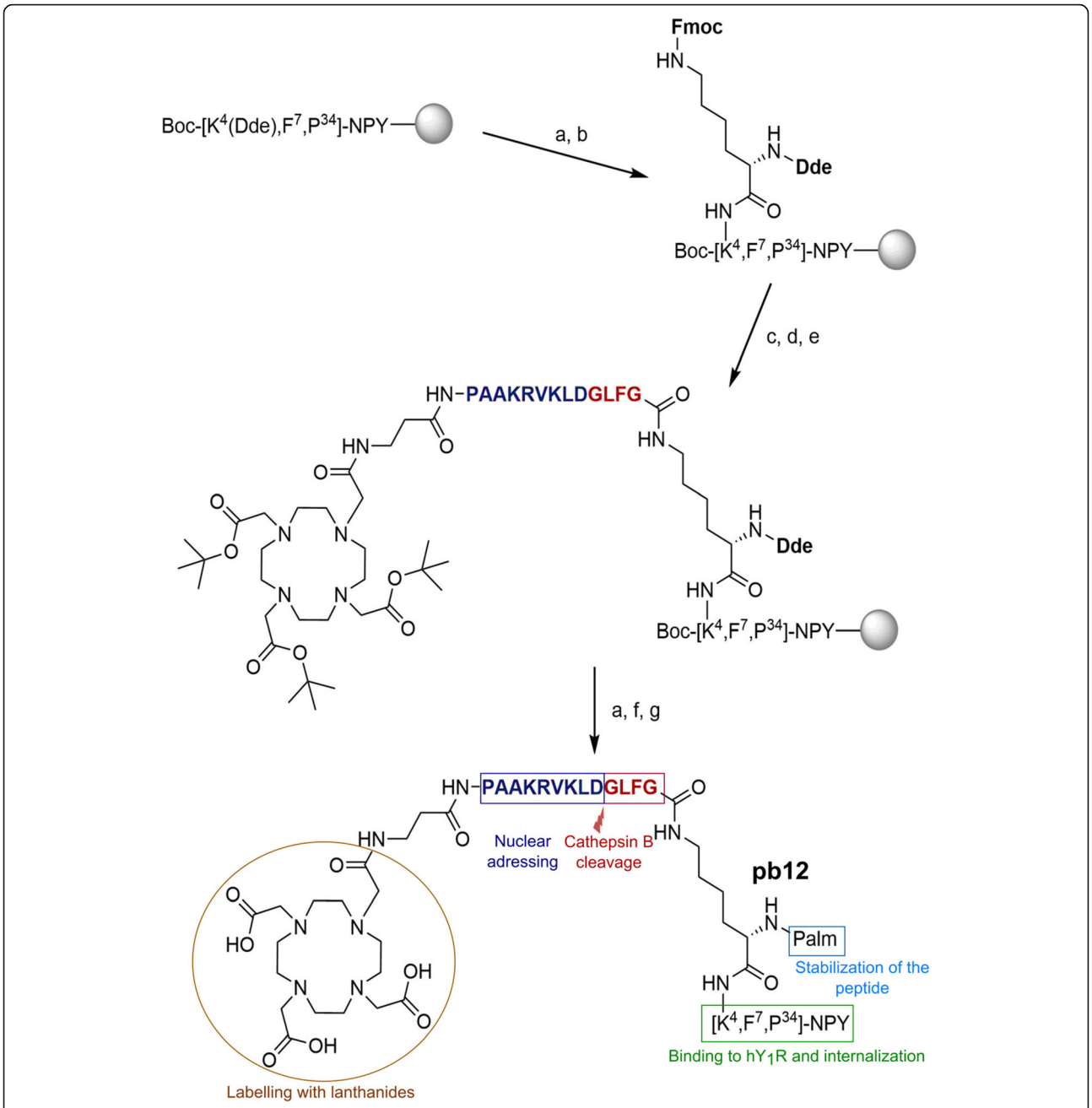

Fig. 1 Synthesis scheme for the hY_1R-targeted, multifunctional NPY conjugate pb12. Dde, 4,4-dimethyl-2,6-dioxocyclohex-1-ylidenethyl; SPPS, solid phase peptide synthesis; Fmoc, 9-fluorenylmethoxycarbonyl; DMF, dimethylformamide; HOBt, 1-hydroxybenzotriazole; DIC, *N,N'*-diisopropylcarbodiimide; NLS, nuclear localization sequence; DOTA, 1,4,7,10-tetraazacyclododecane-1,4,7,10-tetraacetic acid; TFA, trifluoroacetic acid; TA, thioanisole; TC, thiocresole; Palm, palmitic acid. The cathepsin B-cleavable linker is marked in red and the nuclear localization sequence in blue. a Dde cleavage, b coupling, c Fmoc cleavage, d extension with β-Ala NLS GLFG sequence, e DOTA coupling, f palm coupling, g full cleavage

Determination of lipophilicity

The lipophilicity of ^{111}In-labeled peptides was assessed by the water-octanol partition/distribution coefficient method as described in detail in supporting information.

Assessment of cathepsin B-mediated cleavage of pb12

Two micromolar of pb12 were incubated with 0.74 U of recombinant cathepsin B for 0, 0.25, 0.5, 1, and 2 hours at 37 °C. Analysis was conducted by HPLC and peptide

stability was monitored with UV-HPLC with and without the cathepsin B inhibitor CA-074.

Cell culture, hY_1R, and cathepsin B expressions assessed using western blot and immunofluorescence on MCF-7 cells and cathepsin B activity of MCF-7 cells determined using ELISA assay are described in supporting information.

Receptor activation, receptor internalization, membrane integrity assay, PIXE experiment, and metabolic stability are also described in supporting information.

Saturation radioligand binding assay

Saturation binding assays were conducted on hY_1R-expressing MCF-7 breast cancer cells following the methodology of Ginj et al. used for [^{111}In]In-DOTA-NLS-TOC [18]. The blocking agent used was the hY_1R antagonist BIBP3226 (1 μM).

Determination of specific internalization of radiolabeled NPY conjugates

The cellular accumulation of the ^{111}In-labeled NPY conjugates was performed as described by Maschauer et al. [19], with only minor modifications (MCF-7 cells were seeded at a density of 1 million cells per well in 6-well plates and incubated overnight; 50 kBq of the respective ^{111}In-labeled NPY conjugates was used, and membrane-bound radioligand was removed with 20 mM acetate buffer (pH 5)). Each peptide was tested in three independent experiments.

Determination of cellular efflux of [^{111}In]In-pb12

For efflux experiments, MCF-7 cells were seeded at a density of 1 million cells per well in 6-well plates and cultured overnight. A total of 50 kBq of [^{111}In]In-pb12 (with or without pre-incubation of the efflux inhibitor probenecid at a concentration of 10 μM) was added to the medium and the cells were incubated (in triplicates) for 1 h at 37 °C. Three minutes before the end of the incubation time, internalization was stopped on ice, and the supernatant was removed. Each well was washed with 1 mL of ice-cold PBS. The membrane-bound fraction was retrieved in 2 mL sodium acetate buffer (20 mM, pH 5) for 2 min; each well was rinsed a second time with 1 mL ice-cold PBS, and fresh culture medium was added. At each time point (0.5, 1, 2, 4, and 24 h), the efflux was stopped by collecting the medium and washing cells twice with ice-cold PBS. Finally, cells were treated with NaOH (1 M). The radioactivity of the collected culture medium supernatant, the PBS wash fractions, and the total internalized fraction were measured in a gamma counter. The experiment was performed three times independently.

Determination of nuclear uptake of ^{111}In

To determine the amount of radioactivity in the nucleus, we proceeded similar to the radioligand internalization experiments. As additional control, the cathepsin-B inhibitor CA-074 Me was pre-incubated at a concentration of 10 μM for 1 h in selected wells. Instead of adding NaOH at the last step, 500 μL of trypsin was added to each well and incubated for 3 min at 37 °C. The content of each well was then centrifuged (5 min, 1800×*g*, 4 °C). The supernatant was removed; 1 mL of hypotonic buffer was added and incubated for 15 min on ice. Subsequently, the samples were again centrifuged (5 min, 1800×*g*, 4 °C), and the resulting supernatant corresponds to the cellular fraction, and the pellet corresponds to the nuclear fraction. Both fractions were separated and measured in a gamma counter. Finally, the percentage of radioactivity in the nucleus relative to the overall specifically internalized radioactivity or the total amount of used radioactivity was calculated. Experiments were independently performed at least two times in triplicates.

In vivo [^{111}In]In-pb12 SPECT/CT imaging

The MCF-7 tumor model was established as described by Hofmann et al [17]. Whole body SPECT/CT scans (duration 17 s each) of mice (23.5 ± 4.2 g, n = 3) bearing MCF-7 xenografts injected with [^{111}In]In-pb12 (2.5 ± 0.2 MBq, 0.77 ± 0.07 μg, 71.7 ± 2.2 μL, 0.1 ± 0.01 nmol) in the tail vein were performed using a NanoSPECT/CT Plus (Mediso Medical Imaging System Ltd) at 12, 20, 29, 37, 46, 54, 63, 71, 80, 88, 96, 104, 240, and 1440 minutes post-injection. A second group of three mice were pre-injected with 50 μg (7.8 nmol) of pb12; 25 minutes before injection of [^{111}In]In-pb12 (one mouse died at 2 h). CT parameters were X-ray, 45 kVp, exposition 500 ms, binning 1:4, and projection 180. Aperture was pinhole 102 Rat STD, whole body 2.2 mm. Region of interest (ROI) was manually drawn on reconstructed images using the Nucline software (v1.02) on several organs (MCF-7 tumors, lungs, heart, kidneys, liver, stomach, brain, bones, and muscle) at each time point, and data were expressed as percentage of injected activity per volume of tissue (%IA/mm^3). SPECT and CT dicom files were fused using PMOD v3.5 (PMOD Technologies Ltd., Switzerland)

Results

Chemistry

Peptide conjugates were prepared by a combination of automated and manual SPPS (Fig. 1). The sequences and the names of the generated compounds are listed in Table 1. All compounds were highly pure (> 95%) (see supplemental Table 1 and supplemental Figure 1).

Table 1 Nomenclature of the prepared NPY conjugates pb12, [^{nat}Tb]Tb-pb12, [^{111}In]In-pb12, and the non-binding control peptides pb13, [^{nat}Tb]Tb-pb13, and [^{111}In]In-pb13

compound	*peptide*
NPY	YPSKPDNPGEDAPAEDLARYYSALRHYINLITRQRY-NH_2
[F^7,P^{34}]-NPY	YPSKPD**F**PGEDAPAEDLARYYSALRHYINLITR**P**RY-NH_2
pb12	[K^4(N_α(Palm)-Lys-N_ε(GFLGDLKVRKAAP-βAla-DOTA)),F^7,P^{34}]-NPY
[^{nat}Tb]Tb-pb12	[K^4(N_α(Palm)-Lys-N_ε(GFLGDLKVRKAAP-βAla-([^{nat}Tb]Tb-DOTA))),F^7,P^{34}]-NPY
[^{111}In]In-pb12	[K^4(N_α(Palm)-Lys-N_ε(GFLGDLKVRKAAP-βAla-([^{111}In]In-DOTA))),F^7,P^{34}]-NPY
pb13	[K^4(N_α(Palm)-Lys-N_ε(GFLGDLKVRKAAP-βAla-DOTA)),F^7,A^{33},P^{34},A^{35}]-NPY
[^{nat}Tb]Tb-pb13	[K^4(N_α(Palm)-Lys-N_ε(GFLGDLKVRKAAP-βAla-([^{nat}Tb]Tb-DOTA))),F^7,A^{33},P^{34},A^{35}]-NPY
[^{111}In]In-pb13	[K^4(N_α(Palm)-Lys-N_ε(GFLGDLKVRKAAP-βAla-([^{111}In]In-DOTA))),F^7,A^{33},P^{34},A^{35}]-NPY

The cathepsin B-cleavable linker is marked in red and the c-Myc nuclear localization sequence in blue. *Palm* palmitic acid, *DOTA* 1,4,7,10-tetraazacyclododecane-1,4,7,10-tetraacetic acid

Characterization of pb12 and [^{nat}Tb]Tb-pb12 compared with the control compounds pb13 and [^{nat}Tb]Tb-pb13

Cleavage of pb12 by cathepsin-B

The pb12 peptide cleavage mediated by recombinant cathepsin B was investigated in vitro and monitored using UV-HPLC as first proof of concept. Cathepsin B metabolite formation increases over time and was significantly inhibited by the cathepsin B inhibitor CA074 (Fig. 2)

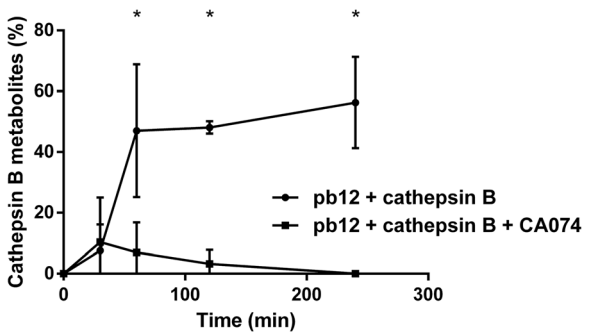

Fig. 2 Kinetics of cathepsin B metabolite formation with and without the cathepsin B inhibitor CA074

Affinity, receptor activation, and internalization

The specific receptor binding of the non-radioactive conjugates pb12 and [^{nat}Tb]Tb-pb12 (Fig. 3) and the control peptides pb13 and [^{nat}Tb]Tb-pb13 (Supplemental Figure 5) were investigated on MCF-7 cells along with the reference compound [F^7,P^{34}]-NPY. First, saturation binding curves were measured by plasmon-waveguide resonance (PWR) spectroscopy. The pb12 conjugate displayed only a slightly decreased affinity compared with [F^7,P^{34}]-NPY (Fig. 3a) with a K_D of 3.1 ± 0.8 nM (Fig. 3b and Table 2). Labeling with ^{nat}Tb, however, led to a ten-fold decrease in binding affinity (K_D 30 ± 3.7 nM for [^{nat}Tb]Tb-pb12, Fig. 3c) compared with the unlabeled pb12 molecule.

For the non-affine control peptides pb13 and [^{nat}Tb]Tb-pb13, no saturation binding up to a concentration of 1 μM could be observed (Supplemental Figure 5A and 5B).

As additional experiment, binding of pb12 and [^{nat}Tb]Tb-pb12 to non-hY_1R-expressing HEK293 cells was investigated and some non-specific membrane interaction was measured (Supplemental Figure 5E and 5F).

Receptor activation of the hY_1R and hY_2R was investigated for the unlabeled DOTA-NLS-[F^7,P^{34}]-NPY

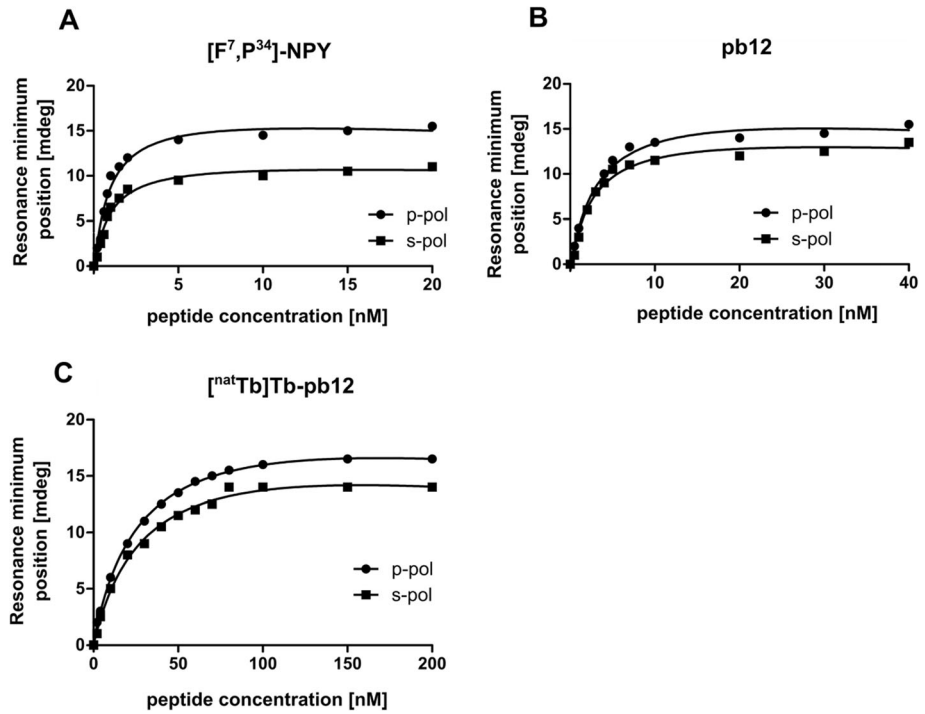

Fig. 3 Affinity of [F^7,P^{34}]-NPY (control, **a**), pb12 (**b**), and [^{nat}Tb]Tb-pb12 (**c**) determined using PWR on MCF-7 cell fragments. p-pol stands for the light component that is perpendicular to the sensor surface and so the lipid membrane, and s-pol stands for the light axis component that is parallel

conjugates pb12 and [^{nat}Tb]Tb-pb12 on COS-7 cells stably co-expressing the hY_1R or hY_2R and the chimeric G protein $G\alpha_{\Delta 6qi4myr}$ which switches the endogenous $G\alpha_i$-coupled signaling pathway of the activated NPY receptors to the $G\alpha_q$-coupled pathway, which results in the intracellular generation of inositol phosphates (Fig. 4a). Unlabeled conjugate pb12 is a full agonist at the hY_1R and displayed only a slightly lower potency compared with NPY and [F^7,P^{34}]-NPY with an EC_{50} of 1.6 nM. Labeling with ^{nat}Tb in pb12 did not change the nanomolar activity of the conjugate at the hY_1R (EC_{50} 1.2 nM). Considering hY_2R activation, pb12 and [^{nat}Tb]Tb-pb12 were able to activate the hY_2R only at very high concentration (10 μM). As regards the non-binding control [^{nat}Tb]Tb-pb13, it was nearly inactive for the hY_1R and completely inactive at the hY_2R.

Table 2 Affinity values of NPY-conjugates to the hY_1R

Compounds	K_D at the hY_1R (nM)
[F^7,P^{34}]-NPY	0.94 ± 0.08
pb12	3.1 ± 0.8
[^{111}In]In-pb12	5.1 ± 3.5
[^{nat}Tb]Tb-pb12	30 ± 3.7
pb13	No specific binding
[^{111}In]In-pb13	No specific binding
[^{nat}Tb]Tb-pb13	No specific binding

[^{nat}Tb]Tb-pb12 and the unlabeled control peptide pb13 were also investigated in live-cell fluorescence microscopy studies for their capability to induce internalization of the hY_1R and hY_2R (Fig. 4b). In the unstimulated state, the fluorescence-tagged hY_1R and hY_2R (green) were predominantly localized in the plasma membrane. [^{nat}Tb]Tb-pb12 was able to stimulate internalization of the hY_1R comparable to the endogenous ligand NPY, whereas no internalization of the hY_2R was observed (Fig. 4b), thus confirming the retained hY_1R selectivity of [^{nat}Tb]Tb-pb12 as determined in the receptor activation assay. The non-binding control pb13 was not able to induce internalization of either hY_1R or hY_2R.

Membrane integrity after application of pb12, [^{nat}Tb]Tb-pb12 compared with the control peptide pb13 and non-exposed cells

Given the identification of some non-specific association of pb12 and [^{nat}Tb]Tb-pb12 in experiments with non-hY_1R-expressing HEK293 and potential impact in membrane organization and integrity, we also tested MCF-7 membrane integrity using a LDH release assay after application of the respective peptides (pb13 peptide and

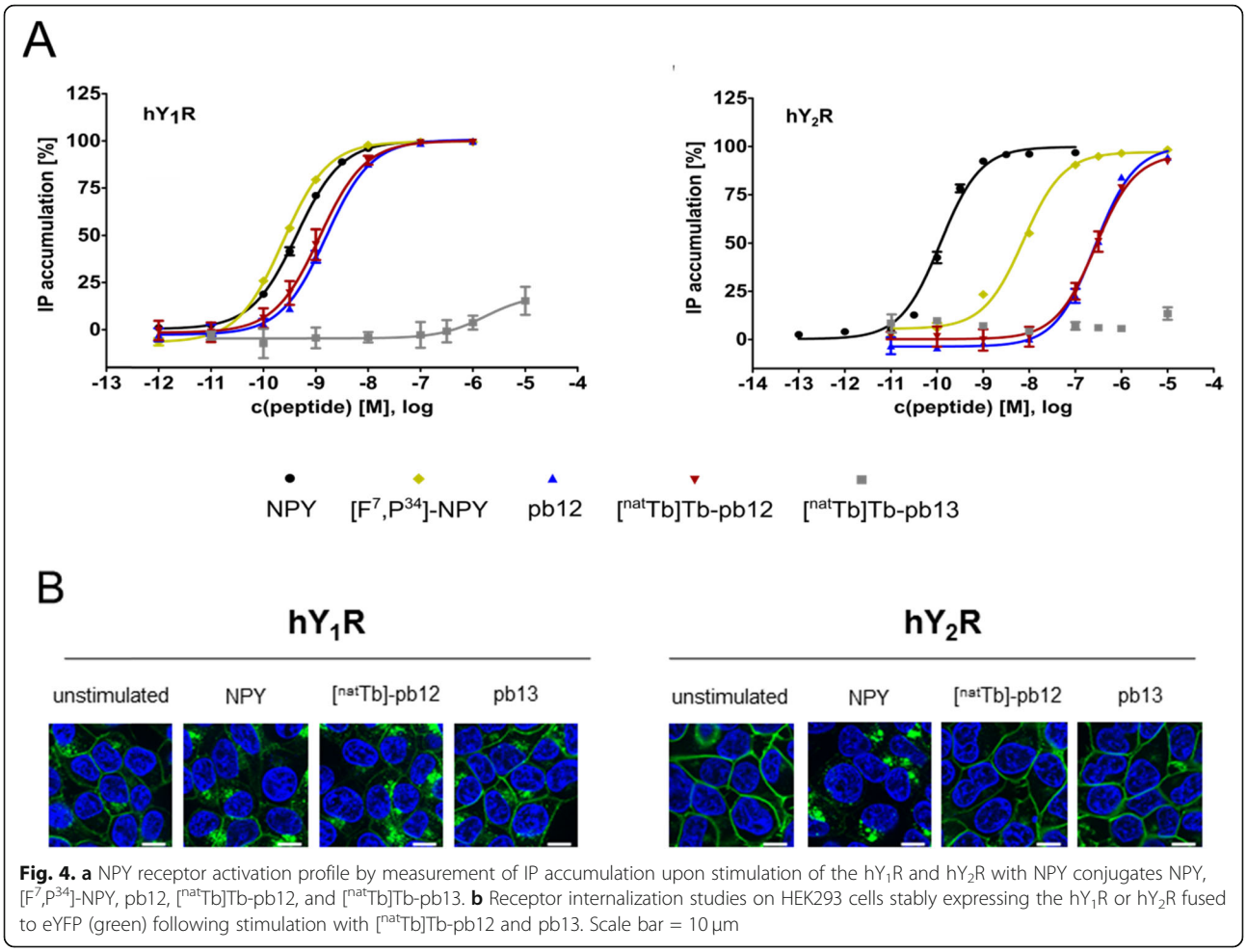

Fig. 4. a NPY receptor activation profile by measurement of IP accumulation upon stimulation of the hY_1R and hY_2R with NPY conjugates NPY, [F^7,P^{34}]-NPY, pb12, [^{nat}Tb]Tb-pb12, and [^{nat}Tb]Tb-pb13. **b** Receptor internalization studies on HEK293 cells stably expressing the hY_1R or hY_2R fused to eYFP (green) following stimulation with [^{nat}Tb]Tb-pb12 and pb13. Scale bar = 10 μm

non-exposed cells were used as controls). Overall, LDH release was low for all peptides tested (around 5%) and comparable to control measurements ($p > 0.05$).

PIXE experiment using [^{nat}Tb]Tb-p12

Because [^{nat}Tb]Tb-pb12 displayed somewhat lower affinity than [^{111}In]In-pb12 at the hY_1R and to illustrate that the multivalent construct pb12 may enable delivery of terbium into MCF-7 cells, we performed PIXE experiments on MCF-7 cells pre-incubated with [^{nat}Tb]Tb-pb12 as surrogate of [^{161}Tb]Tb-pb12. After irradiation with 3 MeV protons and signal quantification, we were able to demonstrate that the pb12 construct is a suitable shuttle for terbium in hY_1R-expressing cells. The amount of native terbium carried by [^{nat}Tb]Tb-pb12 was significantly higher than in non-exposed cells ($p = 0.041$).

Characterization of the radiolabeled [^{111}In]In-pb12 and the control compound [^{111}In]In-pb13

^{111}In radiolabeling

NPY conjugates pb12 and pb13 were subsequently labeled with the Auger electron- and γ-emitting ^{111}In as surrogate for radiolanthanides because terbium isotopes are not yet widely available [20]. [^{111}In]In-pb12 and [^{111}In]In-pb13 were obtained in high radiochemical purity (> 92%), high enough for pre-clinical characterization. All preclinical characterizations were performed at a volumic activity of 20 MBq/mL except for in vivo imaging which was performed at 47 MBq/mL.

Hydrophilicity

By using the partition method, a LogD (pH 5) value of – 0.27 ± 0.19, a LogP (pH 7) value of – 1.20 ± 0.27, and a LogP (pH 7.4) value of – 0.99 ± 0.16 were found for [^{111}In]In-pb12.

Affinity, internalization, efflux rate, and nuclear delivery of [^{111}In]In-pb12 compared with [^{111}In]In-pb13

[^{111}In]In-pb12 and [^{111}In]In-pb13 were investigated in a saturation radioligand binding assay on MCF-7 cells. [^{111}In]In-pb12 displayed a retained, high-hY_1R binding affinity (K_D 5.1 ± 3.5 nM, Supplemental Figure 5C and Table 2), comparable to unlabeled pb12. The control peptide [^{111}In]In-pb13 showed no specific binding to the

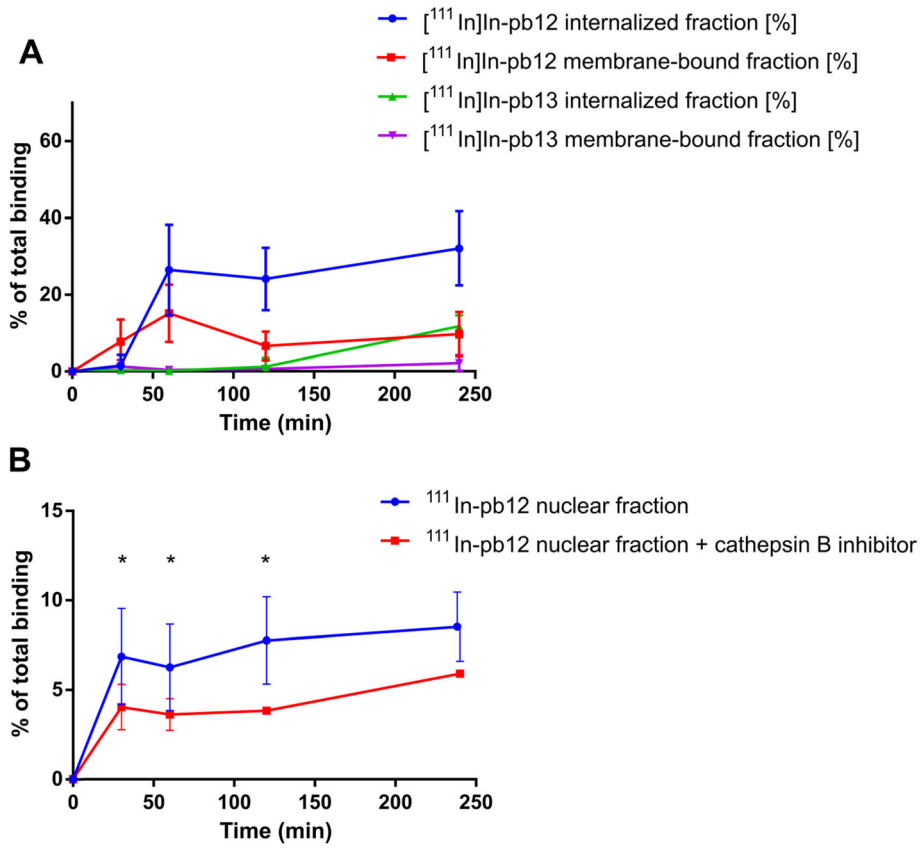

Fig. 5 Determination of the internalized fraction and membrane-bound fraction of [^{111}In]In-pb12 and control peptide [^{111}In]In-pb13 (**a**) and nuclear fractions of [^{111}In]In-pb12 with and without the cathepsin B inhibitor CA074Me (**b**) into endogenously hY_1R-expressing MCF-7 cells. Data points represent the mean ± SD of at least two independent experiments

hY_1R on MCF-7 cells (Supplemental Figure 5D) For easier comparison, Table 2 summarizes affinity values of all compounds evaluated in this work.

Next, the hY_1R-mediated internalization of the radiolabeled conjugates [^{111}In]In-pb12 and [^{111}In]In-pb13 into MCF-7 cells was analyzed (Fig. 4a). For conjugate [^{111}In]In-pb12, specific, time-dependent internalization into MCF-7 cells was observed with a maximum of 32.0 ± 9.7% of the total amount of used radiopeptide being internalized after 4 h (vs 11.7 ± 2.9% for the control peptide [^{111}In]In-pb13 at 4 h, differences were significant at 1 h, 2 h and 4 h).

In another set of experiments, the nuclear delivery of ^{111}In after internalization of [^{111}In]In-pb12 into MCF-7 cells was investigated (Fig. 5b). Incubation of MCF-7 cells with the multifunctional conjugate [^{111}In]In-pb12 resulted in a time-dependent nuclear uptake of ^{111}In. After incubation for 2 h, a maximum of 7.7 ± 2.4% of the total radioactivity was found to be located in the nucleus (Fig. 5b). This value would yield to 24.1% of the internalized fraction addressed to the nucleus. A significant reduction of nuclear uptake of ^{111}In at 3.8 ± 0.1% ($p < 0.01$) was observed when cells were pre-incubated with a cathepsin B inhibitor (Fig. 5b).

[^{111}In]In-pb12 was further evaluated regarding cellular efflux. A high and fast efflux of radioactivity was found for [^{111}In]In-pb12 (Fig. 6). Already after 30 min post internalization, 77 ± 5% of the total internalized radioactivity was detected in the medium outside the cells.

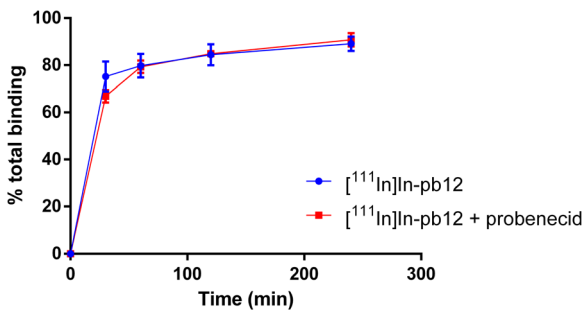

Fig. 6 Investigation of the cellular efflux of [^{111}In]In-pb12 with and without the efflux inhibitor probenecid. Data points represent the mean ± SD of three independent experiments

This further increased to 88 ± 3% extracellular radioactivity after 4 h post internalization. However, the observed efflux was not inhibited by the efflux inhibitor probenecid (Fig. 6) and the control conjugate [^{111}In]In-pb13 displayed a similar efflux profile (not shown).

Plasma stability of [^{111}In]In-pb12

Metabolic stability of [^{111}In]In-pb12 was evaluated in vitro in human plasma. Unfortunately, fast degradation of conjugate [^{111}In]In-pb12 was observed, with ~20% of the initial radiopeptide left intact 1 h after incubation at 37 °C.

SPECT/CT imaging of [^{111}In]In-pb12

Given the low plasmatic stability of [^{111}In]In-pb12, we focused on the first imaging time point at 12 minutes post-injection. [^{111}In]In-pb12 showed preferential elimination via the liver (Fig. 7a, b; 0.205 ± 0.07%IA/mm^3). Non-specific signal was also quantified in the heart (0.121 ±

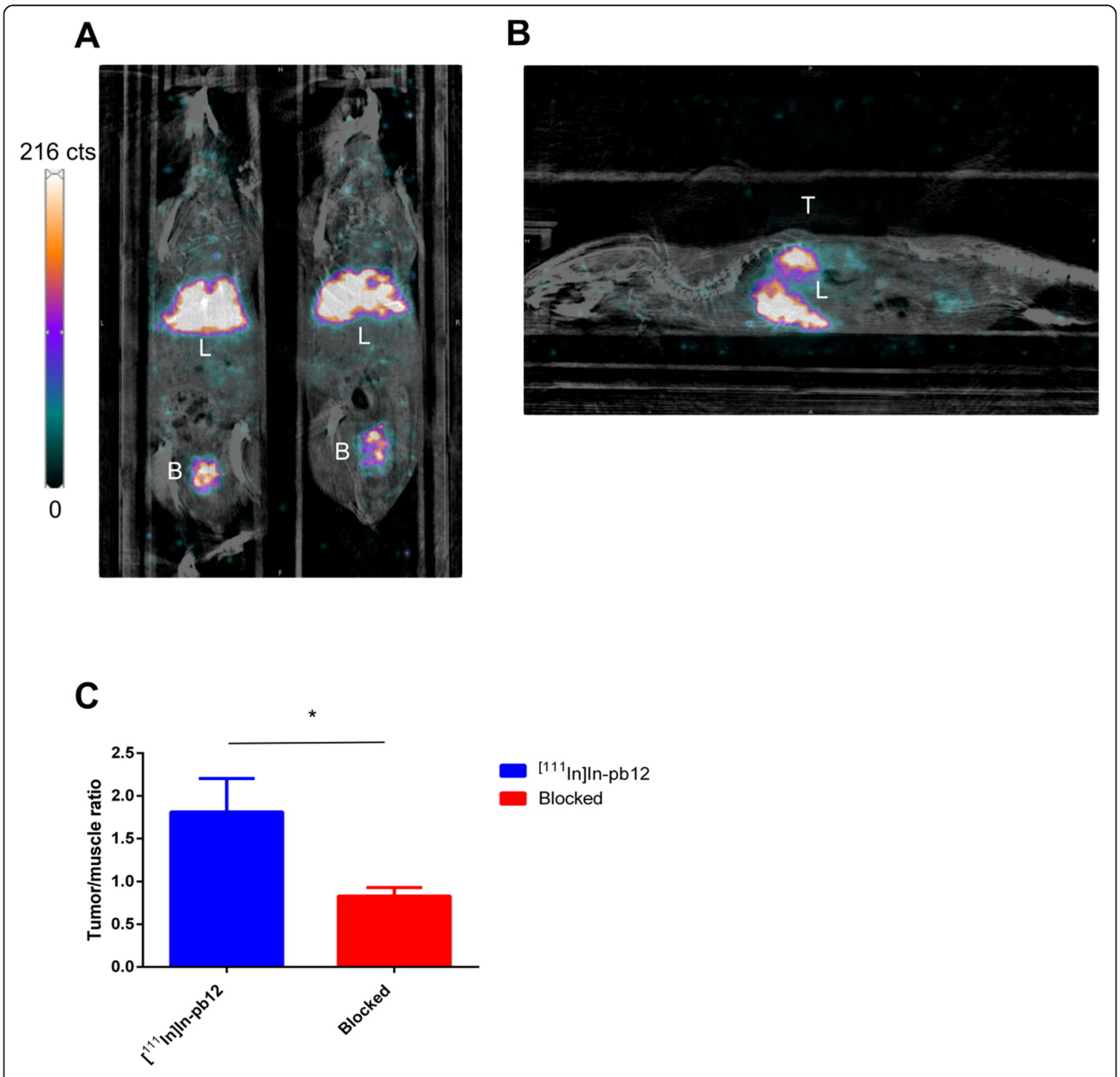

Fig. 7 In vivo behavior of [^{111}In]In-pb12 in MCF-7 xenograft mice. **a** Representative SPECT/CT coronal image at 12 min post-injection showing major elimination of [^{111}In]In-pb12 by the liver and minor elimination by the bladder. **b** Representative SPECT/CT sagittal image at 12 min post-injection showing major elimination of [^{111}In]In-pb12 by the liver. **c** Tumor/muscle ratio at 12 min post-injection of [^{111}In]In-pb12 in MCF-7 xenografted mice determined on the SPECT/CT images. Co-injection of non-labeled pb12 (blocked group) significantly decreases the tumor/muscle ratio. L stands for liver, B means bladder and T stands for MCF-7 tumor

0.03%IA/mm^3) and the lungs (0.109 ± 0.05 %IA/mm^3). Interestingly, low but specific uptake was noted in MCF-7 tumor (vs the blocked group, $p = 0.001$). Also, the tumor/muscle ratio was highly significantly reduced in the cold pb12-blocked mice (Fig. 7c, $p = 0.01$).

Discussion

Targeted radionuclide therapy holds promise to deliver radiation to tumor cells over-expressing peptide receptors. In this work, we aimed to explore the feasibility of enhanced-TRT by using a subcellular active (radio) pharmaceutical able to deliver Auger-electron emitter like ^{161}Tb, in tumors over-expressing the hY$_1$R. Several strategies have been used to develop NPY ligands for imaging and therapy (non-peptide ligands, antagonistic-truncated peptides, or agonistic full-length peptides) with variable success [19, 21, 22]. The full-length hY$_1$R-preferring peptide analog [F^7,P^{34}]-NPY allows selective delivery of cargos such as radioisotopes [12, 17, 23]. We described here the multivalent construct pb12 based on the hY$_1$R-preferring [F^7,P^{34}]-NPY sequence, which rapidly internalizes into acidic endosomes after agonistic stimulation of the hY$_1$R, modified with a cathepsin B-cleavable linker able to release a nuclear localization sequence (NLS) linked to a DOTA chelator to convey lanthanides into the nucleus using importins [24]. For therapy perspective, a profound in vitro characterization is needed to fully understand the biological mechanisms which might impact the efficacy. Receptor binding studies demonstrated that the advanced modification of [F^7, P^{34}]-NPY with a DOTA-NLS-GLFG unit and a fatty acid in pb12 did not influence the high hY$_1$R affinity of the peptide. In addition, labeling with ^{nat}Tb results in a decrease in affinity from 3 to 30 nM but the activity and biological behavior of the ^{nat}Tb-labeled conjugate was hopefully maintained as demonstrated by PIXE experiments. pb12 was also radiolabeled with ^{111}In as "surrogate" of lanthanides, and we showed that, in this case, the high hY$_1$R affinity was preserved. The difference in affinity between the ^{111}In-labeled version of pb12 and its ^{nat}Tb counterpart illustrates the necessity of carefully determining affinity of metallated compounds for imaging and therapy. Importantly, these nanomolar affinity values compete well with other full-length peptides [17] or non-peptide ligands [21] and are better than those reported for truncated peptides [22].

We then looked for the hydrophilicity of [^{111}In]In-pb12, and results showed that this compound is fairly hydrophilic. Addition of the lipophilic palmitic acid moiety might be responsible for the increased lipophilicity of our compound and lead to some non-specific binding of the peptide to the cell membrane. However, this interaction does not compromise cell membrane integrity as demonstrated by the LDH assay. Previous studies have shown that palmitoylation is an effective approach to enhance association of peptides with cell membrane and therefore increasing their proximity to the target, which is an important parameter for TRT with ^{161}Tb [25]. Exploring the additional radiobiological impact of ^{161}Tb on tumor cell membrane would be interesting [26].

To envision the use of Auger-electron emitters for enhanced TRT, the "shuttle" pb12 should be internalized. In living cells, the high affinity [^{nat}Tb]Tb-pb12 displayed similar internalization to the endogenous peptide NPY. When radiolabeled with ^{111}In, pb12 displayed a time dependent, specific internalization reaching 30% of total binding corresponding to the maximum of hY$_1$R internalization capacity, reflecting the full agonist behavior of [^{111}In]In-pb12 [27]. Moreover, hY$_1$R internalization is rapid and leads to membrane recycling of the receptor [28] illustrated by a significant rapid increase of [^{111}In]In-pb12 bound to the cell membrane which stayed constant over the course of 4 h. (Fig. 5).

After hY$_1$R-mediated internalization followed by endocytosis [29], our compound was designed to be cleaved by cathepsin B to release the ^{111}In-DOTA-NLS unit, which is next addressed to the nucleus after binding to importins. We demonstrated that the recombinant cathepsin-B enzyme effectively cleaved the pb12 sequence (Fig. 2) and this cleavage is necessary to maximize the addressing of ^{111}In to the nucleus. In general, cytosol-located molecules with a molecular weight < 45 kDa are able to enter the nucleus via passive diffusion, while bigger molecules require a NLS to be transported by the nuclear pore complex [30]. Therefore, conjugation with NLS moieties was mostly performed for targeted antibodies such as trastuzumab [31]. The NLS conjugation to smaller molecules, as in this study, was also reported to be successful. A trifunctional [^{111}In]In-DOTA-NLS-TOC conjugate facilitated nuclear uptake of ^{111}In compared with [^{111}In]In-DOTA-TOC [18]. In our experiments, we cannot exclude a passive transport of ^{111}In (via interactions with membranes as demonstrated above for pb12 and [^{nat}Tb]Tb-pb12) into the nucleus, as the addition of the cathepsin B inhibitor did not fully inhibit the nuclear uptake of ^{111}In.

Another requirement for TRT radiopeptides is their low efflux rate. Indeed, a high efflux would result in suboptimal irradiation of tumor cells, particularly with short-range particles, and higher off-target dose delivery. [^{111}In]In-pb12 demonstrated high efflux which was not inhibited by the efflux inhibitor probenecid. However, using PWR, we demonstrate that compounds pb12 and [^{nat}Tb]Tb-pb12 interact with membrane lipids in a non-specific manner (Supplemental Figure 5E and 5F). Taken together, the efflux of [^{111}In]In-pb12 we measured probably reflects the association of the peptide with the cell membrane rather than a high efflux, representing a significant improvement compared with truncated peptides [19].

To envision clinical application of our concept, the [^{111}In]In-pb12 conjugate needs to remain stable in vivo although full length peptides might be highly sensitive proteases. Despite its palmitic acid modification, known to increase resistance against proteolysis [32], [^{111}In]In-pb12 is rapidly metabolized potentially limiting its availability for tumor uptake. In a previous study, [F^{7}, P^{34}]-NPY conjugated to methotrexate by the GFLG-linker exhibited much higher plasma stability [13]. Therefore, the reason for the fast degradation of [^{111}In]In-pb12 is most likely high susceptibility of the arginine/lysine-rich c-Myc NLS (PAAKRVKLD) to proteolysis and stabilization of this sequence is required for further application. We would like to point out that the metabolic stability regarding nucleus targeting studies was never reported in the literature, and this data, although disappointing, is of high interest for laboratories working in this research field. To give more insight in plasmatic stability, we intravenously injected [^{111}In]In-pb12 in mice bearing a MCF-7 xenograft. At an early time point, before major radiopeptide degradation, we noted a specific uptake in MCF-7 tumor, confirming the interest of [^{111}In]In-pb12 to target the hY_1R. High accumulation was noted in the liver, consistent with the lipophilicity of the radiopeptide. Another limitation of this work was the low availability of ^{161}Tb. Therefore, we performed preliminary experiments with ^{nat}Tb which may be only partially representative of the behavior of the ^{161}Tb-counterpart as the radiolabeled fraction might be different. In the future, we plan to improve stability of the conjugate and to perform cellular studies comparing the radiotoxicity of different products, including ^{111}In, ^{90}Y, ^{177}Lu, and ^{161}Tb-labeled molecules (we are seeking European collaboration to receive ^{161}Tb).

Conclusion

In summary, we have developed a first multifunctional NPY analog allowing nuclear delivery of radiolanthanides. Our results suggest that the sequential mode of action of the construct works, i.e., hY_1R binding with high affinity and selectivity, hY_1R-mediated internalization, low efflux, cathepsin B-mediated cleavage of the multifunctional NPY analog, and finally nuclear delivery of the radiolanthanide. However, increasing metabolic stabilization is now needed for future application.

Supplementary information

Supplementary information accompanies this paper at https://doi.org/10.1186/s13550-020-0612-8.

Additional file 1. Analytical data, supplemental methods, characterization of MCF-7 cells and affinity values of pb13, [^{nat}Tb]Tb-pb13, [^{111}In]In-pb12, [^{111}In]In-pb13, pb12 and [^{nat}Tb]Tb-pb12 are presented in Additional file 1.

Acknowledgements

We thank the technical staff members of the AIFIRA facility P. Alfaurt and S. Sorieul. We thank G. Devegraves, H. Seznec, and P. Barberet for their help during the sample preparation and data analysis.
Imaging of samples for PIXE experiments was performed on the Bordeaux Imaging Center, member of the France-BioImaging national infrastructure (ANR-10-INBS-04). Authors also thank Prof B. Guillet (CERIMED, Aix Marseille-University) and E. Gontier (University of Bordeaux) for their support.

Authors' contributions

AC performed most in vitro experiments using ^{111}In-labeled peptides and approved the final manuscript. DJW performed chemical synthesis of all compounds as well as cellular experiments using transfected cells, analyzed data, wrote, and approved the final manuscript. IDA performed PWR experiments, analyzed data, and approved the final manuscript. DV performed all ^{111}In-radiolabeling and approved the final manuscript. MP performed electron microscopy and helped in sample preparation for PIXE experiments. SF and PG performed in vivo imaging of [^{111}In]In-pb12 in nude mice bearing MCF-7 xenograft. PF approved the final manuscript. EH helps in funding request and approved the final manuscript. ABS participates in funding requests, analyzed data, wrote the manuscript, and approved its final version. CM performed ^{111}In-radiolabeling, some in vitro experiments, analyzed data, is the recipient of the funding, wrote the manuscript, and approved its final version. The author(s) read and approved the final manuscript.

Funding

This work was achieved and funded within the context of the Laboratory of Excellence TRAIL ANR-10-LABX-57 (INNOVATHER project). The AIFIRA facility is financially supported by the CNRS, the University of Bordeaux, and the Region Nouvelle Aquitaine.

Availability of data and materials

The datasets used and/or analyzed during the current study are available from the corresponding author on reasonable request

Ethics approval and consent to participate

Fresh human plasma was obtained from "Etablissement Francais du Sang." after evaluation by the Ethics Committee "Etablissement Français du Sang 16PLER.023,". COS7 cells were obtained from DSMZ, #ACC 60. Authentication confirmed species and the presence of SV40 T antigen. MCF-7 cells were obtained from N. Jones (Univ. Bordeaux, France), and no additional authentication was performed by the authors of this study. HEK293 cells were obtained from J. Javitch (Univ. Columbia, USA), and no additional authentication was performed by the authors of this study.
Animal experiments were authorized by APAFiS #14191 on 2018/12/05 for 5 years after evaluation by the Ethics committee CE71. Animals were handled following national guidelines R.214-87 and R.214-126.

Consent for publication

Not applicable

Competing interests

The authors declare that they have no competing interests.

Author details

[1]Department of Nuclear Medicine, University Hospital of Bordeaux, F-33076 Bordeaux, France. [2]University of Bordeaux, INCIA UMR 5287, F-33400 Talence, France. [3]CNRS, INCIA UMR 5287, F-33400 Talence, France. [4]Institute of Biochemistry, Faculty of Life Sciences, Leipzig University, Brüderstr. 34, 04103 Leipzig, Germany. [5]Institute of Chemistry & Biology of Membranes & Nano-objects (CBMN), CNRS UMR 5248, University of Bordeaux, F-33600 Pessac, France. [6]University of Bordeaux, Bordeaux Imaging Center, F-33000 Bordeaux, France. [7]Aix-Marseille University, INSERM, Institut National de la Recherche Agronomique, Centre de Recherche en Cardiovasculaire et Nutrition, 13385 Marseille, France. [8]Aix-Marseille University, Centre Européen de Recherche en Imagerie Médicale, 13005 Marseille, France.

Received: 9 January 2020 Accepted: 18 February 2020
Published online: 02 March 2020

References

1. Strosberg J, El-Haddad G, Wolin E, et al. Phase 3 trial of ^{177}Lu-DOTATATE for midgut neuroendocrine tumors. N Engl J Med. 2017;376:125–35.
2. Hofman MS, Violet J, Hicks RJ, et al. [^{177}Lu]-PSMA-617 radionuclide treatment in patients with metastatic castration-resistant prostate cancer (LuPSMA trial): a single-centre, single-arm, phase 2 study. Lancet Oncol. 2018;19:825–33.
3. Haller S, Pellegrini G, Vermeulen C, et al. Contribution of auger/conversion electrons to renal side effects after radionuclide therapy: preclinical comparison of ^{161}Tb-folate and ^{177}Lu-folate. EJNMMI Res. 2016;6.
4. Hindié E, Zanotti-Fregonara P, Quinto MA, Morgat C, Champion C. Dose deposits from ^{90}Y, ^{177}Lu, ^{111}In, and ^{161}Tb in micrometastases of various sizes: implications for radiopharmaceutical therapy. J Nucl Med. 2016;57:759–64.
5. Champion C, Quinto MA, Morgat C, Zanotti-Fregonara P, Hindié E. Comparison between three promising ß-emitting radionuclides, ^{67}Cu, ^{47}Sc and ^{161}Tb, with emphasis on doses delivered to minimal residual disease. Theranostics. 2016;6:1611–8.
6. Müller C, Umbricht CA, Gracheva N, et al. Terbium-161 for PSMA-targeted radionuclide therapy of prostate cancer. Eur J Nucl Med Mol Imaging. 2019.
7. Müller C, Reber J, Haller S, et al. Direct in vitro and in vivo comparison of ^{161}Tb and ^{177}Lu using a tumour-targeting folate conjugate. Eur J Nucl Med Mol Imaging. 2014;41:476–85.
8. Bavelaar BM, Lee BQ, Gill MR, Falzone N, Vallis KA. Subcellular targeting of theranostic radionuclides. Front Pharmacol. 2018;9:996.
9. Morgat C, Mishra AK, Varshney R, Allard M, Fernandez P, Hindié E. Targeting neuropeptide receptors for cancer imaging and therapy: perspectives with bombesin, neurotensin, and neuropeptide-Y receptors. J Nucl Med. 2014;55:1650–7.
10. Morgat C, Macgrogan G, Brouste V, et al. Expression of gastrin-releasing peptide receptor in breast cancer and its association with pathologic, biologic, and clinical parameters: a study of 1,432 primary tumors. J Nucl Med. 2017:1401–7.
11. Reubi JC, Gugger M, Waser B, Schaer JC. Y_1-mediated effect of neuropeptide-Y in cancer: breast carcinomas as targets. Cancer Res. 2001;61:4636–41.
12. Söll RM, Dinger MC, Lundell I, Larhammer D, Beck-Sickinger AG. Novel analogues of neuropeptide-Y with a preference for the Y_1-receptor. Eur J Biochem. 2001;268:2828–37.
13. Böhme D, Beck-Sickinger AG. Controlling toxicity of peptide-drug conjugates by different chemical linker structures. ChemMedChem. 2015;10:804–14.
14. Worm DJ, Hoppenz P, Els-Heindl S, et al. Selective neuropeptide-Y conjugates with maximized carborane loading as promising boron delivery agents for boron neutron capture therapy. J Med Chem. 2019. https://doi.org/10.1021/acs.jmedchem.9b01136.
15. Zhong Y-J, Shao L-H, Li Y. Cathepsin B-cleavable doxorubicin prodrugs for targeted cancer therapy. Int J Oncol. 2013;42:373–83.
16. Dang CV, Lee WM. Identification of the human c-myc protein nuclear translocation signal. Mol Cell Biol. 1988;8:4048–54.
17. Hofmann S, Maschauer S, Kuwert T, Beck-Sickinger AG, Prante O. Synthesis and in vitro and in vivo evaluation of an ^{18}F-labeled neuropeptide-Y analogue for imaging of breast cancer by PET. Mol Pharmaceutics. 2015;12:1121–30.
18. Ginj M, Hinni K, Tschumi S, Schulz S, Maecke HR. Trifunctional somatostatin-based derivatives designed for targeted radiotherapy using Auger electron emitters. J Nucl Med. 2005;46:2097–103.
19. Maschauer S, Ott JJ, Bernhardt G, Kuwert T, Keller M, Prante O. ^{18}F-labelled triazolyl-linked argininamides targeting the neuropeptide-Y Y_1R for PET imaging of mammary carcinoma. Sci Rep. 2019;9:1–12.
20. Müller C, Zhernosekov K, Köster U, et al. A unique matched quadruplet of terbium radioisotopes for PET and SPECT and for α- and β−-radionuclide therapy: an in vivo proof-of-concept study with a new receptor-targeted folate derivative. J Nucl Med. 2012;53:1951–9.
21. Keller M, Maschauer S, Brennauer A, et al. Prototypic ^{18}F-labeled argininamide-type neuropeptide-Y Y_1R antagonists as tracers for PET imaging of mammary carcinoma. ACS Med Chem Lett. 2017;8:304–9.
22. Zhang C, Pan J, Lin K-S, et al. Targeting the neuropeptide-Y_1 receptor for cancer imaging by positron emission tomography using novel truncated peptides. Mol Pharmaceutics. 2016;13:3657–64.
23. Zwanziger D, Khan IU, Neundorf I, et al. Novel chemically modified analogues of neuropeptide-Y for tumor targeting. Bioconjugate Chem. 2008;19:1430–8.
24. Yoneda Y, Hieda M, Nagoshi E, Miyamoto Y. Nucleocytoplasmic protein transport and recycling of Ran. Cell Struct Funct. 1999;24:425–33.
25. Avadisian M, Gunning PT. Extolling the benefits of molecular therapeutic lipidation. Mol BioSyst. 2013;9:2179–88.
26. Pouget J-P, Lozza C, Deshayes E, Boudousq V, Navarro-Teulon I. Introduction to radiobiology of targeted radionuclide therapy. Front Med (Lausanne). 2015;2:12.
27. Mäde V, Babilon S, Jolly N, et al. Peptide modifications differentially alter G protein-coupled receptor internalization and signaling bias. Angew Chem Int Ed Engl. 2014;53:10067–71.
28. Lundell I, Rabe Bernhardt N, Johnsson A-K, Larhammar D. Internalization studies of chimeric neuropeptide-Y receptors Y_1 and Y_2 suggest complex interactions between cytoplasmic domains. Regul Pept. 2011;168:50–8.
29. Wanka L, Babilon S, Kaiser A, Mörl K, Beck-Sickinger AG. Different mode of arrestin-3 binding at the human Y_1 and Y_2 receptor. Cell Signal. 2018;50:58–71.
30. Wagstaff KM, Jans DA. Nuclear drug delivery to target tumour cells. Eur J Pharmacol. 2009;625:174–80.
31. Costantini DL, Chan C, Cai Z, Vallis KA, Reilly RM. ^{111}In-labeled Trastuzumab (Herceptin) modified with nuclear localization sequences (NLS): an auger electron-emitting radiotherapeutic agent for HER2/neu-amplified breast cancer. J Nucl Med. 2007;48:1357–68.
32. Hofmann S, Bellmann-Sickert K, Beck-Sickinger AG. Chemical modification of neuropeptide-Y for human Y_1 receptor targeting in health and disease. Biological Chemistry. 2019;400:299–311.

Publisher's Note

EXPERIMENTAL SECTION

CHEMISTRY

Materials for peptide synthesis

9-Fluorenylmethoxycarbonyl (Fmoc)- and *tert*-butyloxycarbonyl (Boc)-protected amino acids were purchased from Orpegen OPC (Heidelberg, Germany), Iris Biotech (Marktredwitz, Germany) and Sigma-Aldrich (Taufkirchen, Germany). NovaSyn TGR R resin was obtained from Novabiochem (Darmstadt, Germany), DOTA-tris(*t*Bu)ester was from CheMatech (Dijon, France) and 1-hydroxybenzotriazole (HOBt), *N,N′*-diisopropylcarbodiimide (DIC) and ethyl 2-cyano-2-(hydroxyimino)acetate (Oxyma) were purchased from Iris Biotech. Dimethylformamide (DMF) and dichloromethane (DCM) were obtained from Biosolve (Valkenswaard, The Netherlands) and acetonitrile (ACN) was from VWR (Darmstadt, Germany). Palmitic acid, dimethylsulfoxide (DMSO), hydrazine, piperidine, thioanisole (TA), trifluoroacetic acid (TFA), terbium(III) chloride hexahydrate and 1-octanol were purchased from Sigma-Aldrich. Thiocresole (TC) was from Alfa Aesar (Ward Hill, MA, USA), diethyl ether was obtained from Merck (Darmstadt, Germany) and ammonium acetate was purchased from Fluka (Buchs, Switzerland).

Synthesis of NPY conjugates

Synthesis of the NPY conjugates was accomplished by a combination of automated solid phase peptide synthesis (SPPS) using a SYRO I peptide synthesizer (MultiSynTech, Bochum, Germany) and manual SPPS. The Fmoc/tert-butyl (Fmoc/tBu) strategy was applied and NovaSyn TGR R resin (15-µmol scale, 0.19 mmol/g) was used to obtain peptides with C-terminal amidation. Amino acids were N-α-Fmoc-protected, except of the N-terminal amino acid of the peptide conjugates, which was N-α-Boc-protected. Full-length peptide backbones Boc-[K^4(Dde),F^7,P^{34}]-NPY and Boc-[K^4(Dde),F^7,A^{33},P^{34},A^{35}]-NPY were prepared by automated SPPS. In the automated synthesis, an 8-fold molar excess of amino acid was coupled with equimolar amounts of Oxyma and DIC (8 equiv, 120 µmol) in DMF for 2 × 40 min. The N-terminal Fmoc protecting group was cleaved with 40 % (v/v) piperidine in DMF for 3 min and again 20 % (v/v) piperidine in DMF for 10 min. Removal of the 4,4-dimethyl-2,6-dioxocyclohex-1-ylidenethyl (Dde) protecting group at either the α-amino or ε-amino group of lysine residues

was performed with 3 % (v/v) hydrazine in DMF for 10 × 10 min. Manual coupling of amino acids (5 equiv, 75 µmol) was performed with equimolar amounts of HOBt and DIC (5 equiv each) in DMF for at least 2 h. Manual Fmoc deprotection was accomplished with 20 % piperidine in DMF for 2 × 10 min. DOTA-tris(tBu)ester (3 equiv, 45 µmol) was coupled manually with HOBt and DIC (5 equiv each) in DMF overnight. Palmitic acid (5 equiv, 75 µmol) was coupled manually with HOBt and DIC (5 equiv each) in DMF for at least 4 h.

Cleavage of the peptides from the resin and simultaneous side chain deprotection was accomplished using a mixture of TFA/TA/TC (90:5:5, *v*/*v*) for 3.5 h. The crude peptides were precipitated from ice-cold diethyl ether, dissolved in ACN/H_2O, filtered through a 0.22-µm PVDF filter and subsequently lyophilized. Purification of the crude peptides was accomplished by preparative reversed phase (RP)-HPLC using a Phenomenex Aeris® 5u XB-C18 (250 mm × 21.2 mm, 5 µm, 100 Å) column with a flow rate of 15 mL/min, linear gradients of eluent B (0.08 % (*v*/*v*) TFA in ACN) in eluent A (0.1 % (*v*/*v*) TFA in water) and detection at λ = 220 nm. The purity of the peptides was determined by analytical RP-HPLC using a Phenomenex Jupiter® 4u Proteo C12 90 Å (250 mm × 4.6 mm, 4 µm, 90 Å, 0.6 mL/min) and a Phenomenex Aeris® Peptide 3.6u XB-C18 (250 mm × 4.6 mm, 3.6 µm, 100 Å, 1.55 mL/min) or Agilent VariTide RPC (250 mm × 4.6 mm, 6 µm, 200 Å, 1.0 mL/min) column. A linear gradient of 20%-70% eluent B in eluent A over 40 min was applied and chromatograms were recorded at λ = 220 nm. For all peptides, a purity of > 95 % was obtained. MALDI-ToF mass spectrometry (UltraflexIII, Bruker, Bremen, Germany) and ESI Orbitrap (Orbitrap Elite, Thermo Scientific) mass spectrometry were used to confirm the correct identity of the purified peptides.

Materials for biological methods

Dulbecco's modified Eagle's medium (DMEM), Dulbecco's phosphate buffered saline (DPBS), Ham's F12, trypsin/EDTA and Hank's balanced salt solution (HBSS) were purchased from Lonza (Basel, Switzerland). Penicillin-streptomycin and RPMI 1640 were obtained from Gibco/Life Technologies (Carlsbad, CA, USA). Hygromycin B was purchased from InvivoGen (San Diego, CA, USA), G418-sulfate was from Merck and fetal calf serum (FCS) was obtained from Biochrom (Berlin, Germany) or Gibco/Life Technologies. Opti-MEM was purchased from Life Technologies, Hoechst 33342 and LiCl were purchased from Sigma-Aldrich and BIBP3226 was obtained from Tocris Bioscience (Bristol, UK).

Cell culture

All cell lines were maintained under humidified atmosphere at 37 °C and 5 % CO2 in 75 cm2 cell culture flasks. HEK293 cells stably expressing the hY_1R or hY_2R, both C-terminally fused to the enhanced yellow fluorescent protein (eYFP), were cultured in DMEM/Ham's F12 (1:1, v/v) supplemented with 15 % (v/v) FCS and hygromycin (100 µg/mL). COS-7 cells, stably co-transfected with either the hY1R or hY2R, C-terminally fused to eYFP, and the chimeric G protein GαΔ6qi4myr, were cultured in DMEM high glucose supplemented with 10 % (v/v) FCS, hygromycin B (133 µg/mL) and G418-sulfate (1.5 mg/mL). MCF-7 cells and HEK 293 cells (not expressing the hY_1Rwere cultured in RPMI 1640 supplemented with 10 % (v/v) FCS and penicillin-streptomycin (100 µL/mL).

Western Blot

Protein samples (80µg) were denatured for 5 minutes at 90°C and then loaded onto 10% SDS polyacrylamide gels. Following electrophoresis, proteins were transferred onto nitrocellulose membranes (Immobilon®-P). Membrane was blocked with 5% non-fat milk at room temperature for 1h, and incubated for 1h at room temperature with the following primary antibodies : Anti-Y_1 (1:100), Anti-Cathepsine B (1:800) and anti-actine (A2066; Sigma-Aldrich®) (1:5000). Membranes were subsequently incubated with anti-Rabbit IgG (111-035-144 ; Jackson Immunoresearch®) peroxidase-conjugated secondary antibodies (1:10.000) or anti-goat IgG (D1118 ; Santa Cruz Biotechnology®) peroxidase-conjugated secondary antibodies (1:10.000), at room temperature for 45min. Finally, the immunoreactive bands were visualized using ECL Western Blotting detection reagents (RPN2209 ; GE Healthcare®). Semi-quantitative analysis was conducted using ImageJ © (V1.52c) software package to measure densitometric values for each band.

Immunofluorescence

Cells were seeded onto glass cover slips and incubated for 24 hours with complete culture medium. The cells were then rinsed with 2mL of DPBS (14190-094 ;Gibco®), and fixed with 3% paraformaldehyde for 90 minutes. Before the experiment, cells were rinsed three times during 10 minutes with DPBS. The slides were saturated for

90 minutes with PBS/Triton (127K0048 ; Sigma-Aldrich®) 0,3% / BSA (A2153 ; Sigma-Aldrich®) 1% (50µL) and then set in the damp chamber overnight with the primary antibody (Anti-Y_1; GTX54639 ; GeneTex®) or (Anti-Cathepsin B; FWN0217081 ; R&Dsystems®) (1/100) and PBS/Triton 0,3% / BSA 1%. Cells were then rinsed three times during 10 minutes with DPBS and then placed in the damp chamber, protected from light, with the secondary antibody (1/500) and PBS/Triton 0.3%/BSA1% (50µL). The glass cover slips were rinsed once more with DPBS for three times 10 minutes and then mounted on microscope sliders with Prolonlog (P36931; Invitrogen®) and DAPI (1/5000). All images obtained were analyzed using ImageJ© (V1.52c) software package.

Cathepsin B Human Elisa Assay

A standard curve (from 156 to 10.000ng/mL) for multiple measurements was prepared in triplicate. MCF7 samples were then studied in triplicate (1/2; 1/10; 1/100), according manufacturer instruction to verify the presence and activity of cathepsin-B.

Cell fragment immobilization in the PWR sensor and ligand titration

The protocol for adhesion of cell fragments on the PWR sensor (silica outlayer) was adapted from reported work of Vogel and collaborators,[39] and has been thoroughly detailed herein.[35] Briefly, the sensor silica surface was washed with ethanol, and cleaned and activated by plasma cleaner (Diener electronic, Ebhausen, Germany) for 2 min. The sensor silica surface was incubated with a polylysine solution (0.1 mg/mL) for 40 min, followed by a wash with PBS buffer. MCF-7 cells grown to less than 50 % confluence are washed with PBS and covered with water to induce osmotic swelling of the cells. Subsequently, the glass coverslip of the sensor is placed directly onto the cells. Pressure is applied for about 1 min on the glass slide or prism to induce cell rupture and capture of cell fragments. Afterwards, they are removed, ripping off cell fragments containing especially the upper membrane. The sensor is washed with PBS to remove cell debris and maintained in buffer to prevent drying and loss of membrane protein activity. The PWR cell sample (a teflon block with a volume capacity of 250 µL) is placed in contact with the sensor containing the immobilized cell fragments and filled with PBS. After cell fragment deposition, there are positive shifts in the resonance minimum position that are correlated with the total occurring mass gain. We have observed spectral shifts that correlate with those observed for the deposition of lipid model

membrane. In the case presented here, some areas of the sensor are covered with cell membranes and others are uncovered. The PWR signal takes into account both covered and uncovered areas as the laser spot is about 0.5 mm in diameter. At the same time, covered areas include both lipids and proteins, meaning that they possess a higher mass than that of a pure lipid membrane. Following stabilization of the signal (no changes in the resonance minimum position with time), peptide ligand is added in an incremental fashion to the chamber and spectral shifts are followed with time. Ligand affinity to the hY_1R in the MCF-7 cell membrane fragments is calculated by plotting the shifts in the resonance minimum position as a function of ligand concentration and performing an one-site saturation binding fir (Graph Pad Prism). Since between independent experiments the mass of cell membrane fragments and hence receptor quantities vary, which is reflected in the magnitude of the ligand-induced spectral changes, the data is normalized relative to the spectral shifts observed due to cell fragment deposition. Control experiments to investigate ligand binding to cell membrane components other than the receptor (e.g. lipids, sugars) are performed on cell membrane fragments from HEK293 cells that do not express the hY_1R.

Determination of hY_1R receptor saturation binding by plasmon waveguide resonance (PWR) spectroscopy

PWR was used to follow receptor conformational changes upon ligand addition to cell membrane fragments overexpressing the hY_1R that were immobilized in the sensor surface as described below [6]. PWR measurements were performed in a homemade instrument, functioning at a fixed wavelength of 632 nm and variable incident angle with an angular resolution of about 0.5 millidegrees [7]. The polarization angle of the incident light is placed at 45° to allow both p- (parallel to the incident light and perpendicular to the sensor surface) and s-polarized (perpendicular to the incident light and parallel to the sensor surface) light resonances to be obtained within a single angular scan. The sensor consists of a BK-7 prism that is coated with silver and silica to support waveguide modes [7]. All measurements were performed at 22 °C. After cell membrane fragment immobilization, ligand binding was measured by titrating with incremental ligand addition and measuring resonance shifts in both polarizations with time. The system was let to equilibrate before each incremental ligand addition. PWR being sensitive to the optical properties of material deposited on the resonator surface (*i.e.*, of ligand bound to the membrane fragments in the sensor), interference from the material present in the bulk solution (non-bound) is unlikely. Apparent dissociation constants (K_D) were obtained by plotting the resonance minimum position as a function of

the peptide concentration and by fitting the plot through a hyperbolic binding function using GraphPad Prism™ version 5.0a (GraphPad Software, San Diego, California, US).

Inositol monophosphate accumulation (IP-One) assay

Receptor activation by non-radioactive peptides was tested in an IP-One assay. COS-7 cells, stably co-transfected with hY_1R-eYFP or hY_2R-eYFP and a chimeric G-protein ($G\alpha_{\Delta 6qi4myr}$), were seeded in a white 384-well plate (6000-7500 cells/well) and grown for 24 h under humidified atmosphere at 37 C and 5 % CO_2. On the following day, the medium was removed by flipping the plate upside-down and the cells were stimulated with increasing concentrations of peptide in HBSS supplemented with 20 mM LiCl for 1 h at 37 °C and 5 % CO_2. Peptides were tested in a concentration range from 10^{-5} M to 10^{-13} M in triplicates. Generated inositol monophosphate was subsequently quantified by using the Cisbio IP-One Gq HTRF assay kit according to the manufacturer's instructions. For the assay read-out, a Tecan Spark microplate reader was used. Data analysis was performed with GraphPad Prism 5.03. Obtained HTRF values for the compounds were normalized to NPY and EC_{50} and pEC_{50} values were calculated from sigmoidal concentration-response curves. Each peptide was tested at least two times independently.

Receptor internalization studies

HEK293 cells stably transfected with the hY_1R or hY_2R, *C*-terminally fused to eYFP, were seeded into ibiTreat 8-well µ-slides (ibidi, Martinsried, Germany) at a density of 300,000 cells/well and cultured overnight until the cells reached confluency. The culture medium was aspirated and the cells were starved in 200 µL Opti-MEM® with 1 µL nuclear stain Hoechst 33342 (0.5 mg/mL) for 30 min under humidified atmosphere at 37 °C and 5 % CO_2. For the non-stimulated cell control, the starving solution was aspirated and 200 µL Opti-MEM® were added. For testing the receptor internalization of non-radioactive NPY conjugates, the starving medium was aspirated and 200 µL Opti-MEM® containing 100 nM peptide (hY_1R) or 1 µM peptide (hY_2R) were added to the cells. After 1 h of stimulation at 37 °C, the cells were washed and maintained in Opti-MEM®. For fluorescence image acquisition, a Zeiss Axio Observer microscope with an ApoTome.2 Imaging System and a 63× immersion oil

objective was used. The nuclear stain Hoechst 33342 was visualized by the DAPI filter (excitation 335−383 nm; emission 420−470 nm) and the eYFP-tag on the receptor by the YFP filter (excitation 488−512 nm; emission 520−550 nm). Image processing was performed with Zeiss ZEN 2 software.

Lipophilicity

The lipophilicity of radiolabeled peptides was assessed by the water-octanol partition/distribution coefficient method. In a centrifuge tube, 500 µL of 1-octanol was added to 500 µL of phosphate-buffered saline (pH 7.4 or pH 5) or water containing the radiolabeled peptide (50 kBq). After equilibrium, the solution was vigorously stirred for 5 min at room temperature and subsequently centrifuged (4000 rpm, 5 min) to yield two immiscible layers. Aliquots of 200 µL were taken from each layer and the radioactivity in the samples was determined by a gamma counter (Perkin Elmer, Waltham, MA, USA).

Metabolic stability

2 MBq of ^{111}In-labeled NPY conjugate **3c** were incubated in 2 mL of human blood plasma at 37 °C. At designated time points, samples of 50 µL were taken and 100 µL ethanol was added to precipitate the plasma proteins. The mixture was centrifuged (5 min, 13000 rpm), 50 µL of supernatant were diluted with 150 µL water and analyzed by UV-radio RP-HPLC. The quantity of intact peptide was referred to the control at 0 h (set at 100%). The experiment was performed two times independently.

Membrane integrity assay

For cytotoxicity assay, MCF-7 cells were seeded at a density of 10 000 cells per well (5µL) in 96-well plates and incubated overnight with 95µL of medium (RPMI1640 containing 10% FBS, penicillin-streptomycin (100µg/mL)). Approximately 10^{-8}M of the respective pb12, ^{nat}Tb-pb12 and control peptide pb13 were added to the medium, and the cells were incubated in triplicates for 4.5 h at 37 °C. Plates were then removed from the incubator and equilibrated to room temperature (approximately 20 minutes). Then, 100µL of Cytotox-One reagent was added to each well, shaken for 30 seconds and incubated for 10 minutes at room temperature. Stop solution

(50µL) was added to each well and shaken for 10 seconds. Fluorescence was measured in a plate reader with an excitation wavelength of 560nm and an emission wavelength of 590nm.

Particle Induced X-ray Emission (PIXE) of [^{nat}Tb]Tb-pb12

Cell monolayers were prepared and freeze-dried for ion beam analysis according to published protocol [8]. Nuclear microprobe analysis of intracellular chemical element contents was performed at the AIFIRA facility, using a 3.0 MeV proton beam focused onto the sample surface, ending with a beam diameter of 1 µm and a beam current of approximately 100 pA [9]. The beam was continuously scanned over square-shaped regions of interest of approximately 150 µm in width. Typical acquisition time for a single analysis was 1 to 2 hours. X-rays emitted after sample-beam interaction were measured using 2 Si(Li) x-ray photon detectors symmetrically placed at 20 mm from sample surface with an angle of 45°. X-ray detectors were covered with a carbon "funny" filter (filter with a pinhole) in order to prevent backscattered protons to blind them. The number of protons delivered during an acquisition, as used for quantification, was measured at the same time by RBS analysis using a PIPS (passivated implanted planar silicon) detector (Canberra PD 50-11-300 AM) placed at a 135° from incoming beam direction. A set of reference samples (GdF_3, CuS, Fe and ZnTe) with certified elemental concentration (100 µg/cm² ± 5%) was used to measure quantification accuracy of the overall set-up (beam geometry – detectors configuration – filters). Calibration of our experimental set-up resulted in concentration measurements in agreement with certified values for element above potassium (X-ray energy > 3.7 keV). Lighter elements producing X-ray photons with lower energy cannot be quantified with a reasonable accuracy due to photons absorption by the funny filter. Results are expressed in percentage of limit of detection.

RESULTS

PEPTIDE SYNTHESIS

Analytical data of all compounds studied in this work are summarized in Supplemental table 1. Exemplary analytical data is shown for conjugate pb12 and [^{nat}Tb]Tb-pb12 in Supplemental figure 1 below.

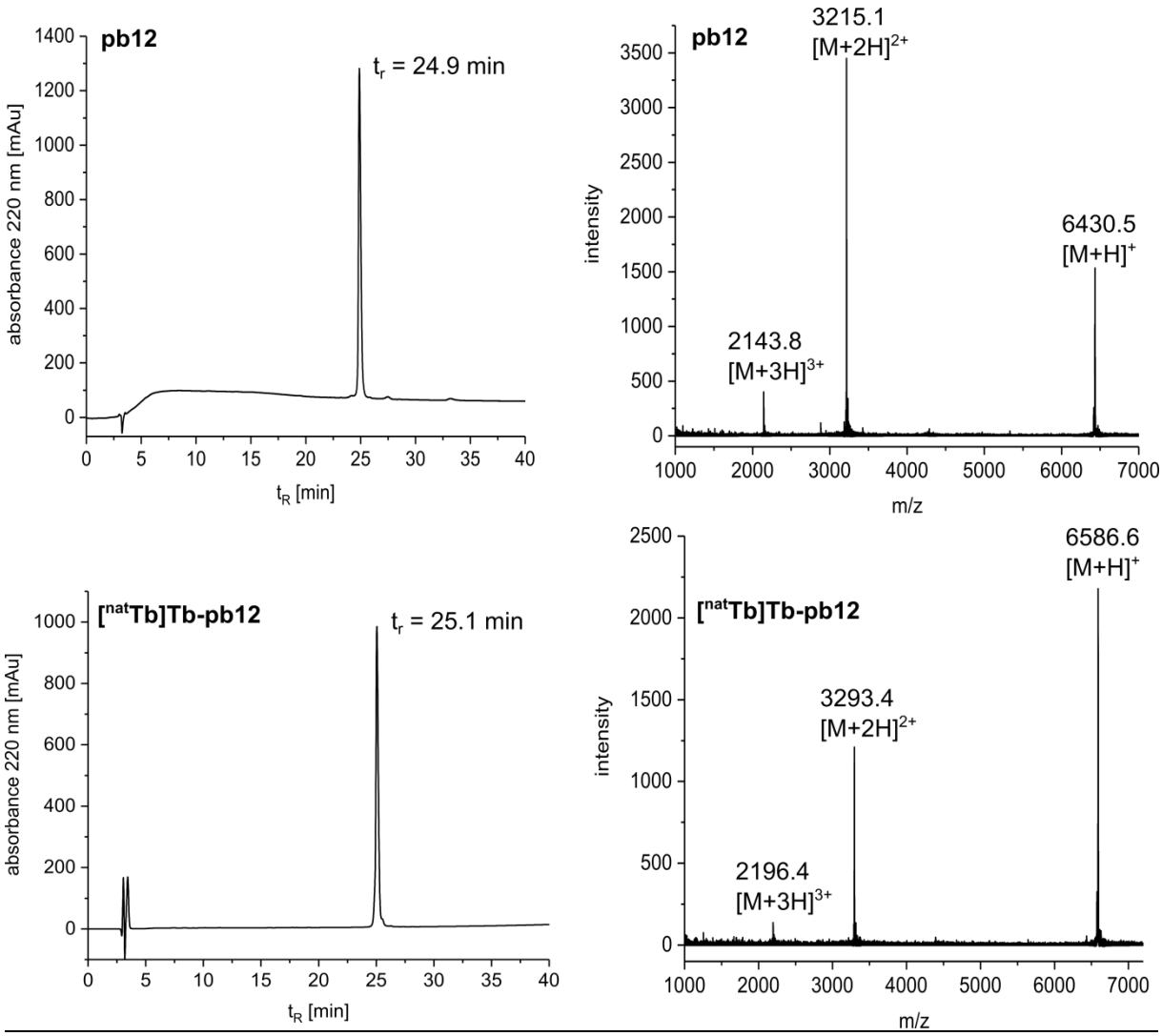

Supplemental figure 1: Analytical data of the peptide conjugate pb12 and the ^{nat}Tb-labeled version [^{nat}Tb]Tb-pb12. Top left: RP-HPLC analysis of pb12 using an Agilent VariTide RPC 200 Å column and a linear gradient of 20%-70% (*v/v*) eluent B in eluent A over 40 min. Eluent A: H_2O + 0.1 % (*v/v*) TFA, eluent B: acetonitrile + 0.08 % (*v/v*) TFA. Top right: MALDI-ToF mass spectrum showing the single-, double- and triple-charged molecular ion species of pb12. M_{exact} (calc.): 6429.5 Da. Bottom left: RP-HPLC analysis of ^{nat}Tb-labeled [^{nat}Tb]Tb-pb12 using an Agilent VariTide RPC 200 Å column and a linear gradient of 20%-70% (*v/v*) eluent B in eluent A over 40 min. Bottom right: MALDI-ToF mass spectrum showing the single-, double- and triple-charged molecular ion species of ^{nat}Tb-labeled pb12. M_{exact} (calc.): 6585.4 Da.

compound	Analyt. RP-HPLC		MALDI-ToF MS		purity
	t_R^1 [min][a]	t_R^2 [min]	M_{exact} (calc.)[d]	M_{exact} (exp.)[e]	

			[Da]	$[M+H]^+$	
NPY	21.3	16.2[b]	4251.1	4252.1	> 95 %
$[F^7,P^{34}]$-NPY	21.0	15.2[b]	4253.1	4254.1	> 95 %
pb12	27.1	24.9[c]	6429.5	6430.5	> 95 %
[^{nat}Tb]Tb-pb12	-	25.1[c]	6585.4	6586.6	> 95 %
pb13	28.5	25.4[c]	6259.4	6260.3	> 95 %
[^{nat}Tb]Tb-pb13	-	25.1[c]	6415.3	6416.4	> 95 %

Supplemental Table 1. Analysis of synthesized peptides by analytical RP-HPLC and MALDI-ToF MS.

[a]Retention time t_R^1 was determined on a Phenomenex Jupiter® 4u Proteo C12 90 Å column using a linear gradient of 20%-70% eluent B in eluent A over 40 min. [b]Retention time t_R^2 for NPY and $[F^7,P^{34}]$-NPY was determined on a Phenomenex Aeris® Peptide 3.6u XB-C18 column using a linear gradient of 20%-70% eluent B in eluent A over 40 min. [c]Retention time t_R^2 for pb12, [^{nat}Tb]Tb-pb12, pb13 and [^{nat}Tb]Tb-pb13 was determined on a Agilent VariTide RPC 200 Å column using a linear gradient of 20%-70% eluent B in eluent A over 40 min. [d]M_{exact} (calc.): calculated monoisotopic mass in Dalton. [e]M_{exact} (exp.): experimentally measured monoisotopic mass.

CHARACTERIZATION OF MCF-7 CELLS

Western Blot

Immunoblots confirmed that MCF-7 cells effectively express the hY_1R (designated as Y_1 on the Supplemental Figure 2 below) and the cathepsin B enzyme. They are suitable cells to investigate our NPY-conjugates.

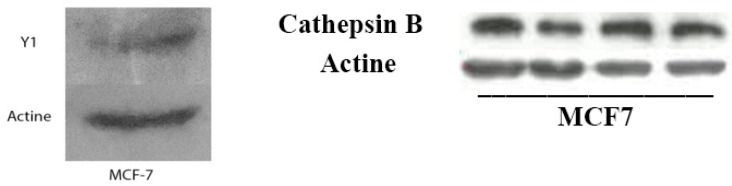

Supplemental Figure 2: Western Blot of hY_1R and cathepsin-B in MCF-7 cells

Immunofluorescence

Using immunofluorescence experiments, we confirmed that MCF-7 cells expressed the hY_1R. Moreover, a membranous labelling was seen for hY_1R as expected with G-protein coupled receptor.

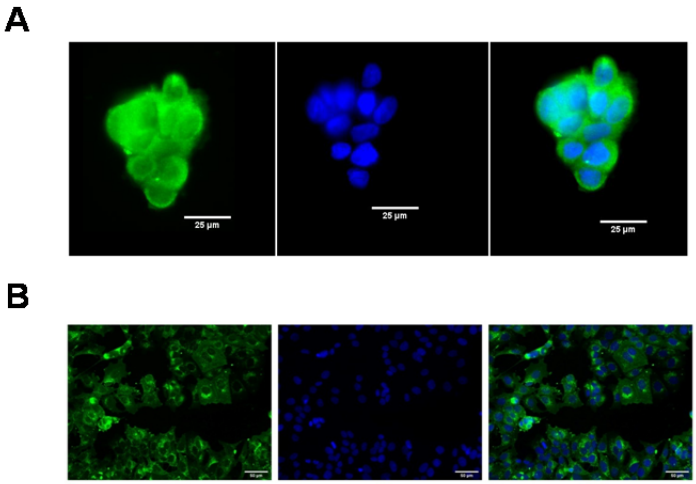

Supplemental figure 3: Immunofluorescence of hY_1R and cathepsin-B in MCF-7 cells at magnification X20. A – left image: subcellular localization of hY_1R assessed by immunofluorescence. Membranous hY_1R expression is seen on MCF-7 cells (green). Middle: DNA staining with DAPI (blue). Right image: fused image. B – left image: subcellular localization of cathepsin-B assessed by immunofluorescence. Granular cytoplasmic staining of cathepsin-B is seen on MCF-7 cells (green). Middle: DNA staining with DAPI (blue). Right image: fused image. Scale bar = 25µm

Cathepsin B Human Elisa Assay

Using ELISA, cathepsin B activity was found to be 57.11 ± 6.13 ng/mL confirming that MCF-7 cells could be used to study our NPY-conjugates metabolized by the cathepsin B.

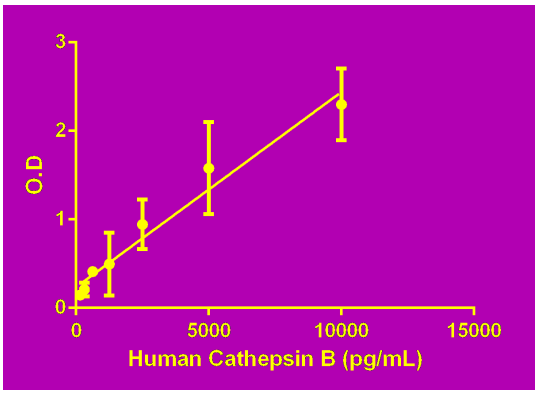

Supplemental Figure 4: ELISA experiment to determine cathepsin B activity in MCF-7 cells. O.D stands for optical density.

All together, these approaches confirm that MCF-7 cells possess all biological equipment (hY_1R and active cathepsin-B enzyme) suitable to study our NPY-multivalent compound.

Affinity values of pb13, [^{nat}Tb]Tb-pb13, [^{111}In]In-pb12, [^{111}In]In-pb13, pb12 and [^{nat}Tb]Tb-pb12

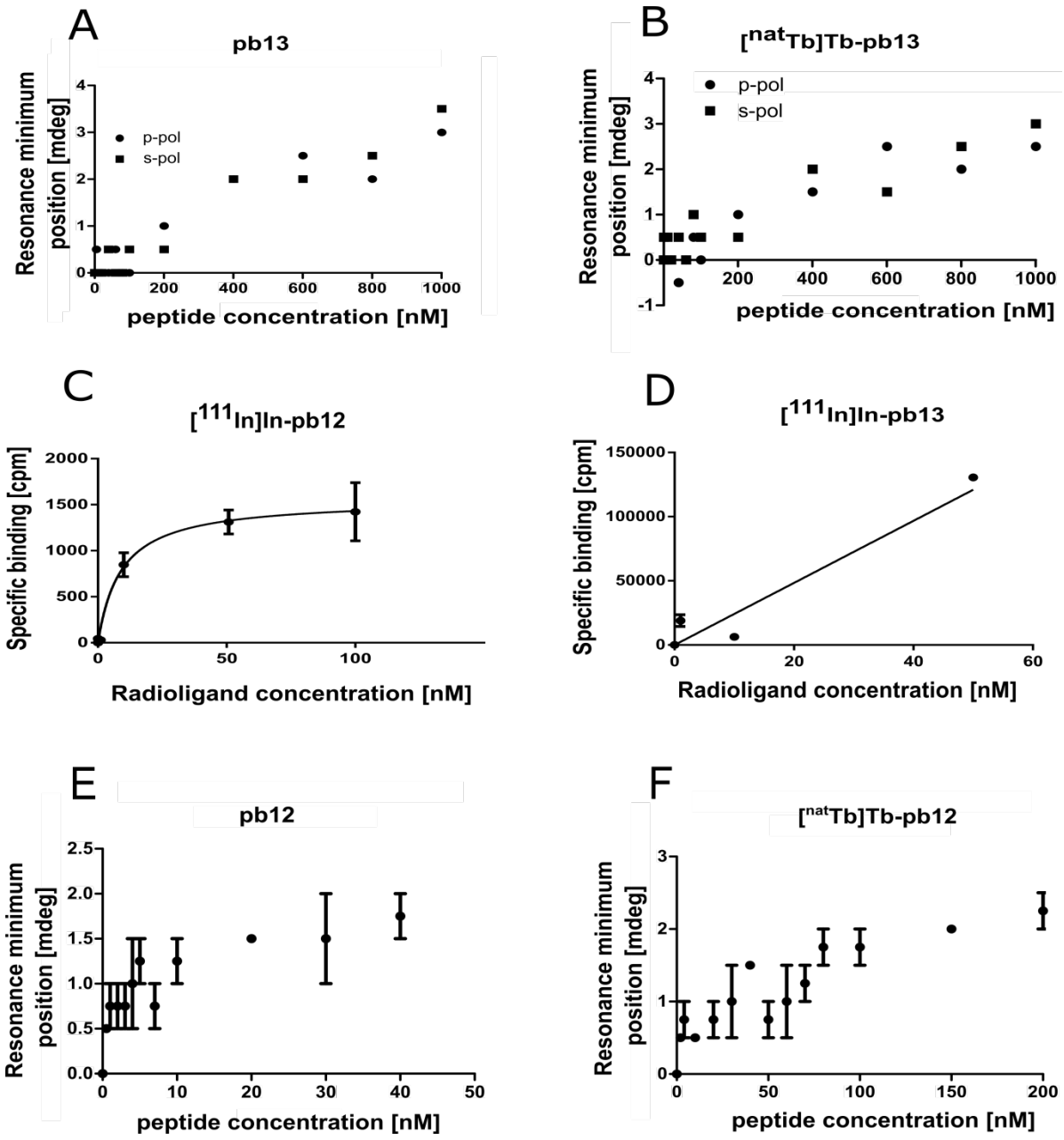

Supplemental figure 5. Affinity values of some NPY-conjugates developed in this work to the hY_1R determined by PWR (A, B, E, F) and radiolabelling assay (C, D). The unlabeled control peptide pb13 (A), the terbium-labelled control peptide [^{nat}Tb]Tb-pb13 (B) and the radiolabeled control peptide [^{111}In]In-pb13 (D) showed no specific binding to MCF-7 fragments The [^{111}In]In-pb12 (C) exhibit specific binding to MCF-7. As additional control experiments, pb12 (E) and [^{nat}Tb]Tb-pb12 present some non-specific interaction to hY_1R-negative HEK293 cells.

REFERENCES

1. Böhme D, Beck-Sickinger AG. Controlling toxicity of Peptide-drug conjugates by different chemical linker structures. ChemMedChem. 2015;10:804–14.

2. Worm DJ, Hoppenz P, Els-Heindl S, Kellert M, Kuhnert R, Saretz S, et al. Selective Neuropeptide Y Conjugates with Maximized Carborane Loading as Promising Boron Delivery Agents for Boron Neutron Capture Therapy. J Med Chem. 2019

3. Zhong Y-J, Shao L-H, Li Y. Cathepsin B-cleavable doxorubicin prodrugs for targeted cancer therapy (Review). Int J Oncol. 2013;42:373–83.

4. Dang CV, Lee WM. Identification of the human c-myc protein nuclear translocation signal. Mol Cell Biol. 1988;8:4048–54.

5. Hofmann S, Maschauer S, Kuwert T, Beck-Sickinger AG, Prante O. Synthesis and in Vitro and in Vivo Evaluation of an ^{18}F-Labeled Neuropeptide Y Analogue for Imaging of Breast Cancer by PET. Mol Pharmaceutics. 2015;12:1121–30.

6. Boyé K, Billottet C, Pujol N, Alves ID, Bikfalvi A. Ligand activation induces different conformational changes in CXCR3 receptor isoforms as evidenced by plasmon waveguide resonance (PWR). Sci Rep. 2017;7.

7. Harté E, Maalouli N, Shalabney A, Texier E, Berthelot K, Lecomte S, et al. Probing the kinetics of lipid membrane formation and the interaction of a nontoxic and a toxic amyloid with plasmon waveguide resonance. Chem Commun. 2014;50:4168–71.

8. Muggiolu G, Simon M, Lampe N, Devès G, Barberet P, Michelet C, et al. In Situ Detection and Single Cell Quantification of Metal Oxide Nanoparticles Using Nuclear Microprobe Analysis. J Vis Exp. 2018;

9. Sorieul S, Alfaurt Ph, Daudin L, Serani L, Moretto Ph. Aifira: An ion beam facility for multidisciplinary research. Nuclear Instruments and Methods in Physics Research Section B: Beam Interactions with Materials and Atoms. 2014;332:68–73.

Discussion générale :

L'approche théranostique en RIV à l'aide d'analogues de neuropeptides est en plein développement. Il y a notamment les analogues de la somatostatine ciblant SST_2 dans les TNE avec entres autres la lutathérapie (Lutathera® ou [^{177}Lu]Lu-oxodotréotide, ayant l'AMM depuis 2017) et le [^{68}Ga]Ga-DOTATOC ([^{68}Ga]Ga-édotréotide, ayant l'AMM depuis 2017). Des analogues dérivés de la bombésine ciblant le GRPR, tel que le RM2, sont actuellement évalués en essais cliniques chez l'homme[134,135,136]. J'ai notamment eu l'occasion de travailler sur un nouveau kit de RM2 pour faciliter le radiomarquage manuel au ^{68}Ga dans le cadre de ma thèse d'exercice de pharmacie[137] (cf. annexe).

L'objectif de ce travail, s'inscrivant dans la continuité de ces études, a été le développement de nouveaux radiopharmaceutiques, analogues de neuropeptides, ciblant des récepteurs surexprimés à la surface de tumeurs, à visée théranostique dans divers cancers.

Nous avons caractérisé deux nouvelles molécules d'intérêt, l'analogue de la neurotensine JMV6659 et l'analogue du neuropeptide Y pb12. Afin de pouvoir étudier ces molécules, il a fallu développer de nouvelles méthodes expérimentales dans notre laboratoire (INCIA CNRS-UMR-5287 Bordeaux), pour mesurer in vitro l'internalisation et l'efflux cellulaire, ainsi que l'affinité pour le récepteur cible. Ceci a notamment impliqué le choix du ligand froid à utiliser pour déterminer l'internalisation et l'efflux médié par le récepteur étudié (analogue froid du conjugué étudié, antagoniste spécifique ou peptide endogène…). Pour cela il a fallu notamment prendre en compte l'aspect économique ainsi que les données de la littérature. En effet, il a été crucial de rapprocher les conditions expérimentales à celles rapportées dans la littérature afin de pouvoir ensuite comparer les résultats. La mise en place de ces nouvelles méthodes au sein du laboratoire nous permet d'effectuer à l'avenir l'ensemble des expériences in vitro et ex-vivo précliniques pour d'autres analogues de neuropeptides. N'ayant pas de micro-PET à notre disposition à Bordeaux à ce jour, les études in-vivo avec souris nude ne sont pas réalisables au sein de notre laboratoire et la collaboration avec d'autres équipes au cours de ce travail a été nécessaire et enrichissante.

Nos deux molécules d'intérêt, bien que prometteuses ont pour inconvénient leur faible stabilité plasmatique. Ceci est particulièrement vrai pour le pb12 qui a une demi-vie d'environ 20 minutes ex-vivo. De plus, sa captation tumorale spécifique chez la souris n'a pu être observée qu'à des temps très précoce post-injection, alors qu'aux temps plus tardifs la dégradation enzymatique plasmatique a empêché le renforcement de la captation, nécessaire à une bonne

visualisation en imagerie et bien sûr à une action thérapeutique ciblée. Au vu de l'amélioration de la stabilité plasmatique observée suite à l'insertion d'acides aminés non naturels dans le JMV6659, il serait intéressant de faire des modifications similaires pour pb12. De plus, il n'y a pas à ce jour d'analogues de neuropeptide Y entiers contenant des acides aminés non naturels décrits dans la littérature. Seuls des analogues tronqués possédant des acides aminés non naturels ont été décrits, ayant une amélioration de la stabilité plasmatique[120,138]. Il serait donc intéressant de modifier pb12 en substituant les acides aminés des sites de clivage par des acides aminés non naturels. Concernant notre analogue de la neurotensine JMV6659 (contenant des acides aminés non-naturels), malgré son excellente affinité pour NTS_1 et captation tumorale chez la souris, sa demi-vie reste trop courte pour une utilisation confortable en pratique clinique. Notre équipe est en train de travailler sur une 2ème génération d'analogues issues du JMV6659 dont l'objectif est d'améliorer la stabilité plasmatique tout en conservant ses caractéristiques pharmacologiques. Nous nous intéressons plus particulièrement au site de clivage peptide-DOTA en modifiant le linker ou le site de liaison linker-peptide.

Les deux analogues de neuropeptide que nous avons étudié sont internalisés par les cellules tumorales cibles. Cependant, au-delà de l'internalisation cellulaire, un des intérêts de pb12 est son adressage nucléaire via la séquence NLS. L'adressage nucléaire permet d'amener les molécules vectrices et leur atome radioactif au plus près de l'ADN cellulaire ce qui permettrait d'envisager l'emploi de radioéléments novateurs, notamment des émetteurs Auger (déposant de fortes énergies sur de très faibles distances)[139]. Cette approche a déjà été explorée avec d'autres analogues, notamment des analogues radiomarqués de la somatostatine[133]. Pour l'[^{111}In]In-Pb12, bien que l'introduction de la séquence NLS a permis une internalisation nucléaire significativement plus importante, nous n'avons toutefois pas pu exclure une contribution non spécifique par diffusion passive car l'ajout d'un inhibiteur de la cathepsine B n'a pas entièrement inhibé l'internalisation nucléaire. Ceci suggère que l'apport d'une NLS pour l'adressage nucléaire reste encore modéré et il serait intéressant d'améliorer cet adressage pour potentialiser l'efficacité de l'atome radioactif choisi pour la thérapie. Par ailleurs, afin de pouvoir exploiter l'adressage nucléaire à l'aide de la NLS, il est indispensable que la molécule à adresser soit dans le cytoplasme[130], ce qui sera à prendre en compte lors du développement d'autres analogues radiomarqués.

Amener un analogue radiomarqué au sein du noyau cellulaire permet de déposer l'énergie libérée par l'atome radioactif au plus près de l'ADN cellulaire provoquant la mort cellulaire par divers mécanismes (mort mitotique, apoptose, etc.). On peut ainsi employer des atomes déposant une très forte énergie à très courte distance (potentialisant leur action par rapport à

une simple internalisation cytoplasmique). C'est ainsi que le Terbium-161 (émetteur bêta moins et Auger) est particulièrement intéressant et étudié en ce moment par plusieurs équipes. Notre équipe a notamment effectué plusieurs études in sillico évaluant la dose délivrée par le ^{161}Tb[128,129,140]. Il a été ainsi démontré que le Terbium 161 dépose une quantité plus importante d'énergie sur des distance plus faible que le Lutétium 177, ce qui rend cet atome particulièrement attractif pour traiter des micrométastases (<1mm, et plus particulièrement ≤100µm). Ainsi, dans le cas spécifique d'une cellule tumorale isolée de 10 micromètres de diamètre, le ^{161}Tb déposerait 3,5 fois plus d'énergie que le ^{177}Lu. L'équipe de C. Müller a effectué des études in vitro d'analogues radiomarqués au ^{161}Tb[124,126] avec des résultats encourageants. Ils ont en effet pu obtenir une pureté radiochimique de leur analogue radiomarqué au ^{161}Tb >98%, et un profil pharmacologique comparable entre les molécules marquées au ^{177}Lu et celles marquées ^{161}Tb. Ils ont pu confirmer que le terbium dépose 3 fois plus d'énergie que le ^{177}Lu. Ainsi le terbium peut probablement se substituer au ^{177}Lu sans impacter significativement les caractéristiques pharmacocinétiques d'un analogue d'intérêt. Un des autres avantages du Terbium est l'existence d'isotopes émetteurs bêta plus (^{152}Tb) et gamma (^{155}Tb) utilisables à visée diagnostique en TEP et SPECT respectivement. C'est donc un radioélément très intéressant dans une perspective d'utilisation en théranostique et des efforts à l'échelle européenne sont en cours afin d'augmenter sa disponibilité et permettre son utilisation en recherche clinique. Pour maximiser l'effet du terbium 161, ou d'émetteurs Auger purs, il faudra à l'avenir renforcer les différentes techniques d'adressage nucléaire[139].

Conclusion

L'utilisation de radiopharmaceutiques dans une démarche théranostique en médecine nucléaire, où l'imagerie des cibles tumorales est suivie d'une radiothérapie interne vectorisée (RIV), est en plein essor. Le ciblage des récepteurs de neuropeptides surexprimés dans plusieurs cancers est une des voies les plus prometteuses. Notre travail de thèse s'est inscrit dans ce cadre avec pour objectif d'affiner le ciblage du récepteur NTS_1 de la neurotensine et le ciblage du récepteur Y_1 du neuropeptide-Y.

Ainsi, nous avons au cours de ce travail pu contribuer au développement, marquage et caractérisation, de deux analogues : l'analogue de la neurotensine « JMV6659 » et l'analogue du neuropeptide Y « pb12 ».

Les résultats obtenus avec le JMV6659 montrent que l'utilisation d'acides aminés non naturels dans les analogues peptidiques est une piste très intéressante pour améliorer la stabilité plasmatique de ces radioligands de la neurotensine. Ainsi, notre équipe de l'INCIA travaille actuellement sur une $2^{ème}$ génération d'analogues issues du JMV6659 dont l'objectif est d'améliorer la stabilité plasmatique tout en conservant ses caractéristiques pharmacologiques.

Le pb12 a été développé avec pour objectif l'adressage nucléaire grâce à la séquence NLS que porte ce conjugué. L'adressage nucléaire permet d'amener les molécules vectrices et leur atome radioactif au plus près de l'ADN cellulaire. L'insertion de la séquence NLS dans le pb12 a permis son adressage nucléaire ce qui élargit les possibilités théranostiques avec la perspective d'utiliser les émetteurs Auger tels que le ^{161}Tb. Un travail d'optimisation de la structure afin de la protéger de la dégradation enzymatique est maintenant nécessaire et ce travail se poursuit au sein de l'INCIA.

Bibliographie

1 E. L. Mazzaferri et S. M. Jhiang, « Long-Term Impact of Initial Surgical and Medical Therapy on Papillary and Follicular Thyroid Cancer », *The American Journal of Medicine* 97, no 5 (novembre 1994): 418-28.

2 *Elif Hindié et al., « Functioning Pulmonary Metastases of Thyroid Cancer: Does Radioiodine Influence the Prognosis? », European Journal of Nuclear Medicine and Molecular Imaging* 30, no 7 (juillet 2003): 974-81, https://doi.org/10.1007/s00259-003-1174-5.

3 Elif Hindié et al., « Bone Metastases of Differentiated Thyroid Cancer: Impact of Early 131I-Based Detection on Outcome », *Endocrine-Related Cancer* 14, no 3 (septembre 2007): 799-807, https://doi.org/10.1677/ERC-07-0120.

4 Dorina Ylli, Douglas Van Nostrand, et Leonard Wartofsky, « Conventional Radioiodine Therapy for Differentiated Thyroid Cancer », *Endocrinology and Metabolism Clinics of North America, Thyroid Cancer*, 48, no 1 (1 mars 2019): 181-97, https://doi.org/10.1016/j.ecl.2018.11.005.

5 C. A. Hoefnagel et al., « Radionuclide Diagnosis and Therapy of Neural Crest Tumors Using Iodine-131 Metaiodobenzylguanidine », *Journal of Nuclear Medicine: Official Publication*, Society of Nuclear Medicine 28, no 3 (mars 1987): 308-14.

6 *James Nagarajah et al., « Iodine Symporter Targeting with 124I/131I Theranostics », Journal of Nuclear Medicine: Official Publication*, Society of Nuclear Medicine 58, no Suppl 2 (2017): 34S-38S, https://doi.org/10.2967/jnumed.116.186866.

7 Thomas E. Witzig et al., « Randomized Controlled Trial of Yttrium-90-Labeled Ibritumomab Tiuxetan Radioimmunotherapy versus Rituximab Immunotherapy for Patients with Relapsed or Refractory Low-Grade, Follicular, or Transformed B-Cell Non-Hodgkin's Lymphoma », *Journal of Clinical Oncology: Official Journal of the American Society of Clinical Oncology* 20, no 10 (15 mai 2002): 2453-63, https://doi.org/10.1200/JCO.2002.11.076.

8 Franck Morschhauser et al., « Phase III Trial of Consolidation Therapy with Yttrium-90-Ibritumomab Tiuxetan Compared with No Additional Therapy after First Remission in Advanced Follicular Lymphoma », Journal of Clinical Oncology: Official Journal of the American Society of Clinical Oncology 26, no 32 (10 novembre 2008): 5156-64, https://doi.org/10.1200/JCO.2008.17.2015.

9 Françoise Kraeber-Bodéré et al., « Radioimmunoconjugates for the Treatment of Cancer », Seminars in Oncology 41, no 5 (octobre 2014): 613-22, https://doi.org/10.1053/j.seminoncol.2014.07.004.

10 Flavio Forrer et al., « Targeted Radionuclide Therapy with 90Y-DOTATOC in Patients with Neuroendocrine Tumors », Anticancer Research 26, no 1B (février 2006): 703-7.

11 Rachel Levine et Eric P. Krenning, « Clinical History of the Theranostic Radionuclide Approach to Neuroendocrine Tumors and Other Types of Cancer: Historical Review Based on an Interview of Eric P. Krenning by Rachel Levine », Journal of Nuclear Medicine: Official Publication, Society of Nuclear Medicine 58, no Suppl 2 (2017): 3S-9S, https://doi.org/10.2967/jnumed.116.186502.

12 B. L. R. Kam et al., « Lutetium-Labelled Peptides for Therapy of Neuroendocrine Tumours », European Journal of Nuclear Medicine and Molecular Imaging 39 Suppl 1 (février 2012): S103-112, https://doi.org/10.1007/s00259-011-2039-y.

13 Kambiz Rahbar et al., « Radioligand Therapy With 177Lu-PSMA-617 as A Novel Therapeutic Option in Patients With Metastatic Castration Resistant Prostate Cancer », Clinical Nuclear Medicine 41, no 7 (juillet 2016): 522-28, https://doi.org/10.1097/RLU.0000000000001240.

14 Michael S. Hofman et al., « [177Lu]-PSMA-617 Radionuclide Treatment in Patients with Metastatic Castration-Resistant Prostate Cancer (LuPSMA Trial): A Single-Centre, Single-Arm, Phase 2 Study », The Lancet Oncology 19, no 6 (1 juin 2018): 825-33, https://doi.org/10.1016/S1470-2045(18)30198-0.

15 Kambiz Rahbar, Lisa Bodei, et Michael J. Morris, « Is the Vision of Radioligand Therapy for Prostate Cancer Becoming a Reality? An Overview of the Phase III VISION Trial and Its Importance for the Future of Theranostics », Journal of Nuclear Medicine 60, no 11 (11 janvier 2019): 1504-6, https://doi.org/10.2967/jnumed.119.234054.

16 Christophe M. Deroose et al., « Molecular Imaging of Gastroenteropancreatic Neuroendocrine Tumors: Current Status and Future Directions », Journal of Nuclear Medicine: Official Publication, Society of Nuclear Medicine 57, no 12 (décembre 2016): 1949-56, https://doi.org/10.2967/jnumed.116.179234.

17 Jaap J. M. Teunissen et al., « Nuclear Medicine Techniques for the Imaging and Treatment of Neuroendocrine Tumours », Endocrine-Related Cancer 18 Suppl 1 (octobre 2011): S27-51, https://doi.org/10.1530/ERC-10-0282.

18 Ali Afshar-Oromieh et al., « The Theranostic PSMA Ligand PSMA-617 in the Diagnosis of Prostate Cancer by PET/CT: Biodistribution in Humans, Radiation Dosimetry, and First Evaluation of Tumor Lesions », Journal of Nuclear Medicine: Official Publication, Society of Nuclear Medicine 56, no 11 (novembre 2015): 1697-1705, https://doi.org/10.2967/jnumed.115.161299.

19 Melpomeni Fani, João P. André, et Helmut R. Maecke, « 68Ga-PET: A Powerful Generator-Based Alternative to Cyclotron-Based PET Radiopharmaceuticals », Contrast Media & Molecular Imaging 3, no 2 (avril 2008): 67-77, https://doi.org/10.1002/cmmi.232.

20 Richard P. Baum et Harshad R. Kulkarni, « THERANOSTICS: From Molecular Imaging Using Ga-68 Labeled Tracers and PET/CT to Personalized Radionuclide Therapy - The Bad Berka Experience », Theranostics 2, no 5 (2012): 437-47, https://doi.org/10.7150/thno.3645.

21 Clément Morgat et al., « Targeting Neuropeptide Receptors for Cancer Imaging and Therapy: Perspectives with Bombesin, Neurotensin, and Neuropeptide-Y Receptors », Journal of Nuclear Medicine: Official Publication, Society of Nuclear Medicine 55, no 10 (octobre 2014): 1650-57, https://doi.org/10.2967/jnumed.114.142000.

22 Renzo Cescato et al., « Bombesin Receptor Antagonists May Be Preferable to Agonists for Tumor Targeting », Journal of Nuclear Medicine: Official Publication, Society of Nuclear Medicine 49, no 2 (février 2008): 318-26, https://doi.org/10.2967/jnumed.107.045054.

23 Guillaume P. Nicolas et al., « Sensitivity Comparison of 68Ga-OPS202 and 68Ga-DOTATOC PET/CT in Patients with Gastroenteropancreatic Neuroendocrine Tumors: A Prospective Phase II Imaging Study », Journal of Nuclear Medicine: Official Publication, Society of Nuclear Medicine 59, no 6 (2018): 915-21, https://doi.org/10.2967/jnumed.117.199760.

24 Robert Carraway et Susan E. Leeman, « The Isolation of a New Hypotensive Peptide, Neurotensin, from Bovine Hypothalami », Journal of Biological Chemistry 248, no 19 (10 octobre 1973): 6854-61.

25 R. Carraway et S. E. Leeman, « The Synthesis of Neurotensin. », Journal of Biological Chemistry 250, no 5 (3 octobre 1975): 1912-18.

26 Stefanie Geisler et al., « Brain Neurotensin, Psychostimulants, and Stress – Emphasis on Neuroanatomical Substrates », Peptides, Neurotensin: Roles and Mechanisms, 27, no 10 (1 octobre 2006): 2364-84, https://doi.org/10.1016/j.peptides.2006.03.037.

27 Bradley V. Clineschmidt et Jodie C. McGuffin, « Neurotensin Administered Intracisternally Inhibits Responsiveness of Mice to Noxious Stimuli », European Journal of Pharmacology 46, no 4 (15 décembre 1977): 395-96, https://doi.org/10.1016/0014-2999(77)90236-9.

28 Lucio Gullo et al., « Plasma Cholecystokinin and Neurotensin after an Ordinary Meal in Humans », EM-Consulte, Gastroenterol Clin Biol, 1998, https://www.em-consulte.com/article/97861/alertePM.

29 John G. Wood et al., « Effect of Neurotensin on Pancreatic and Gastric Secretion and Growth in Rats », Pancreas 3, no 3 (mai 1988): 332–339.

30 Robert P. Thomas et al., « Role of Gastrointestinal Hormones in the Proliferation of Normal and Neoplastic Tissues », Endocrine Reviews 24, no 5 (1 octobre 2003): 571-99, https://doi.org/10.1210/er.2002-0028.

31 William H. Rostène et Mark J. Alexander, « Neurotensin and Neuroendocrine Regulation », Frontiers in Neuroendocrinology 18, no 2 (1 avril 1997): 115-73, https://doi.org/10.1006/frne.1996.0146.

32 Pascale Chalon et al., « Molecular Cloning of a Levocabastine-Sensitive Neurotensin Binding Site », FEBS Letters 386, no 2-3 (1996): 91-94, https://doi.org/10.1016/0014-5793(96)00397-3.

33 Zherui Wu et al., « Neurotensin and its high affinity receptor 1 as a potential pharmacological target in cancer therapy », Frontiers in Endocrinology 3 (17 janvier 2013), https://doi.org/10.3389/fendo.2012.00184.

34 M. Méndez et al., « High Affinity Neurotensin Receptor MRNA Distribution in Rat Brain and Peripheral Tissues. Analysis by Quantitative RT-PCR », Journal of Molecular Neuroscience: MN 9, no 2 (octobre 1997): 93-102, https://doi.org/10.1007/BF02736853.

35 Shengyang Qiu et al., « Characterisation of the Expression of Neurotensin and Its Receptors in Human Colorectal Cancer and Its Clinical Implications », Biomolecules 10, no 8 (5 août 2020), https://doi.org/10.3390/biom10081145.

36 Manfred Rettenbacher et Jean Reubi, « Localization and Characterization of Neuropeptide Receptors in Human Colon », Naunyn-Schmiedeberg's Archives of Pharmacology 364, no 4 (1 octobre 2001): 291-304, https://doi.org/10.1007/s002100100454.

37 Jean Mazella et al., « Structure, Functional Expression, and Cerebral Localization of the Levocabastine-Sensitive Neurotensin/Neuromedin N Receptor from Mouse Brain », The Journal of Neuroscience 16, no 18 (15 septembre 1996): 5613-20, https://doi.org/10.1523/JNEUROSCI.16-18-05613.1996.

38 Claude Granier et al., « Synthesis and Characterization of Neurotensin Analogues for Structure/Activity Relationship Studies », European Journal of Biochemistry 124, no 1 (1982): 117-25, https://doi.org/10.1111/j.1432-1033.1982.tb05913.x.

39 Séverine Barroso et al., « Identification of Residues Involved in Neurotensin Binding and Modeling of the Agonist Binding Site in Neurotensin Receptor 1 », Journal of Biological Chemistry 275, no 1 (1 juillet 2000): 328-36, https://doi.org/10.1074/jbc.275.1.328.

40 Patrick Kitabgi, « Functional Domains of the Subtype 1 Neurotensin Receptor (NTS1) », Peptides, Neurotensin: Roles and Mechanisms, 27, no 10 (1 octobre 2006): 2461-68, https://doi.org/10.1016/j.peptides.2006.02.013.

41 Jim F. White et al., « Structure of the agonist-bound neurotensin receptor », Nature 490, no 7421 (25 octobre 2012): 508-13, https://doi.org/10.1038/nature11558.

42 Hideaki E. Kato et al., « Conformational transitions of a neurotensin receptor 1–Gi1 protein complex », Nature 572, no 7767 (août 2019): 80-85, https://doi.org/10.1038/s41586-019-1337-6.

43 Élie Besserer-Offroy et al., « The Signaling Signature of the Neurotensin Type 1 Receptor with Endogenous Ligands », European Journal of Pharmacology 805 (15 juin 2017): 1-13, https://doi.org/10.1016/j.ejphar.2017.03.046.

44 J. C. Bozou et al., « Neurotensin-Mediated Inhibition of Cyclic AMP Formation in Neuroblastoma N1E115 Cells: Involvement of the Inhibitory GTP-Binding Component of Adenylate Cyclase. », Molecular Pharmacology 29, no 5 (1 mai 1986): 489-96.

45 Sandra Dupouy et al., « The Potential Use of the Neurotensin High Affinity Receptor 1 as a Biomarker for Cancer Progression and as a Component of Personalized Medicine in Selective Cancers », Biochimie 93, no 9 (1 septembre 2011): 1369-78, https://doi.org/10.1016/j.biochi.2011.04.024.

46 Robert H. Oakley et al., « Molecular Determinants Underlying the Formation of Stable Intracellular G Protein-Coupled Receptor-β-Arrestin Complexes after Receptor Endocytosis* », Journal of Biological Chemistry 276, no 22 (6 janvier 2001): 19452-60, https://doi.org/10.1074/jbc.M101450200.

47 Emmanuel Hermans et Jean-Marie Maloteaux, « Mechanisms of Regulation of Neurotensin Receptors », Pharmacology & Therapeutics 79, no 2 (1 août 1998): 89-104, https://doi.org/10.1016/S0163-7258(98)00009-6.

48 Jean-Marie Botto et al., « Stable Expression of the Mouse Levocabastine-Sensitive Neurotensin Receptor in HEK 293 Cell Line: Binding Properties, Photoaffinity Labeling, and Internalization Mechanism », Biochemical and Biophysical Research Communications 243, no 2 (13 février 1998): 585-90, https://doi.org/10.1006/bbrc.1997.8071.

49 F. Vandenbulcke et al., « Ligand-Induced Internalization of Neurotensin in Transfected COS-7 Cells: Differential Intracellular Trafficking of Ligand and Receptor », Journal of Cell Science 113, no 17 (1 septembre 2000): 2963-75.

50 Cheryl Savdie et al., « Cell-Type-Specific Pathways of Neurotensin Endocytosis », Cell and Tissue Research 324, no 1 (1 avril 2006): 69-85, https://doi.org/10.1007/s00441-005-0102-3.

51 Mohamad Younes et al., « Neurotensin (NTS) and Its Receptor (NTSR1) Causes EGFR, HER2 and HER3 over-Expression and Their Autocrine/Paracrine Activation in Lung Tumors, Confirming Responsiveness to Erlotinib », Oncotarget 5, no 18 (30 septembre 2014): 8252-69, https://doi.org/10.18632/oncotarget.1633.

52 Meike Körner et al., « Neurotensin Receptors in Pancreatic Ductal Carcinomas », EJNMMI Research 5 (2015): 17, https://doi.org/10.1186/s13550-015-0094-2.

53 Sandra Dupouy et al., « Activation of EGFR, HER2 and HER3 by Neurotensin/Neurotensin Receptor 1 Renders Breast Tumors Aggressive yet Highly Responsive to Lapatinib and Metformin in Mice », Oncotarget 5, no 18 (30 septembre 2014): 8235-51, https://doi.org/10.18632/oncotarget.1632.

54 Sandra Dupouy et al., « The Neurotensin Receptor-1 Pathway Contributes to Human Ductal Breast Cancer Progression », PloS One 4, no 1 (2009): e4223, https://doi.org/10.1371/journal.pone.0004223.

55 Younes et al., « Neurotensin (NTS) and Its Receptor (NTSR1) Causes EGFR, HER2 and HER3 over-Expression and Their Autocrine/Paracrine Activation in Lung Tumors, Confirming Responsiveness to Erlotinib ».

56 Marco Alifano et al., « Neurotensin Receptor 1 Determines the Outcome of Non–Small Cell Lung Cancer », Clinical Cancer Research 16, no 17 (1 septembre 2010): 4401-10, https://doi.org/10.1158/1078-0432.CCR-10-0659.

57 Stephanie L. Swift, Julie E. Burns, et Norman J. Maitland, « Altered Expression of Neurotensin Receptors Is Associated with the Differentiation State of Prostate Cancer », Cancer Research 70, no 1 (1 janvier 2010): 347-56, https://doi.org/10.1158/0008-5472.CAN-09-1252.

58 Tingting He et al., « Evaluation of Neurotensin Receptor 1 as Potential Biomarker for Prostate Cancer Theranostic Use », European Journal of Nuclear Medicine and Molecular Imaging 46, no 10 (septembre 2019): 2199-2207, https://doi.org/10.1007/s00259-019-04355-y.

59 Charlie D. Chen et al., « Molecular Determinants of Resistance to Antiandrogen Therapy », Nature Medicine 10, no 1 (janvier 2004): 33-39, https://doi.org/10.1038/nm972.

60 Mary-Ellen Taplin, « Drug Insight: Role of the Androgen Receptor in the Development and Progression of Prostate Cancer », Nature Clinical Practice Oncology 4, no 4 (avril 2007): 236-44, https://doi.org/10.1038/ncponc0765.

61 Kohei Hashimoto et al., « The Potential of Neurotensin Secreted from Neuroendocrine Tumor Cells to Promote Gelsolin-Mediated Invasiveness of Prostate Adenocarcinoma Cells », Laboratory Investigation; a Journal of Technical Methods and Pathology 95, no 3 (mars 2015): 283-95, https://doi.org/10.1038/labinvest.2014.165.

62 Clément Morgat et al., « Neurotensin Receptor-1 Expression in Human Prostate Cancer: A Pilot Study on Primary Tumors and Lymph Node Metastases », International Journal of Molecular Sciences 20, no 7 (7 avril 2019), https://doi.org/10.3390/ijms20071721.

63 Bruno Vincent, Jean-Pierre Vincent, et Frédéric Checler, « Neurotensin and Neuromedin N Undergo Distinct Catabolic Processes in Murine Astrocytes and Primary Cultured Neurons », European Journal of Biochemistry 221, no 1 (1994): 297-306, https://doi.org/10.1111/j.1432-1033.1994.tb18741.x.

64 Elisa García-Garayoa et al., « In Vitro and in Vivo Evaluation of New Radiolabeled Neurotensin(8–13) Analogues with High Affinity for NT1 Receptors », Nuclear Medicine and Biology 28, no 1 (1 janvier 2001): 75-84, https://doi.org/10.1016/S0969-8051(00)00190-6.

65 Panagiotis Kanellopoulos et al., « Key-Protease Inhibition Regimens Promote Tumor Targeting of Neurotensin Radioligands », Pharmaceutics 12, no 6 (9 juin 2020), https://doi.org/10.3390/pharmaceutics12060528.

66 García-Garayoa et al., « In Vitro and in Vivo Evaluation of New Radiolabeled Neurotensin(8–13) Analogues with High Affinity for NT1 Receptors ».

67 Peter Bläuenstein et al., « Improving the Tumor Uptake of 99mTc-Labeled Neuropeptides Using Stabilized Peptide Analogues », Cancer Biotherapy and Radiopharmaceuticals 19, no 2 (1 avril 2004): 181-88, https://doi.org/10.1089/108497804323071959.

68 J. Couder et al., « Synthesis and Biological Activities of Psi (CH2NH) Pseudopeptide Analogues of the C-Terminal Hexapeptide of Neurotensin », International Journal of Peptide and Protein Research 41, no 2 (février 1993): 181-84, https://doi.org/10.1111/j.1399-3011.1993.tb00129.x.

69 Christof Sparr et al., « Syntheses, Receptor Bindings, in Vitro and in Vivo Stabilities and Biodistributions of DOTA-Neurotensin(8-13) Derivatives Containing β-Amino Acid Residues - a Lesson about the Importance of Animal Experiments », Chemistry & Biodiversity 10, no 12 (décembre 2013): 2101-21, https://doi.org/10.1002/cbdv.201300331.

70 Remya Ramesh et D. Srinivasa Reddy, « Quest for Novel Chemical Entities through Incorporation of Silicon in Drug Scaffolds », Journal of Medicinal Chemistry 61, no 9 (10 2018): 3779-98, https://doi.org/10.1021/acs.jmedchem.7b00718.

71 Florine Cavelier, Damien Marchand, et Jean Martinez, « Alpha,Alpha'-Disubstituted Amino Acids with Silylated Side Chains as Lipophilic Building Blocks for the Synthesis of Peptaibol Analogues », Chemistry & Biodiversity 5, no 7 (juillet 2008): 1279-87, https://doi.org/10.1002/cbdv.200890114.

72 Roberto Fanelli et al., « Synthesis and Characterization in Vitro and in Vivo of (l)-(Trimethylsilyl)Alanine Containing Neurotensin Analogues », Journal of Medicinal Chemistry 58, no 19 (8 octobre 2015): 7785-95, https://doi.org/10.1021/acs.jmedchem.5b00841.

73 Alba Mascarin, Ibai E. Valverde, et Thomas L. Mindt, « Structure-Activity Relationship Studies of Amino Acid Substitutions in Radiolabeled Neurotensin Conjugates », ChemMedChem 11, no 1 (5 janvier 2016): 102-7, https://doi.org/10.1002/cmdc.201500468.

74 Veronique Maes et al., « Novel 99mTc-Labeled Neurotensin Analogues with Optimized Biodistribution Properties », Journal of Medicinal Chemistry 49, no 5 (9 mars 2006): 99, https://doi.org/10.1021/jm051172f.

75 Faisal Alshoukr et al., « Novel DOTA-Neurotensin Analogues for 111In Scintigraphy and 68Ga PET Imaging of Neurotensin Receptor-Positive Tumors », Bioconjugate Chemistry 22, no 7 (20 juillet 2011): 1374-85, https://doi.org/10.1021/bc200078p.

76 D. Gully et al., « Biochemical and Pharmacological Profile of a Potent and Selective Nonpeptide Antagonist of the Neurotensin Receptor », Proceedings of the National Academy of Sciences of the United States of America 90, no 1 (1 janvier 1993): 65-69, https://doi.org/10.1073/pnas.90.1.65.

77 D. Gully et al., « Biochemical and Pharmacological Activities of SR 142948A, a New Potent Neurotensin Receptor Antagonist », The Journal of Pharmacology and Experimental Therapeutics 280, no 2 (février 1997): 802-12.

78 Jörg Schulz et al., « Comparative Evaluation of the Biodistribution Profiles of a Series of Nonpeptidic Neurotensin Receptor-1 Antagonists Reveals a Promising Candidate for Theranostic Applications », Journal of Nuclear Medicine: Official Publication, Society of Nuclear Medicine 57, no 7 (juillet 2016): 1120-23, https://doi.org/10.2967/jnumed.115.170530.

79 Richard P. Baum et al., « 177Lu-3BP-227 for Neurotensin Receptor 1-Targeted Therapy of Metastatic Pancreatic Adenocarcinoma: First Clinical Results », Journal of Nuclear Medicine: Official Publication, Society of Nuclear Medicine 59, no 5 (2018): 809-14, https://doi.org/10.2967/jnumed.117.193847.

80 Alba Mascarin et al., « 1,2,3-Triazole Stabilized Neurotensin-Based Radiopeptidomimetics for Improved Tumor Targeting », Bioconjugate Chemistry 26, no 10 (21 octobre 2015): 2143-52, https://doi.org/10.1021/acs.bioconjchem.5b00444.

81 Simone Maschauer et al., « (18)F- and (68)Ga-Labeled Neurotensin Peptides for PET Imaging of Neurotensin Receptor 1 », Journal of Medicinal Chemistry 59, no 13 (14 juillet 2016): 6480-92, https://doi.org/10.1021/acs.jmedchem.6b00675.

82 Aurélie Prignon et al., « Preclinical Evaluation of 68Ga-DOTA-NT-20.3: A Promising PET Imaging Probe To Discriminate Human Pancreatic Ductal Adenocarcinoma from Pancreatitis », Molecular Pharmaceutics, 23 avril 2019, https://doi.org/10.1021/acs.molpharmaceut.9b00283.

83 Marina Hodolic et al., « Safety and Tolerability of 68Ga-NT-20.3, a Radiopharmaceutical for Targeting Neurotensin Receptors, in Patients with Pancreatic Ductal Adenocarcinoma: The First in-Human Use », European Journal of Nuclear Medicine and Molecular Imaging, 2 octobre 2020, https://doi.org/10.1007/s00259-020-05045-w.

84 Schulz et al., « Proof of Therapeutic Efficacy of a Novel (177)Lu-Labeled Neurotensin Receptor 1-Antagonist in a Colon Carcinoma Xenograft Model », J. Nucl. Med, 02 mars 2017, https://doi.org/10.2967/jnumed.116.185140

85 Anne Roivainen et al., « Plasma Pharmacokinetics, Whole-Body Distribution, Metabolism, and Radiation Dosimetry of 68Ga Bombesin Antagonist BAY 86-7548 in Healthy Men », Journal of Nuclear Medicine 54, no 6 (1 juin 2013): 867-72, https://doi.org/10.2967/jnumed.112.114082.

86 K. Tatemoto, « Neuropeptide Y: Complete Amino Acid Sequence of the Brain Peptide », Proceedings of the National Academy of Sciences of the United States of America 79, no 18 (septembre 1982): 5485-89, https://doi.org/10.1073/pnas.79.18.5485.

87 Wagner et al. « Proteolytic degradation of neuropeptide Y (NPY) from head to toe : Identification of novel NPY-cleaving peptidases and potential drug interactions in CNS an Periphery », Journal of neurochemistry, 7 octobre 2015, https://doi.org/10.1111/jnc.13378.

88 Lei Zhang, Martijn S. Bijker, et Herbert Herzog, « The Neuropeptide Y System: Pathophysiological and Therapeutic Implications in Obesity and Cancer », Pharmacology & Therapeutics 131, no 1 (juillet 2011): 91-113, https://doi.org/10.1016/j.pharmthera.2011.03.011.

89 E. Ekblad et al., « Neuropeptide Y Co-Exists and Co-Operates with Noradrenaline in Perivascular Nerve Fibers », Regulatory Peptides 8, no 3 (avril 1984): 225-35, https://doi.org/10.1016/0167-0115(84)90064-8.

90 C. Wahlestedt, N. Yanaihara, et R. Håkanson, « Evidence for Different Pre-and Post-Junctional Receptors for Neuropeptide Y and Related Peptides », Regulatory Peptides 13, no 3-4 (février 1986): 307-18, https://doi.org/10.1016/0167-0115(86)90048-0.

91 J. A. Bard et al., « Cloning and Functional Expression of a Human Y4 Subtype Receptor for Pancreatic Polypeptide, Neuropeptide Y, and Peptide YY », The Journal of Biological Chemistry 270, no 45 (10 novembre 1995): 26762-65, https://doi.org/10.1074/jbc.270.45.26762.

92 M. C. Michel et al., « XVI. International Union of Pharmacology Recommendations for the Nomenclature of Neuropeptide Y, Peptide YY, and Pancreatic Polypeptide Receptors », Pharmacological Reviews 50, no 1 (mars 1998): 143-50.

93 H. Herzog et al., « Cloned Human Neuropeptide Y Receptor Couples to Two Different Second Messenger Systems », Proceedings of the National Academy of Sciences of the United States of America 89, no 13 (1 juillet 1992): 5794-98, https://doi.org/10.1073/pnas.89.13.5794.

94 A. G. Beck-Sickinger et G. Jung, « Structure-Activity Relationships of Neuropeptide Y Analogues with Respect to Y1 and Y2 Receptors », Biopolymers 37, no 2 (1995): 123-42, https://doi.org/10.1002/bip.360370207.

95 S. Hoffmann et al., « Structure-Affinity Studies of C-Terminally Modified Analogs of Neuropeptide Y Led to a Novel Class of Peptidic Y1 Receptor Antagonist », Regulatory Peptides 65, no 1 (27 août 1996): 61-70, https://doi.org/10.1016/0167-0115(96)00073-0.

96 A. G. Beck-Sickinger et al., « Complete L-Alanine Scan of Neuropeptide Y Reveals Ligands Binding to Y1 and Y2 Receptors with Distinguished Conformations », European Journal of Biochemistry 225, no 3 (1 novembre 1994): 947-58, https://doi.org/10.1111/j.1432-1033.1994.0947b.x.

97 C. Cabrele et A. G. Beck-Sickinger, « Molecular Characterization of the Ligand-Receptor Interaction of the Neuropeptide Y Family », Journal of Peptide Science: An Official Publication of the European Peptide Society 6, no 3 (mars 2000): 97-122, https://doi.org/10.1002/(SICI)1099-1387(200003)6:3<97::AID-PSC236>3.0.CO;2-E.

98 Diana Lindner et al., « Functional Role of the Extracellular N-Terminal Domain of Neuropeptide Y Subfamily Receptors in Membrane Integration and Agonist-Stimulated Internalization », Cellular Signalling 21, no 1 (janvier 2009): 61-68, https://doi.org/10.1016/j.cellsig.2008.09.007.

99 M. Sautel et al., « Role of a Hydrophobic Pocket of the Human Y1 Neuropeptide Y Receptor in Ligand Binding », Molecular and Cellular Endocrinology 112, no 2 (11 août 1995): 215-22, https://doi.org/10.1016/0303-7207(95)03603-5.

100 M. Sautel et al., « Neuropeptide Y and the Nonpeptide Antagonist BIBP 3226 Share an Overlapping Binding Site at the Human Y1 Receptor », Molecular Pharmacology 50, no 2 (août 1996): 285-92.

101 T. Kannoa et al., « Different Binding Sites for the Neuropeptide Y Y1 Antagonists 1229U91 and J-104870 on Human Y1 Receptors », Peptides 22, no 3 (mars 2001): 405-13, https://doi.org/10.1016/s0196-9781(01)00350-3.

102 Paula Sjödin et al., « Re-evaluation of receptor–ligand interactions of the human neuropeptide Y receptor Y1: a site-directed mutagenesis study », Biochemical Journal 393, no Pt 1 (1 janvier 2006): 161-69, https://doi.org/10.1042/BJ20050708.

103 Nicole Merten et al., « Receptor Subtype-Specific Docking of Asp6.59 with C-Terminal Arginine Residues in Y Receptor Ligands », The Journal of Biological Chemistry 282, no 10 (9 mars 2007): 7543-51, https://doi.org/10.1074/jbc.M608902200.

104 Zhenlin Yang et al., « Structural Basis of Ligand Binding Modes at the Neuropeptide Y Y1 Receptor », Nature 556, no 7702 (2018): 520-24, https://doi.org/10.1038/s41586-018-0046-x.

105 P. J. Mannon et J. M. Mele, « Peptide YY Y1 Receptor Activates Mitogen-Activated Protein Kinase and Proliferation in Gut Epithelial Cells via the Epidermal Growth Factor Receptor », The Biochemical Journal 350 Pt 3 (15 septembre 2000): 655-61.

106 D. E. Hansel, B. A. Eipper, et G. V. Ronnett, « Neuropeptide Y Functions as a Neuroproliferative Factor », Nature 410, no 6831 (19 avril 2001): 940-44, https://doi.org/10.1038/35073601.

107 Ilka Böhme et al., « Agonist Induced Receptor Internalization of Neuropeptide Y Receptor Subtypes Depends on Third Intracellular Loop and C-Terminus », Cellular Signalling 20, no 10 (octobre 2008): 1740-49, https://doi.org/10.1016/j.cellsig.2008.05.017.

108 Ambikaipakan Balasubramaniam, « Neuropeptide Y Family of Hormones: Receptor Subtypes and Antagonists », Peptides 18, no 3 (1 janvier 1997): 445-57, https://doi.org/10.1016/S0196-9781(96)00347-6.

109 D. A. Keire et al., « Structure and Receptor Binding of PYY Analogs », Peptides 23, no 2 (février 2002): 305-21, https://doi.org/10.1016/s0196-9781(01)00602-7.

110 Meike Körner et Jean Claude Reubi, « NPY Receptors in Human Cancer: A Review of Current Knowledge », Peptides 28, no 2 (février 2007): 419-25, https://doi.org/10.1016/j.peptides.2006.08.037.

111 Meike Körner et Jean Claude Reubi, « Neuropeptide Y Receptors in Primary Human Brain Tumors: Overexpression in High-Grade Tumors », Journal of Neuropathology and Experimental Neurology 67, no 8 (août 2008): 741-49, https://doi.org/10.1097/NEN.0b013e318180e618.

112 Meike Körner, Beatrice Waser, et Jean Claude Reubi, « Neuropeptide Y Receptors in Renal Cell Carcinomas and Nephroblastomas », International Journal of Cancer 115, no 5 (10 juillet 2005): 734-41, https://doi.org/10.1002/ijc.20948.

113 Meike Körner, Beatrice Waser, et Jean Claude Reubi, « Neuropeptide Y Receptor Expression in Human Primary Ovarian Neoplasms », Laboratory Investigation; a Journal of Technical Methods and Pathology 84, no 1 (janvier 2004): 71-80, https://doi.org/10.1038/labinvest.3700009.

114 P. Magni et M. Motta, « Expression of Neuropeptide Y Receptors in Human Prostate Cancer Cells », Annals of Oncology: Official Journal of the European Society for Medical Oncology 12 Suppl 2 (2001): S27-29, https://doi.org/10.1093/annonc/12.suppl_2.s27.

115 Massimiliano Ruscica et al., « Activation of the Y1 Receptor by Neuropeptide Y Regulates the Growth of Prostate Cancer Cells », Endocrinology 147, no 3 (mars 2006): 1466-73, https://doi.org/10.1210/en.2005-0925.

116 Massimiliano Ruscica et al., « Modulatory Actions of Neuropeptide Y on Prostate Cancer Growth: Role of MAP Kinase/ERK 1/2 Activation », Advances in Experimental Medicine and Biology 604 (2007): 96-100, https://doi.org/10.1007/978-0-387-69116-9_7.

117 K. Rudolf et al., « The First Highly Potent and Selective Non-Peptide Neuropeptide Y Y1 Receptor Antagonist: BIBP3226 », European Journal of Pharmacology 271, no 2-3 (27 décembre 1994): R11-13, https://doi.org/10.1016/0014-2999(94)90822-2.

118 Max Keller et al., « Prototypic 18F-Labeled Argininamide-Type Neuropeptide Y Y1R Antagonists as Tracers for PET Imaging of Mammary Carcinoma », ACS Medicinal Chemistry Letters 8, no 3 (9 mars 2017): 304-9, https://doi.org/10.1021/acsmedchemlett.6b00467.

119 Brigitte Guérin et al., « [Lys(DOTA)4]BVD15, a Novel and Potent Neuropeptide Y Analog Designed for Y1 Receptor-Targeted Breast Tumor Imaging », Bioorganic & Medicinal Chemistry Letters 20, no 3 (1 février 2010): 950-53, https://doi.org/10.1016/j.bmcl.2009.12.068.

120 Chengcheng Zhang et al., « Targeting the Neuropeptide Y1 Receptor for Cancer Imaging by Positron Emission Tomography Using Novel Truncated Peptides », Molecular Pharmaceutics 13, no 11 (07 2016): 3657-64, https://doi.org/10.1021/acs.molpharmaceut.6b00464.

121 R. M. Söll et al., « Novel Analogues of Neuropeptide Y with a Preference for the Y1-Receptor », European Journal of Biochemistry 268, no 10 (mai 2001): 2828-37, https://doi.org/10.1046/j.1432-1327.2001.02161.x.

122 Sven Hofmann et al., « Synthesis and in Vitro and in Vivo Evaluation of an (18)F-Labeled Neuropeptide Y Analogue for Imaging of Breast Cancer by PET », Molecular Pharmaceutics 12, no 4 (6 avril 2015): 1121-30, https://doi.org/10.1021/mp500601z.

123 Cristina Müller et al., « A Unique Matched Quadruplet of Terbium Radioisotopes for PET and SPECT and for α- and β- Radionuclide Therapy: An in Vivo Proof-of-Concept Study with a New Receptor-Targeted Folate Derivative », Journal of Nuclear Medicine: Official Publication, Society of Nuclear Medicine 53, no 12 (décembre 2012): 1951-59, https://doi.org/10.2967/jnumed.112.107540.

124 Cristina Müller et al., « Direct in Vitro and in Vivo Comparison of (161)Tb and (177)Lu Using a Tumour-Targeting Folate Conjugate », European Journal of Nuclear Medicine and Molecular Imaging 41, no 3 (mars 2014): 476-85, https://doi.org/10.1007/s00259-013-2563-z.

1251 Jürgen Grünberg et al., « Anti-L1CAM Radioimmunotherapy Is More Effective with the Radiolanthanide Terbium-161 Compared to Lutetium-177 in an Ovarian Cancer Model », European Journal of Nuclear Medicine and Molecular Imaging 41, no 10 (octobre 2014): 1907-15, https://doi.org/10.1007/s00259-014-2798-3.

126 Cristina Müller et al., « Terbium-161 for PSMA-Targeted Radionuclide Therapy of Prostate Cancer », European Journal of Nuclear Medicine and Molecular Imaging 46, no 9 (août 2019): 1919-30, https://doi.org/10.1007/s00259-019-04345-0.

127 Stephanie Haller et al., « Contribution of Auger/Conversion Electrons to Renal Side Effects after Radionuclide Therapy: Preclinical Comparison of (161)Tb-Folate and (177)Lu-Folate », EJNMMI Research 6, no 1 (décembre 2016): 13, https://doi.org/10.1186/s13550-016-0171-1.

128 Elif Hindié et al., « Dose Deposits from 90Y, 177Lu, 111In, and 161Tb in Micrometastases of Various Sizes: Implications for Radiopharmaceutical Therapy », Journal of Nuclear Medicine: Official Publication, Society of Nuclear Medicine 57, no 5 (2016): 759-64, https://doi.org/10.2967/jnumed.115.170423.

129 Mario E. Alcocer-Ávila et al., « Radiation Doses from 161Tb and 177Lu in Single Tumour Cells and Micrometastases », EJNMMI Physics 7, no 1 (19 mai 2020): 33, https://doi.org/10.1186/s40658-020-00301-2.

130 Y. Yoneda et al., « Nucleocytoplasmic Protein Transport and Recycling of Ran », Cell Structure and Function 24, no 6 (décembre 1999): 425-33, https://doi.org/10.1247/csf.24.425.

131 Melpomeni Fani et al., « Unexpected Sensitivity of Sst2 Antagonists to N-Terminal Radiometal Modifications », Journal of Nuclear Medicine: Official Publication, Society of Nuclear Medicine 53, no 9 (septembre 2012): 1481-89, https://doi.org/10.2967/jnumed.112.102764.

132 Veronika Mäde et al., « Peptide Modifications Differentially Alter G Protein-Coupled Receptor Internalization and Signaling Bias », Angewandte Chemie (International Ed. in English) 53, no 38 (15 septembre 2014): 10067-71, https://doi.org/10.1002/anie.201403750.

133 Mihaela Ginj et al., « Trifunctional Somatostatin-Based Derivatives Designed for Targeted Radiotherapy Using Auger Electron Emitters », Journal of Nuclear Medicine: Official Publication, Society of Nuclear Medicine 46, no 12 (décembre 2005): 2097-2103.

134 Schollhammer R et al., « 68Ga-PSMA-617 Compared With 68Ga-RM2 and 18F-FCholine PET/CT for the Initial Staging of High-Risk Prostate Cancer. », Clin Nucl Med. 2019 Sep;44(9):e535-e536

135 Minamimoto et al « Pilot Comparison of ^{68}Ga-RM2 PET and ^{68}Ga-PSMA-11 PET in Patients with Biochemically Recurrent Prostate Cancer », J Nucl Med, Avril 2016, https://doi.org/10.2967/jnumed/115.168393

136 Touijer et al « Prospective Study of the Radiolabeled GRPR Antagonist BAY86-7548 for Positron Emission Tomography/Computed Tomography Imaging of Newly Diagnosed Prostate Cancer », Eur urol oncol, 2 mars 2019, https://doi.org/10.1016/j.euo.2018.08.011

137 Adrien Chastel, « Mise au point du radiomarquage au gallium-68 et validation d'une trousse pour le ciblage du récepteur du Gastrin-Releasing Peptide (GRP-R) » (Thèse d'exercice de Pharmacie, Université de Toulouse, 2020).

138 Chengcheng Zhang et al., « Stabilizing Truncated Peptides Targeting the Neuropeptide Y1 Receptor for Cancer Imaging », Journal of Nuclear Medicine 58, no supplement 1 (5 janvier 2017): 693-693.

139 Andrey A. Rosenkranz et al., « Exploiting Active Nuclear Import for Efficient Delivery of Auger Electron Emitters into the Cell Nucleus », International Journal of Radiation Biology, 14 septembre 2020, 1-11, https://doi.org/10.1080/09553002.2020.1815889.

140 Christophe Champion et al., « Comparison between Three Promising SS-Emitting Radionuclides, (67)Cu, (47)Sc and (161)Tb, with Emphasis on Doses Delivered to Minimal Residual Disease », Theranostics 6, no 10 (2016): 1611-18, https://doi.org/10.7150/thno.15132.

Production scientifique

Publications

Morgat C, **Chastel A**, Molinie V, Schollhammer R, Macgrogan G, Vélasco V, Malavaud B, Fernandez P, Hindié E ; Neurotensin Receptor-1 Expression in Human Prostate Cancer: A Pilot Study on Primary Tumors and Lymph Node Metastases ; *International Journal of Molecular Sciences, 20(7). pii: E1721, 2019*

Chastel A, Worm D J, Alves I D, Vimont D, Petrel M, Fernandez S, Garrigue P, Fernandez P, Hindié E, Beck-Sickinger A G, Morgat C ; Design, synthesis, and biological evaluation of a multifunctional neuropeptide-Y conjugate for selective nuclear delivery of radiolanthanides, *EJNMMI Res, 10(1):16, 2020*

Fanelli R, **Chastel A,** Previti S, Hindié E, Vimont D, Zanotti-Fregonara P, Fernandez P, Garrigue P, Lamare F, Schollhammer R, Balasse L, Guillet B, Rémond E, Morgat C, Cavelier F ; Silicon-Containing Neurotensin Analogues as Radiopharmaceuticals for NTS1-Positive Tumors Imaging ; *Bioconjugate Chemistry*, sous presse

Communications orales

Previti S, **Chastel A**, Fanelli R, Hindié E, Rémond E, Morgat C, Cavelier F ; Novel radiopharmaceutical neurotensin analogues as potential agents for cancer theranostic, *Groupe français des peptides et des protéines : GFPP21, Amboise, France, Mai 2019*

Chastel A, Fanelli R, Previti S, Vimont D, Zanotti-Frégonara P, Guillet B, Fernandez P, Rémond E, Hindié E, Cavelier F, Morgat C ; Novel radiolabelled neurotensin analogues containing silylated amino acid for improved neurotensin receptor-1 (NTS1) targeting, *EANM 2019, Octobre 2019*

Communications affichées

Chastel A, Worm D J, Alves I D, Vimont D, Petrel M, Fernandez P, Hindié E, Beck-Sickinger A, Morgat C ; Development of a multivalent NPY analogue for selective nuclear delivery of terbium-161, *EANM 2019, Octobre 2019*

Annexe

Thèse d'exercice de Pharmacie, Chastel A

TITRE : Mise au point du radiomarquage au gallium-68 et validation d'une trousse pour le ciblage du récepteur du Gastrin-Releasing Peptide (GRP-R)

RÉSUMÉ : Les médicaments radiopharmaceutiques employés en médecine nucléaire sont en plein développement. Nous étudions ici le radiomarquage au 68Ga d'une trousse au RM2 pour le ciblage du récepteur du gastrin-releasing peptide connu pour être surexprimé dans plusieurs cancers. Nous avons d'abord optimisé les conditions de radiomarquage pour être conforme à la pharmacopée européenne, puis réalisé une évaluation in vitro des caractéristiques pharmacologiques du radiopharmaceutique. Enfin, nous avons évalué les coûts de l'emploi de cette technique en routine clinique comparée à un marquage par module. Le radiomarquage a été réussi avec l'obtention d'un produit répondant aux exigences. Les caractéristiques pharmacologiques (hydrophilie, affinité, internalisation et efflux) ont pu être déterminées, complétant ainsi les connaissances disponibles à ce jour dans la littérature. Enfin, la synthèse du 68Ga-RM2 par trousse s'est avérée moins onéreuse que la synthèse par module.

MOTS-CLÉS : Gastrin Releasing Peptide Receptor, GRP-R, RM2, Oncologie, Radiopharmaceutique, Gallium-68, Trousse, Module

Titre : Exploration de nouvelles approches en radiothérapie interne vectorisée à l'aide d'analogues de neuropeptides

Résumé :

La radiothérapie interne vectorisée (RIV) utilise des radionucléides couplés à des molécules vectrices (radiopharmaceutiques) capables de cibler des récepteurs surexprimés par les cellules tumorales ou leur microenvironnement. Parmi les approches utilisées en RIV, celle basée sur des analogues de peptides radiomarqués, comme le [^{177}Lu]Lu-DOTATATE ou le [^{177}Lu]Lu-PSMA, est en pleine expansion. Ces traitements s'inscrivent dans une approche théranostique personnalisée, où une molécule compagnon, marquée à l'aide d'un émetteur de positons comme le ^{68}Ga, sert à l'imagerie en TEP en préambule à la RIV. Ce travail de Thèse explore le potentiel offert par le ciblage de deux récepteurs de neuropeptides, le récepteur NTS_1 de la neurotensine et le récepteur Y_1R du neuropeptide Y connus pour être surexprimés dans plusieurs cancers.

Concernant le ciblage de NTS_1, le design de radiopharmaceutiques peptidiques est difficile en raison de la courte demi-vie du peptide endogène neurotensine. Dans la première partie de travail, nous avons exploré l'impact d'acides aminés non naturels au sein d'analogues de la neurotensine, radiomarqués au ^{68}Ga. L'insertion d'une alanine silylée en position N-terminale a permis de stabiliser le peptide [^{68}Ga]Ga-JMV6659 tout en conservant un bon profil d'affinité et de sélectivité. In vivo, l'analogue [^{68}Ga]Ga-JMV6659 a montré une excellente captation tumorale chez des souris nude porteuses d'une xénogreffe HT-29 faisant de ce composé un bon candidat pour l'imagerie TEP.

Les orientations futures de la RIV nécessitent d'augmenter la dose déposée à la tumeur pour mieux contrôler la pathologie cancéreuse. Une stratégie émergente, aujourd'hui peu explorée, consiste en l'adressage nucléaire d'émetteurs thérapeutiques à faible parcours comme le terbium-161, riche en électrons Auger. Dans cette optique, , nous avons exploré la faisabilité d'un adressage nucléaire via le récepteur Y_1R d'un analogue agoniste du neuropeptide Y modifié, à l'aide d'une séquence de clivage par la cathepsine B endosomale libérant par la suite une séquence d'adressage nucléaire (NLS) prise en charge par des importines cytoplasmiques assurant le transport au noyau. Ainsi, le composé Pb12 a été étudié après radiomarquage à l'^{111}In, comme substitut au ^{161}Tb. Les résultats obtenus sur des cellules mammaires cancéreuses MCF7 exprimant Y_1R ont montré que cette technologie d'adressage nucléaire multi-étapes fonctionne ouvrant des perspectives prometteuses avec d'autres émetteurs thérapeutiques à courte portée comme les émetteurs alpha.

Mots clés : Radiothérapie interne vectorisée, cancer, NTS_1, Y_1R, radiopharmaceutiques

---

Title: Exploration of new approaches to targeted radionuclide therapy with neuropeptide analogs

Abstract :

Targeted Radionuclide Therapy (TRT) uses radionuclides coupled to carrier molecules (radiopharmaceuticals) capable of targeting receptors overexpressed by tumor cells or their microenvironment. Among the approaches used in TRT, the one based on analogs of radiolabeled peptides, such as [^{177}Lu]Lu-DOTATATE or [^{177}Lu]Lu-PSMA, is in full expansion. These treatments are part of a personalized theranostic approach, where a companion molecule labeled with a positron emitter such as ^{68}Ga is used for PET imaging as a preamble to TRT. This Thesis work explores the potential offered by the targeting of two neuropeptide receptors, the neurotensin receptor NTS_1 and the neuropeptide Y receptor Y_1R, known to be overexpressed in several cancers.

Regarding the targeting of NTS_1, the design of peptide radiopharmaceuticals is difficult due to the short half-life of the endogenous neurotensin peptide. In the first part of this work, we explored the impact of unnatural amino acids in neurotensin analogs, radiolabelled with ^{68}Ga. Insertion of a silylated alanine in the N-terminal position stabilized the [^{68}Ga]Ga-JMV6659 peptide while maintaining a good affinity and selectivity profile. In vivo, the analog [^{68}Ga]Ga-JMV6659 showed excellent tumor uptake in nude mice carrying an HT-29 xenograft making this compound a good candidate for PET imaging.

Future development of TRT requires increasing the dose deposited to the tumor to better control the cancerous pathology. An emerging strategy, little explored today, consists of the nuclear targeting of therapeutic short-course emitters such as terbium-161, rich in Auger electrons. With this in mind, we explored the feasibility of nuclear addressing via the Y_1R receptor of an agonist analogue of the modified neuropeptide Y, using a cleavage sequence by endosomal cathepsin B subsequently releasing a nuclear localization sequence (NLS) supported by cytoplasmic importins providing transport to the nucleus. Thus, the compound Pb12 was studied after radiolabelling with ^{111}In, as a substitute for ^{161}Tb. Results obtained on MCF7 breast cancer cells expressing Y_1R showed that this multi-step nuclear addressing technology works, opening promising prospects with other short-range therapeutic emitters such as alpha emitters.

Keywords: Targeted radionuclide therapy, NTS_1, Y_1R, radiopharmaceuticals

---

Unité de recherche

Institut des Neurosciences Cognitives et Intégratives d'Aquitaine (INCIA), UMR-CNRS 5287, 146 Rue Léo Saignat, 33000 Bordeaux